NONDESTRUCTIVE ELECTROMAGNETIC CHARACTERIZATION OF

UNIAXIAL MATERIALS

DISSERTATION

Neil G. Rogers, Captain, USAF

AFIT-ENG-DS-14-S-05

DEPARTMENT OF THE AIR FORCE
AIR UNIVERSITY

AIR FORCE INSTITUTE OF TECHNOLOGY

Wright-Patterson Air Force Base, Ohio

AFIT-ENG-DS-14-S-05

NONDESTRUCTIVE ELECTROMAGNETIC CHARACTERIZATION OF UNIAXIAL

MATERIALS

DISSERTATION

Presented to the Faculty

Graduate School of Engineering and Management

Air Force Institute of Technology

Air University

Air Education and Training Command

in Partial Fulfillment of the Requirements for the

Degree of Doctor of Philosophy

Neil G. Rogers, B.S.E.E.,M.S.E.E

Captain, USAF

September 2014

AFIT-ENG-DS-14-S-05

NONDESTRUCTIVE ELECTROMAGNETIC CHARACTERIZATION OF UNIAXIAL

MATERIALS

Neil G. Rogers, B.S.E.E.,M.S.E.E

Captain, USAF

Approved:

//signed//	24 June 2014
Michael J. Havrilla, PhD (Chairman)	Date
//signed//	24 June 2014
William P. Baker, PhD (Member)	Date
//signed//	24 June 2014
Major Milo Hyde, PhD (Member)	Date

Accepted:

//signed//	24 July 2014
ADEDEJI B. BADIRU, PhD, PE	Date

Dean, Graduate School of Engineering
and Management

AFIT-ENG-DS-14-S-05

Abstract

In this dissertation, a method for the simultaneous non-destructive extraction of the permittivity and permeability of a dielectric magnetic uniaxial anisotropic media is developed and several key contributions are demonstrated. The method utilizes a single fixture in which the MUT is clamped between two rectangular waveguides with 6" × 6" PEC flanges. The transmission and reflection coefficients are measured, then compared with theoretically calculated coefficients to find a least squares solution to the minimization problem. One of the key contributions of this work is the development of the total parallel plate spectral-domain Green's function by two independent methods. The Green's function is thereby shown to be correct in form and in physical meaning. A second significant contribution of this work to the scientific community is the evaluation of one of the inverse Fourier transform integrals in the complex plane. This significantly enhances the efficiency of the extraction code. A third significant contribution is the measurement of a number of uniaxial anisotropic materials, many of which were envisioned, designed and constructed in-house using 3D printing technology. The results are shown to be good in the transverse dimension, but mildly unstable in the longitudinal dimension. A secondary contribution of this work that warrants mention is the inclusion of a flexible, complete, working code for the extraction process. Although such codes have been written before, they have not been published in the literature for broader use.

iv

To my wife: I am blessed and thankful to have you 'till death do us part.

To my boys: may you be better men than I am.

Acknowledgments

A work of this magnitude is a team effort and would never be possible as the work of a single individual. Several people deserve special recognition for their invaluable part in bringing this work to fruition. First and foremost, I would like to thank the Lord Jesus Christ, without whose constant help I would be utterly lost in any endeavor. My wife and my three sons have given me unwavering support through the longest three years of our life together. Any accomplishment is meaningless without their encouragement and enthusiasm and they have given those in abundance. I would also like to thank Dr. Havrilla for his countless hours of instruction and forbearance, as I grappled with the many complex facets of this research. Without his dedication and expertise, this work would undoubtedly remain half finished. I also owe a debt of gratitude to Maj Milo Hyde for his invaluable insight into all things MATLAB and, of course, the tFWMT. Dr. Andrew Bogle was a constant companion - helping me understand the complexities of lab measurements and always a willing sounding board. Dr. Jeffery Allen was invaluable in constructing material samples and giving independent advice. To my church, Apex, and my friends: you kept me going when I didn't think I could make it; you helped me finish strong. Finally, the AFIT machine shop was an unexpected ally, their outstanding products and responsiveness helped turn my lab workflow into a process that produced consistent results day in and day out.

Neil G. Rogers

Table of Contents

List of Figures

xiv

xv

List of Tables

List of Acronyms

Acronym	Definition
tFWMT	Two-Flanged Waveguide Measurement Technique
LO	Low Observable
MUT	Material Under Test
NDE	Nondestructive Evaluation
CIT	Cauchty's Integral Theorem
MoM	Method of Moments
TRL	Thru-Line-Reflect
DNG	Double-Negative Materials
LHM	Left-Handed Materials
ENG	Epsilon-Negative Materials
MNG	Mu-Negative Materials
SRR	Split Ring Resonators
TL	Transmission Line
CEM	Computational Electromagnetics
S/FS	Short/Free-Space
TTM	Two Thickness Method
TLM	Two Layer Method
FV	Frequency Varying
DWP	Dual Wavguide Probe
GTD	Geometrical Theory of Diffraction
UTD	Uniform Theory of Diffraction
PTD	Physical Theory of Diffraction

Acronym	Definition
MFIE	Magnetic Field Integral Equation
PEC	Perfect Electrical Conductor
UHP	Upper Half Plane
LHP	Lower Half Plane
PPWG	Parallel Plate Waveguide
TRR	Trust Region Reflective
L-M	Levenburg-Marquardt
NRW	Nicholson-Ross-Weir
VNA	Vector Network Analyzer
WRWST	Waveguide Rectangular to Waveguide Square Technique
FBMT	Focused Beam Measurement Technique
RWMT	Rectangular Waveguide Measurement Technique
CAD	Computer-aided Design

NONDESTRUCTIVE ELECTROMAGNETIC CHARACTERIZATION OF UNIAXIAL MATERIALS

I. Introduction

1.1 Introduction

Electromagnetic characterization of a material refers to the general process of obtaining the constitutive parameters of medium, $\overset{\leftrightarrow}{\varepsilon} = \overset{\leftrightarrow}{\varepsilon}_{re} + j\overset{\leftrightarrow}{\varepsilon}_{im}$ and $\overset{\leftrightarrow}{\mu} = \overset{\leftrightarrow}{\mu}_{re} + j\overset{\leftrightarrow}{\mu}_{im}$, for the case of anisotropic media. In the case of isotropic media, the constitutive parameter dyads can be reduced to scalars. Clearly, an anisotropic or bianisotropic media requires more parameters for an accurate characterization. The electromagnetic characterization of media is an area of active research; most methods rely on measuring scattering from any number of possible geometries, then solve the minimization problem between the theoretical scattering and the experimental results. Accurate measurements are difficult enough in isotropic media, in which boundary conditions based on the geometry are applied to Maxwell's equations and the inverse problem solved by a numerical root search or non-linear least squares method. In anisotropic media, though, the problem is further complicated through the coupling induced in the transverse and/or longitudinal axes of the material. This complexity manifests itself, mathematically, through increasingly complicated Green's functions and additional constitutive parameters. However, given the explosion of interest in complex media, it is now desirable to develop methods with which we can accurately extract the constitutive parameters of complex media. For example, in an environment of increasing reliance on Low Observable (LO) materials to defeat highly sensitive radars, complete knowledge of the electromagnetic scattering characteristics of complex media is required

to achieve accurate engineering designs and operational performance. Such precision is also required for the design of advanced scanning antennas, polarization shifters, advanced ground planes for electronics and myriad other cutting edge applications of metamaterials. The electromagnetic characterization of these complex materials is quickly being outpaced by the theoretical applications. This work proposes to fill a small gap in the characterization capability.

Broadly, characterization methods can be broken into destructive measurement techniques and nondestructive techniques. In destructive techniques, a machined sample is required to fit inside a waveguiding region, such as a coaxial or rectangular waveguide. However, it is not always practical to machine a sample of a Material Under Test (MUT), due to the uniqueness of a sample, precision mounting constraints, or other potential concerns. This has led to a great interest in Nondestructive Evaluation (NDE) techniques. Although there are many choices for NDE, this work seeks to extend an existing NDE method, which has been proven effective for the simultaneous extraction of complex permittivity and permeability of both lossless and lossy isotropic materials.

1.2 Problem Statement

Up to this point, many characterization methods for materials in the microwave regime have focused on isotropic materials. We seek a NDE method to measure the complex permittivity and permeability of anisotropic uniaxial media. The exact characteristics which differentiate the categories of complex media and the foundational work of those who have pioneered this area will be discussed in detail in the next section, in the context of what we will call the metamaterial "revolution". The problem at hand is a multi-faceted one, which requires employment of many mathematical, analytical, computational and experimental tools. We begin our solution with a rigorous spectral-domain examination of Maxwell's equations, which is specialized for uniaxial materials.

2

Although a few individuals have pioneered the Green's functions of certain classes of complex media before, we undertake a novel method of obtaining them, producing a simple solution which clearly demonstrates the physics of the geometry and is also shown to reduce to the isotropic case. Application of complex plane analysis, including Cauchty's Integral Theorem (CIT), Jordan's Lemma and Cauchy's Integral Formula (see Appendix A), leads to identification of spectral-domain Green's functions, to which we apply the PEC boundary conditions for uniaxial media sandwiched between parallel-plates. Using this total Green's function, we re-visit the theory for a flanged-waveguide measurement apparatus, employ a Method of Moments (MoM) solution and reformulate the required MFIE's, which relate the source field of the network analyzer to the theoretical reflection (S_{11}) and transmission (S_{21}) coefficients. In the laboratory, appropriate calibration is accomplished using the Thru-Line-Reflect (TRL) technique and the data processed by MATLAB®, which, given the appropriate measurements, performs a non-linear optimization method to extract the complex permittivity and permeability.

To the knowledge of the author, the derivation of the parallel-plate Green's function, application of this Green's function to the Two-Flanged Waveguide Measurement Technique (tFWMT) and measurement of a uniaxial material in a nondestructive apparatus all represent original work. Additionally, they are considered to be significant contributions to the scientific community at large, so that NDE methods may be applied to an increasing number of classes of materials. Naturally, this research stands on the shoulders of giants and pioneers, whose work is now reviewed and referenced in considerably more detail.

1.3 Metamaterial Revolution

Although we intend in this section to review the recent metamaterial "revolution", we must first set forth a few fundamental concepts upon which all electromagnetic material

characterization are built. Most introductory texts on electromagnetics restrict their treatments of electromagnetic scattering and associated phenomena to simple media, which are defined to be linear, homogeneous and isotropic. In contrast, complex media are materials which possess one or more characteristics outside of the simple media arena (i.e., non-linear, inhomogeneous and/or non-isotropic). Complex media can be sub-classified as either anisotropic, in which the permittivity ($\overleftrightarrow{\varepsilon}$) and permeability ($\overleftrightarrow{\mu}$) are dyadic and non-zero, while the magnetoelectric dyads ($\overleftrightarrow{\xi}, \overleftrightarrow{\zeta}$) are zero; or they may be classified as bianisotropic, in which both the constitutive parameters and magnetoelectric dyads are dyadic and non-zero. This work will focus on anisotropic media, but we will now examine some general characteristics of bianisotropic media in order to facilitate a more comprehensive understanding scope of the problem at hand. Assuming an $e^{+j\omega t}$ time dependence and omitting the spatial and frequency dependencies for notational convenience, Maxwell's equations for the more general case (bianisotropic) are

$$\nabla \times \vec{E} = -\vec{J_h} - j\omega\vec{B}$$

$$\nabla \times \vec{H} = \vec{J_e} + j\omega\vec{D}$$

$$\text{(1.1)}$$

$$\vec{B} = \overleftrightarrow{\mu} \cdot \vec{H} + \overleftrightarrow{\zeta} \cdot \vec{E}$$

$$\vec{D} = \overleftrightarrow{\xi} \cdot \vec{H} + \overleftrightarrow{\varepsilon} \cdot \vec{E}$$

where the constitutive parameters take the dyadic form

$$\overleftrightarrow{\sigma} = \begin{bmatrix} \sigma_{xx} & \sigma_{xy} & \sigma_{xz} \\ \sigma_{yx} & \sigma_{yy} & \sigma_{yz} \\ \sigma_{zx} & \sigma_{zy} & \sigma_{zz} \end{bmatrix} \quad , \quad \sigma = \overleftrightarrow{\varepsilon}, \overleftrightarrow{\mu}, \overleftrightarrow{\zeta}, \overleftrightarrow{\xi} \quad \text{(1.2)}$$

Here, $\overleftrightarrow{\varepsilon}$ and $\overleftrightarrow{\mu}$ are the permittivity and permeability dyads, respectively and $\overleftrightarrow{\zeta}$ and $\overleftrightarrow{\xi}$ are the magnetoelectric dyads. Clearly, the more complex the media, there exist a greater number

of parameters (36 in the most general case) [1] to "tune" the electromagnetic scattering parameters. However, the price one pays for such flexibility is an increased difficulty in the theoretical characterization of a complex material. For anisotropic media, the coupling constants are zero, resulting in a much simplified system, but still allowing for a significant degree of tuning of the electromagnetic fields. Additionally, a result of the great interest in developing metamaterials is a significant increase in the ease and precision with which one can manufacture such complex media. For example, many media displaying dyadic constitutive parameters may now be easily manufactured or printed with a 3D printer. Within the more general realm of complex media, we can describe materials based on symmetries within their constitutive dyads. Specifically, we restrict our attention to two of these sub-categories:

$$\text{gyrotropic} \quad \rightarrow \quad \overset{\leftrightarrow}{\sigma} = \begin{bmatrix} \sigma_t & -j\sigma_g & 0 \\ j\sigma_g & \sigma_t & 0 \\ 0 & 0 & \sigma_z \end{bmatrix} \quad (1.3)$$

$$\text{uniaxial} \quad \rightarrow \quad \overset{\leftrightarrow}{\sigma} = \begin{bmatrix} \sigma_t & 0 & 0 \\ 0 & \sigma_t & 0 \\ 0 & 0 & \sigma_z \end{bmatrix} \quad (1.4)$$

Natural examples of uniaxial crystals are sapphire, calcite and ruby. These crystals are known to possess unusual characteristics in the optical regime, such as birefringence [48]. Gyrotropic media are less abundant in nature, but include some dielectric and magnetic materials, such as plasmas and ferrites [30, 112]. Clearly, the form of the constitutive parameter dyads are tied to the physical structure and of the material (crystal structure) and the molecular content of that structure. Now that we have a broad understanding of complex media, let us examine the most prolific application of such media: metamaterials.

---

[1]There is some debate [60, 75] on the so-called Post constraint, which limits the equations to 35 total parameters.

This work does not presume to undertake a full review of the exponential growth of metamaterials over the last 40 years - many recent articles have undertaken such a task with far more completeness than is given here. In fact, a recent internet search has shown Veselago's initial article on metamaterials [92] to have been cited in more than 7,000 articles. However, it is productive to survey some of the highlights of the recent explosion of interest in the development of metamaterials. An exact definition of metamaterials is elusive, but one of the most encompassing definitions comes from Cui [30]: "a metamaterial is a macroscopic composite of periodic or non-periodic structure whose function is due to both the cellular architecture and the chemical composition." It is also well-understood that metamaterials are man-made materials which possess physical characteristics "outside of" or "above" naturally occurring materials, such as negative values for constitutive parameters in a certain frequency range.

In a seminal paper, written in 1968, Veselago [92] first postulated the idea of Double-Negative Materials (DNG) (materials with simultaneously negative values of permittivity and permeability) and the properties such materials would have, although he readily admitted knowing of no existing material with such constitutive parameters. From an analysis of Maxwell's equations, he quickly concluded that such Left-Handed Materials (LHM) would have a negative group velocity and a positive phase velocity, leading to several interesting physical phenomena. He primarily postulated that LHM would demonstrate several unusual characteristics: a reverse Doppler effect; a reverse Vavilov-Cerenkov radiation; a negative index of refraction; and a light "tension" (or attraction), rather than the usual light pressure. Furthermore, in an analysis relative to the motivation of our work, he noted that it is possible for gyrotropic materials to be Epsilon-Negative Materials (ENG), Mu-Negative Materials (MNG) or DNG, depending on the structure of $\overleftrightarrow{\varepsilon}$ and $\overleftrightarrow{\mu}$. A plasma in a magnetic field (gyrotropic in $\overleftrightarrow{\varepsilon}$) would be a good example of an ENG material, while there exist certain gyrotropic magnetic materials which could be classified

as MNG. Pure ferromagnetic metals (for example, nickel) and even some semi-conductors (Indium Antimonide, Chalcopyrite, etc.) could potentially be DNG. Again, it is worth noting that Veselago provided no experimental evidence - he was purely hypothesizing about the properties and, in some cases, the existence of such materials.

Although Veselago's paper is frequently credited with being the foundation of the metamaterial revolution, he was not the first to observe the negative group velocity phenomenon. In fact, Mandel'shtam [64] reported negative group velocity in some crystal structures. However, Veselago was the first to highlight potential properties of such materials. His paper was largely unregarded until Pendry began publishing a number of papers in the late 1990's [70, 71, 73, 74], observing shifts in material properties based on the physical structure of a given material. For example, in [71], he noted a depression of the plasma frequency into the GHz band by including periodic structures of *thin wires*, a phenomenon which could produce some of the novel effects of an ENG material postulated by Veselago. Pendry then began to recognize the ability to tune the constitutive parameters, including permeability, to "values not accessible in naturally occuring materials" [70] by a periodic structure of magnetic metallic cylinders or Split Ring Resonators (SRR). Effectively, Pendry made the connection between the work of Mandel'shtam and Veselago, noting that periodic structures could be utilized in producing ENG, MNG or DNG materials. It is worthwhile to mention that he often compares this new idea to that of composites, crystals and semi-conductors, thus solidifying the link between his experiments and the analysis some 30 years before. Therefore, Pendry can be thought in many ways as the father of the metamaterials revolution in the midst of which we now find ourselves.

The potential applications of Pendry's metamaterials piqued the interest of research organizations around the world. In the decade or so since Pendry's papers, thousands of papers have been published touting advances in a wide range of research areas and

practical applications. However, in this review, we will focus on the areas with the most relevant military utility: antennas and controlled electromagnetic scattering. A number of high-profile applications are detailed by Shamonina in [84]: perfect lenses; slow wave structures; super-directivity; super-resolution; sub-wavelength focusing and imaging; photonic band-gap materials; and nanoparticles. Pendry [74] detailed how a negative-index slab could be used as a perfect lens, demonstrating separate configurations for both optical and microwave applications. Shelby, et al. [85] presented the first apparent experimental verification of negative refraction in the microwave frequency band, using a 2D array of unit cells consisting of copper strips and SRR's. A gradient index material, which would be useful for lensing and filtering, was designed and tested with good results. Ziolkowski [112] presents a good review of how metamaterials are now being investigated for improvements in electrically small antennas, highly directive antennas using (near) zero-index materials and sub-wavelength antennas. Of course, since the electromagnetic fields can be controlled "at will" [72], cloaking has become an area of high interest. Waveguide miniaturization using a uniaxial MNG material was shown in [50]. Therefore, we see a plethora of applications are envisioned for metamaterials. For a great many more applications, [37, 39] are fantastic references.

So far, we have concerned ourselves with volumetric metamaterials, in which repeating unit cells are arranged such that negative permeability, negative permittivity, or both are obtained over a certain bandwidth. However, it is important to note that applications of these structures focus on utilizing the resonant mode(s), which invites high loss and a relatively narrow bandwidth. In the Transmission Line (TL) theory of metamaterials, an electrical system of series capacitances and shunt inductances are shown to produce a LHM [16], with broader bandwidth characteristics and lower loss. In this comprehensive work, Caloz demonstrates a number of guided wave and radiating structures. For our work, the composition and production of the metamaterial is tailored to be uniaxial via

a tetragonal lattice design. This will allow for the development of a generalized parallel-plate Green's function and, eventually, NDE of a uniaxial material.

1.4 Material Characterization Background and Methods

Before we begin, let's provide a bit of motivation for accurately determining the constitutive parameters of a material. In essence, the complex permittivity and permeability are required for current Computational Electromagnetics (CEM) codes to accurately and precisely predict scattering characteristics. CEM codes are used in many research and development laboratories to investigate and design stealthy materials, novel antennas and many other applications. However, without an efficient, accessible, reproducible, and non-destructive method of determining the constitutive parameters of an actual material, the results of CEM codes cannot be transitioned into real-world applications. In other words, when producing a material, how do you know you made what you wanted to make? This question becomes even more poignant when referring to complex media. As was discussed in 1.3, production and manufacturing negative- and double negative-index materials, LHM and all other manner of postulated materials is now becoming a reality. The goal of this work is to contribute to the efficient and accurate characterization of such materials, so that development and application of these materials may confidently proceed.

Many methods exist for the electromagnetic characterization of materials in the microwave regime. The effectiveness of any given method is contingent upon many factors: material type, analytical model (including the underlying assumptions), laboratory setup (including frequency range and measurement configuration) and numerical solution techniques (including computational efficiency, convergence and error minimization). This section presents a review of prominent examples of research in each of these areas.

1.4.1 Isotropic Materials - Background and Review of Previous Work.

Much work has been accomplished in characterizing the constitutive parameters of isotropic materials. Since this research builds on that foundation, it is appropriate to review some of the milestones in this area before proceeding to complex media. First note, as with any well-posed mathematical problem, the number of measurements must correspond to the number of unknowns.[2] Therefore, for isotropic materials, in order to simultaneously determine complex permittivity and permeability, two independent measurements are required. Thus, for uniaxial anisotropic media, four independent measurements are required.

A number of varying measurement configurations have been utilized in the NDE characterization of isotropic materials, each possessing different strengths and shortcomings [22]. These configurations include: free-space, single probe and dual probe. Clearly, the frequency range of interest also affects the selected method, therefore, we note that the goal of this research is NDE of anisotropic uniaxial materials in the X-band (8-12GHz). One could utilize a mixing formula, as in [113], but these are tied heavily to similarities in the constituent materials and rely heavily on estimation. Therefore, we seek a more accurate, rigorous and extensible method.

1.4.1.1 Free Space Methods.

Free space methods utilize a monostatic or bi-static configuration, with horn antennas situated on either side of the MUT. They do not require physical contact with the MUT and allow characterization at either vertical or horizontal polarization (in both the transmit and receive plane). Additionally, reflection coefficients may be easily obtained at a variety of incident angles and over a wider bandwidth than waveguide methods. However, as is

---

[2]This is only true since we wish to avoid optimization techniques for under-determined systems, which may significantly complicate the issue.

noted by Stewart [86], error is introduced in many ways. One source of error is due to edge diffraction and variation of the wavefront at the sample, which will violate the plane wave incidence assumption. Additionally, the assumption of infinite transverse dimensions may prove invalid, depending on the illumination pattern of the antennas and the distance of the sample from the source. Finally, these systems require precision positioning of the sample, large focusing lenses and, due to the far-field requirement, take up more space than waveguide probe systems. All of these factors can lead to a tedious measurement process. Such a monostatic system was demonstrated in [2], where two variations on the two-thickness technique were used to provide two independent measurements, reporting an error of up 10%.

A bistatic system is employed by Ghodgaonkar [43], in which a MUT is placed in between two horn antennas. The reflection and transmission coefficients are measured after calibration by the well-known TRL calibration method. This configuration allows for reduction in the error due to edge diffraction effects by using spot-focusing lenses. However, the lenses are 30cm in diameter, demonstrating the large size of such a measurement apparatus.

1.4.1.2   Single Probe Methods.

In general, NDE methods can be sub-classified as reflection-only methods and transmission/reflection methods. Either one permits simultaneous measurement of the constitutive parameters, given the appropriate configuration and the correct number of independent measurements. In reflection-only methods, samples are backed either by free-space or a conductor (PEC) and the reflection coefficient measured. In order to obtain simultaneous extraction of ε and μ, a second independent measurement is required. One way to obtain the second measurement is the Short/Free-Space (S/FS) method [7,62,89]. In this method, one measurement is made with a PEC backing applied to the MUT and the second measurement

11

is made with a free-space backing. As is noted by Hyde [52], it is shown to produce very accurate results, because the two methods are the complement of one another; that is, the PEC-backed sample is interrogated by a strong magnetic field and the free-space backed sample is interrogated by a strong electric field. Both a Two Thickness Method (TTM) and a Frequency Varying (FV) technique are demonstrated in [65]. In the TTM, the first measurement is made with an open-ended waveguide and a PEC-backed MUT; the second measurement is made with a sample of the MUT of a different thickness. However, Moade uses an approximate form of the input admittance and, for the FV technique, some *a priori* knowledge of the frequency behavior of the constitutive parameters is necessary for the most accurate results. We seek to avoid errors introduced by approximate formulations, especially when the availability of rigorous solutions and sufficient computational resources makes such approximations unnecessary. Additionally, *a priori* knowledge of the frequency response of the material is not always available. It is found from uncertainty analysis that great errors can stem from variations in the thicknesses of the samples, or the relative difference in the thicknesses of the two samples [19] when using the TTM. In the search for a second independent measurement, Dester, et al., [33] propose an alternative to TTM, the Two Layer Method (TLM). This method utilizes the standard open-ended waveguide method as the first measurement, then places a material whose constitutive parameters are known on top of the MUT. The two-layer parallel plate Green's function is then used as the second set of equations from which complex permittivity and permeability may be extracted. Unfortunately, it is found that the errors associated with this method are higher than the TTM and TLM should be used only in circumstances when two samples of the MUT are not available (such as *in situ* measurements). Even so, the known material should be as low-loss as possible, to permit as much of the interrogating electric field as possible to penetrate to the MUT. Hyde presents a new TLM in [52], in which the second measurement is made placing the known material *behind* the MUT. This allows for a stronger

12

interrogation field and results in more accurate extraction of the constitutive parameters. Although not ideally suited to *in situ* measurements, this method proves useful when thin materials may bow and produce an air gap, which would skew the results. Finally, Dester presents a two-iris method [35], in which a second independent measurement is obtained by presenting a reduced aperture to the material. His results seem comparable to the new TLM offered by Hyde [52] and seem of more practical use for *in situ* measurements.

Most of the traditional literature focuses on single probe characterization, both of open-ended coaxial probes and open-ended rectangular waveguides. Coaxial probes offer a wide bandwidth and good accuracy and are used extensively as canonical treatments throughout textbooks and literature [22, 41, 110, 113]. A relatively early review [88] article details several coaxial configurations and points out some of the errors related to each method. Perhaps the largest source of error is related to air gaps between the center conductor and the sample. Scott [82] suggests several ways of mitigating this issue, the most practical of which is a spring-loaded center conductor. However, this adds complexity to an already delicate and precision measurement procedure. Additionally, it is found [79] that accuracy of the measurement depends on the frequency at which the measurement is taken. Pournarpoulos demonstrates the wide bandwidth nature of the coaxial probe method in [76], demonstrating NDE characterization of several materials up to 40GHz.

Rectangular waveguide probes are more restrictive in bandwidth, but provide a very good accuracy, along with a more rugged form factor, as well as a better matching with free space impedance [22]. Additionally, rectangular waveguides benefit from a deeper penetration of the radiating fields into the material and the linear polarization of the waves in the waveguide, which allows for measurement of anisotropic materials. A number of configurations have been investigated for NDE using a single-probe rectangular waveguide configuration. Zoughi [113] presents a fine example of using an open-ended rectangular waveguide for surface crack detection. A great number of publications report success

in utilizing variations on the open-ended flanged rectangular waveguide configuration to extract complex permittivity and permeability, most notably [15, 18, 32, 33, 65, 87, 90]. Similar configurations have been used in the successful measurement of a stratified, continuously varying profile dielectric, representing inhomogeneous media [68, 80]. One drawback of the flanged waveguide measurement technique is the requirement to suppress unwanted reflections from the edge of the flanges. In order to do so, the lossiness of the material must be balanced by the size of the flanges in order to prevent two-way reflections from affecting the desired measurements. Thus, a lower loss material requires unreasonably sized flanges. However, Hyde [54] presents a time-gating technique which allows for the relaxation of such requirements. The reflection data is analyzed in the time domain, where the edge reflections are clearly seen, and these reflections are essentially gated from the data. Then, a Fourier transform allows for the extraction of the constitutive parameters in the frequency-domain. In this dominant mode-only analysis, error is shown to increase with frequency, but inclusion of higher order modes in the calculation is expected to improve correlation with established values. This technique allows for the use of very small flanges, even in low-loss materials. Although single probe methods are desirable, due to their simplicity in configuration, much work in the rectangular waveguide area in the last few years has transitioned to focus on dual-probe methods.

1.4.1.3 *Dual Probe Methods.*

In dual probe methods, or transmission/reflection methods, we need not search for additional measurement techniques, as a sufficient number of independent measurements is inherent (for isotropic media). Using such a method, one is able to efficiently perform measurements simultaneously and extract the complex constitutive parameters. This method is also useful for *in situ* measurement of materials or when a second sample of identical material with a differing thickness is not available. In a novel application of the dual probe method, Stewart presents a rigorous development [87] of the MFIE's for

14

Dual Wavguide Probe (DWP) NDE of a conductor-backed sample. Using the S_{11} and S_{21} measurements, Stewart successfully extracts both complex constitutive parameters for several dielectric-magnetic materials and compares them with the single probe TTM and traditional destructive rectangular waveguide measurements. These measurements were based on a dominant-mode only reflection assumption, leading to errors of less than 10%. Further consideration of a full-wave modal solution would undoubtedly improve the accuracy of this method. This method is promising in many areas, as it allows for a single set of measurements, as opposed to the TTM, which requires multiple sets of measurements. Additionally, Stewart's dual-probe method is rugged, allowing for the possibility of use in the field, and rigorous in EM theoretical development.

A number of papers have been written considering dual-probe flanged waveguide methods [51–56, 83], successfully demonstrating simple, precise and accurate measurements. The method is shown to be relatively insensitive to small misalignment of the waveguides in the transverse dimensions [51, 56] and immune to some of the sources of error inherent in the traditional (destructive) waveguide method, where precise machining and positioning are required to eliminate edge reflections and air gaps. In the case of tFWMT, the material is only required to be lossy enough (or the flanges large enough) to prevent reflections from the flange edges from being detected at the probes. However, even in the case when such large flanges are not available or desirable, time-gating signal processing may be used to filter out the edge reflections and still produce remarkably accurate results [55]. The time-gating technique is then used to reduce the dimensions of the flanges, resulting in a more compact measurement apparatus. Finally, prompted by the comparison of PEC-backed and FS-backed DWP configurations, Seal utilizes a combination of the tFWMT measurement and the new TLM [52] in an attempt to improve the accuracy of the extracted parameters. He finds, though, that a combination of the PEC-backed and FS-backed methods still gives the most accurate results. In the isotropic case, this amounts to solving an overdetermined

15

system (8 equations with 2 unknowns). The discovery that the combination PEC/FS-backed method is best arises from the fact that the PEC-backed method provides a large interrogating magnetic field to the MUT, while the FS-backed method provides a large electric field to the MUT, thereby allowing good fidelity in extracting both ε_r and μ_r. In fact, it is always difficult to extract precise permittivity values from a PEC-backed sample [56], even more so when the MUT is electrically thin.

1.4.2 *Analytical Models.*

Now that we have discussed the physical measurement apparatus, we review several potential analytical models. Clearly, the accuracy of the NDE method is tied to the accuracy of the analytical model. In general, the analytical models fall into two categories - asymptotic methods and full-wave methods.

1.4.2.1 *Asymptotic Methods.*

The most common high frequency methods are Geometrical Theory of Diffraction (GTD), Uniform Theory of Diffraction (UTD) and Physical Theory of Diffraction (PTD) [66]. These techniques have been applied to parallel plate geometries as a special case of the canonical wedge [31, 61]. One of the fundamental restrictions on any of these methods is that the size of the scatterer must be large in terms of the incident wavelength [66]. However, we note that, at the middle of the X-band, the wavelength is approximately 2cm. Therefore, this requirement is invalid for many of our samples, which are considerably thinner and the largest dimension of the X-band waveguide is $\approx$ 2.2cm.

1.4.2.2 *Full Wave Methods.*

Full wave methods can be further sub-classified as approximate or rigorous. Approximate methods make use of the principle of least action [8, 28, 42, 65, 113], thereby avoiding the differential equations of a rigorous solution. Authors in the previously cited literature

employ approximations of the admittance at the aperture, allowing for extraction of the constitutive parameters. However, as has been mentioned before, we wish to avoid the errors introduced by approximations, especially given the ready availability of powerful computational resources.

Rigorous full-wave solutions start with Maxwell's equations and incorporate all scattering phenomena associated with the MUT. Balanis provides a solid foundation for such rigorous solutions in his eminent book [9]. Since the entirety of radiation phenomena are accounted for through Maxwell's equations and the application of appropriate boundary conditions, no special treatment of edge diffraction, creeping waves, surface waves or material properties is required. The rigorous method of Stewart in [86, 87] begins with Maxwell's equations to formulate an integral equation solution in the form of a Green's function kernel, utilizes appropriate boundary conditions in conjunction with Love's equivalence principle and applies a field expansion of the reflected modes through use of the MoM. This results in the rigorous formulation of a set of MFIE's, which may then be subjected to a root search, such as the Newton-Raphson method, to extract the desired constitutive parameters. Accuracy is clearly tied to the number of modes that are used in the expansion of the MoM solution.

Typically, as in [86], the first 20 modes are used in the expansion of the MoM solution. Although including more modes in the MoM solution results in a greater accuracy, the computational cost rises quadratically with the number of modes. However, Dester [34] recognizes that the assumption of convergence within the first 20 modes may not provide the most accurate or efficient means of achieving true convergence (as is assumed by many authors [15]). Consequently, he proposes a hybrid method which uses the first twenty modes and an extrapolation technique to obtain results that are nearly identical to those obtained when using the first 160 modes.

This work will utilize such advances in rigorous full-wave methods in order to maximize accuracy, while simultaneously seeking the highest possible computational efficiency. In light of those goals, we can reduce the computational burden by finding closed-form integrals where possible, through careful application of complex plane analysis (including Cauchy's Integral Theorem, Principle Value Theorem and Jordan's Lemma) [4].

1.4.3 Numerical Solution Techniques.

In spite of our aforementioned desire to minimize the computational burden, the solution to the MFIE's cannot be found in a completely closed form, so we must utilize a numerical method to extract the desired parameters. Numerical techniques are used at two critical junctions in the NDE process: solution of analytical model (forward problem) and error minimization when extracting the constitutive parameters from the experimental data and the theoretical model (inverse problem).

In the course of solving the spectral-domain MFIE's of the forward problem, the MoM is the chosen method [24, 25, 45, 67]. By carefully choosing the basis and testing functions, the forward problem can be significantly simplified. In the case of a rectangular waveguide, choosing the (infinite number of) waveguide modes serves exactly this purpose, as will be shown in Chapter 4. The primary concern in utilizing a MoM solution is the number of modes to use in the expansion. Since the basis and testing functions consist of the infinite number of modes in the waveguide, a truncation is necessary, as was mentioned in the previous section. The computation time grows proportional to N^2 (where N is the number of modes included in the solution), therefore, we must balance our desire for accuracy with available computational resources.

Since measurements are performed at discrete frequencies throughout the band of interest (for X-band, 8.2GHz-12.4GHz), we may extract the constitutive parameters on a point-by-point basis when solving the reverse problem. The Newton-Raphson method is well-

18

suited to this type of analysis [56, 86]. Both the 1-D and 2-D algorithms are fairly simple to implement in computational form. However, a variety of methods of non-linear least squares analysis (detailed in [63]) have been implemented in many works [6, 51, 52, 90]. Using a non-linear least squares method to extract the parameters allows for a better characterization of the uncertainties and frequency dependence of the extracted parameters. Methods such as the Gauss-Newton, Levenberg-Marquardt or Trust Region Reflective (TRR) method can be implemented fairly easily in MATLAB® [63, 69].

1.5 Anisotropic Materials

Although NDE of anisotropic media is not a new problem, far less research has been dedicated to the study of such complex media than to isotropic media. Recent interest in the characterization of complex media has been sparked by concurrent improvements in the manufacturing of such media, along with a slew of research theorizing a wide range of applications for such materials [14, 36, 50]. Uniaxial media is the simplest type of anisotropic media, which is also fairly easily manufactured [26]. In addition to the added complexity of the Green's function due the dyadic form of the constitutive parameters, anisotropic materials require a larger number of independent measurements. For the dielectric-magnetic uniaxial case, we now require four independent measurements, or reflection and transmission measurements for two separate configurations.

Resonator methods have been used in the accurate extraction of complex constitutive parameters from both isotropic and anisotropic uniaxial materials [59]. While this method provides a high accuracy, it is a destructive method, in which the sample is required to be placed inside a modestly sized resonator cavity.

Belhadj-Tahar successfully measured the complex permittivity of uniaxial alumina and sapphire in the context of a coaxial line probe [12]. However, he also uses a destructive technique which requires precise placement of the sample within the coaxial line and an

exacting preparation of the sample. Additionally, his technique runs into difficulty with the low-loss nature of the samples.

In a more relevant work, Chang [17] uses an open-ended rectangular waveguide method to measure the permittivity of a dielectric-fiber composite material, noting that ε_z is unstable in his experiments, due to a high conductance of the material and a thin sample. In order to obtain the required number of independent measurements, he measures the material at a 30, 60 and 90 degree angle with respect to the longitudinal axis. This rotation of the material may prove more difficult to recreate precise measurements, especially when considering a non-laboratory environment.

In order to build on the preponderance of recent research and take advantage of the precision and accuracy of the method, this work will focus on extending the tFWMT to include uniaxial media.

1.6 Green's Functions

In most cases, it is useful to frame the solution to Maxwell's equations in terms of a Green's function kernel. Directly solving Maxwell's equations is a lengthy process, one which is usually avoided, but is ambitiously employed in [46]. Traditionally, vector potentials have been used to aid in these solutions [9, 24, 27, 44]. More recently, scalar potential techniques have been developed for a number of different classes of anisotropic materials (gyrotropic,chiral and uniaxial) [47, 77, 78, 94–100, 103–105, 107–109]. The use of scalar potentials not only dramatically simplifies the analysis, but provide a unique and particularly elegant physical insight, as most methods utilize a decomposition into transverse and longitudinal terms.

In any case, obtaining the Green's function kernel is no trivial matter. Even though Weiglhofer and his colleagues are most certainly to be applauded for their pioneering

work in the area of theoretical electromagnetics, we have been unable to demonstrate that certain consistency in which the potentials for the more general cases (e.g., gyrotropic bianistotropic) clearly reduce to the simpler cases (uniaxial anisotropic or isotropic). The potential methods used in [47] for a dielectric uniaxial media clearly demonstrate this property, therefore, this work utilizes similar methods to extend the Green's function derived in [47] to the more general case of dielectric and magnetic uniaxial media immersed in a parallel plate environment.

1.6.1 Direct Field Approach.

In general, direct solutions to Maxwell's equations are tedious and involve considerably more work than the potential-based approaches. This is primarily due to the inversion of a 6x6 matrix that is required to find the electric and magnetic fields. Additionally, unless a vectorized form of the 6x6 matrix can be found, the entire process must be repeated term-by-term, resulting in tedious, repetitive mathematical manipulations. To demonstrate this, consider Maxwell's equations for homogeneous, bianisotropic gyrotropic media.

$$
\left(\nabla \times \overleftrightarrow{I} + j\omega \overleftrightarrow{\zeta} \right) \cdot \vec{E} = -\vec{J}_h - j\omega \overleftrightarrow{\mu} \cdot \vec{H}
$$

$$
\left(\nabla \times \overleftrightarrow{I} - j\omega \overleftrightarrow{\xi} \right) \cdot \vec{H} = \vec{J}_e + j\omega \overleftrightarrow{\varepsilon} \cdot \vec{E}
\tag{1.5}
$$

where the constituent parameters are dyads of the generalized gyrotropic form:

$$
\overleftrightarrow{\sigma} = \begin{bmatrix} \sigma_{xx} & -j\sigma_{xy} & 0 \\ j\sigma_{yx} & \sigma_{yy} & 0 \\ 0 & 0 & \sigma_{zz} \end{bmatrix} \qquad \sigma = \varepsilon, \mu, \zeta, \xi
\tag{1.6}
$$

21

It can be shown (and will be shown, for anisotropic uniaxial media, in Chapter 2) that the magnetic field, using the direct-field method can be expressed as (with $\overset{\leftrightarrow}{\vec{k}} = \omega^2 \overset{\leftrightarrow}{\varepsilon} \cdot \overset{\leftrightarrow}{\mu}$):

$$\left[\overset{\leftrightarrow}{\varepsilon} \cdot \left(\nabla \times \overset{\leftrightarrow}{I} + j\omega \overset{\leftrightarrow}{\zeta} \right) \cdot \overset{\leftrightarrow}{\varepsilon}^{-1} \cdot \left(\nabla \times \overset{\leftrightarrow}{I} - j\omega \overset{\leftrightarrow}{\xi} \right) - \overset{\leftrightarrow}{k}^2 \right] \cdot \vec{H}$$

$$= -j\omega \overset{\leftrightarrow}{\varepsilon} \cdot \vec{J}_h + \overset{\leftrightarrow}{\varepsilon} \cdot \left(\nabla \times \overset{\leftrightarrow}{I} + j\omega \overset{\leftrightarrow}{\zeta} \right) \cdot \overset{\leftrightarrow}{\varepsilon}^{-1} \cdot \vec{J}_e$$

(1.7)

or:

$$\vec{H} = \overset{\leftrightarrow}{\mathsf{w}}_h^{-1} \cdot \vec{s}_1 \tag{1.8}$$

where $\overset{\leftrightarrow}{\mathsf{w}}_h$ is the eigenvector matrix and $\vec{s}_1$ is the source term. The specific forms of these terms will be discussed in detail in later sections. From (1.7) and (1.8), we can see that, when the constitutive parameter dyads are of full rank, $\overset{\leftrightarrow}{\mathsf{w}}_h$ is a 3x3 matrix of full rank, the inversion of which is a very lengthy process. We will demonstrate the extent of the difficulties involved in this process in Chapter 3, where the direct field method is used to find the total parallel-plate Green's function for anisotropic uniaxial media.

1.6.2 Potential-based approach.

Effectively, potential-based method can be used to reduce, to varying degrees, the size of the matrix operating on the fields when solving Maxwell's equations. Weiglhofer [103] demonstrated that the most general material that may represented by the potential-based methods is the gyrotropic material. Therefore, in order to illustrate the concept of how simplification occurs, we consider the same gyrotropic material as from the previous subsection (a more complete development is found in Chapter 2). Using a partial decomposition of the fields into transverse and longitudinal portions, we are able to determine the transverse ($\vec{E}_t$ and $\vec{H}_t$) and $z-$directed ($\vec{E}_z = \hat{\mathbf{z}} E_z$ and $\vec{H}_z = \hat{\mathbf{z}} H_z$) fields in terms of the scalar potentials ψ and θ (Φ and Π are, themselves, potentials and related to ψ

22

and θ, respectively):

$$\vec{E_t} = \nabla_t \Phi - \hat{\mathbf{z}} \times \nabla_t \theta \qquad \vec{H_t} = \nabla_t \Pi - \hat{\mathbf{z}} \times \nabla_t \psi$$

$$E_z = -\frac{1}{j\omega\varepsilon_z} \left(\nabla_t^2 \psi + J_{ez} \right) \qquad H_z = \frac{1}{j\omega\mu_z} \left(\nabla_t^2 \theta - J_{mz} \right)$$

The scalar potentials are then solutions of the system of equations:

$$L_1 \psi + L_2 \theta = s_1 \qquad L_3 \psi + L_4 \theta = s_2$$

where the L_n operators are scalar differential operators and s_1 and s_2 are source terms. Again, the specific forms of these terms will be given in later sections. Therefore, we can use a Fourier transform technique and fundamental algebra to invert the 2x2 **L** matrix. The field recovery is then a matter of simple differentiation. These two steps represent a considerably more straightforward solution method than the inversion of the $\overleftrightarrow{\mathbf{w}}_e$ and $\overleftrightarrow{\mathbf{w}}_h$ matrices in the direct-field solutions. However, in order to confirm our results and illustrate the advantages of the potential-based method, we will derive the total parallel-plate Green's function using both the potential-based method in Chapter 2 and the direct-field method in Chapter 3.

1.7 Scope

Although Veselago and many others have emphasized gyrotropic materials as a means to realizing metamaterials, we note that uniaxial materials are also given due consideration in a number of publications [13, 14, 16, 109]. Since uniaxial materials are seen to be a specialization of gyrotropic materials, in which the constitutive dyads are greatly simplified (and, by correlation, the solution to Maxwell's equations), this work focuses primarily on characterizing uniaxial materials. Therefore, we will focus primarily on uniaxial material throughout development of the parallel-plate Green's function, tFWMT theory and subsequent implementation. It is understood that this is merely a stepping stone to the greater goal of generalized gyrotropic material characterization. It will be shown using

our method of potential development, that the potentials for a gyrotropic material reduce quite easily to that for a uniaxial material and the potentials for the uniaxial case reduce quite easily to the isotropic case. This has not been clearly demonstrated in previous works. Therefore, we will be able to characterize a wide range of materials using a single extraction technique.

1.8   Research Goals and Contribution to Science

- Determine principal and total parallel-plate Green's function for anisotropic uniaxial media

  Through the rigorous analysis of EM propagation in an anisotropic uniaxial material, this research contributes significantly to the general understanding of EM propagation in metamaterials. The development of the magnetic, electric and magneto-electric spectral-domain principal and parallel-plate Green's functions in two different manners (using scalar potentials and direct field methods) provides an intuitive kernel through which propagation in anisotropic uniaxial media can be studied in great confidence. Physical insight will be gleaned throughout the theoretical development, demonstrating how the math and the physics are tied together in the solution.

- Formulate Magnetic Field Integral Equation (MFIE)'s for tFWMT measurement setup

- Measure complex permittivity for electrically uniaxial material using dominant mode approximation

  The theoretical and experimental model for the tFWMT using the dominant-mode only will be extended from isotropic materials to incorporate the anisotropic uniaxial case. This will provide additional utility to an already proven method. Experiments

will also be conducted to ensure the isotropic results correspond with previous results. The ability to characterize uniaxial and isotropic materials using a single measurement technique represents a significant step forward in the goal of a fast and efficient measurement of complex media in general.

1.9 Assumptions

This work makes a few basic assumptions in order to simplify the analysis. These assumptions are not unreasonable and are commonly used in previous works in similar areas.

- The $e^{j\omega t}$ time dependence is assumed and suppressed throughout

- The distinguished (longitudinal) axis is the z axis and the transverse axes are x and y

- Any conducting surface, such as the waveguide walls or parallel plates, are treated as Perfect Electrical Conductor (PEC).

- The transverse dimensions of the material sample and parallel plates are infinite

- Rectangular waveguides contain only free space with constitutive parameters ε_0 and μ_0

- MUT sample is linear, anisotropic, dielectric, magnetic; additionally, the sample is of uniform thickness and homogeneous

- The waveguide probes are perfectly aligned in all dimensions - this eliminates one potential complexity in the evaluation of spectral integrals

- The constitutive parameters $\varepsilon_t, \varepsilon_z, \mu_t$ and μ_z are all assumed to be the multiplication of a relative constitutive parameter and the free space constitutive parameter, such

that:

$$\sigma_\alpha = \sigma_{\alpha r}\sigma_0 \qquad \dots \begin{cases} \sigma = \varepsilon, \mu \\ \\ \alpha = t, z \end{cases}$$

1.10 Notation

Complex notation is required in the development of certain expressions. As such, it is worthwhile to explain certain basic principles that this document adheres to. In the case of Green's functions and Electric fields, it is necessary to specify both the source and the field maintained by that source. For example, the symbol

$$\widetilde{G}_{eh,xy}$$

refers to the x component of the electric field (e) which is **maintained** by a y-directed magnetic (h) source. This convention applies to the placement of elements within a matrix, such that the element in the first row and second column is the (x, y) component and represents the x-directed field maintained by a y-directed source.

Additionally, this document utilizes Fourier Transform methods and these transforms are performed with respect to the transverse (x, y) variables and the longitudinal variable (z) separately. As such, it is important to distinguish between the two transform domain. To this effect, we represent the spectral variables by λ terms. Additionally a single overset tilde represents a quantity that has been transformed with respect to the transverse variables and exists in the single transform (λ_ρ, z) domain (e.g., $\widetilde{G}$). Similarly, two overset tildes represent a quantity that has been transformed with respect to both the transverse and longitudinal variables and exists in the double transform domain $(\vec{\lambda}_\rho, lamz)$. Table 1.1 is given as a quick reference.

26

Table 1.1: The conventions used in this document for spatial and spectral quantities. The last column is an example of how quantities are represented and is applied to Green's function terms, field terms, etc.

Spatial Variable	Spectral Variable	Domain Representation	Quantities
x	λ_x		
		$\vec{\lambda}_\rho$	$\widetilde{G}$
y	λ_y		
z	λ_z	λ_z	$\widetilde{\widetilde{G}}$

1.11 Mission Impact

Due to their dispersive characteristics, the small dimensions of the elements of their unit cells and the difficulty of fabrication, designing metamaterials is a laborious and difficult process. Accordingly, uncertainty regarding the manufactured product results in less than optimal performance from the final system, whether it be a flat, highly-directive antenna, a sub-wavelength lens or a high-scattering surface. In a quickly-evolving world of today's technology, enemy detection systems are constantly improving in their low-observable detection. Therefore, our ability to accurately characterize the response of our systems must also improve. The ability to simultaneously accurately measure complex permittivity and permeability from complex media will enable material scientists to accurately tune the effective bandwidth and electromagnetic scattering properties of next-generation metamaterials with confidence. Rather than follow a costly and time-consuming trial and error process, a material can be designed to meet a certain engineering requirement, measured for accurate production and incorporated into a system faster than ever before.

1.12 Sponsorship

1.13 Overview and Organization

This chapter has provided the background and motivation for the NDE of anisotropic uniaxial materials. The general categories of complex media were set forth, along with a brief review of the genesis of metamaterials. Several methods of NDE were also reviewed, along with milestones in the general field of NDE. This included the requisite theoretical and analytical models, as well as numerical solution techniques. We also considered several significant contributions to the development of Green's functions for anisotropic materials and presented reasons for seeking a new development of these Green's functions. In light of the explosion of interest in developing new metamaterials and new applications for those metamaterials, we seek to fill the gap in our capability to accurately and precisely measure an increasing number of materials using a single measurement technique. The next two chapters (chapters 2 and 3) will focus on developing the required parallel-plate Green's functions for use in the tFWMT via two different methods. The use of the potential-based method and the direct-field method will add confidence to our development, since the two results are seen to be exactly the same. Chapter 4 will extend the tFWMT theory for uniaxial media, utilizing the newly developed Green's function. Chapter 5 will present results for measured materials. Finally, chapter 6 will present the conclusions of this work and suggest topics for future consideration.

II. Potential Formulation and Total Parallel-Plate Green's Function for Anisotropic Uniaxial Media

Before we extend the theory of the tFWMT [51] to include anisotropic uniaxial media, we need to develop the total parallel plate Green's function. Although the principal Green's function is not a novel problem, as it has been previously explored by authors (e.g., [46,102,104,106] among others). However, the principal problem has not been treated in any higher level of detail. Additionally, the development of the scattered solution and total Green's function for a dielectric and magnetic uniaxial media contained in a parallel plate geometry has, to the knowledge of the author, never been presented in the literature. Therefore the threefold contribution of this chapter is to use a scalar potential method to develop the principal Green's function for dielectric-magnetic uniaxial anisotropic media, find the scattered Green's function in a parallel plate geometry and find the total Green's function subject to the PPWG boundary conditions. In [47], Havrilla uses a potential formulation to find the Green's function for a magnetic current contained in a waveguide filled with an electrically uniaxial ($\overset{\leftrightarrow}{\varepsilon} = \mathbf{\hat{x}\hat{x}}\varepsilon_t + \mathbf{\hat{y}\hat{y}}\varepsilon_t + \mathbf{\hat{z}\hat{z}}\varepsilon_z$), magnetically isotropic material ($\overset{\leftrightarrow}{\mu} = \mathbf{\hat{x}\hat{x}}\mu_0 + \mathbf{\hat{y}\hat{y}}\mu_0 + \mathbf{\hat{z}\hat{z}}\mu_0$). This chapter will follow his methodology, but, for the sake of completeness, we will develop this Green's function assuming the media is both uniaxial in the dielectric and magnetic sense, and contains both electric and magnetic sources. As was previously mentioned, discrepancies were found in some of the previous literature when comparing the varying results for the principal Green's function. This is the primary motivation for starting with the principal Green's function. Furthermore, in the next chapter, we will repeat the derivation using the direct field solution method, which will show the two methods produce the exact same result. Therefore, using the two different methods will provide us with the necessary confidence in moving forward.

2.1 Potential-Based Formulation

Maxwell's equations for a linear, inhomogeneous (in *z*), electrically and magnetically anisotropic uniaxial medium, generalized with an electric and magnetic source are

$$\nabla \times \vec{E}(\vec{\rho}, z) = -\vec{J}_h(\vec{\rho}, z) - j\omega \overset{\leftrightarrow}{\mu}(z) \cdot \vec{H}(\vec{\rho}, z) \tag{2.1}$$

$$\nabla \times \vec{H}(\vec{\rho}, z) = \vec{J}_e(\vec{\rho}, z) + j\omega \overset{\leftrightarrow}{\varepsilon}(z) \cdot \vec{E}(\vec{\rho}, z) \tag{2.2}$$

where:

$$\overset{\leftrightarrow}{\varepsilon} = \varepsilon_t \overset{\leftrightarrow}{I}_t + \hat{\mathbf{z}} \varepsilon_z \hat{\mathbf{z}}$$

$$\overset{\leftrightarrow}{\mu} = \mu_t \overset{\leftrightarrow}{I}_t + \hat{\mathbf{z}} \mu_z \hat{\mathbf{z}}$$

$$\overset{\leftrightarrow}{I}_t = \hat{\mathbf{x}}\hat{\mathbf{x}} + \hat{\mathbf{y}}\hat{\mathbf{y}}$$

In matrix form, the constitutive dyads are given by

$$\overset{\leftrightarrow}{\varepsilon} = \begin{bmatrix} \varepsilon_t & 0 & 0 \\ 0 & \varepsilon_t & 0 \\ 0 & 0 & \varepsilon_z \end{bmatrix} \qquad \overset{\leftrightarrow}{\mu} = \begin{bmatrix} \mu_t & 0 & 0 \\ 0 & \mu_t & 0 \\ 0 & 0 & \mu_z \end{bmatrix} \tag{2.3}$$

Given the nature of a uniaxial material and our definitions of the constitutive dyads, we call the longitudinal ($\hat{\mathbf{z}}$) axis the distinguished (or principal) axis. Therefore, it is reasonable to decompose (2.1) and (2.2) into longitudinal and transverse parts by defining a transverse differential operator $\nabla_t = \hat{\mathbf{x}}\frac{\partial}{\partial x} + \hat{\mathbf{y}}\frac{\partial}{\partial y}$ and writing

$$\left(\nabla_t + \hat{\mathbf{z}}\frac{\partial}{\partial z}\right) \times \left(\vec{E}_t + \hat{\mathbf{z}}E_z\right) = -\vec{J}_{ht} - \hat{\mathbf{z}}J_{hz} - j\omega\mu_t\vec{H}_t - \hat{\mathbf{z}}j\omega\mu_z H_z$$

$$\implies \nabla_t \times \vec{E}_t + \overbrace{\nabla_t \times \hat{\mathbf{z}}E_z}^{-\hat{\mathbf{z}} \times \nabla_t E_z} + \frac{\partial}{\partial z}\hat{\mathbf{z}} \times \vec{E}_t = -\vec{J}_{ht} - \hat{\mathbf{z}}J_{hz} - j\omega\mu_t\vec{H}_t - \hat{\mathbf{z}}j\omega\mu_z H_z \tag{2.4}$$

30

and

$$\left(\nabla_t + \hat{\mathbf{z}}\frac{\partial}{\partial z}\right) \times \left(\vec{H}_t + \hat{\mathbf{z}}H_z\right) = \vec{J}_{et} + \hat{\mathbf{z}}J_{ez} + j\omega\varepsilon_t\vec{E}_t + \hat{\mathbf{z}}j\omega\varepsilon_zE_z$$

$$\implies \nabla_t \times \vec{H}_t + \overbrace{\nabla_t \times \hat{\mathbf{z}}H_z}^{-\hat{\mathbf{z}}\times\nabla_tH_z} + \frac{\partial}{\partial z}\hat{\mathbf{z}} \times \vec{H}_t = \vec{J}_{et} + \hat{\mathbf{z}}J_{ez} + j\omega\varepsilon_t\vec{E}_t + \hat{\mathbf{z}}j\omega\varepsilon_zE_z \qquad (2.5)$$

By examining the forms of (2.4) and (2.5), we see that they include both transverse and longitudinal terms, which are, by definition, orthogonal and thus linearly independent. Therefore, we can equate the transverse and longitudinal components of (2.4) to find

$$-\hat{\mathbf{z}} \times \nabla_tE_z + \frac{\partial}{\partial z}\hat{\mathbf{z}} \times \vec{E}_t = -\vec{J}_{ht} - j\omega\mu_t\vec{H}_t \qquad (2.6)$$

$$\nabla_t \times \vec{E}_t = -\hat{\mathbf{z}}J_{hz} - \hat{\mathbf{z}}j\omega\mu_zH_z \qquad (2.7)$$

and, similarly, for (2.5)

$$-\hat{\mathbf{z}} \times \nabla_tH_z + \frac{\partial}{\partial z}\hat{\mathbf{z}} \times \vec{H}_t = \vec{J}_{et} + j\omega\varepsilon_t\vec{E}_t \qquad (2.8)$$

$$\nabla_t \times \vec{H}_t = \hat{\mathbf{z}}J_{ez} + \hat{\mathbf{z}}j\omega\varepsilon_zE_z \qquad (2.9)$$

According to the usual method, we seek to introduce potentials in keeping with Helmholtz's theorem, which states a vector field $\vec{V}$ can be uniquely specified by a superposition of a divergence-free and a curl-free contribution. In the general mathematical sense, taking w to be a scalar field and $\vec{V}$ to be a vector field, this means

$$\vec{V} = \nabla w + \nabla \times \vec{A} \implies \vec{V}_t = \nabla_tw + \nabla_t \times \hat{\mathbf{z}}A_z = \nabla_tw - \hat{\mathbf{z}} \times \nabla_tA_z \qquad (2.10)$$

This allows us to write the transverse parts of the fields and currents given by Faraday's Law and Ampere's Law in (2.6) and (2.8) as

$$\vec{E}_t = \nabla_t\Phi + \nabla_t \times \vec{\theta} = \nabla_t\Phi + \nabla_t \times \hat{\mathbf{z}}\theta = \nabla_t\Phi - \hat{\mathbf{z}} \times \nabla_t\theta \qquad (2.11)$$

$$\vec{H}_t = \nabla_t\Pi + \nabla_t \times \vec{\psi} = \nabla_t\Pi + \nabla_t \times \hat{\mathbf{z}}\psi = \nabla_t\Pi - \hat{\mathbf{z}} \times \nabla_t\psi \qquad (2.12)$$

$$\vec{J}_{et} = \nabla_tu_e + \nabla_t \times \vec{v}_e = \nabla_tu_e + \nabla_t \times \hat{\mathbf{z}}v_e = \nabla_tu_e - \hat{\mathbf{z}} \times \nabla_tv_e \qquad (2.13)$$

$$\vec{J}_{ht} = \nabla_tu_h + \nabla_t \times \vec{v}_h = \nabla_tu_h + \nabla_t \times \hat{\mathbf{z}}v_h = \nabla_tu_h - \hat{\mathbf{z}} \times \nabla_tv_h \qquad (2.14)$$

31

In developing these equations, only $\hat{\mathbf{z}}$-directed scalar potentials are used, since an $\hat{\mathbf{x}}$- or $\hat{\mathbf{y}}$- directed vector potential would produce longitudinal (i.e., non-transverse) components after the transverse curl operates on it. Now, we seek expressions for the longitudinal field components in terms of the scalar potentials Φ, θ, Π, and ψ. They can be found by inserting (2.12) into (2.9) and inserting (2.11) into (2.7), and using the vector identities $\nabla_t \times \nabla_t w = 0$, $\nabla_t \cdot \hat{\mathbf{z}} w = 0$ and $\nabla_t \times \nabla_t \times \vec{A} = \nabla_t (\nabla_t \cdot \vec{A}) - \nabla_t^2 \vec{A}$ (where w is a generic scalar field and $\vec{A}$ is a generic vector field):

$$E_z = -\frac{1}{j\omega\varepsilon_z} \left(\nabla_t^2 \psi + J_{ez} \right) \tag{2.15}$$

$$H_z = \frac{1}{j\omega\mu_z} \left(\nabla_t^2 \theta - J_{hz} \right) \tag{2.16}$$

The complete representation for the fields (transverse and longitudinal components) in a uniaxial media are found in (2.11) - (2.16), in terms of the potentials Φ, θ, Π and ψ. The final step in the potential method is to find the governing equations for the potentials. Inserting (2.11), (2.12) and (2.14) into (2.6) and noting $\hat{\mathbf{z}} \times \hat{\mathbf{z}} \times \nabla_t \theta = -\nabla_t \theta$, we find

$$
\begin{aligned}
- \hat{\mathbf{z}} \times \nabla_t E_z &+ \frac{\partial}{\partial z} \hat{\mathbf{z}} \times \nabla_t \Phi + \frac{\partial}{\partial z} \nabla_t \theta \\
&= -\nabla_t u_h + \hat{\mathbf{z}} \times \nabla_t v_h - j\omega\mu_t \nabla_t \Pi + j\omega\mu_t \hat{\mathbf{z}} \times \nabla_t \psi
\end{aligned}
\tag{2.17}
$$

Examining the last two terms on the right hand side of (2.17), we find

$$\overleftrightarrow{\mu}_t \cdot \nabla_t \Pi = (\hat{\mathbf{x}}\mu_t\hat{\mathbf{x}} + \hat{\mathbf{y}}\mu_t\hat{\mathbf{y}}) \cdot \left(\hat{\mathbf{x}}\frac{\partial \Pi}{\partial x} + \hat{\mathbf{y}}\frac{\partial \Pi}{\partial y} \right) = \hat{\mathbf{x}}\left(\mu_t\frac{\partial \Pi}{\partial x} \right) + \hat{\mathbf{y}}\left(\mu_t\frac{\partial \Pi}{\partial y} \right)$$

$$= \mu_t \nabla_t \Pi \tag{2.18}$$

and

$$\overleftrightarrow{\mu}_t \cdot \hat{\mathbf{z}} \times \nabla_t \psi = (\hat{\mathbf{x}}\mu_t\hat{\mathbf{x}} + \hat{\mathbf{y}}\mu_t\hat{\mathbf{y}}) \cdot \left(-\hat{\mathbf{x}}\frac{\partial \psi}{\partial y} + \hat{\mathbf{y}}\frac{\partial \psi}{\partial x} \right) = \hat{\mathbf{x}}\left(-\mu_t\frac{\partial \psi}{\partial y} \right) + \hat{\mathbf{y}}\left(\mu_t\frac{\partial \psi}{\partial x} \right)$$

$$= \mu_t \hat{\mathbf{z}} \times \nabla_t \psi \tag{2.19}$$

Using (2.18) and (2.19) in (2.17) and noting that the $\frac{\partial}{\partial z}$ operator and the constitutive relations (which depend on z only) can be interchanged with ∇_t, we have (2.17) as

$$-\hat{\mathbf{z}} \times \nabla_t E_z + \hat{\mathbf{z}} \times \nabla_t \frac{\partial \Phi}{\partial z} + \nabla_t \frac{\partial \theta}{\partial z} = -\nabla_t u_h + \hat{\mathbf{z}} \times \nabla_t v_h - \nabla_t j\omega\mu_t \Pi + \hat{\mathbf{z}} \times \nabla_t j\omega\mu_t \psi \quad (2.20)$$

Observing that ∇_t and $\hat{\mathbf{z}} \times \nabla_t$ are orthogonal and subsequently equating the ∇_t and $\hat{\mathbf{z}} \times \nabla_t$ terms on each side of the equation leads to

$$\frac{\partial \theta}{\partial z} = -u_h - j\omega\mu_t \Pi + C_1(z) \quad (2.21)$$

and

$$-E_z + \frac{\partial \Phi}{\partial z} = v_h + j\omega\mu_t \psi + C_2(z) \quad (2.22)$$

Here we see the appearance of the scalar fields C_1 and C_2 from the inversion of the transverse gradient and curl operators, respectively. Since the field recovery process via (2.11)-(2.14) implicate the ∇_t operator, the fields $C_1(z)$ and $C_2(z)$, which are seen to be constants in the transverse dimensions, do not influence the field calculations and can be set to zero without loss of generality. A more stringent condition that the potentials satisfy the radiation condition may also be imposed, leading to the same result ($C_1(z)$ and $C_2(z) = 0$). Therefore, (2.21) simplifies to

$$\boxed{\Pi = -\frac{1}{j\omega\mu_t} \left(\frac{\partial \theta}{\partial z} + u_h \right)} \quad (2.23)$$

and (2.22) simplifies to

$$-E_z + \frac{\partial \Phi}{\partial z} = v_h + j\omega\mu_t \psi \quad (2.24)$$

Inserting (2.24) into (2.15) leads to

$$\boxed{\frac{1}{j\omega\varepsilon_z} \left(\nabla_t^2 \psi + J_{ez} \right) + \frac{\partial \Phi}{\partial z} = v_h + j\omega\mu_t \psi} \quad (2.25)$$

33

We can find the other two governing equations for the potentials by inserting (2.11) - (2.13) into (2.8) and following the same method as above. This leads to

$$\Phi = \frac{1}{j\omega\varepsilon_t}\left(\frac{\partial\psi}{\partial z} - u_e\right) \tag{2.26}$$

and

$$-\frac{1}{j\omega\mu_z}\left(\nabla_t^2\theta - J_{hz}\right) + \frac{\partial\Pi}{\partial z} = -v_e - j\omega\varepsilon_t\theta \tag{2.27}$$

Finally, from (2.23), (2.25), (2.26) and (2.27), and multiplying by the appropriate factor of either $-\frac{\varepsilon_t}{\varepsilon_z}$ or $-\frac{\mu_t}{\mu_z}$, we have the governing differential equations for the scalar potentials in inhomogeneous media:

$$-\frac{\varepsilon_t}{\varepsilon_z}\nabla_t^2\psi - \varepsilon_t\frac{\partial}{\partial z}\frac{1}{\varepsilon_t}\frac{\partial\psi}{\partial z} - k_t^2\psi = -\varepsilon_t\frac{\partial}{\partial z}\frac{1}{\varepsilon_t}u_e + \frac{\varepsilon_t}{\varepsilon_z}J_{ez} - j\omega\varepsilon_t v_h \tag{2.28}$$

$$-\frac{\mu_t}{\mu_z}\nabla_t^2\theta - \mu_t\frac{\partial}{\partial z}\frac{1}{\mu_t}\frac{\partial\theta}{\partial z} - k_t^2\theta = \mu_t\frac{\partial}{\partial z}\frac{1}{\mu_t}u_h - \frac{\mu_t}{\mu_z}J_{hz} - j\omega\mu_t v_e \tag{2.29}$$

For a homogeneous medium, (2.28) and (2.29) reduce to:

$$-\frac{\varepsilon_t}{\varepsilon_z}\nabla_t^2\psi - \frac{\partial^2\psi}{\partial z^2} - k_t^2\psi = -\frac{\partial u_e}{\partial z} + \frac{\varepsilon_t}{\varepsilon_z}J_{ez} - j\omega\varepsilon_t v_h \tag{2.30}$$

$$-\frac{\mu_t}{\mu_z}\nabla_t^2\theta - \frac{\partial^2\theta}{\partial z} - k_t^2\theta = \frac{\partial u_h}{\partial z} - \frac{\mu_t}{\mu_z}J_{hz} - j\omega\mu_t v_e \tag{2.31}$$

Lastly, we can take the divergence and curl of the transverse source current relations (2.13) and (2.14) to obtain

$$\boxed{\nabla_t \cdot \vec{J}_{et} = \nabla_t^2 u_e} \tag{2.32}$$

$$\boxed{\nabla_t \times \vec{J}_{et} = -\hat{\mathbf{z}} \nabla_t^2 v_e} \tag{2.33}$$

$$\boxed{\nabla_t \cdot \vec{J}_{ht} = \nabla_t^2 u_h} \tag{2.34}$$

$$\boxed{\nabla_t \times \vec{J}_{ht} = -\hat{\mathbf{z}} \nabla_t^2 v_h} \tag{2.35}$$

2.1.1 Summary of Potentials.

The potential formulation for a uniaxial, homogeneous media can be written in a concise operator form.

Fields:

$$\vec{E} = \vec{E}_t + \hat{\mathbf{z}} E_z \qquad \text{and} \qquad \vec{H} = \vec{H}_t + \hat{\mathbf{z}} H_z$$

$$\vec{E}_t = \nabla_t \Phi + \nabla_t \times \hat{\mathbf{z}}\theta = \nabla_t \Phi - \hat{\mathbf{z}} \times \nabla_t \theta \qquad E_z = -\frac{1}{j\omega\varepsilon_z}\left(\nabla_t^2 \psi + J_{ez}\right)$$

$$\vec{H}_t = \nabla_t \Pi + \nabla_t \times \hat{\mathbf{z}}\psi = \nabla_t \Pi - \hat{\mathbf{z}} \times \nabla_t \psi \qquad H_z = \frac{1}{j\omega\mu_z}\left(\nabla_t^2 \theta - J_{hz}\right)$$

Potentials:

$$\Pi = -\frac{1}{j\omega\mu_t}\left(\frac{\partial\theta}{\partial z} + u_h\right) \qquad \Phi = \frac{1}{j\omega\varepsilon_t}\left(\frac{\partial\psi}{\partial z} - u_e\right)$$

Where θ and ψ satisfy the coupled 2nd order differential equations:

$$L_1\psi = s_1 \qquad L_2\theta = s_2$$

$$L_1 = -\frac{\varepsilon_t}{\varepsilon_z}\nabla_t^2 - \frac{\partial^2}{\partial z^2} - k_t^2 \qquad L_2 = -\frac{\mu_t}{\mu_z}\nabla_t^2 - \frac{\partial^2}{\partial z^2} - k_t^2$$

$$s_1 = -\frac{\partial u_e}{\partial z} + \frac{\varepsilon_t}{\varepsilon_z}J_{ez} - j\omega\varepsilon_t v_h \qquad s_2 = \frac{\partial u_h}{\partial z} - \frac{\mu_t}{\mu_z}J_{hz} - j\omega\mu_t v_e$$

Auxiliary Relations:

$$\nabla_t \cdot \vec{J}_{et} = \nabla_t^2 u_e \qquad \nabla_t \times \vec{J}_{et} = -\hat{\mathbf{z}}\nabla_t^2 v_e$$

$$\nabla_t \cdot \vec{J}_{ht} = \nabla_t^2 u_h \qquad \nabla_t \times \vec{J}_{ht} = -\hat{\mathbf{z}}\nabla_t^2 v_h$$

$$k_t^2 = \omega^2 \varepsilon_t \mu_t$$

It can be shown, with $\varepsilon_t = \varepsilon_z = \varepsilon$ and $\mu_t = \mu_z = \mu$, that these potentials reduce to those of the isotropic case (often referred to as $\vec{A}$ and $\vec{F}$), although care must be taken to understand the terms which result from the scalarization of the source currents, since vector potential methods do not expand the source current.

2.2   Principal Solution

The differential equations of the previous section must now be solved. In order to do so, we take the typical approach for linear non-homogeneous differential equations. Namely, the solution is composed of the superposition of a forced, unbounded (principal) solution and an unforced, bounded (scattered) solution. The appropriate boundary conditions are then enforced on the total **fields** in order to find the total solution for the parallel plate geometry. We begin with the principal solution. Since the principal solution exists in unbounded space, we are prompted to perform a Fourier Transform. Using the generic transform pair

$$\text{Forward} \rightarrow \tilde{f}(\vec{\lambda}_\rho, z) = \iint\limits_{-\infty}^{\infty} f(\vec{\rho}, z) e^{-j\vec{\lambda}_\rho \cdot \vec{\rho}} d^2\rho \tag{2.36}$$

$$\text{Reverse} \rightarrow f(\vec{\rho}, z) = \frac{1}{(2\pi)^2} \iint\limits_{-\infty}^{\infty} \tilde{f}(\vec{\lambda}_\rho, z) e^{j\vec{\lambda}_\rho \cdot \vec{\rho}} d^2\lambda_\rho \tag{2.37}$$

where $d^2\lambda_\rho = d\lambda_x d\lambda_y$, $d^2\rho = dxdy$, $\vec{\lambda}_\rho = \hat{\mathbf{x}}\lambda_x + \hat{\mathbf{y}}\lambda_y$.

We can now write the equations and the operators in the single transform $(\vec{\lambda}_\rho, z)$ domain (quantities in this domain are denoted by the single overset tilde in this work, so we will frequently drop the domain notation except in certain circumstances when it is necessary to be absolutely clear):

$$\tilde{L}_1 \tilde{\psi}^p = \tilde{s}_1 \qquad \text{and} \qquad \tilde{L}_2 \tilde{\theta}^p = \tilde{s}_2$$

$$\tilde{L}_1 = \frac{\varepsilon_t}{\varepsilon_z} \lambda_\rho^2 - \frac{\partial^2}{\partial z^2} - k_t^2$$

$$\tilde{L}_2 = \frac{\mu_t}{\mu_z} \lambda_\rho^2 - \frac{\partial^2}{\partial z^2} - k_t^2 \tag{2.38}$$

$$\tilde{s}_1 = -\frac{\partial \tilde{u}_e}{\partial z} + \frac{\varepsilon_t}{\varepsilon_z} \tilde{J}_{ez} - j\omega\varepsilon_t \tilde{v}_h$$

$$\tilde{s}_2 = \frac{\partial \tilde{u}_h}{\partial z} - \frac{\mu_t}{\mu_z} \tilde{J}_{hz} - j\omega\mu_t \tilde{v}_e$$

37

We can transform again on the longitudinal variable z into the double transform $(\vec{\lambda}_\rho, \lambda_z)$ domain (denoted by the double overset tildes), using the generic transform pairs

$$\text{Forward} \rightarrow \tilde{\tilde{f}}(\vec{\lambda}_\rho, \lambda_z) = \int_{-\infty}^{\infty} \tilde{f}(\vec{\lambda}_\rho, z)e^{-j\lambda_z z}dz \tag{2.39}$$

$$\text{Reverse} \rightarrow \tilde{f}(\vec{\lambda}_\rho, z) = \frac{1}{2\pi} \int_{-\infty}^{\infty} \tilde{\tilde{f}}(\vec{\lambda}_\rho, \lambda_z)e^{j\lambda_z z}d\lambda_z \tag{2.40}$$

and the system becomes

$$\tilde{\tilde{L}}_1 \tilde{\tilde{\psi}}^p = \tilde{\tilde{s}}_1 \qquad \text{and} \qquad \tilde{\tilde{L}}_2 \tilde{\tilde{\theta}}^p = \tilde{\tilde{s}}_2$$

$$\tilde{\tilde{L}}_1 = \frac{\varepsilon_t}{\varepsilon_z}\lambda_\rho^2 + \lambda_z^2 - k_t^2$$

$$\tilde{\tilde{L}}_2 = \frac{\mu_t}{\mu_z}\lambda_\rho^2 + \lambda_z^2 - k_t^2 \tag{2.41}$$

$$\tilde{\tilde{s}}_1 = -j\lambda_z\tilde{\tilde{u}}_e + \frac{\varepsilon_t}{\varepsilon_z}\tilde{\tilde{J}}_{ez} - j\omega\varepsilon_t\tilde{\tilde{v}}_h$$

$$\tilde{\tilde{s}}_2 = j\lambda_z\tilde{\tilde{u}}_h - \frac{\mu_t}{\mu_z}\tilde{\tilde{J}}_{hz} - j\omega\mu_t\tilde{\tilde{v}}_e$$

In order to simplify the notation, we define

$$\lambda_{z\psi}^2 = k_t^2 - \frac{\varepsilon_t}{\varepsilon_z}\lambda_\rho^2 \tag{2.42}$$

$$\lambda_{z\theta}^2 = k_t^2 - \frac{\mu_t}{\mu_z}\lambda_\rho^2 \tag{2.43}$$

which condenses the linear operators to the form

$$\tilde{\tilde{L}}_1 = \lambda_z^2 - \lambda_{z\psi}^2 = (\lambda_z - \lambda_{z\psi})(\lambda_z + \lambda_{z\psi})$$

$$\tilde{\tilde{L}}_2 = \lambda_z^2 - \lambda_{z\theta}^2 = (\lambda_z - \lambda_{z\theta})(\lambda_z + \lambda_{z\theta}) \tag{2.44}$$

Now, we have the solutions to the system of equations (2.41) as

$$\tilde{\tilde{\psi}}^p = \frac{\tilde{\tilde{s}}_1}{\tilde{\tilde{L}}_1} = \frac{-j\lambda_z\tilde{\tilde{u}}_e + \frac{\varepsilon_t}{\varepsilon_z}\tilde{\tilde{J}}_{ez} - j\omega\varepsilon_t\tilde{\tilde{v}}_h}{(\lambda_z - \lambda_{z\psi})(\lambda_z + \lambda_{z\psi})} \tag{2.45}$$

38

and

$$\widetilde{\widetilde{\theta}}^p = \frac{\widetilde{\widetilde{s}}_2}{\widetilde{\widetilde{L}}_2} = \frac{j\lambda_z\widetilde{\widetilde{u}}_h - \frac{\mu_t}{\mu_z}\widetilde{\widetilde{J}}_{hz} - j\omega\mu_t\widetilde{\widetilde{v}}_e}{(\lambda_z - \lambda_{z\theta})(\lambda_z + \lambda_{z\theta})} \tag{2.46}$$

The roots of (2.45) and (2.46) represent the TE^z and TM^z modes of the upward and downward propagating waves in the unbounded media. The modal relationship will become clear later in the development. It is possible to further simplify this system, by applying the transforms of (2.36) and (2.39) to the auxiliary divergence and curl relationships to write

$$\nabla_t \cdot \vec{J}_{et} = \nabla_t^2 u_e \xrightarrow{FT} j\vec{\lambda}_\rho \cdot \widetilde{\vec{\widetilde{J}}}_{et} = -\lambda_\rho^2\widetilde{\widetilde{u}}_e \qquad \Longrightarrow \widetilde{\widetilde{u}}_e = -\frac{j\vec{\lambda}_\rho \cdot \widetilde{\vec{\widetilde{J}}}_{et}}{\lambda_\rho^2} = -\frac{j\vec{\lambda}_\rho \cdot \widetilde{\vec{\widetilde{J}}}_e}{\lambda_\rho^2} \tag{2.47a}$$

$$\nabla_t \cdot \vec{J}_{ht} = \nabla_t^2 u_h \xrightarrow{FT} j\vec{\lambda}_\rho \cdot \widetilde{\vec{\widetilde{J}}}_{et} = -\lambda_\rho^2\widetilde{\widetilde{u}}_h \qquad \Longrightarrow \widetilde{\widetilde{u}}_h = -\frac{j\vec{\lambda}_\rho \cdot \widetilde{\vec{\widetilde{J}}}_{ht}}{\lambda_\rho^2} = -\frac{j\vec{\lambda}_\rho \cdot \widetilde{\vec{\widetilde{J}}}_h}{\lambda_\rho^2} \tag{2.47b}$$

$$\nabla_t \times \vec{J}_{et} = -\hat{\mathbf{z}}\nabla_t^2 v_e \xrightarrow{FT} j\vec{\lambda}_\rho \times \widetilde{\vec{\widetilde{J}}}_{et} = \hat{\mathbf{z}}\lambda_\rho^2\widetilde{\widetilde{v}}_e \qquad \Longrightarrow \widetilde{\widetilde{v}}_e = \frac{j\hat{\mathbf{z}} \times \vec{\lambda}_\rho \cdot \widetilde{\vec{\widetilde{J}}}_{et}}{\lambda_\rho^2} = \frac{j\hat{\mathbf{z}} \times \vec{\lambda}_\rho \cdot \widetilde{\vec{\widetilde{J}}}_e}{\lambda_\rho^2} \tag{2.47c}$$

$$\nabla_t \times \vec{J}_{ht} = -\hat{\mathbf{z}}\nabla_t^2 v_h \xrightarrow{FT} j\vec{\lambda}_\rho \times \widetilde{\vec{\widetilde{J}}}_{ht} = \hat{\mathbf{z}}\lambda_\rho^2\widetilde{\widetilde{v}}_h \qquad \Longrightarrow \widetilde{\widetilde{v}}_h = \frac{j\hat{\mathbf{z}} \times \vec{\lambda}_\rho \cdot \widetilde{\vec{\widetilde{J}}}_{ht}}{\lambda_\rho^2} = \frac{j\hat{\mathbf{z}} \times \vec{\lambda}_\rho \cdot \widetilde{\vec{\widetilde{J}}}_h}{\lambda_\rho^2} \tag{2.47d}$$

where the transverse nature of $\vec{\lambda}_\rho$ is utilized in substituting $\widetilde{\vec{\widetilde{J}}}_{e,m}$ for $\widetilde{\vec{\widetilde{J}}}_{et,mt}$. Using the results of (2.47) and simplifying, we can re-write (2.45) as

$$\widetilde{\widetilde{\psi}}^p = \left(\frac{-\frac{\lambda_z\vec{\lambda}_\rho}{\lambda_\rho^2} + \frac{\varepsilon_t}{\varepsilon_z}\hat{\mathbf{z}}}{(\lambda_z - \lambda_{z\psi})(\lambda_z + \lambda_{z\psi})} \right) \cdot \widetilde{\vec{\widetilde{J}}}_e + \left(\frac{\omega\varepsilon_t\frac{\hat{\mathbf{z}}\times\vec{\lambda}_\rho}{\lambda_\rho^2}}{(\lambda_z - \lambda_{z\psi})(\lambda_z + \lambda_{z\psi})} \right) \cdot \widetilde{\vec{\widetilde{J}}}_h \tag{2.48}$$

Similarly, we can re-write (2.46) as

$$\widetilde{\widetilde{\theta}}^p = \left(\frac{\omega\mu_t\frac{\hat{\mathbf{z}}\times\vec{\lambda}_\rho}{\lambda_\rho^2}}{(\lambda_z - \lambda_{z\theta})(\lambda_z + \lambda_{z\theta})} \right) \cdot \widetilde{\vec{\widetilde{J}}}_e - \left(\frac{-\frac{\lambda_z\vec{\lambda}_\rho}{\lambda_\rho^2} + \frac{\mu_t}{\mu_z}\hat{\mathbf{z}}}{(\lambda_z - \lambda_{z\theta})(\lambda_z + \lambda_{z\theta})} \right) \cdot \widetilde{\vec{\widetilde{J}}}_h \tag{2.49}$$

39

To summarize the results from this section, we now have the principal solution to the potentials in the $(\vec{\lambda}_\rho, \lambda_z)$ domain as

$$
\widetilde{\widetilde{\psi}}^p = \left(\frac{-\frac{\lambda_z \vec{\lambda}_\rho}{\lambda_\rho^2} + \frac{\varepsilon_t}{\varepsilon_z}\hat{\mathbf{z}}}{(\lambda_z - \lambda_{z\psi})(\lambda_z + \lambda_{z\psi})} \right) \cdot \vec{\widetilde{\widetilde{J}}}_e + \left(\frac{\omega\varepsilon_t \frac{\hat{\mathbf{z}} \times \vec{\lambda}_\rho}{\lambda_\rho^2}}{(\lambda_z - \lambda_{z\psi})(\lambda_z + \lambda_{z\psi})} \right) \cdot \vec{\widetilde{\widetilde{J}}}_h
$$

$$
\widetilde{\widetilde{\theta}}^p = \left(\frac{\omega\mu_t \frac{\hat{\mathbf{z}} \times \vec{\lambda}_\rho}{\lambda_\rho^2}}{(\lambda_z - \lambda_{z\theta})(\lambda_z + \lambda_{z\theta})} \right) \cdot \vec{\widetilde{\widetilde{J}}}_e - \left(\frac{-\frac{\lambda_z \vec{\lambda}_\rho}{\lambda_\rho^2} + \frac{\mu_t}{\mu_z}\hat{\mathbf{z}}}{(\lambda_z - \lambda_{z\theta})(\lambda_z + \lambda_{z\theta})} \right) \cdot \vec{\widetilde{\widetilde{J}}}_h
$$

$$
\lambda_{z\psi_g}^2 = k_t^2 - \frac{\varepsilon_t}{\varepsilon_z}\lambda_\rho^2 \qquad \lambda_{z\theta_g}^2 = k_t^2 - \frac{\mu_t}{\mu_z}\lambda_\rho^2
$$

2.3   Determination of Principal Green's Functions

Note that these potentials are written in the notional form:

$$
\widetilde{\widetilde{\psi}}^p = \vec{\widetilde{\widetilde{G}}}_{\psi_e}^p \cdot \vec{\widetilde{\widetilde{J}}}_e + \vec{\widetilde{\widetilde{G}}}_{\psi_h}^p \cdot \vec{\widetilde{\widetilde{J}}}_h \qquad \text{and} \qquad \widetilde{\widetilde{\theta}}^p = \vec{\widetilde{\widetilde{G}}}_{\theta_e}^p \cdot \vec{\widetilde{\widetilde{J}}}_e + \vec{\widetilde{\widetilde{G}}}_{\theta_h}^p \cdot \vec{\widetilde{\widetilde{J}}}_h
$$

The principal spectral-domain vector Green's functions $\vec{\widetilde{\widetilde{G}}}_{\psi_e}^p, \vec{\widetilde{\widetilde{G}}}_{\theta_e}^p$ represent the element of potential $\widetilde{\widetilde{\psi}}^p, \widetilde{\widetilde{\theta}}^p$ maintained by the electric current density $\vec{\widetilde{\widetilde{J}}}_e$. Similarly, the principal spectral-domain vector Green's functions $\vec{\widetilde{\widetilde{G}}}_{\psi_h}^p, \vec{\widetilde{\widetilde{G}}}_{\theta_h}^p$ represent the element of potential $\widetilde{\widetilde{\psi}}^p, \widetilde{\widetilde{\theta}}^p$ maintained by the magnetic current density $\vec{\widetilde{\widetilde{J}}}_h$. Now, we can use the inverse Fourier

Transform from (2.40) to transform these back to the $(\vec{\lambda}_\rho, z)$ domain:

$$\widetilde{\psi}^p(\vec{\lambda}_\rho, z) = \frac{1}{2\pi} \int\limits_{-\infty}^{\infty} \widetilde{\widetilde{\psi}}^p(\vec{\lambda}_\rho, \lambda_z) e^{j\lambda_z z} d\lambda_z$$

$$= \frac{1}{2\pi} \int\limits_{-\infty}^{\infty} \widetilde{\vec{\widetilde{G}}}^p_{\psi_e}(\vec{\lambda}_\rho, \lambda_z) \cdot \widetilde{\vec{\widetilde{J}}}_e(\vec{\lambda}_\rho, \lambda_z) e^{j\lambda_z z} d\lambda_z + \frac{1}{2\pi} \int\limits_{-\infty}^{\infty} \widetilde{\vec{\widetilde{G}}}^p_{\psi_h}(\vec{\lambda}_\rho, \lambda_z) \cdot \widetilde{\vec{\widetilde{J}}}_h(\vec{\lambda}_\rho, \lambda_z) e^{j\lambda_z z} d\lambda_z$$

(2.50a)

$$\widetilde{\theta}^p(\vec{\lambda}_\rho, z) = \frac{1}{2\pi} \int\limits_{-\infty}^{\infty} \widetilde{\widetilde{\theta}}^p(\vec{\lambda}_\rho, \lambda_z) e^{j\lambda_z z} d\lambda_z$$

$$= \frac{1}{2\pi} \int\limits_{-\infty}^{\infty} \widetilde{\vec{\widetilde{G}}}^p_{\theta_e}(\vec{\lambda}_\rho, \lambda_z) \cdot \widetilde{\vec{\widetilde{J}}}_e(\vec{\lambda}_\rho, \lambda_z) e^{j\lambda_z z} d\lambda_z + \frac{1}{2\pi} \int\limits_{-\infty}^{\infty} \widetilde{\vec{\widetilde{G}}}^p_{\theta_h}(\vec{\lambda}_\rho, \lambda_z) \cdot \widetilde{\vec{\widetilde{J}}}_h(\vec{\lambda}_\rho, \lambda_z) e^{j\lambda_z z} d\lambda_z$$

(2.50b)

Note, the current densities are described mathematically by

$$\widetilde{\vec{\widetilde{J}}}_{e,h}(\vec{\lambda}_\rho, \lambda_z) = \int\limits_{-\infty}^{\infty} \widetilde{\vec{J}}_{e,h}(\vec{\lambda}_\rho, z') e^{-j\lambda_z z'} dz' = \int\limits_{a}^{b} \widetilde{\vec{J}}_{e,h}(\vec{\lambda}_\rho, z') e^{-j\lambda_z z'} dz'$$

where the second equation takes into account the realistic physical extent of the currents, which are assumed to exist continuously only in the region $a < z < b$. By the Convolution Theorem, we can write (2.50) as

$$\widetilde{\psi}^p(\vec{\lambda}_\rho, z) = \int\limits_{a}^{b} \widetilde{\vec{G}}^p_{\psi_e}(\vec{\lambda}_\rho, z - z') \cdot \widetilde{\vec{J}}_e(\vec{\lambda}_\rho, z') dz' + \int\limits_{a}^{b} \widetilde{\vec{G}}^p_{\psi_h}(\vec{\lambda}_\rho, z - z') \cdot \widetilde{\vec{J}}_h(\vec{\lambda}_\rho, z') dz' \qquad (2.51a)$$

$$\widetilde{\theta}^p(\vec{\lambda}_\rho, z) = \int\limits_{a}^{b} \widetilde{\vec{G}}^p_{\theta_e}(\vec{\lambda}_\rho, z - z') \cdot \widetilde{\vec{J}}_e(\vec{\lambda}_\rho, z') dz' + \int\limits_{a}^{b} \widetilde{\vec{G}}^p_{\theta_h}(\vec{\lambda}_\rho, z - z') \cdot \widetilde{\vec{J}}_h(\vec{\lambda}_\rho, z') dz' \qquad (2.51b)$$

where the dyadic Green's functions are

$$\vec{\bar{G}}^p_{\psi_e}(\vec{\lambda}_\rho, z-z') = \frac{1}{2\pi}\int\limits_{-\infty}^{\infty}\vec{\tilde{\bar{G}}}^p_{\psi_e}(\vec{\lambda}_\rho, \lambda_z)e^{j\lambda_z(z-z')}d\lambda_z \tag{2.52a}$$

$$\vec{\bar{G}}^p_{\psi_h}(\vec{\lambda}_\rho, z-z') = \frac{1}{2\pi}\int\limits_{-\infty}^{\infty}\vec{\tilde{\bar{G}}}^p_{\psi_h}(\vec{\lambda}_\rho, \lambda_z)e^{j\lambda_z(z-z')}d\lambda_z \tag{2.52b}$$

$$\vec{\bar{G}}^p_{\theta_e}(\vec{\lambda}_\rho, z-z') = \frac{1}{2\pi}\int\limits_{-\infty}^{\infty}\vec{\tilde{\bar{G}}}^p_{\theta_e}(\vec{\lambda}_\rho, \lambda_z)e^{j\lambda_z(z-z')}d\lambda_z \tag{2.52c}$$

$$\vec{\bar{G}}^p_{\theta_h}(\vec{\lambda}_\rho, z-z') = \frac{1}{2\pi}\int\limits_{-\infty}^{\infty}\vec{\tilde{\bar{G}}}^p_{\theta_h}(\vec{\lambda}_\rho, \lambda_z)e^{j\lambda_z(z-z')}d\lambda_z \tag{2.52d}$$

These real integrals can be evaluated using the complex plane analysis techniques described in Appendix A. In order to evaluate the integrals of (2.52a)-(2.52d), it is important to examine the exponential term and the implications of its form on the closure conditions in the application of Jordan's Lemma. Since λ_z is complex, we can write it in the form $\lambda_z = \text{Re}\{\lambda_z\} + j\text{Im}\{\lambda_z\} = \lambda_{z,re} + j\lambda_{z,im}$. Therefore, we can write the exponential as

$$e^{j\lambda_z(z-z')} = e^{-\lambda_{z,im}(z-z')}e^{j\lambda_{z,re}(z-z')}$$

which allows us to determine the closure conditions on the contour path of the integral:

$$z - z' > 0 \implies \text{UHPC (i.e., } \lambda_{z,im} > 0)$$
$$z - z' < 0 \implies \text{LHPC (i.e., } \lambda_{z,im} < 0)$$

This closure is required by Jordan's Lemma to ensure the integral values decay to zero as $R \to \infty$ on the semi-circular contour of Figure 2.1. Now, we have $\vec{\bar{G}}^p_{\psi_e}$ from (2.48) and (2.52a):

42

$$\vec{G}^p_{\psi_e} = \frac{1}{2\pi} \int\limits_{-\infty}^{\infty} \tilde{\vec{G}}^p_{\psi_e} e^{j\lambda_z(z-z')} d\lambda_z$$

$$= \frac{1}{2\pi} \int\limits_{-\infty}^{\infty} \frac{-\frac{\lambda_z \vec{\lambda}_\rho}{\lambda_\rho^2} + \hat{\mathbf{z}}\frac{\varepsilon_t}{\varepsilon_z}}{(\lambda_z + \lambda_{z\psi})(\lambda_z - \lambda_{z\psi})} e^{j\lambda_z(z-z')} d\lambda_z \qquad (2.53)$$

We see that $\pm\lambda_{z\psi}$ are the two simple poles of (2.53). These are plotted in the λ_z complex plane, along with the Cauchy integral contour in Figure 2.1. We can show that the positive value of $\lambda_{z\psi}$ term from 2.42 is located in the Lower Half Plane (LHP) and the negative value of the $\lambda_{z\psi}$ term is located in the Upper Half Plane (UHP), which will be required for the complex plane analysis to come. By factoring out a k_t out of the square root sign, we have

$$\lambda_{z\psi} = k_t \sqrt{1 - \frac{\lambda_\rho^2}{\omega^2 \varepsilon_z \mu_t}} \qquad (2.54)$$

First, we recognize that the complex permittivity and permeability can be written in the form $\rho e^{j\phi}$. For most real, passive materials, the $\omega^2 \varepsilon_z \mu_t$ term will have the argument ϕ as a negative value (since the real part will be positive and the imaginary part will be negative), which is in the lower half plane. Inverting $\rho e^{j\phi}$ leads to an inversion around the real axis. Therefore, $\frac{\lambda_\rho^2}{\omega^2 \varepsilon_z \mu_t}$ is in the upper half plane, regardless of the sign of the imaginary part of $\vec{\lambda}_\rho$. Negating this term leads to a counter-clockwise rotation around the origin. Therefore, $1 - \frac{\lambda_\rho^2}{\omega^2 \varepsilon_z \mu_t}$ will be in the lower half plane. Since the square root term will always produce a positive real part (with the branch cut along the negative real axis), we see that the term $\sqrt{1 - \frac{\lambda_\rho^2}{\omega^2 \varepsilon_z \mu_t}}$ will be restricted to the 4th quadrant. Finally, multiplying by k_t (which will have a value in the lower half plane) will place $\lambda_{z\psi} = k_t \sqrt{1 - \frac{\lambda_\rho^2}{\omega^2 \varepsilon_z \mu_t}}$ in the lower half plane. A similar analysis shows the negative value to be in the UHP and also shows these relations are true for both values of $\lambda_{z\theta}$.
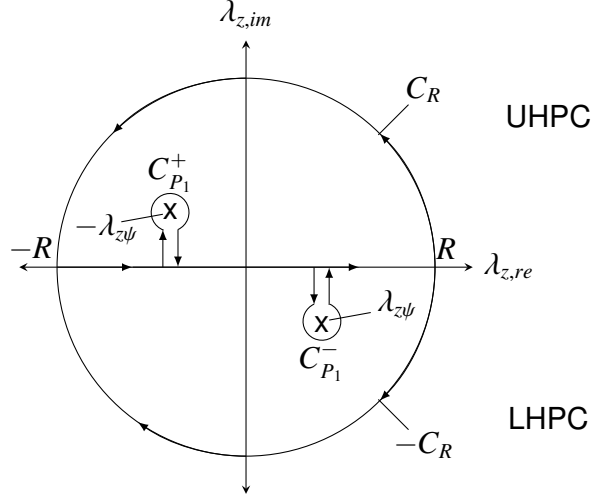
Figure 2.1: The complex λ_z plane and Cauchy's integral contour. For reference the contour deformation $C_{P_1}^+$ is around the pole $-\lambda_{z\psi}$ and the deformation $C_{P_1}^-$ is around the pole $\lambda_{z\psi}$. Note that the distance between the paths around the singularities are exaggerated so as to give a better view of the overall contour path for implementing Cauchy's Integral Theorem. In reality, they lie on top of each other.

According to Cauchy's Integral Theorem, for the case of $z - z' > 0$, we have the integration around the semi-circular contour in the UHP as the concatenation of the three contours:

$$\lim_{R\to\infty} \left[\int_{-R}^{R} + \oint_{C_p^+} + \int_{C_R^+} \right] = 0 \tag{2.55}$$

According to Jordan's Lemma and the closure conditions specified above, the third term is zero, which, when combined with Cauchy's Integral Formula, leads to

$$\lim_{R\to\infty} \int_{-R}^{R} = -\oint_{C_p^+} = \oint_{C_p^+} = j2\pi\mathrm{Res}(f, C_{p1}^+) \tag{2.56}$$

44

where we have introduced the negative sign in order to account for direction of contour integration. We can determine the Green's function from 2.56

$$\vec{\vec{G}}^p_{\psi_e}(z-z') = j2\pi \left[\frac{1}{2\pi} \left(\frac{-\vec{\lambda}_\rho \frac{\lambda_z}{\lambda_\rho^2} + \hat{\mathbf{z}}\frac{\varepsilon_t}{\varepsilon_z}}{\lambda_z - \lambda_{z\psi}} \right) e^{j\lambda_z(z-z')} \right]\Bigg|_{\lambda_z = -\lambda_{z\psi}} \tag{2.57}$$

Which, after some algebraic manipulation gives

$$\vec{\vec{G}}^p_{\psi_e}(z-z') = -j \frac{\vec{\lambda}_\rho \frac{\lambda_{z\psi}}{\lambda_\rho^2} + \hat{\mathbf{z}}\frac{\varepsilon_t}{\varepsilon_z}}{2\lambda_{z\psi}} e^{-j\lambda_{z\psi}(z-z')} \qquad \dots \text{for } z - z' > 0$$

Now, we proceed similarly for the $z-z' < 0$ case (the LHP). Again, using Cauchy's Integral Theorem, Jordan's Lemma and Cauchy's Integral Formula, we have

$$\lim_{R \to \infty} \left[\int_{-R}^{R} + \oint_{C_p^-} + \overbrace{\int_{C_R^-}}^{0} \right] = 0$$

$$\implies \int_{-\infty}^{\infty} = -\oint_{C_p^-} = -j2\pi \mathrm{Res}(f, C_{p1}^-)$$

$$\implies \vec{\vec{G}}^p_{\psi_e}(z-z') = -j2\pi \left[\frac{1}{2\pi} \left(\frac{-\vec{\lambda}_\rho \frac{\lambda_z}{\lambda_\rho^2} + \hat{\mathbf{z}}\frac{\varepsilon_t}{\varepsilon_z}}{\lambda_z + \lambda_{z\psi}} \right) e^{j\lambda_z(z-z')} \right]\Bigg|_{\lambda_z = \lambda_{z\psi}}$$

$$= -j \frac{-\vec{\lambda}_\rho \frac{\lambda_z}{\lambda_\rho^2} + \hat{\mathbf{z}}\frac{\varepsilon_t}{\varepsilon_z}}{2\lambda_{z\psi}} e^{j\lambda_{z\psi}(z-z')} \qquad \dots \text{for } z - z < 0$$

These two cases can be written succinctly as

$$\boxed{\vec{\vec{G}}^p_{\psi_e}(z-z') = -j \frac{\vec{\lambda}_\rho \frac{\mathrm{sgn}(z-z')\lambda_{z\psi}}{\lambda_\rho^2} + \hat{\mathbf{z}}\frac{\varepsilon_t}{\varepsilon_z}}{2\lambda_{z\psi}} e^{-j\lambda_{z\psi}|z-z'|}} \tag{2.58}$$

Recognizing $\vec{\vec{G}}^p_{\theta_h} = -\vec{\vec{G}}^p_{\psi_e}$ and, by duality, replacing $\varepsilon_t, \varepsilon_z$ with $-\mu_t, -\mu_z$ and $\lambda_{z\psi}$ with $\lambda_{z\theta}$, we can readily write

$$\boxed{\vec{\vec{G}}^p_{\theta_h}(z-z') = j \frac{\vec{\lambda}_\rho \frac{\mathrm{sgn}(z-z')\lambda_{z\theta}}{\lambda_\rho^2} + \hat{\mathbf{z}}\frac{\mu_t}{\mu_z}}{2\lambda_{z\theta}} e^{-j\lambda_{z\theta}|z-z'|}} \tag{2.59}$$

Proceeding similarly with $\tilde{\vec{\vec{G}}}^p_{\psi_h}$, we find

$$\boxed{\tilde{\vec{\vec{G}}}^p_{\psi_h}(z - z') = -\frac{\hat{\mathbf{z}} \times \vec{\lambda}_\rho \frac{j\omega\varepsilon_t}{\lambda_\rho^2}}{2\lambda_{z\psi}} e^{-j\lambda_{z\psi}|z-z'|}}$$

(2.60)

As before, we see that $\tilde{\vec{\vec{G}}}^p_{\psi_h} = -\tilde{\vec{\vec{G}}}^p_{\theta_e}$, if, by duality, we replace $\lambda_{z\psi}$ with $\lambda_{z\theta}$, ε_t with $-\mu_t$, and we can readily write

$$\boxed{\tilde{\vec{\vec{G}}}^p_{\theta_e}(z - z') = -\frac{\hat{\mathbf{z}} \times \vec{\lambda}_\rho \frac{j\omega\mu_t}{\lambda_\rho^2}}{2\lambda_{z\theta}} e^{-j\lambda_{z\theta}|z-z'|}}$$

(2.61)

2.3.1 *Potential Principal Green's Function Summary (in the $(\vec{\lambda}_\rho, z)$ domain).*

$$\boxed{\begin{aligned}
\tilde{\vec{\vec{G}}}^p_{\psi_e}(\vec{\lambda}_\rho|z-z') &= -j\frac{\vec{\lambda}_\rho \frac{\mathrm{sgn}(z-z')\lambda_{z\psi}}{\lambda_\rho^2} + \hat{\mathbf{z}}\frac{\varepsilon_t}{\varepsilon_z}}{2\lambda_{z\psi}} e^{-j\lambda_{z\psi}|z-z'|} = \vec{\vec{g}}^p_{\psi_e} e^{-j\lambda_{z\psi}|z-z'|} \\
\tilde{\vec{\vec{G}}}^p_{\psi_h}(\vec{\lambda}_\rho|z-z') &= -\frac{\hat{\mathbf{z}} \times \vec{\lambda}_\rho \frac{j\omega\varepsilon_t}{\lambda_\rho^2}}{2\lambda_{z\psi}} e^{-j\lambda_{z\psi}|z-z'|} = \vec{\vec{g}}^p_{\psi_h} e^{-j\lambda_{z\psi}|z-z'|} \\
\tilde{\vec{\vec{G}}}^p_{\theta_e}(\vec{\lambda}_\rho|z-z') &= -\frac{\hat{\mathbf{z}} \times \vec{\lambda}_\rho \frac{j\omega\mu_t}{\lambda_\rho^2}}{2\lambda_{z\theta}} e^{-j\lambda_{z\theta}|z-z'|} = \vec{\vec{g}}^p_{\theta_e} e^{-j\lambda_{z\theta}|z-z'|} \\
\tilde{\vec{\vec{G}}}^p_{\theta_h}(\vec{\lambda}_\rho|z-z') &= j\frac{\vec{\lambda}_\rho \frac{\mathrm{sgn}(z-z')\lambda_{z\theta}}{\lambda_\rho^2} + \hat{\mathbf{z}}\frac{\mu_t}{\mu_z}}{2\lambda_{z\theta}} e^{-j\lambda_{z\theta}|z-z'|} = \vec{\vec{g}}^p_{\theta_h} e^{-j\lambda_{z\theta}|z-z'|}
\end{aligned}}$$

2.4 Cancellation of Transverse Depolarizing Dyad Artifact

The u_e and u_h terms (which are transverse in nature) in the potentials Φ and Π are not intuitive, since they appear to be analogous to the well-known longitudinal depolarizing dyad terms [3,5,11,21,23,40,47,57,91,93,101,111], which are clearly seen in (2.23) and (2.26) . These findings discuss methods of handling the source point discontinuity, when $z = z'$. The authors employ a method of dividing the source region into two regions along the longitudinal axis, $V - V_\delta$ and V_δ. V_δ is seen to be a small volume around the source point and will be allowed to become infinitesimally small as $\delta \to 0$. For a geometry such as that in Figure 2.2, dividing the region in such a manner causes the walls around V_δ to build

up charge, due to the longitudinal current, much like a parallel-plate capacitor, instigating an electric field. The depolarizing terms and corresponding gap electric field offset the resulting gap field. This offsetting field is necessary since the original continuous volume does not have a gap field. However, for the geometry shown in Figure 2.2, these terms are not expected in the transverse direction, since a transverse current produces no charge buildup. Havrilla [47] has shown that careful application of the Leibnitz rule in the case of a dielectric uniaxial material reveals a residual term that exactly cancels these depolarizing terms. The next sections demonstrated that these terms are, in fact, non-physical (as they are mathematically cancelled) in the present case as well.

Figure 2.2: A graphical depiction of the source point discontinuity. The integration is performed around the source region, in order to account for the discontinuity when $z = z'$. When the entire region of interest is broken up in this manner, z-directed "gap" fields originate from the charging effect of the boundary on each side of the region $z - \delta \leqslant z \leqslant z + \delta$. The well-known depolarizing fields $(\vec{E}_d, \vec{H}_d)$ serve to correct for these anomalous gap fields $(\vec{E}_g, \vec{H}_g)$.

2.4.1 $\tilde{\Phi}$ *Potential.*

From the summary in Section 2.1.1, $\tilde{\Phi}^p$ can be written as:

$$\tilde{\Phi}^p = \frac{1}{j\omega\varepsilon_t}\left(\frac{\partial\tilde{\psi}^p}{\partial z} - \tilde{u}_e\right) \tag{2.62}$$

where:

$$\tilde{\psi}^p = \int_a^b \vec{\vec{G}}_{\psi_e}^p(\vec{\lambda}_\rho|z-z')\cdot\vec{\tilde{J}}_e(\vec{\lambda}_\rho|z')dz' + \int_a^b \vec{\vec{G}}_{\psi_h}^p(\vec{\lambda}_\rho|z-z')\cdot\vec{\tilde{J}}_h(\vec{\lambda}_\rho|z')dz' \tag{2.63}$$

Noting the partial derivative of $\tilde{\psi}$ with respect to z in (2.62), we seek to move the derivative operator inside of the integration operators shown in (2.63). Before doing so, we recognize that differentiation under the integrand is only justified when the function (f) and it's derivative (f') are continuous [49]. In our case, even though the source current and its derivative are assumed to be continuous, we see that $f = \vec{\vec{G}}_{\psi_e}(\vec{\lambda}_\rho|z-z')\cdot\vec{\tilde{J}}_e(\vec{\lambda}_\rho|z')$ is not continuous, due to the sgn $(z-z')$ term in the numerator. Furthermore, $\frac{\partial f}{\partial z}$ is not continuous, due to the $|z-z'|$ term in the exponential. Looking at $\vec{\vec{G}}_{\psi_h}$, a similar argument applies. However, breaking the region of interest into two subregions, as shown in Figure 2.2, leads to a Principal Value integration of the form

$$PV\int_a^b dz' = \lim_{\delta\to0}\left[\int_a^{z-\delta} dz' + \int_{z+\delta}^b dz'\right]$$

Now, on each interval, we recognize that f and f' are continuous, thereby satisfying the requirements for interchanging the integral and the differentiation operators. However, we have now introduced variable limits of integration. In order to solve this issue, we use a careful application of the Leibnitz rule. This process will now be demonstrated for $\vec{\vec{G}}_{\psi_e}^p$ and

$\vec{\tilde{G}}^p_{\psi_h}$. Observe that we can now write:

$$\frac{\partial \widetilde{\psi}}{\partial z} = \frac{\partial}{\partial z} \int_a^b \vec{\tilde{G}}^p_{\psi_e}(\vec{\lambda}_\rho | z - z') \cdot \vec{\tilde{J}}_e(\vec{\lambda}_\rho | z') dz' + \frac{\partial}{\partial z} \int_a^b \vec{\tilde{G}}^p_{\psi_h}(\vec{\lambda}_\rho | z - z') \cdot \vec{\tilde{J}}_h(\vec{\lambda}_\rho | z') dz'$$

$$= \frac{\partial}{\partial z} \int_a^b \vec{\tilde{g}}^p_{\psi_e} e^{-j\lambda_{z\psi}|z-z'|} \cdot \vec{\tilde{J}}_e(\vec{\lambda}_\rho, z') dz' + \frac{\partial}{\partial z} \int_a^b \vec{\tilde{g}}^p_{\psi_h} e^{-j\lambda_{z\psi}|z-z'|} \cdot \vec{\tilde{J}}_h(\vec{\lambda}_\rho, z') dz' \qquad (2.64)$$

2.4.1.1 $\vec{\tilde{G}}_{\psi_e}(\vec{\lambda}_\rho, z)$ *Leibnitz Integration.*

Following the prescribed procedure, we break the region of interest into two intervals, such that $[a, b] = \lim_{\delta \to 0} [a, z - \delta) \cup (z + \delta, b]$. This is equivalent to dividing the region into two subregions, $V - V_\delta$ and V_δ, where, in the specified limit, $V_\delta = 0$. Thus, recognizing the first term of (2.64) can be written such that the limits of integration vary according to z:

$$\frac{\partial}{\partial z} \int_a^{z-\delta} \vec{\tilde{g}}^p_{\psi_e} e^{-j\lambda_{z\psi}(z-z')} \cdot \vec{\tilde{J}}_e dz' \qquad \ldots \text{for } z > z' \qquad (2.65a)$$

$$\frac{\partial}{\partial z} \int_{z+\delta}^b \vec{\tilde{g}}^p_{\psi_e} e^{j\lambda_{z\psi}(z-z')} \cdot \vec{\tilde{J}}_e dz' \qquad \ldots \text{for } z < z' \qquad (2.65b)$$

In this case, we see that the signum terms and the absolute value terms take on continuous values on the specified intervals. This allows us to apply the Leibnitz integration rule to (2.65a). Noting $z^- = z - \delta$ and $\lim_{\delta \to 0} z^- = z$ results in

$$\frac{\partial}{\partial z}\int_a^{z^-} \vec{\vec{g}}^{\,p}_{\psi_e} e^{-j\lambda_{z\psi}(z-z')} \cdot \vec{J}_e(z')dz'$$

$$= \lim_{z^-\to z}\left[\int_a^{z^-} \frac{\partial}{\partial z}\vec{\vec{g}}^{\,p}_{\psi_e} e^{-j\lambda_{z\psi}(z-z')} \cdot \vec{J}_e(z')dz' - \overset{0}{\cancel{\frac{\partial a}{\partial z}}}\vec{\vec{g}}^{\,p}_{\psi_e}(z'=a)e^{-j\lambda_{z\psi}(z-a)} \cdot \vec{J}_e(z'=a) \right.$$

$$\left. + \overset{1}{\cancel{\frac{\partial z^-}{\partial z}}}\vec{\vec{g}}^{\,p}_{\psi_e}(z'=z^-)\overbrace{e^{-j\lambda_{z\psi}(z-z^-)}}^{1} \cdot \vec{J}_e(z'=z^-) \right]$$

$$= -\int_a^{z^-} j\lambda_{z\psi}\vec{\vec{g}}^{\,p}_{\psi_e}(\vec{\lambda}_\rho)e^{-j\lambda_{z\psi}(z-z')} \cdot \vec{J}_e(z')dz' + \vec{\vec{g}}^{\,p}_{\psi_e}(z'=z^-)\cdot\vec{J}_e(z) \qquad \dots \text{for } z>z'$$

$$(2.66)$$

Here we have assumed that the source current is continuous, such that $\lim_{\delta\to 0}\vec{J}_e(z-\delta)=\vec{J}_e(z)$. Similarly, applying the Leibnitz integration rule to (2.65b), noting $z^+=z+\delta$ and $\lim_{\delta\to 0}z^+=z$ leads to

$$\frac{\partial}{\partial z}\int_{z^+}^b \vec{\vec{g}}^{\,p}_{\psi_e} e^{j\lambda_{z\psi}(z-z')} \cdot \vec{J}_e(z')dz'$$

$$= \lim_{z^+\to z}\left[\int_{z^+}^b \frac{\partial}{\partial z}\vec{\vec{g}}^{\,p}_{\psi_e} e^{j\lambda_{z\psi}(z-z')} \cdot \vec{J}_e(z')dz' - \overset{1}{\cancel{\frac{\partial z^+}{\partial z}}}\vec{\vec{g}}^{\,p}_{\psi_e}(z'=z^+)\overbrace{e^{-j\lambda_{z\psi}(z-z^+)}}^{1} \cdot \vec{J}_e(z'=z^+) \right.$$

$$\left. + \overset{0}{\cancel{\frac{\partial b}{\partial z}}}\vec{\vec{g}}^{\,p}_{\psi_e}(z'=b)e^{j\lambda_{z\psi}(z-b)} \cdot \vec{J}_e(z'=b) \right]$$

$$= \int_{z^+}^b j\lambda_{z\psi}\vec{\vec{g}}^{\,p}_{\psi_e}(\vec{\lambda}_\rho)e^{j\lambda_{z\psi}(z-z')} \cdot \vec{J}_e(z')dz' - \vec{\vec{g}}^{\,p}_{\psi_e}(z'=z^+)\cdot\vec{J}_e(z) \qquad \dots \text{for } z<z' \quad (2.67)$$

Using (2.66) and (2.67), we can write the electric term in (2.64) as

$$\frac{\partial}{\partial z} \int_a^b \vec{\vec{g}}_{\psi_e}^p e^{-j\lambda_{z\psi}|z-z'|} \cdot \vec{J}_e dz'$$

$$= -j\lambda_{z\psi}\operatorname{sgn}(z-z') \int_a^b \vec{\vec{g}}_{\psi_e}^p e^{-j\lambda_{z\psi}|z-z'|} \cdot \vec{J}_e dz' + \left[\vec{\vec{g}}_{\psi_e}^p(z'=z^-) - \vec{\vec{g}}_{\psi_e}^p(z'=z^+)\right] \cdot \vec{J}_e(z)$$

$$(2.68)$$

Observing the relationship

$$z > z' = z^- \implies \operatorname{sgn}(z - z^-) = +1$$

$$z < z' = z^+ \implies \operatorname{sgn}(z - z^+) = -1$$

We find the Leibnitz contribution:

$$\left[\vec{\vec{g}}_{\psi_e}^p(z'=z^-) - \vec{\vec{g}}_{\psi_e}^p(z'=z^+)\right] \cdot \vec{J}_e(z) = \left[-j\frac{\vec{\lambda}_\rho \frac{\lambda_{z\psi}}{\lambda_\rho^2} + \hat{\mathbf{z}}\frac{\varepsilon_t}{\varepsilon_z}}{2\lambda_{z\psi}} + j\frac{-\vec{\lambda}_\rho \frac{\lambda_{z\psi}}{\lambda_\rho^2} + \hat{\mathbf{z}}\frac{\varepsilon_t}{\varepsilon_z}}{2\lambda_{z\psi}}\right] \cdot \vec{J}_e(z)$$

$$= -\vec{\lambda}_\rho \frac{j}{\lambda_\rho^2} \cdot \vec{J}_e(z) = \tilde{u}_e(\vec{\lambda}_\rho, z)$$

2.4.1.2 $\vec{\vec{G}}_{\psi_h}^p(\vec{\lambda}_\rho, z)$ *Leibnitz Rule.*

Following the same procedure as the previous section, we calculate the Leibnitz contribution for the second term of (2.64) as:

$$\left[\vec{\vec{g}}_{\psi_h}^p(z'=z^-) - \vec{\vec{g}}_{\psi_h}^p(z'=z^+)\right] \cdot \vec{J}_m(z) = \left[-\frac{\hat{\mathbf{z}} \times \vec{\lambda}_\rho \frac{j\omega\varepsilon_t}{\lambda_\rho^2}}{2\lambda_{z\psi}} + \frac{\hat{\mathbf{z}} \times \vec{\lambda}_\rho \frac{j\omega\varepsilon_t}{\lambda_\rho^2}}{2\lambda_{z\psi}}\right] \cdot \vec{J}_m(z) = 0$$

$$(2.69)$$

51

2.4.1.3 $\tilde{u}_e$ Depolarizing Dyad Cancellation.

Recalling the form of $\tilde{\Phi}^p$:

$$
\begin{aligned}
\tilde{\Phi}^p &= \frac{1}{j\omega\varepsilon_t}\left[\frac{\partial\tilde{\psi}^p}{\partial z} - \tilde{u}_e\right] \\[2mm]
&= \frac{1}{j\omega\varepsilon_t}\left\{\int_a^b \frac{\partial}{\partial z}\vec{\tilde{G}}^p_{\psi_e}\cdot\vec{\tilde{J}}_e dz' + \int_a^b \frac{\partial}{\partial z}\vec{\tilde{G}}^p_{\psi_h}\cdot\vec{\tilde{J}}_h dz' - \tilde{u}_e + \tilde{u}_e\right\} \\[2mm]
&= -\frac{1}{j\omega\varepsilon_t}\left[\int_a^b j\lambda_{z\psi}\,\mathrm{sgn}\,(z-z')\,\vec{\tilde{G}}^p_{\psi_e}(\vec{\lambda}_\rho|z-z')\cdot\vec{\tilde{J}}_e(\vec{\lambda}_\rho,z')dz'\right. \\[2mm]
&\qquad\left. + \int_a^b j\lambda_{z\psi}\,\mathrm{sgn}\,(z-z')\,\vec{\tilde{G}}^p_{\psi_h}(\vec{\lambda}_\rho|z-z')\cdot\vec{\tilde{J}}_h(\vec{\lambda}_\rho,z')dz'\right]
\end{aligned}
\tag{2.70}
$$

Therefore, we see that the depolarizing dyad cancels for $\tilde{\Phi}^p$, which is the expected result, since we expect no depolarizing effect in the transverse direction!

2.4.2 $\tilde{\Pi}^p$ Potential.

From the summary in Section 2.1.1, $\tilde{\Pi}^p$ can be written as:

$$
\tilde{\Pi}^p = -\frac{1}{j\omega\mu_t}\left(\frac{\partial\tilde{\theta}^p}{\partial z} + \tilde{u}_h\right)
\tag{2.71}
$$

where:

$$
\tilde{\theta}^p = \int_a^b \vec{\tilde{G}}^p_{\theta_e}(\vec{\lambda}_\rho|z-z')\cdot\vec{\tilde{J}}_e(\vec{\lambda}_\rho,z')dz' + \int_a^b \vec{\tilde{G}}^p_{\theta_h}(\vec{\lambda}_\rho|z-z')\cdot\vec{\tilde{J}}_h(\vec{\lambda}_\rho,z')dz'
\tag{2.72}
$$

Following the same procedure as in the previous section reveals a Leibnitz contribution that exactly cancels the $\tilde{u}_h$ term, allowing us to write the expected result:

$$\tilde{\Pi}^p = \frac{1}{j\omega\mu_t} \left[\int_a^b j\lambda_{z\theta}\mathrm{sgn}\,(z-z')\, \bar{\bar{G}}^p_{\theta_e}(\vec{\lambda}_\rho|z - z')\cdot\vec{\tilde{J}}_e(\vec{\lambda}_\rho, z')dz' \right.$$

$$\left. + \int_a^b j\lambda_{z\theta}\mathrm{sgn}\,(z-z')\, \bar{\bar{G}}^p_{\theta_h}(\vec{\lambda}_\rho|z - z')\cdot\vec{\tilde{J}}_h(\vec{\lambda}_\rho, z')dz' \right]$$

(2.73)

2.5 Scattered Solution for Parallel Plate Wave Guide (PPWG) Boundary Conditions

Now that we have determined the principal solution in the transform domain for unbounded uniaxial media, we will find the scattered solution inside a Parallel Plate Waveguide (PPWG), since this is the physical form of the tFWMT. Then, finally, we will combine the principal and scattered solutions and enforce the boundary conditions for a PPWG. Recall the principal Green's function was found from the system of coupled differential equations derived from the application of Helmholtz's theorem to Maxwell's equations. Due to the presence of the parallel plate walls in the z dimension, we are only able to transform on the transverse dimensions in this case. Therefore, the scattered solution is the solution to the system of homogeneous forms of (2.38) (found by setting $\tilde{s}_1 = \tilde{s}_2 = 0$):

$$\tilde{L}_1\tilde{\psi}^s = 0$$
$$\tilde{L}_2\tilde{\theta}^s = 0$$

(2.74)

A non-trivial solution to (2.74) only exists for $\tilde{\psi}^s$ and $\tilde{\theta}^s$ with $\lambda_z = \pm\lambda_{z\psi}$ and $\lambda_z = \pm\lambda_{z\theta}$, respectively. Because we expect upward and downward propagating waves, we assume a solution of the form

$$\tilde{\psi}^s = \tilde{\psi}^+e^{-j\lambda_{z\psi}z} + \tilde{\psi}^-e^{j\lambda_{z\psi}z}$$
$$\tilde{\theta}^s = \tilde{\theta}^+e^{-j\lambda_{z\theta}z} + \tilde{\theta}^-e^{j\lambda_{z\theta}z}$$

(2.75)

53

Then, we can express the total potentials as:

$$\widetilde{\psi} = \widetilde{\psi}^p + \widetilde{\psi}^s = \widetilde{\psi}^p + \widetilde{\psi}^+ e^{-j\lambda_{z\psi}z} + \widetilde{\psi}^- e^{j\lambda_{z\psi}z} \tag{2.76}$$

$$\widetilde{\theta} = \widetilde{\theta}^p + \widetilde{\theta}^s = \widetilde{\theta}^p + \widetilde{\theta}^+ e^{-j\lambda_{z\theta}z} + \widetilde{\theta}^- e^{j\lambda_{z\theta}z} \tag{2.77}$$

where $\widetilde{\psi}^+, \widetilde{\psi}^-, \widetilde{\theta}^+$ and $\widetilde{\theta}^-$ are the unknown scattering coefficients, which can be found by applying the appropriate boundary conditions.

2.5.1 PPWG Boundary Conditions.

Since the walls of the PPWG are assumed to be PEC, the boundary conditions are enforced on the tangential electric fields, which will in turn give the appropriate boundary conditions for the potentials. It is assumed the walls of the parallel plate waveguide lie in planes of constant z. The walls of the parallel plate are assumed to have infinite conductivity (PEC). For such a material, the boundary condition is $\hat{n} \times \vec{E} = 0$, or $\vec{E}_t = 0$. Enforcing this on our form of the tangential electric field leads to:

$$\vec{E}_t = \nabla_t \Phi + \nabla_t \times \hat{\mathbf{z}} \theta = 0 \tag{2.78}$$

It is important to remember that the boundary conditions are imposed on the *total* fields, thus the boundary conditions must be imposed on the *total* potentials. Since the potentials are based on Helmholtz's theorem, they are independent and therefore must independently satisfy the boundary conditions. This leads to four equations for our four unknown scattering coefficients:

$$\widetilde{\Phi}\Big|_{z=0} = \frac{1}{j\omega\varepsilon_t}\left(\frac{\partial\widetilde{\psi}(z=0)}{\partial z} - \widetilde{u}_e(z=0)\right) = 0 \tag{2.79}$$

$$\widetilde{\theta}\Big|_{z=0} = 0 \tag{2.80}$$

$$\widetilde{\Phi}\Big|_{z=d} = \frac{1}{j\omega\varepsilon_t}\left(\frac{\partial\widetilde{\psi}(z=d)}{\partial z} - \widetilde{u}_e(z=d)\right) = 0 \tag{2.81}$$

$$\widetilde{\theta}\Big|_{z=d} = 0 \tag{2.82}$$

Now, we can apply these boundary conditions to find the total Green's function. In the process, we have inserted reflection coefficients $(R_\psi, \overline{R}_\psi, R_\theta, \overline{R}_\theta)$ in order to keep track of the terms. This might at first seem unnecessary, but will provide a very useful physical interpretation of the final solution. Additionally, we note that the integration limits z_1' and z_2' are used to derive generalized expressions and will eventually be replaced with values that represent the actual extent of the system.

- $\widetilde{\Phi}$ at z=0

$$\left.\widetilde{\Phi}\right|_{z=0} = 0 = \left.\frac{1}{j\omega\varepsilon_t}\left[\frac{\partial\widetilde{\psi}}{\partial z} - \widetilde{u}_e\right]\right|_{z=0}$$

$$0 = \left.\left[\frac{\partial\widetilde{\psi}^p}{\partial z} - \widetilde{u}_e + \frac{\partial\widetilde{\psi}^s}{\partial z}\right]\right|_{z=0}$$

$$0 = \left.\left[\int_{z_1'}^{z_2'}\frac{\partial}{\partial z}\vec{\vec{G}}_{\psi_e}^p\cdot\vec{J}_e dz' + \int_{z_1'}^{z_2'}\frac{\partial}{\partial z}\vec{\vec{G}}_{\psi_h}^p\cdot\vec{J}_h dz' - j\lambda_{z\psi}\widetilde{\psi}^+ e^{-j\lambda_{z\psi}z} + j\lambda_{z\psi}\widetilde{\psi}^- e^{j\lambda_{z\psi}z}\right]\right|_{z=0}$$

$$0 = \left[-j\lambda_{z\psi}\mathrm{sgn}\,(z-z')\int_{z_1'}^{z_2'}\vec{\vec{G}}_{\psi_e}^p\cdot\vec{J}_e dz' - j\lambda_{z\psi}\mathrm{sgn}\,(z-z')\int_{z_1'}^{z_2'}\vec{\vec{G}}_{\psi_h}^p\cdot\vec{J}_h dz'\right.$$

$$\left.\left. - j\lambda_{z\psi}\widetilde{\psi}^+ e^{-j\lambda_{z\psi}z} + j\lambda_{z\psi}\widetilde{\psi}^- e^{j\lambda_{z\psi}z}\right]\right|_{z=0}$$

$$0 = \overbrace{\underbrace{\int_{z_1'}^{z_2'}\vec{\vec{G}}_{\psi_e}^p(z=0)\cdot\vec{J}_e dz'}_{V_{\psi_e}^-} + \underbrace{\int_{z_1'}^{z_2'}\vec{\vec{G}}_{\psi_h}^p(z=0)\cdot\vec{J}_h dz'}_{V_{\psi_h}^-}}^{V_\psi^-} -\widetilde{\psi}^+ + \widetilde{\psi}^-$$

$$\boxed{\widetilde{\psi}^+ = R_\psi V_\psi^- + R_\psi\widetilde{\psi}^- \rightarrow R_\psi = 1} \qquad (2.83)$$

55

- $\widetilde{\Phi}$ at z=d

$$\widetilde{\Phi}\Big|_{z=d} = 0 = \frac{1}{j\omega\varepsilon_t}\left[\frac{\partial\widetilde{\psi}}{\partial z} - \widetilde{u}_e\right]\Big|_{z=d}$$

$$0 = \left[-j\lambda_{z\psi}\int_{z_1'}^{z_2'}\mathrm{sgn}\,(z-z')\,\vec{\bar{G}}_{\psi_e}^p\cdot\vec{\widetilde{J}}_e dz' - j\lambda_{z\psi}\int_{z_1'}^{z_2'}\mathrm{sgn}\,(z-z')\,\vec{\bar{G}}_{\psi_h}^p\cdot\vec{\widetilde{J}}_h dz'\right.$$

$$\left.-\,j\lambda_{z\psi}\widetilde{\psi}^+ e^{-j\lambda_{z\psi}z} + j\lambda_{z\psi}\widetilde{\psi}^- e^{j\lambda_{z\psi}z}\right]\Bigg|_{z=d}$$

$$0 = -\int_{z_1'}^{z_2'}\vec{\bar{G}}_{\psi_e}^p(z=d)\cdot\vec{\widetilde{J}}_e dz' - \int_{z_1'}^{z_2'}\vec{\bar{G}}_{\psi_h}^p(z=d)\cdot\vec{\widetilde{J}}_h dz' - \widetilde{\psi}^+ e^{-j\lambda_{z\psi}d} + \widetilde{\psi}^- e^{j\lambda_{z\psi}d}$$

$$0 = -e^{-j\lambda_{z\psi}d}\int_{z_1'}^{z_2'}\vec{\bar{g}}_{\psi_e}^p(z=d)e^{j\lambda_{z\psi}z'}\cdot\vec{\widetilde{J}}_e dz' - e^{-j\lambda_{z\psi}d}\int_{z_1'}^{z_2'}\vec{\bar{g}}_{\psi_h}^p(z=d)e^{j\lambda_{z\psi}z'}\cdot\vec{\widetilde{J}}_h dz'$$

$$-\,\widetilde{\psi}^+ e^{-j\lambda_{z\psi}d} + \widetilde{\psi}^- e^{j\lambda_{z\psi}d}$$

$$0 = \overbrace{\underbrace{-\int_{z_1'}^{z_2'}\vec{\bar{g}}_{\psi_e}^p(z=d)e^{j\lambda_{z\psi}z'}\cdot\vec{\widetilde{J}}_e dz'}_{V_{\psi_e}^+} \underbrace{-\int_{z_1'}^{z_2'}\vec{\bar{g}}_{\psi_h}^p(z=d)e^{j\lambda_{z\psi}z'}\cdot\vec{\widetilde{J}}_h dz'}_{V_{\psi_h}^+}}^{V_\psi^+} -\widetilde{\psi}^+ + \widetilde{\psi}^- e^{j2\lambda_{z\psi}d}$$

$$\boxed{\widetilde{\psi}^- = \overline{R}_\psi V_\psi^+ e^{-j2\lambda_{z\psi}d} + \overline{R}_\psi\widetilde{\psi}^+ e^{-j2\lambda_{z\psi}d} \rightarrow \overline{R}_\psi = 1} \qquad (2.84)$$

- $\widetilde{\theta}$ at z=0

$$\widetilde{\theta}\Big|_{z=0} = 0 = \left[\int_{z_1'}^{z_2'}\vec{\bar{G}}_{\theta_e}^p\cdot\vec{\widetilde{J}}_e dz' + \int_{z_1'}^{z_2'}\vec{\bar{G}}_{\theta_h}^p\cdot\vec{\widetilde{J}}_h dz' + \widetilde{\theta}^+ e^{-j\lambda_{z\theta}z} + \widetilde{\theta}^- e^{j\lambda_{z\theta}z}\right]\Bigg|_{z=0}$$

56

$$0 = \overbrace{\underbrace{\int_{z_1'}^{z_2'} \vec{\vec{G}}_{\theta_e}^p(z=0) \cdot \vec{J}_e dz'}_{V_{\theta_e}^-} + \underbrace{\int_{z_1'}^{z_2'} \vec{\vec{G}}_{\theta_h}^p(z=0) \cdot \vec{J}_h dz'}_{V_{\theta_h}^-}}^{V_\theta^-} + \tilde{\theta}^+ + \tilde{\theta}^-$$

$$\boxed{\tilde{\theta}^+ = R_\theta V_\theta^- + R_\theta \tilde{\theta}^- \rightarrow R_\theta = -1} \tag{2.85}$$

- $\tilde{\theta}$ at z=d

$$\tilde{\theta}\Big|_{z=d} = 0 = \int_{z_1'}^{z_2'} \vec{\vec{g}}_{\theta_e}^p(z=d) e^{j\lambda_{z\theta}z'} e^{-j\lambda_{z\theta}d} \cdot \vec{J}_e dz' + \int_{z_1'}^{z_2'} \vec{\vec{g}}_{\theta_h}^p(z=d) e^{j\lambda_{z\theta}z'} e^{-j\lambda_{z\theta}d} \cdot \vec{J}_h dz'$$

$$+ \tilde{\theta}^+ e^{-j\lambda_{z\theta}d} + \tilde{\theta}^- e^{j\lambda_{z\theta}d}$$

$$0 = \overbrace{\underbrace{\int_{z_1'}^{z_2'} \vec{\vec{g}}_{\theta_e}^p(z=d) e^{j\lambda_{z\theta}z'} \cdot \vec{J}_e dz'}_{V_{\theta_e}^+} + \underbrace{\int_{z_1'}^{z_2'} \vec{\vec{g}}_{\theta_h}^p(z=d) e^{j\lambda_{z\theta}z'} \cdot \vec{J}_h dz'}_{V_{\theta_h}^+}}^{V_\theta^+} + \tilde{\theta}^+ + \tilde{\theta}^- e^{j2\lambda_{z\theta}d}$$

$$\boxed{\tilde{\theta}^- = \overline{R}_\theta V_\theta^+ e^{-j2\lambda_{z\theta}d} + \overline{R}_\theta \tilde{\theta}^+ e^{-j2\lambda_{z\theta}d} \rightarrow \overline{R}_\theta = -1} \tag{2.86}$$

Now that we have applied the boundary conditions, we seek the unknown scattering coefficients. Substituting (2.84) into (2.83), we find:

$$\boxed{\tilde{\psi}^+ = \frac{R_\psi V_\psi^- + R_\psi \overline{R}_\psi V_\psi^+ e^{-j2\lambda_{z\psi}d}}{1 - R_\psi \overline{R}_\psi e^{-j2\lambda_{z\psi}d}}} \tag{2.87}$$

Substituting (2.83) into (2.84), we find

$$\boxed{\tilde{\psi}^- = \frac{\overline{R}_\psi V_\psi^+ e^{-j2\lambda_{z\psi}d} + R_\psi \overline{R}_\psi V_\psi^- e^{-j2\lambda_{z\psi}d}}{1 - R_\psi \overline{R}_\psi e^{-j2\lambda_{z\psi}d}}} \tag{2.88}$$

Similarly, substituting (2.86) into (2.85), we find

$$\widetilde{\theta}^+ = \frac{R_\theta V_\theta^- + R_\theta \overline{R}_\theta V_\theta^+ e^{-j2\lambda_{z\theta}d}}{1 - R_\theta \overline{R}_\theta e^{-j2\lambda_{z\theta}d}} \tag{2.89}$$

Finally, substituting (2.85) into (2.86), we find

$$\widetilde{\theta}^- = \frac{\overline{R}_\theta V_\theta^+ e^{-j2\lambda_{z\theta}d} + R_\theta \overline{R}_\theta V_\theta^- e^{-j2\lambda_{z\theta}d}}{1 - R_\theta \overline{R}_\theta e^{-j2\lambda_{z\theta}d}} \tag{2.90}$$

2.5.2 Scattered Solution Summary.

$$\widetilde{\psi}^s = \widetilde{\psi}^+ e^{-j\lambda_{z\psi}z} + \widetilde{\psi}^- e^{j\lambda_{z\psi}z} \qquad \widetilde{\theta}^s = \widetilde{\theta}^+ e^{-j\lambda_{z\theta}z} + \widetilde{\theta}^- e^{j\lambda_{z\theta}z}$$

$$\widetilde{\psi}^+ = \frac{R_\psi V_\psi^- + R_\psi \overline{R}_\psi V_\psi^+ e^{-j2\lambda_{z\psi}d}}{1 - R_\psi \overline{R}_\psi e^{-j2\lambda_{z\psi}d}} \qquad \widetilde{\psi}^- = \frac{\overline{R}_\psi V_\psi^+ e^{-j2\lambda_{z\psi}d} + R_\psi \overline{R}_\psi V_\psi^- e^{-j2\lambda_{z\psi}d}}{1 - R_\psi \overline{R}_\psi e^{-j2\lambda_{z\psi}d}}$$

$$\widetilde{\theta}^+ = \frac{R_\theta V_\theta^- + R_\theta \overline{R}_\theta V_\theta^+ e^{-j2\lambda_{z\theta}d}}{1 - R_\theta \overline{R}_\theta e^{-j2\lambda_{z\theta}d}} \qquad \widetilde{\theta}^- = \frac{\overline{R}_\theta V_\theta^+ e^{-j2\lambda_{z\theta}d} + R_\theta \overline{R}_\theta V_\theta^- e^{-j2\lambda_{z\theta}d}}{1 - R_\theta \overline{R}_\theta e^{-j2\lambda_{z\theta}d}}$$

$$R_\psi, \overline{R}_\psi = 1 \qquad \text{and} \qquad R_\theta, \overline{R}_\theta = -1$$

$$V_\psi^- = V_{\psi_e}^- + V_{\psi_h}^- = \int_0^d \vec{\vec{g}}_{\psi_e}^{\,p}(z=0)e^{-j\lambda_{z\psi}z'} \cdot \vec{\vec{J}}_e dz' + \int_0^d \vec{\vec{g}}_{\psi_h}^{\,p}(z=0)e^{-j\lambda_{z\psi}z'} \cdot \vec{\vec{J}}_h dz'$$

$$V_\psi^+ = V_{\psi_e}^+ + V_{\psi_h}^+ = \int_0^d \vec{\vec{g}}_{\psi_e}^{\,p}(z=d)e^{j\lambda_{z\psi}z'} \cdot \vec{\vec{J}}_e dz' + \int_0^d \vec{\vec{g}}_{\psi_h}^{\,p}(z=d)e^{j\lambda_{z\psi}z'} \cdot \vec{\vec{J}}_h dz'$$

$$V_\theta^- = V_{\theta_e}^- + V_{\theta_h}^- = \int_0^d \vec{\vec{g}}_{\theta_e}^{\,p}(z=0)e^{-j\lambda_{z\theta}z'} \cdot \vec{\vec{J}}_e dz' + \int_0^d \vec{\vec{g}}_{\theta_h}^{\,p}(z=0)e^{-j\lambda_{z\theta}z'} \cdot \vec{\vec{J}}_h dz'$$

$$V_\theta^+ = V_{\theta_e}^+ + V_{\theta_h}^+ = \int_0^d \vec{\vec{g}}_{\theta_e}^{\,p}(z=d)e^{j\lambda_{z\theta}z'} \cdot \vec{\vec{J}}_e dz' + \int_0^d \vec{\vec{g}}_{\theta_h}^{\,p}(z=d)e^{j\lambda_{z\theta}z'} \cdot \vec{\vec{J}}_h dz'$$

$$\tag{2.91}$$

Here we have changed the integration limits from $a > z' > b$ to $d > z' > 0$ in anticipation of the physical geometry of a parallel plate system of width d. The next step is to expand the solutions found above and evaluate the scattered potentials. This will allow us to subsequently find the total potentials.

2.5.3 $\widetilde{\psi}^s$ Potential.

We can find the scattered potential $\widetilde{\psi}^s$ by substituting in the scattering coefficients and simplifying.

$$
\begin{aligned}
\widetilde{\psi}^s &= \widetilde{\psi}^+ e^{-j\lambda_{z\psi} z} + \widetilde{\psi}^- e^{j\lambda_{z\psi} z} \\
&= \frac{R_\psi V_\psi^- e^{-j\lambda_{z\psi} z} + R_\psi \overline{R}_\psi V_\psi^+ e^{-j\lambda_{z\psi}(2d+z)} + R_\psi V_\psi^+ e^{-j\lambda_{z\psi}(2d-z)} + R_\psi \overline{R}_\psi V_\psi^- e^{-j\lambda_{z\psi}(2d-z)}}{1 - R_\psi \overline{R}_\psi e^{-j2\lambda_{z\psi} d}}
\end{aligned}
\tag{2.92}
$$

Since V_ψ^- and V_ψ^+ both contain electric and magnetic terms, we break $\widetilde{\psi}$ into those two separate terms, for convenience. Therefore, recognizing $\widetilde{\psi} = \widetilde{\psi}_e + \widetilde{\psi}_h$, we can write

$$
\begin{aligned}
\widetilde{\psi}^s_{(e,h)} &= \frac{R_\psi V_{\psi_{(e,h)}}^- e^{-j\lambda_{z\psi} z} + R_\psi \overline{R}_\psi V_{\psi_{(e,h)}}^+ e^{-j\lambda_{z\psi}(2d+z)}}{1 - R_\psi \overline{R}_\psi e^{-j2\lambda_{z\psi} d}} \\
&\quad + \frac{\overline{R}_\psi V_{\psi_{(e,h)}}^+ e^{-j\lambda_{z\psi}(2d-z)} + R_\psi \overline{R}_\psi V_{\psi_{(e,h)}}^- e^{-j\lambda_{z\psi}(2d-z)}}{1 - R_\psi \overline{R}_\psi e^{-j2\lambda_{z\psi} d}} \\[2mm]
&= \int_0^d \left\{ \frac{R_\psi \vec{\vec{g}}_{\psi_{(e,h)}}(z=0) e^{-j\lambda_{z\psi}(z+z')} + R_\psi \overline{R}_\psi \vec{\vec{g}}_{\psi_{(e,h)}}(z=d) e^{-j\lambda_{z\psi}(2d+z-z')}}{1 - R_\psi \overline{R}_\psi e^{-j2\lambda_{z\psi} d}} \right. \\
&\quad \left. + \frac{\overline{R}_\psi \vec{\vec{g}}_{\psi_{(e,h)}}(z=d) e^{-j\lambda_{z\psi}(2d-z-z')} + R_\psi \overline{R}_\psi \vec{\vec{g}}_{\psi_{(e,h)}}(z=0) e^{-j\lambda_{z\psi}(2d-z+z')}}{1 - R_\psi \overline{R}_\psi e^{-j2\lambda_{z\psi} d}} \right\} \cdot \vec{J}_{(e,h)} dz'
\end{aligned}
\tag{2.93}
$$

$$
= \int_0^d \vec{\vec{G}}^s_{\psi_{(e,h)}} \cdot \vec{J}_{(e,h)} dz'
$$

We can now step back from the mathematics for a moment and compare (2.93) with the expected physical result.
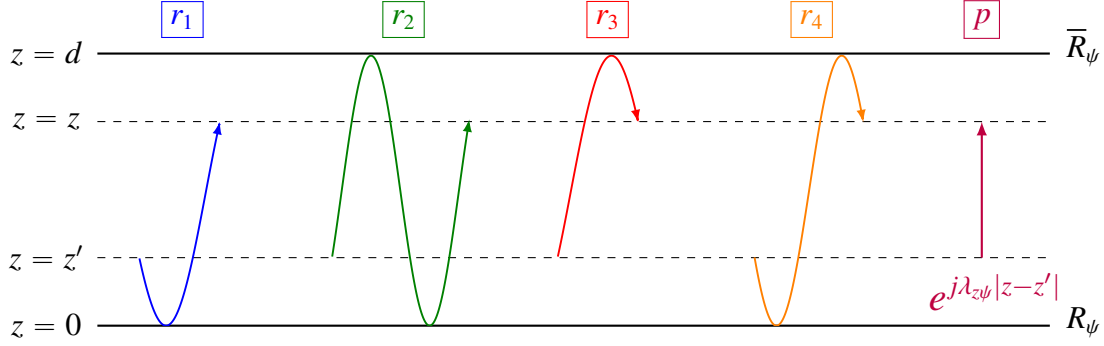
Figure 2.3: A visual representation of the terms given in (2.93). The terms represent waves that are reflected from the top and bottom of the parallel plate. The path r_1 represents the first term, path r_2 represents the second term, path r_3 represents the third term and the path r_4 represents the fourth. The principal solution is also shown on the far right.

From Figure 3.1, we can see that there are 4 distinct possibilities for a wave radiated in a PPWG. The first is a wave that originates at $z = z'$, then propagates downward from the source and is reflected off of the bottom plate, then observed at point z. This is represented by the path r_1 and corresponds to the first term in (2.93), as it contains the appropriate reflection coefficient, R_ψ and the appropriate phase shift in the exponential $(z + z')$. The second possibility is a wave that originates at $z = z'$, then propagates upward, reflects of the top plate, then the bottom plate and is observed at point z. Accordingly, this is represented by path r_2 and corresponds to the second term in (2.93), as it contains both the R_ψ and $\overline{R}_\psi$ reflection terms and the appropriate phase shift in the exponential $(2d + z - z')$. The third possibility is a wave originating at $z = z'$, which propagates upward, reflects off the top plate and is observed at z. This is represented by path r_3 and corresponds to the third term in (2.93), which contains only the reflection coefficient from the top plate

60

and the appropriate phase shift in the exponential $(2d - z - z')$. The last possibility is a wave that originates at $z = z'$, propagates downward, reflects off of the bottom plate, then the top plate and is observed at z. This is represented by path r_4 and corresponds to the fourth term in (2.93), as it contains both the top and bottom reflection coefficients and the appropriate phase shift in the exponential $(2d - z + z')$. Finally, the principal solution is shown as the path p, and is seen to be the direct path between the source and observation. Therefore, we see that the equation we have obtained at this point is in complete agreement with the physically expected situation. In this discussion, we have only considered the four fundamental cases, but the poles in the denominator implicate an infinite sum of this fundamental wave set (since $\lambda_{z\psi}$ contains $\lambda_\rho^2 = \lambda_x^2 + \lambda_y^2$, which will be reverse transformed into the spatial domain using a double integral from $-\infty$ to ∞).

2.5.4 $\widetilde{\theta}^s$ *Potential.*

Now, we turn our attention to the $\widetilde{\theta}^s$ potential, using the same procedure we used for the $\widetilde{\psi}^s$. potential. We can find the scattered potential $\widetilde{\theta}^s$ by substituting in the scattering coefficients and simplifying.

$$
\begin{aligned}
\widetilde{\theta}^s &= \widetilde{\theta}^+ e^{-j\lambda_{z\theta}z} + \widetilde{\theta}^- e^{j\lambda_{z\theta}z} \\
&= \frac{R_\theta V_\theta^- e^{-j\lambda_{z\theta}z} + R_\theta \overline{R}_\theta V_\theta^+ e^{-j\lambda_{z\theta}(2d+z)} + R_\theta V_\theta^+ e^{-j\lambda_{z\theta}(2d-z)} + R_\theta \overline{R}_\theta V_\theta^- e^{-j\lambda_{z\theta}(2d-z)}}{1 - R_\theta \overline{R}_\theta e^{-j2\lambda_{z\theta}d}}
\end{aligned}
$$

Since V_θ^- and V_θ^+ both contain electric and magnetic source terms, we break $\widetilde{\theta}$ into those two separate terms, for convenience. Therefore, recognizing $\widetilde{\theta} = \widetilde{\theta}_e + \widetilde{\theta}_h$, we can write

$$\tilde{\theta}^s_{e,h} = \frac{R_\theta V^-_{\theta_{(e,h)}} e^{-j\lambda_{z\theta} z} + R_\theta \overline{R}_\theta V^+_{\theta_{(e,h)}} e^{-j\lambda_{z\theta}(2d+z)} + \overline{R}_\theta V^+_{\theta_{(e,h)}} e^{-j\lambda_{z\theta}(2d-z)} + R_\theta \overline{R}_\theta V^-_{\theta_{(e,h)}} e^{-j\lambda_{z\theta}(2d-z)}}{1 - R_\theta \overline{R}_\theta e^{-j2\lambda_{z\theta} d}}$$

$$= \int_0^d \left\{ \frac{R_\theta \vec{\tilde{g}}_{\theta_{(e,h)}}(z=0) e^{-j\lambda_{z\theta}(z+z')} + R_\theta \overline{R}_\theta \vec{\tilde{g}}_{\theta_{(e,h)}}(z=d) e^{-j\lambda_{z\theta}(2d+z-z')}}{1 - R_\theta \overline{R}_\theta e^{-j2\lambda_{z\theta} d}} \right.$$

$$\left. + \frac{\overline{R}_\theta \vec{\tilde{g}}_{\theta_{(e,h)}}(z=d) e^{-j\lambda_{z\theta}(2d-z-z')} + R_\theta \overline{R}_\theta \vec{\tilde{g}}_{\theta_{(e,h)}}(z=0) e^{-j\lambda_{z\theta}(2d-z+z')}}{1 - R_\theta \overline{R}_\theta e^{-j2\lambda_{z\theta} d}} \right\} \cdot \vec{\tilde{J}}_{(e,h)} dz'$$

$$= \int_0^d \vec{\tilde{G}}_{\theta_{(e,h)}} \cdot \vec{\tilde{J}}_{(e,h)} dz'$$

(2.94)

which is seen to conform to a similar analysis as the $\tilde{\psi}^s$ potential.

2.6 Total Green's Function

Now that we have found the scattered potentials, we can work towards a total Green's function and, finally, the electric and magnetic fields. We begin by combining the principal and scattered potentials to find the total potentials.

2.6.1 $\tilde{\psi}_e$ Potential.

The total potential, $\tilde{\psi}_e$ is

$$\tilde{\psi}_e = \tilde{\psi}^p_e + \tilde{\psi}^s_e$$

$$= \int_0^d \left\{ \frac{\vec{\tilde{G}}^p_{\psi_e}\left(1 - R_\psi \overline{R}_\psi e^{-j2\lambda_{z\psi} d}\right) + R_\psi \vec{\tilde{g}}^p_{\psi_e}(z=0) e^{-j\lambda_{z\psi}(z+z')} + R_\psi \overline{R}_\psi \vec{\tilde{g}}^p_{\psi_e}(z=d) e^{-j\lambda_{z\psi}(2d+z-z')}}{1 - R_\psi \overline{R}_\psi e^{-j2\lambda_{z\psi} d}} \right.$$

$$\left. + \frac{\overline{R}_\psi \vec{\tilde{g}}^p_{\psi_e}(z=d) e^{-j\lambda_{z\psi}(2d-z-z')} + R_\psi \overline{R}_\psi \vec{\tilde{g}}^p_{\psi_e}(z=0) e^{-j\lambda_{z\psi}(2d-z+z')}}{1 - R_\psi \overline{R}_\psi e^{-j2\lambda_{z\psi} d}} \right\} \cdot \vec{\tilde{J}}_e dz'$$

62

which, after some algebraic manipulation using the Euler identities and letting $R_\psi = \overline{R}_\psi = 1$, can be written as

$$
\tilde{\psi}_e = \int_0^d \left\{ \frac{\vec{\tilde{g}}^{\,p}_{\psi_e} e^{j\lambda_{z\psi}(d-|z-z'|)} - \vec{\tilde{g}}^{\,p}_{\psi_e} R_\psi \overline{R}_\psi e^{-j\lambda_{z\psi}(d+|z-z'|)} + \vec{\tilde{g}}^{\,p}_{\psi_e}(z=0) e^{-j\lambda_{z\psi}(-d+z+z')}}{j2\sin(\lambda_{z\psi}d)} \right.
$$
$$
\left. + \frac{\vec{\tilde{g}}^{\,p}_{\psi_e}(z=d) e^{-j\lambda_{z\psi}(d+z-z')} + \vec{\tilde{g}}^{\,p}_{\psi_e}(z=d) e^{-j\lambda_{z\psi}(d-z-z')} + \vec{\tilde{g}}^{\,p}_{\psi_e}(z=0) e^{-j\lambda_{z\psi}(d-z+z')}}{j2\sin(\lambda_{z\psi}d)} \right\} \cdot \vec{\tilde{J}}_e dz'
$$

$$(2.95)$$

2.6.1.1 $\tilde{\psi}_{et}$ Potential.

From the form of the Green's functions for $\tilde{\psi}$ given in 2.3.1, we see that it is possible to examine the longitudinal and transverse parts of the total potential separately, such that $\tilde{\psi}_e = \tilde{\psi}_{et} + \tilde{\psi}_{ez}$. We will first investigate the transverse portion:

$$
\vec{\tilde{g}}^{\,p}_{\psi_{et}} = -\vec{\lambda}_\rho \frac{j\,\mathrm{sgn}\,(z-z')}{2\lambda_\rho^2}
$$

Using this equation, (2.95) becomes

$$
\tilde{\psi}_{et} = \int_0^d \left(-\frac{\vec{\lambda}_\rho}{2\lambda_\rho^2} \right) \left\{ \frac{\mathrm{sgn}\,(z-z')\,e^{j\lambda_{z\psi}(d-|z-z'|)} - \mathrm{sgn}\,(z-z')\,e^{-j\lambda_{z\psi}(d+|z-z'|)} - e^{-j\lambda_{z\psi}(-d+z+z')}}{2\sin(\lambda_{z\psi}d)} \right.
$$
$$
\left. + \frac{e^{-j\lambda_{z\psi}(d+z-z')} + e^{-j\lambda_{z\psi}(d-z-z')} - e^{-j\lambda_{z\psi}(d-z+z')}}{2\sin(\lambda_{z\psi}d)} \right\} \cdot \vec{\tilde{J}}_e dz'
$$

$$(2.96)$$

While we have now found the total Green's function, we anticipate a solution representing standing waves in the PPWG geometry. We can use the Euler identities to find such a representation of $\tilde{\psi}_{et}$. Due to the $|z-z'|$ term, we must investigate two cases: $z > z'$ and $z < z'$.

- $z > z' \implies |z - z'| = (z - z')$ and $\operatorname{sgn}(z - z') = +1$

$$\widetilde{\psi}_{et} = \int_0^d \left(-\frac{\vec{\lambda}_\rho}{2\lambda_\rho^2} \right) \left\{ \frac{e^{j\lambda_{z\psi}(d-z+z')} - e^{-j\lambda_{z\psi}(d+z-z')} - e^{j\lambda_{z\psi}(d-z-z')}}{2\sin(\lambda_{z\psi}d)} \right.$$

$$\left. + \frac{e^{-j\lambda_{z\psi}(d+z-z')} + e^{-j\lambda_{z\psi}(d-z-z')} - e^{-j\lambda_{z\psi}(d-z+z')}}{2\sin(\lambda_{z\psi}d)} \right\} \cdot \vec{\widetilde{J}}_e dz'$$

$$= \int_0^d \left(-\vec{\lambda}_\rho \frac{j}{2\lambda_\rho^2} \right) \left\{ \frac{\sin(\lambda_{z\psi}[d - (z - z')]) - \sin(\lambda_{z\psi}[d - (z + z')])}{\sin(\lambda_{z\psi}d)} \right\} \cdot \vec{\widetilde{J}}_e dz'$$

$$(2.97)$$

- $z < z' \implies |z - z'| = -(z - z')$ and $\operatorname{sgn}(z - z') = -1$

$$\widetilde{\psi}_{et} = \int_0^d \left(-\frac{\vec{\lambda}_\rho}{2\lambda_\rho^2} \right) \left\{ \frac{-e^{j\lambda_{z\psi}(d+z-z')} + e^{-j\lambda_{z\psi}(d-z+z')} - e^{-j\lambda_{z\psi}(d-z-z')}}{2\sin(\lambda_{z\psi}d)} \right.$$

$$\left. + \frac{+e^{-j\lambda_{z\psi}(d+z-z')} + e^{-j\lambda_{z\psi}(d-z-z')} - e^{-j\lambda_{z\psi}(d-z+z')}}{2\sin(\lambda_{z\psi}d)} \right\} \cdot \vec{\widetilde{J}}_e dz'$$

$$= \int_0^d \left(-\vec{\lambda}_\rho \frac{j}{2\lambda_\rho^2} \right) \left\{ \frac{-\sin(\lambda_{z\psi}[d + (z - z')]) - \sin(\lambda_{z\psi}[d - (z + z')])}{\sin(\lambda_{z\psi}d)} \right\} \cdot \vec{\widetilde{J}}_e dz'$$

$$(2.98)$$

We can write (2.97) and (2.98) concisely as

$$\boxed{\widetilde{\psi}_{et} = \int_0^d \left(-\vec{\lambda}_\rho \frac{j}{2\lambda_\rho^2} \right) \left\{ \frac{\operatorname{sgn}(z-z')\sin(\lambda_{z\psi}[d-|z-z'|]) - \sin(\lambda_{z\psi}[d-(z+z')])}{\sin(\lambda_{z\psi}d)} \right\} \cdot \vec{\widetilde{J}}_e dz'}$$

$$(2.99)$$

2.6.1.2 $\widetilde{\psi}_{ez}$ *Potential.*

Now, we turn our attention to the longitudinal portion of $\widetilde{\psi}$. From Section 2.3.1, we have

$$\vec{g}^{\,p}_{\psi_{ez}} = -\hat{\mathbf{z}}\frac{j\varepsilon_t}{2\lambda_{z\psi}\varepsilon_z}$$

Using this equation and again converting to a standing wave form, (2.95), becomes

$$\widetilde{\psi}_{ez} = \int_0^d \left(-\hat{\mathbf{z}}\frac{\varepsilon_t}{2\lambda_{z\psi}\varepsilon_z}\right) \left\{\frac{\cos\left(\lambda_{z\psi}\left[d - |z - z'|\right]\right) + \cos\left(\lambda_{z\psi}\left[d - (z + z')\right]\right)}{\sin\left(\lambda_{z\psi}d\right)}\right\} \cdot \vec{\tilde{J}}_e dz'$$

$$(2.100)$$

2.6.2 $\widetilde{\psi}_h$ *Potential.*

Examining the form of $\vec{g}^{\,p}_{\psi_h}$

$$\vec{g}^{\,p}_{\psi_h} = -\frac{\hat{\mathbf{z}} \times \vec{\lambda}_\rho j\omega\varepsilon_t}{2\lambda_{z\psi}\lambda_\rho^2} \qquad (2.101)$$

we see that there is no longitudinal part. Therefore, the exponential part of $\vec{g}_{\psi_h}$ will be in the same form as (2.95). This allows us to relatively easily find

$$\widetilde{\psi}_h = \int_0^d \left(-\frac{\hat{\mathbf{z}} \times \vec{\lambda}_\rho \omega\varepsilon_t}{2\lambda_{z\psi}\lambda_\rho^2}\right) \left\{\frac{\cos\left(\lambda_{z\psi}\left[d - |z - z'|\right]\right) + \cos\left(\lambda_{z\psi}\left[d - (z + z')\right]\right)}{\sin\left(\lambda_{z\psi}d\right)}\right\} \cdot \vec{\tilde{J}}_h dz'$$

$$(2.102)$$

2.6.3 $\widetilde{\theta}_e$ *Potential.*

The total potential, $\widetilde{\theta}_e$ is

$$\widetilde{\theta}_e = \widetilde{\theta}_e^p + \widetilde{\theta}_e^s \qquad (2.103)$$

$$
= \int_0^d \left\{ \frac{\vec{\tilde{G}}_{\theta_e}^p \left(1 - R_\theta \overline{R}_\theta e^{-j2\lambda_{z\theta}d}\right) + R_\theta \vec{\tilde{g}}_{\theta_e}^p (z = 0)e^{-j\lambda_{z\theta}(z+z')} + R_\theta \overline{R}_\theta \vec{\tilde{g}}_{\theta_e}^p (z = d)e^{-j\lambda_{z\theta}(2d+z-z')}}{1 - R_\theta \overline{R}_\theta e^{-j2\lambda_{z\theta}d}} \right.
$$

$$
\left. + \frac{\overline{R}_\theta \vec{\tilde{g}}_{\theta_e}^p (z = d)e^{-j\lambda_{z\theta}(2d-z-z')} + R_\theta \overline{R}_\theta \vec{\tilde{g}}_{\theta_e}^p (z = 0)e^{-j\lambda_{z\theta}(2d-z+z')}}{1 - R_\theta \overline{R}_\theta e^{-j2\lambda_{z\theta}d}} \right\} \cdot \vec{\tilde{J}}_e dz'
$$

which, with $R_\theta = \overline{R}_\theta = -1$ and some algebraic effort, can be written as

$$
\tilde{\theta}_e = \int_0^d \left\{ \frac{\vec{\tilde{g}}_{\theta_e}^p e^{j\lambda_{z\theta}(d-|z-z'|)} - \vec{\tilde{g}}_{\theta_e}^p e^{j\lambda_{z\theta}(d-|z-z'|)} - \vec{\tilde{g}}_{\theta_e}^p (z = 0)e^{j\lambda_{z\theta}(d-z-z')}}{j2\sin\left(\lambda_{z\theta}d\right)} \right.
$$
$$
\left. + \frac{\vec{\tilde{g}}_{\theta_e}^p (z = d)e^{-j\lambda_{z\theta}(d+z-z')} - \vec{\tilde{g}}_{\theta_e}^p (z = d)e^{-j\lambda_{z\theta}(d-z-z')} + \vec{\tilde{g}}_{\theta_e}^p (z = 0)e^{-j\lambda_{z\theta}(d-z+z')}}{j2\sin\left(\lambda_{z\theta}d\right)} \right\} \cdot \vec{\tilde{J}}_e dz'
$$
(2.104)

Examining the form of $\vec{\tilde{g}}_{\theta_e}^p$ from 2.3.1

$$
\vec{\tilde{g}}_{\theta_e}^p = -\frac{\hat{\mathbf{z}} \times \vec{\lambda}_\rho j\omega\mu_t}{2\lambda_{z\theta}\lambda_\rho^2}
$$
(2.105)

we see that there is no longitudinal part. Therefore, using (2.104) and converting to sinusoidal form, we find

$$
\boxed{\tilde{\theta}_e = \int_0^d \left(-\frac{\hat{\mathbf{z}} \times \vec{\lambda}_\rho \omega\mu_t}{2\lambda_{z\theta}\lambda_\rho^2}\right) \left\{ \frac{\cos\left(\lambda_{z\theta}\left[d - |z - z'|\right]\right) - \cos\left(\lambda_{z\theta}\left[d - (z + z')\right]\right)}{\sin\left(\lambda_{z\theta}d\right)} \right\} \cdot \vec{\tilde{J}}_e dz'}
$$

(2.106)

2.6.4 $\tilde{\theta}_h$ *Potential.*

As with $\tilde{\psi}_e$, we can examine the transverse and longitudinal parts of the total potential separately, such that $\tilde{\theta}_h = \tilde{\theta}_{ht} + \tilde{\theta}_{hz}$.

66

2.6.4.1 $\widetilde{\theta}_{ht}$ Potential.

We will first investigate the transverse portion. From Section 2.3.1, we have

$$\vec{\tilde{g}}^{p}_{\theta_{ht}} = \vec{\lambda}_{\rho} \frac{j\mathrm{sgn}\,(z - z')}{2\lambda_{\rho}^{2}}$$

Using this equation and noting that the $\widetilde{\theta}_{h}$ potential will have a similar form as (2.104), we have

$$\widetilde{\theta}_{ht} = \int\limits_{0}^{d} \left(\vec{\lambda}_{\rho} \frac{j}{2\lambda_{\rho}^{2}} \right) \left\{ \frac{\mathrm{sgn}\,(z - z')\sin\,(\lambda_{z\theta}\,[d - |z - z'|]) + \sin\,(\lambda_{z\theta}\,[d - (z + z')])}{\sin\,(\lambda_{z\theta}d)} \right\} \cdot \vec{\tilde{J}}_{h}dz'$$

$$(2.107)$$

2.6.4.2 $\widetilde{\theta}_{hz}$ Potential.

Now, we turn our attention to the longitudinal portion of $\widetilde{\theta}$. From Section 2.3.1, we have

$$\vec{\tilde{g}}^{p}_{\theta_{hz}} = \hat{\mathbf{z}} \frac{j\mu_{t}}{2\lambda_{z\theta}\mu_{z}}$$

Using this equation and the form of (2.104), we have

$$\widetilde{\theta}_{hz} = \int\limits_{0}^{d} \left(\hat{\mathbf{z}} \frac{\mu_{t}}{2\lambda_{z\theta}\mu_{z}} \right) \left\{ \frac{\cos\,(\lambda_{z\theta}\,[d - |z - z'|]) - \cos\,(\lambda_{z\theta}\,[d - (z + z')])}{\sin\,(\lambda_{z\theta}d)} \right\} \cdot \vec{\tilde{J}}_{h}dz' \quad (2.108)$$

Examining the form of the $\widetilde{\psi}$ and $\widetilde{\theta}$ potentials (conveniently summarized in the next section), we see that duality could almost be used to obtain one from the other. However, it is important to note that, while duality holds for the principal portion of the Green's function, it breaks down for the scattered portion. This makes sense, as, for a full duality case, one substitutes $\varepsilon_{(t,z)} \leftrightarrow -\mu_{(t,z)}$, $\vec{J}_{e} \leftrightarrow -\vec{J}_{h}$, $\lambda_{z\psi} \leftrightarrow \lambda_{z\theta}$ and exchanges PEC boundary conditions for PMC. For our parallel plate case, all of these substitutions can be made, except for the

67

PEC to PMC substitution, since it woud not satisfy the physical problem. Therefore, the reflection coefficients $(R, \overline{R})$ for the scattered Green's function pick up a negative sign. We see this in the summary, where the second sinusoidal term is oppositely signed between what would otherwise be dual cases (e.g., $\overset{\leftrightarrow}{\tilde{G}}{}^{\psi}_{et} \leftrightarrow \overset{\leftrightarrow}{\tilde{G}}{}^{\theta}_{ht}$, etc.). This will be an important consideration when working through the direct field method in the next chapter.

2.6.5 *Total Potential Summary for $\tilde{\psi}$ and $\tilde{\theta}$.*

$$\tilde{\psi} = \tilde{\psi}_e + \tilde{\psi}_h = \tilde{\psi}_{et} + \tilde{\psi}_{ez} + \tilde{\psi}_h$$

$$\tilde{\psi}_{et} = \int_0^d \left(-\vec{\lambda}_\rho \frac{j}{2\lambda_\rho^2} \right) \left\{ \frac{\operatorname{sgn}(z - z') \sin(\lambda_{z\psi}[d - |z - z'|]) - \sin(\lambda_{z\psi}[d - (z + z')])}{\sin(\lambda_{z\psi}d)} \right\} \cdot \vec{\tilde{J}}_e dz'$$

$$\tilde{\psi}_{ez} = \int_0^d \left(-\hat{\mathbf{z}} \frac{\varepsilon_t}{2\lambda_{z\psi}\varepsilon_z} \right) \left\{ \frac{\cos(\lambda_{z\psi}[d - |z - z'|]) + \cos(\lambda_{z\psi}[d - (z + z')])}{\sin(\lambda_{z\psi}d)} \right\} \cdot \vec{\tilde{J}}_e dz'$$

$$\tilde{\psi}_h = \int_0^d \left(-\frac{\hat{\mathbf{z}} \times \vec{\lambda}_\rho \omega \varepsilon_t}{2\lambda_{z\psi}\lambda_\rho^2} \right) \left\{ \frac{\cos(\lambda_{z\psi}[d - |z - z'|]) + \cos(\lambda_{z\psi}[d - (z + z')])}{\sin(\lambda_{z\psi}d)} \right\} \cdot \vec{\tilde{J}}_h dz'$$

$$\tilde{\theta} = \tilde{\theta}_e + \tilde{\theta}_h = \tilde{\theta}_e + \tilde{\theta}_{ht} + \tilde{\theta}_{hz}$$

$$\tilde{\theta}_e = \int_0^d \left(-\frac{\hat{\mathbf{z}} \times \vec{\lambda}_\rho \omega \mu_t}{2\lambda_{z\theta}\lambda_\rho^2} \right) \left\{ \frac{\cos(\lambda_{z\theta}[d - |z - z'|]) - \cos(\lambda_{z\theta}[d - (z + z')])}{\sin(\lambda_{z\theta}d)} \right\} \cdot \vec{\tilde{J}}_e dz'$$

$$\tilde{\theta}_{ht} = \int_0^d \left(\vec{\lambda}_\rho \frac{j}{2\lambda_\rho^2} \right) \left\{ \frac{\operatorname{sgn}(z - z') \sin(\lambda_{z\theta}[d - |z - z'|]) + \sin(\lambda_{z\theta}[d - (z + z')])}{\sin(\lambda_{z\theta}d)} \right\} \cdot \vec{\tilde{J}}_h dz'$$

$$\tilde{\theta}_{hz} = \int_0^d \left(\hat{\mathbf{z}} \frac{\mu_t}{2\lambda_{z\theta}\mu_z} \right) \left\{ \frac{\cos(\lambda_{z\theta}[d - |z - z'|]) - \cos(\lambda_{z\theta}[d - (z + z')])}{\sin(\lambda_{z\theta}d)} \right\} \cdot \vec{\tilde{J}}_h dz'$$

Therefore, we can write the Green's functions for the potentials $\widetilde{\psi}$ and $\widetilde{\theta}$ as:

$$\widetilde{\psi} = \widetilde{\psi}_e + \widetilde{\psi}_h = \int_0^d \vec{\vec{G}}_{\psi_e}(z|z') \cdot \vec{J}_e(z')dz' + \int_0^d \vec{\vec{G}}_{\psi_h}(z|z') \cdot \vec{J}_h(z')dz'$$

$$\vec{\vec{G}}_{\psi_e} = \vec{\vec{G}}_{\psi_{et}} + \vec{\vec{G}}_{\psi_{ez}}$$

$$\vec{\vec{G}}_{\psi_{et}} = \left(-\vec{\lambda}_\rho \frac{j}{2\lambda_\rho^2} \right) \left\{ \frac{\operatorname{sgn}(z-z')\sin(\lambda_{z\psi}[d-|z-z'|]) - \sin(\lambda_{z\psi}[d-(z+z')])}{\sin(\lambda_{z\psi}d)} \right\}$$

$$\vec{\vec{G}}_{\psi_{ez}} = \left(-\hat{\mathbf{z}}\frac{\varepsilon_t}{2\lambda_{z\psi}\varepsilon_z} \right) \left\{ \frac{\cos(\lambda_{z\psi}[d-|z-z'|]) + \cos(\lambda_{z\psi}[d-(z+z')])}{\sin(\lambda_{z\psi}d)} \right\}$$

$$\vec{\vec{G}}_{\psi_h} = \left(-\frac{\hat{\mathbf{z}} \times \vec{\lambda}_\rho \omega\varepsilon_t}{2\lambda_{z\psi}\lambda_\rho^2} \right) \left\{ \frac{\cos(\lambda_{z\psi}[d-|z-z'|]) + \cos(\lambda_{z\psi}[d-(z+z')])}{\sin(\lambda_{z\psi}d)} \right\}$$

$$\widetilde{\theta} = \widetilde{\theta}_e + \widetilde{\theta}_h = \int_0^d \vec{\vec{G}}_{\theta_e}(z|z') \cdot \vec{J}_e(z')dz' + \int_0^d \vec{\vec{G}}_{\theta_h}(z|z') \cdot \vec{J}_h(z')dz'$$

$$\vec{\vec{G}}_{\theta_h} = \vec{\vec{G}}_{\theta_{ht}} + \vec{\vec{G}}_{\theta_{hz}}$$

$$\vec{\vec{G}}_{\theta_e} = \left(-\frac{\hat{\mathbf{z}} \times \vec{\lambda}_\rho \omega\mu_t}{2\lambda_{z\theta}\lambda_\rho^2} \right) \left\{ \frac{\cos(\lambda_{z\theta}[d-|z-z'|]) - \cos(\lambda_{z\theta}[d-(z+z')])}{\sin(\lambda_{z\theta}d)} \right\}$$

$$\vec{\vec{G}}_{\theta_{ht}} = \left(\vec{\lambda}_\rho \frac{j}{2\lambda_\rho^2} \right) \left\{ \frac{\operatorname{sgn}(z-z')\sin(\lambda_{z\theta}[d-|z-z'|]) + \sin(\lambda_{z\theta}[d-(z+z')])}{\sin(\lambda_{z\theta}d)} \right\}$$

$$\vec{\vec{G}}_{\theta_{hz}} = \left(\hat{\mathbf{z}}\frac{\mu_t}{2\lambda_{z\theta}\mu_z} \right) \left\{ \frac{\cos(\lambda_{z\theta}[d-|z-z'|]) - \cos(\lambda_{z\theta}[d-(z+z')])}{\sin(\lambda_{z\theta}d)} \right\}$$

2.6.6 $\tilde{\Pi}(\vec{\lambda}_\rho, z)$ *Potential.*

Now that we've found the total potentials $\tilde{\psi}$ and $\tilde{\theta}$, we can directly calculate $\tilde{\Pi}$ and $\tilde{\Phi}$. Recall the form of $\tilde{\Pi}$ from (2.73):

$$\tilde{\Pi} = -\frac{1}{j\omega\mu_t} \left[\int_0^d \frac{\partial}{\partial z} \vec{\tilde{G}}_{\theta_e} \cdot \vec{\tilde{J}}_e dz' + \int_0^d \frac{\partial}{\partial z} \vec{\tilde{G}}_{\theta_{ht}} \cdot \vec{\tilde{J}}_h dz' + \int_0^d \frac{\partial}{\partial z} \vec{\tilde{G}}_{\theta_{hz}} \cdot \vec{\tilde{J}}_h dz' \right] \tag{2.109}$$

Therefore, we see the Green's functions for the potential $\tilde{\Pi}$ are:

$$\vec{\tilde{G}}_{\Pi_e} = -\frac{1}{j\omega\mu_t} \frac{\partial \vec{\tilde{G}}_{\theta_e}}{\partial z}$$

$$\vec{\tilde{G}}_{\Pi_h} = \vec{\tilde{G}}_{\Pi_{ht}} + \vec{\tilde{G}}_{\Pi_{hz}} = -\frac{1}{j\omega\mu_t} \frac{\partial \vec{\tilde{G}}_{\theta_{ht}}}{\partial z} - \frac{1}{j\omega\mu_t} \frac{\partial \vec{\tilde{G}}_{\theta_{hz}}}{\partial z}$$

In order to express these Green's functions explicitly, we need to calculate the partial derivatives of the Green's functions for $\tilde{\theta}$. Due to the absolute value and signum terms, we again must look at the two cases $z > z'$ and $z < z'$.

2.6.6.1 $\tilde{\Pi}_e(\vec{\lambda}_\rho, z)$ *Potential.*

$$\vec{\tilde{G}}_{\Pi_e} = -\frac{1}{j\omega\mu_t} \frac{\partial \vec{\tilde{G}}_{\theta_e}}{\partial z}$$

$$= -\frac{1}{j\omega\mu_t} \frac{\partial}{\partial z} \left(-\frac{\hat{\mathbf{z}} \times \vec{\lambda}_\rho \omega \mu_t}{2\lambda_{z\theta}\lambda_\rho^2} \right) \left\{ \frac{\cos(\lambda_{z\theta}[d - |z - z'|]) - \cos(\lambda_{z\theta}[d - (z + z')])}{\sin(\lambda_{z\theta}d)} \right\}$$

$$= \left(-\frac{\hat{\mathbf{z}} \times j\vec{\lambda}_\rho}{2\lambda_{z\theta}\lambda_\rho^2 \sin(\lambda_{z\theta}d)} \right) \frac{\partial}{\partial z} \left\{ \cos(\lambda_{z\theta}[d - |z - z'|]) - \cos(\lambda_{z\theta}[d - (z + z')]) \right\}$$

Since the cosine terms are the only terms that require differentiation, we will examine them seperately, noting that the $|z - z'|$ term requires examining the two possible cases $z > z'$ and $z < z'$.

- $z > z' \implies |z - z'| = (z - z')$

$$\frac{\partial}{\partial z} \left[\cos(\lambda_{z\theta}[d - (z - z')]) - \cos(\lambda_{z\theta}[d - (z + z')]) \right]$$

$$= \lambda_{z\theta}\sin(\lambda_{z\theta}[d - (z - z')]) - \lambda_{z\theta}\sin(\lambda_{z\theta}[d - (z + z')])$$

70

- $z < z' \implies |z - z'| = -(z - z')$

$$\frac{\partial}{\partial z} \left[\cos \left(\lambda_{z\theta} \left[d + (z - z') \right] \right) - \cos \left(\lambda_{z\theta} \left[d - (z + z') \right] \right) \right]$$

$$= -\lambda_{z\theta} \sin \left(\lambda_{z\theta} \left[d + (z - z') \right] \right) - \lambda_{z\theta} \sin \left(\lambda_{z\theta} \left[d - (z + z') \right] \right)$$

These two results can be written succinctly as:

$$\mathrm{sgn}\,(z - z')\, \lambda_{z\theta} \sin \left(\lambda_{z\theta} \left[d - |z - z'| \right] \right) - \lambda_{z\theta} \sin \left(\lambda_{z\theta} \left[d - (z + z') \right] \right) \tag{2.110}$$

Therefore:

$$\boxed{ \vec{\tilde{G}}_{\Pi_e} = \left(-\frac{\hat{\mathbf{z}} \times j\vec{\lambda}_\rho}{2\lambda_\rho^2} \right) \left[\frac{\mathrm{sgn}\,(z - z') \sin \left(\lambda_{z\theta} \left[d - |z - z'| \right] \right) - \sin \left(\lambda_{z\theta} \left[d - (z + z') \right] \right)}{\sin \left(\lambda_{z\theta} d \right)} \right] }$$

$$\tag{2.111}$$

2.6.6.2 $\widetilde{\Pi}_{ht}(\vec{\lambda}_\rho, z)$ *Potential.*

Using this same method, we can also find $\vec{\tilde{G}}_{\theta_{ht}}$.

$$\vec{\tilde{G}}_{\theta_{ht}} = -\frac{1}{j\omega\mu_t} \frac{\partial \vec{\tilde{G}}_{\theta_{ht}}}{\partial z}$$

$$= -\frac{1}{j\omega\mu_t} \frac{\partial}{\partial z} \left(\vec{\lambda}_\rho \frac{j}{2\lambda_\rho^2} \right) \left\{ \frac{\mathrm{sgn}\,(z - z') \sin \left(\lambda_{z\theta} \left[d - |z - z'| \right] \right) + \sin \left(\lambda_{z\theta} \left[d - (z + z') \right] \right)}{\sin \left(\lambda_{z\theta} d \right)} \right\}$$

$$= -\vec{\lambda}_\rho \frac{1}{2\lambda_\rho^2 \omega\mu_t \sin \left(\lambda_{z\theta} d \right)} \frac{\partial}{\partial z} \left[\mathrm{sgn}\,(z - z') \sin \left(\lambda_{z\theta} \left[d - |z - z'| \right] \right) + \sin \left(\lambda_{z\theta} \left[d - (z + z') \right] \right) \right]$$

Again, we must investigate the two cases where $z > z'$ and $z < z'$ for the sine terms, leading to:

$$\boxed{ \vec{\tilde{G}}_{\Pi_{ht}} = \left(\vec{\lambda}_\rho \frac{\lambda_{z\theta}}{2\lambda_\rho^2 \omega\mu_t} \right) \left[\frac{\cos \left(\lambda_{z\theta} \left[d + |z - z'| \right] \right) + \cos \left(\lambda_{z\theta} \left[d - (z + z') \right] \right)}{\sin \left(\lambda_{z\theta} d \right)} \right] } \tag{2.112}$$

2.6.6.3 $\widetilde{\Pi}_{hz}(\vec{\lambda}_\rho, z)$ *Potential.*

Using this same method, we can also find $\vec{\tilde{G}}_{\theta_{hz}}$.

$$\boxed{ \vec{\tilde{G}}_{\Pi_{hz}} = \hat{\mathbf{z}} \frac{j}{2\omega\mu_z} \left[\frac{\mathrm{sgn}\,(z - z') \sin \left(\lambda_{z\theta} \left[d - |z - z'| \right] \right) - \sin \left(\lambda_{z\theta} \left[d - (z + z') \right] \right)}{\sin \left(\lambda_{z\theta} d \right)} \right] } \tag{2.113}$$

71

2.6.7 $\widetilde{\Phi}(\vec{\lambda}_\rho, z)$ *Potential.*

Recall the form of $\widetilde{\Phi}$ from (2.70):

$$\widetilde{\Phi} = \frac{1}{j\omega\varepsilon_t} \left[\int_0^d \frac{\partial}{\partial z} \vec{\widetilde{G}}_{\psi_h} \cdot \vec{\widetilde{J}}_h dz' + \int_0^d \frac{\partial}{\partial z} \vec{\widetilde{G}}_{\psi_{et}} \cdot \vec{\widetilde{J}}_e dz' + \int_0^d \frac{\partial}{\partial z} \vec{\widetilde{G}}_{\psi_{ez}} \cdot \vec{\widetilde{J}}_e dz' \right] \qquad (2.114)$$

Therefore, we see the Green's functions for the potential $\widetilde{\Phi}$ are:

$$\vec{\widetilde{G}}_{\Phi_h} = \frac{1}{j\omega\varepsilon_t} \frac{\partial \vec{\widetilde{G}}_{\psi_h}}{\partial z}$$

$$\vec{\widetilde{G}}_{\Phi_e} = \vec{\widetilde{G}}_{\Phi_{et}} + \vec{\widetilde{G}}_{\Phi_{ez}}$$

$$= \frac{1}{j\omega\varepsilon_t} \frac{\partial \vec{\widetilde{G}}_{\psi_{et}}}{\partial z} + \frac{1}{j\omega\varepsilon_t} \frac{\partial \vec{\widetilde{G}}_{\psi_{ez}}}{\partial z}$$

In order to express these Green's functions explicitly, we need to calculate the partial derivatives of the Green's functions for $\widetilde{\psi}$. Due to the absolute value and signum terms, we must again consider the two cases $z > z'$ and $z < z'$.

2.6.7.1 $\widetilde{\Phi}_h(\vec{\lambda}_\rho, z)$ *Potential.*

Using the same methods as the for the $\widetilde{\Pi}$ potential, we find:

$$\boxed{\vec{\widetilde{G}}_{\Phi_h} = \left(\frac{\hat{\mathbf{z}} \times j\vec{\lambda}_\rho}{2\lambda_\rho^2} \right) \left[\frac{\operatorname{sgn}(z - z') \sin(\lambda_{z\psi}[d - |z - z'|]) + \sin(\lambda_{z\psi}[d - (z + z')])}{\sin(\lambda_{z\psi}d)} \right]}$$

$$(2.115)$$

2.6.7.2 $\widetilde{\Phi}_{et}(\vec{\lambda}_\rho, z)$ *Potential.*

In a similar fashion, we can also find $\vec{\widetilde{G}}_{\Phi_{et}}$.

$$\boxed{\vec{\widetilde{G}}_{\Phi_{et}} = \left(\vec{\lambda}_\rho \frac{\lambda_{z\psi}}{2\lambda_\rho^2 \omega\varepsilon_t} \right) \left[\frac{\cos(\lambda_{z\psi}[d - |z - z'|]) - \cos(\lambda_{z\psi}[d - (z + z')])}{\sin(\lambda_{z\psi}d)} \right]} \qquad (2.116)$$

2.6.7.3 $\widetilde{\Phi}_{ez}(\vec{\lambda}_\rho, z)$ *Potential.*

Finally, we find $\vec{\tilde{G}}_{\psi_{ez}}$ as:

$$\vec{\tilde{G}}_{\Phi_{ez}} = \left(\hat{\mathbf{z}}\frac{j}{2\omega\varepsilon_z}\right)\left[\frac{\mathrm{sgn}\,(z - z')\sin\,(\lambda_{z\psi}\,[d - |z - z'|]) + \sin\,(\lambda_{z\psi}\,[d - (z + z')])}{\sin\,(\lambda_{z\psi}d)}\right]$$

$$(2.117)$$

2.6.8 Summary for Potentials $\widetilde{\Pi}(\vec{\lambda}_\rho, z)$ and $\widetilde{\Phi}(\vec{\lambda}_\rho, z)$.

$$\widetilde{\Pi} = \int_0^d \vec{\vec{G}}_{\Pi_e} \cdot \vec{J}_e dz' + \int_0^d \vec{\vec{G}}_{\Pi_h} \cdot \vec{J}_h dz' = \int_0^d \vec{\vec{G}}_{\Pi_e} \cdot \vec{J}_e dz' + \int_0^d \vec{\vec{G}}_{\Pi_{ht}} \cdot \vec{J}_h dz' + \int_0^d \vec{\vec{G}}_{\Pi_{hz}} \cdot \vec{J}_h dz'$$

$$\vec{\vec{G}}_{\Pi_e} = \left(-\frac{\hat{\mathbf{z}} \times j\vec{\lambda}_\rho}{2\lambda_\rho^2} \right) \left[\frac{\text{sgn}\,(z - z') \sin\,(\lambda_{z\theta}\,[d - |z - z'|]) - \sin\,(\lambda_{z\theta}\,[d - (z + z')])}{\sin\,(\lambda_{z\theta}d)} \right]$$

$$\vec{\vec{G}}_{\Pi_{ht}} = \left(\vec{\lambda}_\rho \frac{\lambda_{z\theta}}{2\lambda_\rho^2 \omega\mu_t} \right) \left[\frac{\cos\,(\lambda_{z\theta}\,[d - |z - z'|]) + \cos\,(\lambda_{z\theta}\,[d - (z + z')])}{\sin\,(\lambda_{z\theta}d)} \right]$$

$$\vec{\vec{G}}_{\Pi_{hz}} = \left(\hat{\mathbf{z}} \frac{j}{2\omega\mu_z} \right) \left[\frac{\text{sgn}\,(z - z') \sin\,(\lambda_{z\theta}\,[d - |z - z'|]) - \sin\,(\lambda_{z\theta}\,[d - (z + z')])}{\sin\,(\lambda_{z\theta}d)} \right]$$

$$\widetilde{\Phi} = \int_0^d \vec{\vec{G}}_{\Phi_h} \cdot \vec{J}_h dz' + \int_0^d \vec{\vec{G}}_{\Phi_e} \cdot \vec{J}_e dz' = \int_0^d \vec{\vec{G}}_{\Phi_h} \cdot \vec{J}_h dz' + \int_0^d \vec{\vec{G}}_{\Phi_{et}} \cdot \vec{J}_e dz' + \int_0^d \vec{\vec{G}}_{\Phi_{ez}} \cdot \vec{J}_e dz'$$

$$\vec{\vec{G}}_{\Phi_h} = \left(\frac{\hat{\mathbf{z}} \times j\vec{\lambda}_\rho}{2\lambda_\rho^2} \right) \left[\frac{\text{sgn}\,(z - z') \sin\,(\lambda_{z\psi}\,[d - |z - z'|]) + \sin\,(\lambda_{z\psi}\,[d - (z + z')])}{\sin\,(\lambda_{z\psi}d)} \right]$$

$$\vec{\vec{G}}_{\Phi_{et}} = \left(\vec{\lambda}_\rho \frac{\lambda_{z\psi}}{2\lambda_\rho^2 \omega\varepsilon_t} \right) \left[\frac{\cos\,(\lambda_{z\psi}\,[d - |z - z'|]) - \cos\,(\lambda_{z\psi}\,[d - (z + z')])}{\sin\,(\lambda_{z\psi}d)} \right]$$

$$\vec{\vec{G}}_{\Phi_{ez}} = \left(\hat{\mathbf{z}} \frac{j}{2\omega\varepsilon_z} \right) \left[\frac{\text{sgn}\,(z - z') \sin\,(\lambda_{z\psi}\,[d - |z - z'|]) + \sin\,(\lambda_{z\psi}\,[d - (z + z')])}{\sin\,(\lambda_{z\psi}d)} \right]$$

$$\vec{G}_{(\psi,\Phi,\theta,\Pi)} = \frac{1}{4\pi^2} \iint_{-\infty}^{\infty} \vec{\vec{G}}_{(\psi,\Phi,\theta,\Pi)} e^{j\vec{\lambda}_\rho \cdot \vec{\rho}} d^2\lambda_\rho$$

2.6.9 Field Recovery.

Now that we have determined the spectral domain potentials $\widetilde{\psi}, \widetilde{\theta}, \widetilde{\Pi}$ and $\widetilde{\Phi}$, the final step in the potential method is to recover the fields. Recall the electric and magnetic fields can be

determined by:

$$\vec{E} = \vec{E}_t + \hat{\mathbf{z}}E_z$$

$$\vec{E}_t = \nabla_t \Phi - \hat{\mathbf{z}} \times \nabla_t \theta \qquad \text{and} \qquad E_z = -\frac{1}{j\omega\varepsilon_z}\left(\nabla_t^2 \psi + J_{ez}\right)$$

$$\vec{H} = \vec{H}_t + \hat{\mathbf{z}}H_z$$

$$\vec{H}_t = \nabla_t \Pi - \hat{\mathbf{z}} \times \nabla_t \psi \qquad \text{and} \qquad H_z = \frac{1}{j\omega\mu_z}\left(\nabla_t^2 \theta - J_{hz}\right)$$

Using the transforms of (2.36), we can write these equations in the single transform domain $(\vec{\lambda}_\rho, z)$:

$$\widetilde{\vec{E}}_t = j\vec{\lambda}_\rho \widetilde{\Phi} - \hat{\mathbf{z}} \times j\vec{\lambda}_\rho \widetilde{\theta} \qquad \widetilde{E}_z = -\frac{1}{j\omega\varepsilon_z}\left(-\lambda_\rho^2 \widetilde{\psi} + \widetilde{J}_{ez}\right)$$

$$\widetilde{\vec{H}}_t = j\vec{\lambda}_\rho \widetilde{\Pi} - \hat{\mathbf{z}} \times j\vec{\lambda}_\rho \widetilde{\psi} \qquad \widetilde{H}_z = \frac{1}{j\omega\mu_z}\left(-\lambda_\rho^2 \widetilde{\theta} - \widetilde{J}_{hz}\right)$$

2.6.9.1 Electric Field.

We start with the electric field:

$$\widetilde{\vec{E}} = \widetilde{\vec{E}}_t + \hat{\mathbf{z}}\widetilde{E}_z$$

$$= j\vec{\lambda}_\rho \widetilde{\Phi} - \hat{\mathbf{z}} \times j\vec{\lambda}_\rho \widetilde{\theta} - \hat{\mathbf{z}}\frac{1}{j\omega\varepsilon_z}\left(-\lambda_\rho^2 \widetilde{\psi} + \widetilde{J}_{ez}\right)$$

$$= j\vec{\lambda}_\rho \widetilde{\Phi} - \hat{\mathbf{z}} \times j\vec{\lambda}_\rho \widetilde{\theta} + \hat{\mathbf{z}}\frac{\lambda_\rho^2}{j\omega\varepsilon_z}\widetilde{\psi} - \hat{\mathbf{z}}\hat{\mathbf{z}} \cdot \frac{\widetilde{\vec{J}}_e}{j\omega\varepsilon_z}$$

$$(2.118)$$

75

We can expand this representation using the Green's functions representations for $\widetilde{\Phi}, \widetilde{\theta}$, and $\widetilde{\psi}$, then group the electric and magnetic source terms together to find:

$$
\vec{\widetilde{E}} = \int_0^d \left\{ \overbrace{\left[j\vec{\lambda}_\rho \vec{\widetilde{G}}_{\Phi_{et}} + j\vec{\lambda}_\rho \vec{\widetilde{G}}_{\Phi_{ez}} - \hat{\mathbf{z}} \times j\vec{\lambda}_\rho \vec{\widetilde{G}}_{\theta_e} + \hat{\mathbf{z}} \frac{\lambda_\rho^2}{j\omega\varepsilon_z} \vec{\widetilde{G}}_{\psi_{et}} + \hat{\mathbf{z}} \frac{\lambda_\rho^2}{j\omega\varepsilon_z} \vec{\widetilde{G}}_{\psi_{ez}} - \hat{\mathbf{z}}\hat{\mathbf{z}} \frac{1}{j\omega\varepsilon_z} \right]}^{\vec{\widetilde{G}}_{ee}} \cdot \vec{\widetilde{J}}_e \right.
$$
$$
\left. + \underbrace{\left[j\vec{\lambda}_\rho \vec{\widetilde{G}}_{\Phi_h} - \hat{\mathbf{z}} \times j\vec{\lambda}_\rho \vec{\widetilde{G}}_{\theta_{ht}} - \hat{\mathbf{z}} \times j\vec{\lambda}_\rho \vec{\widetilde{G}}_{\theta_{hz}} + \hat{\mathbf{z}} \frac{\lambda_\rho^2}{j\omega\varepsilon_z} \vec{\widetilde{G}}_{\psi_{ht}} \right]}_{\vec{\widetilde{G}}_{eh}} \cdot \vec{\widetilde{J}}_h \right\} dz'
$$

(2.119)

It is worth examining the final form of (2.119) in order to reconcile the mathematics with the physically expected picture. The Green's functions are expanded into components in Appendix B. From these, we see $\overset{\leftrightarrow}{\widetilde{G}}_{ee}$ is a dyad of full rank. This is completely intuitive, as $\overset{\leftrightarrow}{\widetilde{G}}_{ee}$ describes the electric field maintained by an electric current. In this case, we would fully expect electric fields with vector components in every direction. However, we would not expect the electric field to have a $\hat{\mathbf{z}}$ component if it were maintained by a $\hat{\mathbf{z}}$-directed magnetic current. Furthermore, the electric field contains a depolarizing term, the $\hat{\mathbf{z}}\hat{\mathbf{z}}$ term, which is only required in the case of an electric field maintained by an electric source current, since a magnetic source current in any direction would not produce any electric charging on the walls of the the V_δ cavity.

Examining $\overset{\leftrightarrow}{\widetilde{G}}_{eh}$ in the same way, we see there is no depolarizing term in the Green's function for an electric field maintained by a magnetic current, which corresponds exactly to the physical picture. These results provide remarkable physical insight into the mathematical results and confirm our intuition about the problem.

2.6.9.2 *Magnetic Field.*

Using the same procedure as with the electric field, we will now recover the magnetic field.

$$
\begin{aligned}
\vec{\tilde{H}} &= \vec{\tilde{H}}_t + \hat{\mathbf{z}}\,\tilde{H}_z \\
&= j\vec{\lambda}_\rho\tilde{\Pi} - \hat{\mathbf{z}} \times j\vec{\lambda}_\rho\tilde{\psi} + \hat{\mathbf{z}}\frac{1}{j\omega\mu_z}\left(-\lambda_\rho^2\tilde{\theta} - \tilde{J}_{hz}\right) \\
&= j\vec{\lambda}_\rho\tilde{\Pi} - \hat{\mathbf{z}} \times j\vec{\lambda}_\rho\tilde{\psi} - \hat{\mathbf{z}}\frac{1}{j\omega\mu_z}\tilde{\theta} - \hat{\mathbf{z}}\hat{\mathbf{z}}\frac{\tilde{J}_h}{j\omega\mu_z}
\end{aligned}
$$

which can again be expanded and grouped as with the electric field:

$$
\vec{\tilde{H}} = \int_0^d \Bigg\{ \overbrace{\left[j\vec{\lambda}_\rho\vec{\tilde{G}}_{\Pi_e} - \hat{\mathbf{z}}\frac{\lambda_\rho^2}{j\omega\mu_z}\vec{\tilde{G}}_{\theta_e} - \hat{\mathbf{z}} \times j\lambda_\rho\vec{\tilde{G}}_{\psi_{et}} - \hat{\mathbf{z}} \times j\lambda_\rho\vec{\tilde{G}}_{\psi_{ez}} \right]}^{\vec{\tilde{\tilde{G}}}_{he}} \cdot \vec{\tilde{J}}_e
$$

$$
+ \underbrace{\left[j\vec{\lambda}_\rho\vec{\tilde{G}}_{\Pi_{ht}} + j\vec{\lambda}_\rho\vec{\tilde{G}}_{\Pi_{hz}} - \hat{\mathbf{z}} \times j\vec{\lambda}_\rho\vec{\tilde{G}}_{\psi_h} - \hat{\mathbf{z}}\frac{\lambda_\rho^2}{j\omega\mu_z}\vec{\tilde{G}}_{\theta_{ht}} - \hat{\mathbf{z}}\frac{\lambda_\rho^2}{j\omega\mu_z}\vec{\tilde{G}}_{\theta_{hz}} - \hat{\mathbf{z}}\hat{\mathbf{z}}\frac{1}{j\omega\mu_z} \right]}_{\vec{\tilde{\tilde{G}}}_{hh}} \cdot \vec{\tilde{J}}_h \Bigg\} dz'
$$

$$
(2.120)
$$

Looking again at the components shown in Appendix B, we see no $\hat{\mathbf{z}}$ term in the magnetic field maintained by an electric source, but we do see a depolarizing term in the magnetic field maintained by a magnetic current. This is exactly the expected behavior, based on our analysis of the electric field.

2.6.10 Total Field Green's Function Grand Summary.

$$\vec{E} = \int\limits_0^d \overset{\leftrightarrow}{\tilde{G}}_{ee} \cdot \vec{J}_e dz' + \int\limits_0^d \overset{\leftrightarrow}{\tilde{G}}_{eh} \cdot \vec{J}_h dz' \qquad\qquad \vec{H} = \int\limits_0^d \overset{\leftrightarrow}{\tilde{G}}_{he} \cdot \vec{J}_e dz' + \int\limits_0^d \overset{\leftrightarrow}{\tilde{G}}_{hh} \cdot \vec{J}_h dz'$$

$$\overset{\leftrightarrow}{\tilde{G}}_{ee} = j\vec{\lambda}_\rho \overset{\vec{\leftrightarrow}}{\tilde{G}}_{\Phi_{et}}(z|z') + j\vec{\lambda}_\rho \overset{\vec{\leftrightarrow}}{\tilde{G}}_{\Phi_{ez}}(z|z') - \hat{\mathbf{z}} \times j\vec{\lambda}_\rho \overset{\vec{\leftrightarrow}}{\tilde{G}}_{\theta_e}(z|z') + \hat{\mathbf{z}}\frac{\lambda_\rho^2}{j\omega\varepsilon_z}\overset{\vec{\leftrightarrow}}{\tilde{G}}_{\psi_{et}}(z|z') + \hat{\mathbf{z}}\frac{\lambda_\rho^2}{j\omega\varepsilon_z}\overset{\vec{\leftrightarrow}}{\tilde{G}}_{\psi_{ez}}(z|z') - \hat{\mathbf{z}}\hat{\mathbf{z}}\frac{1}{j\omega\varepsilon_z}$$

$$\overset{\leftrightarrow}{\tilde{G}}_{eh} = j\vec{\lambda}_\rho \overset{\vec{\leftrightarrow}}{\tilde{G}}_{\Phi_h}(z|z') - \hat{\mathbf{z}} \times j\vec{\lambda}_\rho \overset{\vec{\leftrightarrow}}{\tilde{G}}_{\theta_{ht}}(z|z') - \hat{\mathbf{z}} \times j\vec{\lambda}_\rho \overset{\vec{\leftrightarrow}}{\tilde{G}}_{\theta_{hz}}(z|z') + \hat{\mathbf{z}}\frac{\lambda_\rho^2}{j\omega\varepsilon_z}\overset{\vec{\leftrightarrow}}{\tilde{G}}_{\psi_h}(z|z')$$

$$\overset{\leftrightarrow}{\tilde{G}}_{he} = j\vec{\lambda}_\rho \overset{\vec{\leftrightarrow}}{\tilde{G}}_{\Pi_e}(z|z') - \hat{\mathbf{z}}\frac{\lambda_\rho^2}{j\omega\mu_z}\overset{\vec{\leftrightarrow}}{\tilde{G}}_{\theta_e}(z|z') - \hat{\mathbf{z}} \times j\vec{\lambda}_\rho \overset{\vec{\leftrightarrow}}{\tilde{G}}_{\psi_{et}}(z|z') - \hat{\mathbf{z}} \times j\vec{\lambda}_\rho \overset{\vec{\leftrightarrow}}{\tilde{G}}_{\psi_{ez}}(z|z')$$

$$\overset{\leftrightarrow}{\tilde{G}}_{hh} = j\vec{\lambda}_\rho \overset{\vec{\leftrightarrow}}{\tilde{G}}_{\Pi_{ht}}(z|z') + j\vec{\lambda}_\rho \overset{\vec{\leftrightarrow}}{\tilde{G}}_{\Pi_{hz}}(z|z') - \hat{\mathbf{z}} \times j\vec{\lambda}_\rho \overset{\vec{\leftrightarrow}}{\tilde{G}}_{\psi_h}(z|z') - \hat{\mathbf{z}}\frac{\lambda_\rho^2}{j\omega\mu_z}\overset{\vec{\leftrightarrow}}{\tilde{G}}_{\theta_{ht}}(z|z') - \hat{\mathbf{z}}\frac{\lambda_\rho^2}{j\omega\mu_z}\overset{\vec{\leftrightarrow}}{\tilde{G}}_{\theta_{hz}}(z|z') - \hat{\mathbf{z}}\hat{\mathbf{z}}\frac{1}{j\omega\mu_z}$$

$$\vec{\tilde{G}}_{\Pi_e} = \left(-\frac{\hat{\mathbf{z}} \times \vec{\lambda}_\rho j}{2\lambda_\rho^2}\right) \left[\frac{\operatorname{sgn}(z - z') \sin(\lambda_{z\theta}[d - |z - z'|]) - \sin(\lambda_{z\theta}[d - (z + z')])}{\sin(\lambda_{z\theta}d)}\right]$$

$$\vec{\tilde{G}}_{\Pi_{ht}} = \left(\vec{\lambda}_\rho \frac{\lambda_{z\theta}}{2\lambda_\rho^2 \omega \mu_t}\right) \left[\frac{\cos(\lambda_{z\theta}[d - |z - z'|]) + \cos(\lambda_{z\theta}[d - (z + z')])}{\sin(\lambda_{z\theta}d)}\right]$$

$$\vec{\tilde{G}}_{\Pi_{hz}} = \left(\hat{\mathbf{z}}\frac{j}{2\omega\mu_z}\right) \left[\frac{\operatorname{sgn}(z - z') \sin(\lambda_{z\theta}[d - |z - z'|]) - \sin(\lambda_{z\theta}[d - (z + z')])}{\sin(\lambda_{z\theta}d)}\right]$$

$$\vec{\tilde{G}}_{\Phi_h} = \left(\frac{\hat{\mathbf{z}} \times \vec{\lambda}_\rho j}{2\lambda_\rho^2}\right) \left[\frac{\operatorname{sgn}(z - z') \sin(\lambda_{z\psi}[d - |z - z'|]) + \sin(\lambda_{z\psi}[d - (z + z')])}{\sin(\lambda_{z\psi}d)}\right]$$

$$\vec{\tilde{G}}_{\Phi_{et}} = \left(\vec{\lambda}_\rho \frac{\lambda_{z\psi}}{2\lambda_\rho^2 \omega \varepsilon_t}\right) \left[\frac{\cos(\lambda_{z\psi}[d - |z - z'|]) - \cos(\lambda_{z\psi}[d - (z + z')])}{\sin(\lambda_{z\psi}d)}\right]$$

$$\vec{\tilde{G}}_{\Phi_{ez}} = \left(\hat{\mathbf{z}}\frac{j}{2\omega\varepsilon_z}\right) \left[\frac{\operatorname{sgn}(z - z') \sin(\lambda_{z\psi}[d - |z - z'|]) + \sin(\lambda_{z\psi}[d - (z + z')])}{\sin(\lambda_{z\psi}d)}\right]$$

$$\vec{\tilde{G}}_{\psi_{et}} = \left(-\vec{\lambda}_\rho \frac{j}{2\lambda_\rho^2}\right) \left[\frac{\operatorname{sgn}(z - z') \sin(\lambda_{z\psi}[d - |z - z'|]) - \sin(\lambda_{z\psi}[d - (z + z')])}{\sin(\lambda_{z\psi}d)}\right]$$

$$\vec{\tilde{G}}_{\psi_{ez}} = \left(-\hat{\mathbf{z}}\frac{\varepsilon_t}{2\lambda_{z\psi}\varepsilon_z}\right) \left[\frac{\cos(\lambda_{z\psi}[d - |z - z'|]) + \cos(\lambda_{z\psi}[d - (z + z')])}{\sin(\lambda_{z\psi}d)}\right]$$

$$\vec{\tilde{G}}_{\psi_h} = \left(-\frac{\hat{\mathbf{z}} \times \vec{\lambda}_\rho \omega \varepsilon_t}{2\lambda_{z\psi}\lambda_\rho^2}\right) \left[\frac{\cos(\lambda_{z\psi}[d - |z - z'|]) + \cos(\lambda_{z\psi}[d - (z + z')])}{\sin(\lambda_{z\psi}d)}\right]$$

$$\vec{\tilde{G}}_{\theta_e} = \left(-\frac{\hat{\mathbf{z}} \times \vec{\lambda}_\rho \omega \mu_t}{2\lambda_{z\theta}\lambda_\rho^2}\right) \left[\frac{\cos(\lambda_{z\theta}[d - |z - z'|]) - \cos(\lambda_{z\theta}[d - (z + z')])}{\sin(\lambda_{z\theta}d)}\right]$$

$$\vec{\tilde{G}}_{\theta_{ht}} = \left(\vec{\lambda}_\rho \frac{j}{2\lambda_\rho^2}\right) \left[\frac{\operatorname{sgn}(z - z') \sin(\lambda_{z\theta}[d - |z - z'|]) + \sin(\lambda_{z\theta}[d - (z + z')])}{\sin(\lambda_{z\theta}d)}\right]$$

$$\vec{\tilde{G}}_{\theta_{hz}} = \left(\hat{\mathbf{z}}\frac{\mu_t}{2\lambda_{z\theta}\mu_z}\right) \left[\frac{\cos(\lambda_{z\theta}[d - |z - z'|]) - \cos(\lambda_{z\theta}[d - (z + z')])}{\sin(\lambda_{z\theta}d)}\right]$$

2.6.11 Physical Interpretation of Green's Functions.

We can now take a step back from the mathematics to examine how our results compare with the physically expected results. This follows quite naturally from our potential development. First, we recall (2.6) and (2.7), which are the transverse and longitudinal parts, respectively, of the expanded version of Faraday's law:

$$-\hat{\mathbf{z}} \times \nabla_t E_z + \frac{\partial}{\partial z}\hat{\mathbf{z}} \times \vec{E}_t = -\vec{J}_{ht} - j\omega\overset{\leftrightarrow}{\mu}_t \cdot \vec{H}_t$$

and

$$\nabla_t \times \vec{E}_t = -\hat{\mathbf{z}}J_{hz} - \hat{\mathbf{z}}j\omega\mu_z H_z$$

We can further expand these expressions using the auxiliary functions in (2.13) (which arise from the transverse current sources) and the definition of the Hertz potentials found in (2.11), (2.12),(2.13):

$$\vec{E}_t = \underbrace{\nabla_t\Phi}_{\vec{E}_{t_l}} - \underbrace{\hat{\mathbf{z}} \times \nabla_t\theta}_{\vec{E}_{t_r}}$$

$$\vec{H}_t = \underbrace{\nabla_t\Pi}_{\vec{H}_{t_l}} - \underbrace{\hat{\mathbf{z}} \times \nabla_t\psi}_{\vec{H}_{t_r}}$$

$$\vec{J}_{ht} = \underbrace{\nabla_t u_h}_{\vec{J}_{ht_l}} - \underbrace{\hat{\mathbf{z}} \times \nabla_t v_h}_{\vec{J}_{ht_r}}$$

First, however, we note that the Hertz potentials and auxiliary functions are nothing more than divergence-free and curl-free components to the fields and transverse current density, respectively. This is in keeping with the distinction made in [24], where it is found that transverse fields and sources may be composed of a lamellar (diverging)-only component and rotational-only component. We denote the transverse lamellar components by the subscript t_l and the transverse rotational component by the subscript t_r. We can now write

(2.6) as:

$$-\hat{\mathbf{z}} \times \nabla_t E_z + \frac{\partial}{\partial z}\hat{\mathbf{z}} \times (\nabla_t \Phi - \hat{\mathbf{z}} \times \nabla_t \theta) =$$

$$- (\nabla_t u_h - \hat{\mathbf{z}} \times \nabla_t v_h) - j\omega \overleftrightarrow{\mu}_t \cdot (\nabla_t \Pi - \hat{\mathbf{z}} \times \nabla_t \psi)$$

or

$$-\hat{\mathbf{z}} \times \nabla_t E_z + \frac{\partial}{\partial z}\hat{\mathbf{z}} \times \nabla_t \Phi + \frac{\partial}{\partial z}\hat{\mathbf{z}} \times (-\hat{\mathbf{z}} \times \nabla_t \theta) =$$

$$-\nabla_t u_h - (-\hat{\mathbf{z}} \times \nabla_t v_h) - j\omega \overleftrightarrow{\mu}_t \cdot \nabla_t \Pi - j\omega \overleftrightarrow{\mu}_t \cdot - \hat{\mathbf{z}} \times \nabla_t \psi$$

Equating the $\hat{\mathbf{z}} \times \nabla_t$ terms and the ∇_t terms, we have two new equations:

$$-\hat{\mathbf{z}} \times \nabla_t E_z + \frac{\partial}{\partial z}\hat{\mathbf{z}} \times \overbrace{\nabla_t \Phi}^{\vec{E}_{t_l}} = - \overbrace{(-\hat{\mathbf{z}} \times \nabla_t v_h)}^{\vec{J}_{ht_r}} - j\omega \overleftrightarrow{\mu}_t \cdot \overbrace{(-\hat{\mathbf{z}} \times \nabla_t \psi)}^{\vec{H}_{t_r}} \qquad (2.121)$$

$$\frac{\partial}{\partial z}\hat{\mathbf{z}} \times \underbrace{-\hat{\mathbf{z}} \times \nabla_t \theta}_{\vec{E}_{t_r}} = - \underbrace{\nabla_t u_h}_{\vec{H}_{t_l}} - j\omega \overleftrightarrow{\mu}_t \cdot \underbrace{\nabla_t \Pi}_{\vec{J}_{ht_l}} \qquad (2.122)$$

From (2.121), we see that a $\vec{J}_{ht_r}$ source maintains $E_z, \vec{E}_{t_l}$, and $\vec{H}_{t_r}$. From (2.122), we see $\vec{J}_{ht_l}$ maintains $\vec{E}_{t_r}$ and $\vec{H}_{t_l}$ fields.

In a similar manner, we can write the longitudinal portion of the expanded Faraday's law (2.7) as:

$$\nabla_t \times (\nabla_t \Phi - \hat{\mathbf{z}} \times \nabla_t \theta) = -\hat{\mathbf{z}} J_{hz} - \hat{\mathbf{z}} j\omega \mu_z H_z$$

$$\underbrace{\nabla_t \times \nabla_t \Phi}_{0} + \nabla_t \times \underbrace{(-\hat{\mathbf{z}} \times \nabla_t \theta)}_{\vec{E}_{t_r}} = -\hat{\mathbf{z}} J_{hz} - \hat{\mathbf{z}} j\omega \mu_z H_z \qquad (2.123)$$

From (2.123), we see that J_{hz} maintains $\vec{E}_{t_r}$ and H_z. The field components maintained by a given current type can be summarized as follows:

$$\vec{J}_{ht_r} \rightarrow \begin{cases} E_z \\ \vec{E}_{t_l} \\ \vec{H}_{t_r} \end{cases} \qquad \vec{J}_{ht_l} \rightarrow \begin{cases} \vec{E}_{t_r} \\ \vec{H}_{t_l} \end{cases} \qquad J_{hz} \rightarrow \begin{cases} \vec{E}_{t_r} \\ H_z \end{cases} \tag{2.124}$$

Performing a similar analysis on Ampere's law (or, by duality), we find:

$$\vec{J}_{et_r} \rightarrow \begin{cases} H_z \\ \vec{H}_{t_l} \\ \vec{E}_{t_r} \end{cases} \qquad \vec{J}_{et_l} \rightarrow \begin{cases} \vec{H}_{t_r} \\ \vec{E}_{t_l} \end{cases} \qquad J_{ez} \rightarrow \begin{cases} \vec{H}_{t_r} \\ E_z \end{cases} \tag{2.125}$$

Let us now see if we can make sense of these dependencies, taking as our basis the relationships found in (2.124). It is clear that J_{hz} should produce a transverse rotational electric field ($\vec{E}_{t_r}$) and a longitudinal magentic field (H_z). However, the fields maintained by $\vec{J}_{ht_r}$ and $\vec{J}_{ht_l}$ are not immediately intuitive. Figure 2.4 demonstrates how these dependencies arise. Figure 2.4a shows a traditional view of the radiation pattern of a general loop of constant current [10]. Figure 2.4b shows a simplified view of this radiation pattern for a loop of constant magnetic current, including the direction of the current flow and field lines. We first note the intuitive H_{t_r} field rotating in the opposite direction of the current. Also, it is well known [10] that the direction of maximum radiation for a current loop in this configuration is in the z-direction. Therefore, we note the presence of the E_z field. Finally, we see an electric field diverging from the origin. This field gives us pause, but a further investigation reveals the meaning. Figure 2.4c shows a view of the Figure 2.4b from the $-z$-direction. We see the diverging field lines in this transverse plane appear as a lamellar electric field ($\vec{E}_{t_l}$)! Therefore, we have shown how a transverse rotational magnetic current maintains a transverse (counter-) rotational magnetic field, a z-directed electric field and a transverse lamellar electric field.

82

The transverse lamellar currents may be examined in a similar fashion, as shown in Figure 2.5. Figure 2.5a shows how a diverging lamellar transverse magnetic current leads to a transverse lamellar magnetic field and a curling electric field. When viewed from the $-z$-direction, as in Figure 2.5b, we see the transverse components of the curling electric fields lead to an apparent transverse rotational electric field. Since the lamellar current is, in reality, an infinite number of these diverging currents, the z-components will cancel each other out (as the neighboring currents will be oppositely directed). Therefore, we see how a transverse lamellar magnetic current ($\vec{J}_{ht_l}$) sustains a transverse lamellar magnetic field ($\vec{H}_{t_l}$) and a transverse rotational electric field ($\vec{E}_{t_l}$). We have yet again seen how the mathematics and the physics are in perfect agreement.

Extending this analysis a bit, if we examine the TE^z case, where, by definition, $E_z = 0$, we see also from (2.124) $\vec{J}_{ht_r} = \vec{E}_{t_l} = \vec{H}_{t_r} = 0$. Additionally, from (2.125), we see that $\vec{J}_{et_l} = J_{ez} = 0$. Therefore, we have for the TE^z case that only $J_{hz}, H_z, \vec{J}_{ht_l}, \vec{H}_{t_l}, \vec{E}_{t_r}$ and $\vec{J}_{et_r}$ are non-zero. Similarly, for the TM^z case, only $J_{ez}, E_z, \vec{J}_{et_l}, \vec{E}_{t_l}, \vec{H}_{t_r}$ and $\vec{J}_{ht_r}$ are non-zero. In summary:

$$
\text{TE}^z \implies \begin{cases} E_z = 0 & \vec{E}_{t_r} \neq 0 \\[2mm] \vec{E}_{t_l} = 0 & \vec{H}_{t_l} \neq 0 \\[2mm] \vec{J}_{ht_r} = 0 & \vec{J}_{ht_l} \neq 0 \\[2mm] \vec{H}_{t_r} = 0 & J_{hz} \neq 0 \\[2mm] & H_z \neq 0 \end{cases} \qquad \text{TM}^z \implies \begin{cases} H_z = 0 & \vec{H}_{t_r} \neq 0 \\[2mm] \vec{H}_{t_l} = 0 & \vec{E}_{t_l} \neq 0 \\[2mm] \vec{J}_{et_r} = 0 & \vec{J}_{et_l} \neq 0 \\[2mm] \vec{E}_{t_r} = 0 & J_{ez} \neq 0 \\[2mm] & E_z \neq 0 \end{cases} \quad (2.126)
$$

Finally, when we compare these results with the Green's functions we developed in this section - we find an exact correlation. For example, based on the above results for the TE^z case, we would expect a dyadic Green's function of full rank for a magnetic field due to a magnetic current ($\overleftrightarrow{\widetilde{G}}_{hh}^{\text{TE}}$), since $\vec{H}_{t_l}$ is non-trivially maintained by $\vec{J}_{t_l}$, H_z is non-

trivially maintained by J_{hz} and a curling $\vec{H}$ is produced from $\vec{E}_{tr}$, which is maintained by J_{hz}. Comparing (B.12) with (2.126), we find the *hh* type Green's function is of full rank.

Similarly, comparing the terms of (B.11) with (2.126) for a magnetic field due to electric current ($\overleftrightarrow{\widetilde{G}}_{he}^{\text{TE}}$), we expect $\widetilde{G}_{he,xz}^{\text{TE}}$, $\widetilde{G}_{he,xy}^{\text{TE}}$ $\widetilde{G}_{he,zz}^{\text{TE}}$ would be zero, since $J_{ez} = 0$. We see that the $\widetilde{G}_{he,xx}^{\text{TE}}$, $\widetilde{G}_{he,xy}^{\text{TE}}$, $\widetilde{G}_{he,yx}^{\text{TE}}$ and $\widetilde{G}_{he,yy}^{\text{TE}}$ correspond to the transverse magnetic field maintained by the rotational electric current. The $\widetilde{G}_{he,zx}^{\text{TE}}$ and $\widetilde{G}_{he,zy}^{\text{TE}}$ terms represent the H_z field maintained by the rotational electric current density.

The electric fields follow a similar analysis. For an electric field due to an electric current ($\overleftrightarrow{\widetilde{G}}_{ee}^{\text{TE}}$), we would expect the only non-zero components to be the transverse fields due to transverse currents ($\widetilde{G}_{he,xx}^{\text{TE}}$, $\widetilde{G}_{he,xy}^{\text{TE}}$, $\widetilde{G}_{he,yx}^{\text{TE}}$, $\widetilde{G}_{he,yy}^{\text{TE}}$), since, by definition, $J_{ez} = E_z = 0$. In fact, this is what we find when comparing (B.9) with (2.126).

For an electric field maintained by a magnetic current ($\overleftrightarrow{\widetilde{G}}_{eh}^{\text{TE}}$), we first expect the *z*-directed fields ($\widetilde{G}_{eh,zx}^{\text{TE}}$, $\widetilde{G}_{eh,zy}^{\text{TE}}$ and $\widetilde{G}_{eh,zz}^{\text{TE}}$) to be zero, by definition. Furthermore, we see that a transverse rotational electric field is sustained by J_{hz}, therefore $\widetilde{G}_{eh,xz}^{\text{TE}}$ and $\widetilde{G}_{eh,yz}^{\text{TE}}$ are accordingly non-zero. Finally, we see that a transverse rotational electric field is sustained due to a transverse lamellar current, so $\widetilde{G}_{eh,xx}^{\text{TE}}$, $\widetilde{G}_{eh,xy}^{\text{TE}}$, $\widetilde{G}_{eh,yx}^{\text{TE}}$ and $\widetilde{G}_{eh,yy}^{\text{TE}}$ are all non-zero. Therefore, we again see exact correlation between (B.10) and (2.126).

Another point of interest is that the components of the total Green's function can easily be shown to reduce to the isotropic case when we combine the TE^z and TM^z results and then allow $\varepsilon_t = \varepsilon_z$ and $\mu_t = \mu_z$. Demonstrating the possibility of this specialization is one of the primary reasons for our re-derivation of the principal and total Green's function, as the forms given in the previous literature were not conducive to such an analysis. Now, the system is easily shown to be consistent for uniaxial and isotropic materials. The same consistency will be shown in reducing the gyrotropic case to the uniaxial case (for the principal Green's function) in a future work.

The correlation between the physically expected picture and the rigorous mathematics gives us confidence moving forward. The next chapter will repeat this derivation for the electric Green's functions using the direct field method of solving Maxwell's equations. The goal of doing so is to provide a measure of confidence in our potential development since apparent inconsistencies were found in previous literature. An additional point is to illustrate the simplicity and elegance of the potential based approach and to emphasize the complexities of the direct field solution method.
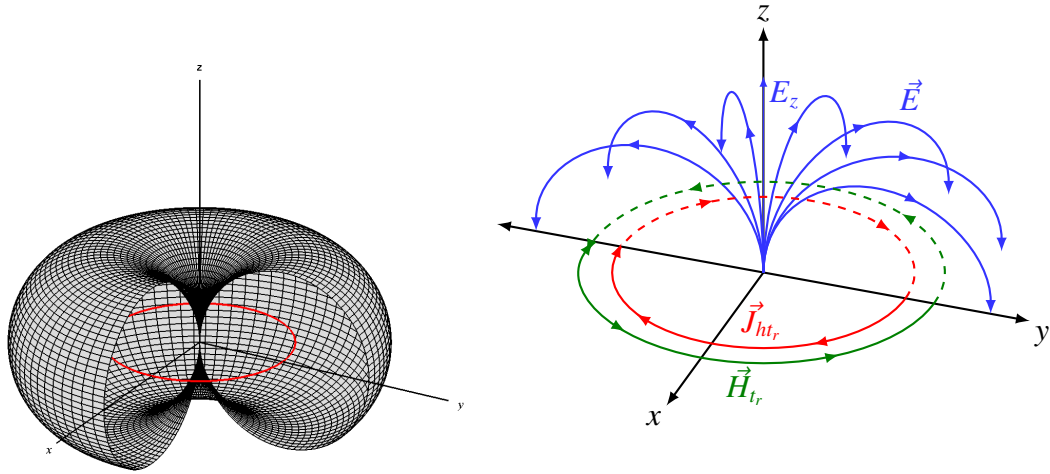
(a) The actual radiation pattern for a loop of constant current.

(b) The 3-D fields for a transverse, rotating magnetic current $\vec{J}_{ht_r}$, viewed from the side.
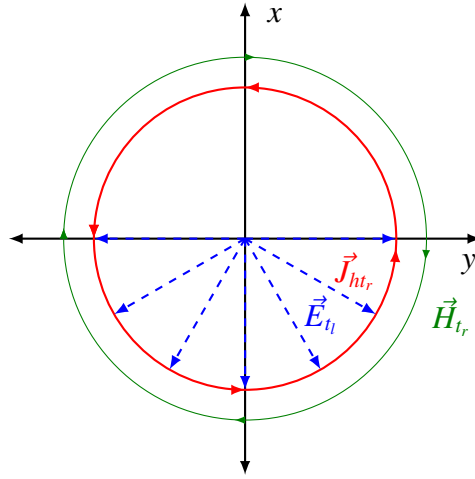
(c) A view down the z-axis of Figure 2.4b. In this case, the electric fields which are diverging from the origin appear as a transverse lamellar field, E_{t_l}.

Figure 2.4: Three different views of the radiation pattern for a constant current loop, showing how $\vec{J}_{ht_r}$ maintains E_z, $\vec{E}_{t_l}$ and $\vec{H}_{t_r}$.
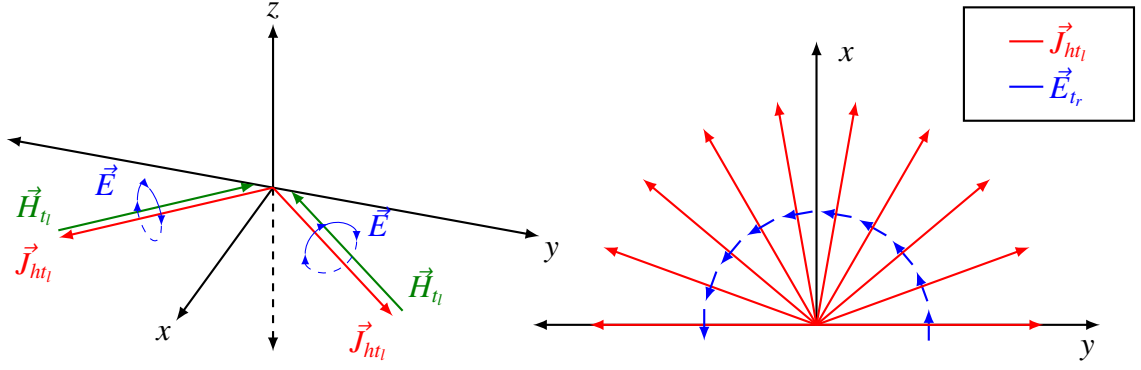
(a) Two notional vectors in a diverging lamellar current, shown in 3-D.

(b) A 2-D view of Figure 2.5a, from the $-z$-direction, where the number of diverging lamellar magnetic currents has been increased to demonstrate the appearance of the transverse rotating electric field $\vec{E}_{t_r}$.

Figure 2.5: Two different views of the transverse lamellar current, showing how $J_{h_t l}$ maintains $\vec{E}_{t_r}$ and $\vec{H}_{t_l}$

.

III.   Direct Field Formulation for the Total Parallel Plate Green's Function of Anisotropic Uniaxial Media

Now that we have found the fields (through the Green's functions) using a potential development, we would like to compare these results with a direct-field solution. This is a lengthy chapter, but provides an in-depth development of the direct field solutions for a uniaxial anisotropic homogeneous media subject to parallel plate waveguide (PPWG) boundary conditions and will compare them to the potential-based method in order to demonstrate their correctness and the benefits of the potential-based method. We take the same approach as before, finding the total solution to be the the superposition of a principal (forced, unbounded) and a reflected (unforced, bounded) solution.

3.1   Principal Solution

Maxwell's equations for an electrically and magnetically uniaxial material with generalized electric and magnetic sources are (with the constitutive dyads taking the usual uniaxial form of (2.3) and noting $\nabla \times \overset{\leftrightarrow}{I} = \overset{\leftrightarrow}{I} \times \nabla$):

$$\nabla \times \vec{E}^p = -\vec{J}_h - j\omega\overset{\leftrightarrow}{\mu}\cdot\vec{H}^p \qquad\qquad \overset{\leftrightarrow}{I} \times \nabla\cdot\vec{E}^p = -\vec{J}_h - j\omega\overset{\leftrightarrow}{\mu}\cdot\vec{H}^p$$
$$\nabla \times \vec{H}^p = \vec{J}_e + j\omega\overset{\leftrightarrow}{\varepsilon}\cdot\vec{E}^p \qquad\Longrightarrow\qquad \overset{\leftrightarrow}{I} \times \nabla\cdot\vec{H}^p = \vec{J}_e + j\omega\overset{\leftrightarrow}{\varepsilon}\cdot\vec{E}^p$$

Since we are seeking the principal solution, which is a forced and unbounded system, we again use the two Fourier Transforms of (2.36) and (2.39), which allow us to write Maxwell's equations as:

$$\overset{\leftrightarrow}{I} \times j\vec{\lambda}\cdot\overset{\approx}{\vec{E}}^p = -\overset{\approx}{\vec{J}}_h - j\omega\overset{\leftrightarrow}{\mu}\cdot\overset{\approx}{\vec{H}}^p \qquad\Longrightarrow\qquad j\vec{\lambda}\cdot\overset{\approx}{\vec{E}}^p = -\overset{\approx}{\vec{J}}_h - j\omega\overset{\leftrightarrow}{\mu}\cdot\overset{\approx}{\vec{H}}^p \qquad (3.1a)$$

$$\overset{\leftrightarrow}{I} \times j\vec{\lambda}\cdot\overset{\approx}{\vec{H}}^p = \overset{\approx}{\vec{J}}_e + j\omega\overset{\leftrightarrow}{\varepsilon}\cdot\overset{\approx}{\vec{E}}^p \qquad\Longrightarrow\qquad j\vec{\lambda}\cdot\overset{\approx}{\vec{H}}^p = \overset{\approx}{\vec{J}}_e + j\omega\overset{\leftrightarrow}{\varepsilon}\cdot\overset{\approx}{\vec{E}}^p \qquad (3.1b)$$

where $\vec{\vec{\lambda}} = \overleftrightarrow{I} \times \vec{\lambda} = \vec{\lambda} \times \overleftrightarrow{I}$. We can now solve the coupled system of Maxwell's equations given in (3.1). Starting with (3.1a), we have the magnetic field as:

$$\frac{j\vec{\vec{\lambda}}\cdot\vec{\tilde{E}}^p + \vec{\tilde{J}}_h}{-j\omega} = \overleftrightarrow{\mu}\cdot\vec{\tilde{H}}^p \implies \vec{\tilde{H}}^p = \frac{\overleftrightarrow{\mu}^{-1}\cdot j\vec{\vec{\lambda}}\cdot\vec{\tilde{E}}^p}{-j\omega} + \frac{\overleftrightarrow{\mu}^{-1}\cdot\vec{\tilde{J}}_h}{-j\omega} \tag{3.2}$$

Substituting this result into (3.1b), and solving for the electric field, we find the electric field directly:

$$\begin{aligned}
\vec{\tilde{E}}^p &= -j\omega\overleftrightarrow{w}_e^{-1}\cdot\overleftrightarrow{\mu}\cdot\vec{\tilde{J}}_e - j\overleftrightarrow{w}_e^{-1}\cdot\overleftrightarrow{\mu}\cdot\vec{\vec{\lambda}}\cdot\overleftrightarrow{\mu}^{-1}\cdot\vec{\tilde{J}}_h \\[2mm]
&= \overleftrightarrow{\tilde{G}}_{ee}^p \cdot\vec{\tilde{J}}_e + \overleftrightarrow{\tilde{G}}_{eh}^p \cdot\vec{\tilde{J}}_h \\[2mm]
\overleftrightarrow{w}_e &= -\overleftrightarrow{\mu}\cdot\vec{\vec{\lambda}}\cdot\overleftrightarrow{\mu}^{-1}\cdot\vec{\vec{\lambda}} - \overleftrightarrow{k}^2 \\[2mm]
\overleftrightarrow{k}^2 &= \omega^2\overleftrightarrow{\mu}\cdot\overleftrightarrow{\varepsilon}
\end{aligned} \tag{3.3}$$

Similarly, we can find the magnetic field to be:

$$\begin{aligned}
\vec{\tilde{H}}^p &= j\overleftrightarrow{w}_h^{-1}\cdot\overleftrightarrow{\varepsilon}\cdot\vec{\vec{\lambda}}\cdot\overleftrightarrow{\varepsilon}^{-1}\cdot\vec{\tilde{J}}_e - j\omega\overleftrightarrow{w}_h^{-1}\cdot\overleftrightarrow{\varepsilon}\cdot\vec{\tilde{J}}_h \\[2mm]
&= \overleftrightarrow{\tilde{G}}_{he}^p \cdot\vec{\tilde{J}}_e + \overleftrightarrow{\tilde{G}}_{hh}^p \cdot\vec{\tilde{J}}_h \\[2mm]
\overleftrightarrow{w}_h &= -\overleftrightarrow{\varepsilon}\cdot\vec{\vec{\lambda}}\cdot\overleftrightarrow{\varepsilon}^{-1}\cdot\vec{\vec{\lambda}} - \overleftrightarrow{k}^2 \\[2mm]
\overleftrightarrow{k}^2 &= \omega^2\overleftrightarrow{\varepsilon}\cdot\overleftrightarrow{\mu}
\end{aligned} \tag{3.4}$$

We note that the $\overleftrightarrow{k}$ terms are equivalent for the $\overleftrightarrow{w}_e$ and $\overleftrightarrow{w}_h$ terms only due to the diagonal nature of the constitutive parameter dyads, $\overleftrightarrow{\varepsilon}$ and $\overleftrightarrow{\mu}$. As a result, we see that $\overleftrightarrow{\varepsilon}\cdot\overleftrightarrow{\mu} = \overleftrightarrow{\mu}\cdot\overleftrightarrow{\varepsilon}$. In a more complex material, such as chiral or gyrotropic, with non-diagonal constitutive dyads, this would not be the case.

3.1.1 Inverse of w_e Dyad.

Although obtaining the expressions for the electric and magnetic fields was straightforward, finding the inverse of $\overleftrightarrow{\mathsf{w}}_e$ is no trivial matter. Havrilla [46] is able to find a vectorized form of $\overleftrightarrow{\mathsf{w}}_e$ in the case of a dielectric uniaxial material, which allows for a simple inversion using an identity given on page 21 of [20]. However, in spite of great efforts, such an expression could not be found when both constitutive parameters are dyadic. This will require each component of the dyadic solution to be determined individually. As such, we will concentrate on the $ee-$ and eh-type Green's functions, which are found from $\overleftrightarrow{\mathsf{w}}_e$. First, we find $\overleftrightarrow{\lambda}$. Recalling the definition of $\overleftrightarrow{\lambda}$, we see it is an anti-symmetric dyad:

$$
\begin{aligned}
\overleftrightarrow{\lambda} = \overleftrightarrow{I} \times \vec{\lambda} &= (\hat{\mathbf{x}}\hat{\mathbf{x}} + \hat{\mathbf{y}}\hat{\mathbf{y}} + \hat{\mathbf{z}}\hat{\mathbf{z}}) \times (\hat{\mathbf{x}}\lambda_x + \hat{\mathbf{y}}\lambda_y + \hat{\mathbf{z}}\lambda_z) \\
&= \begin{bmatrix} 0 & -\lambda_z & \lambda_y \\ \lambda_z & 0 & -\lambda_x \\ -\lambda_y & \lambda_x & 0 \end{bmatrix}
\end{aligned}
\tag{3.5}
$$

Using this expression and some straightforward mathematical manipulation, we find $\overleftrightarrow{\mathsf{w}}_e$:

$$
\overleftrightarrow{\mathsf{w}}_e = -\overleftrightarrow{\mu} \cdot \overleftrightarrow{\lambda} \cdot \overleftrightarrow{\mu}^{-1} \cdot \overleftrightarrow{\lambda} - \overleftrightarrow{k}^2 = \begin{bmatrix} \lambda_z^2 - k_t^2 + \frac{\mu_t}{\mu_z}\lambda_y^2 & -\frac{\mu_t}{\mu_z}\lambda_x\lambda_y & -\lambda_x\lambda_z \\ -\frac{\mu_t}{\mu_z}\lambda_x\lambda_y & \lambda_z^2 - k_t^2 + \frac{\mu_t}{\mu_z}\lambda_x^2 & -\lambda_y\lambda_z \\ -\frac{\mu_z}{\mu_t}\lambda_x\lambda_z & -\frac{\mu_z}{\mu_t}\lambda_y\lambda_z & \frac{\mu_z}{\mu_t}\lambda_\rho^2 - k_z^2 \end{bmatrix}
\tag{3.6}
$$

The inverse of $\overleftrightarrow{\mathsf{w}}_e$ may be found by the adjoint method

$$
\overleftrightarrow{\mathsf{w}}_e^{-1} = \frac{\operatorname{adj} \overleftrightarrow{\mathsf{w}}_e}{\det \overleftrightarrow{\mathsf{w}}_e}
\tag{3.7}
$$

Therefore, we must find the determinant and adjoint of $\overleftrightarrow{\mathsf{w}}_e$.

3.1.1.1 Determinant of w_e Dyad.

Clearly, the determinant of $\overset{\leftrightarrow}{\mathsf{w}}_e$ is a tedious expression:

$$
\det \overset{\leftrightarrow}{\mathsf{w}}_e = \overbrace{\left(\lambda_z{}^2 - k_t{}^2 + \frac{\mu_t}{\mu_z}\lambda_y{}^2 \right) \left[\left(\lambda_z{}^2 - k_t{}^2 + \frac{\mu_t}{\mu_z}\lambda_x{}^2 \right) \left(\frac{\mu_z}{\mu_t}\lambda_\rho^2 - k_z^2 \right) - (-\lambda_y\lambda_z)\left(-\frac{\mu_z}{\mu_t}\lambda_y\lambda_z \right) \right]}^{A}
$$
$$
\overbrace{- \left(-\frac{\mu_t}{\mu_z}\lambda_x\lambda_y \right)\left[\left(-\frac{\mu_t}{\mu_z}\lambda_x\lambda_y \right)\left(\frac{\mu_z}{\mu_t}\lambda_\rho^2 - k_z^2 \right) - (-\lambda_y\lambda_z)\left(-\frac{\mu_z}{\mu_t}\lambda_x\lambda_z \right) \right]}^{B}
$$
$$
\overbrace{+ (-\lambda_x\lambda_z)\left[\left(-\frac{\mu_t}{\mu_z}\lambda_x\lambda_y \right)\left(-\frac{\mu_z}{\mu_t}\lambda_y\lambda_z \right) - \left(\lambda_z{}^2 - k_t{}^2 + \frac{\mu_t}{\mu_z}\lambda_x{}^2 \right)\left(-\frac{\mu_z}{\mu_t}\lambda_x\lambda_z \right) \right]}^{C}
$$

$$\tag{3.8}$$

Due to the length of (3.8), we can examine each piece individually, define $\lambda_{z\psi}^2 = k_t^2 - \frac{\mu_t}{\mu_z}\lambda_\rho^2$ and $\lambda_{z\theta}^2 = k_t^2 - \frac{\varepsilon_t}{\varepsilon_z}\lambda_\rho^2$ and simplify. Glossing over the tedious, yet straightforward, algebraic details, we find the relatively simple expression:

$$
\boxed{\det \overset{\leftrightarrow}{\mathsf{w}}_e = \left(-k_z^2 \right)\left(\lambda_z{}^2 - \lambda_{z\theta}^2 \right)\left(\lambda_z^2 - \lambda_{z\psi}^2 \right)}
$$

$$\tag{3.9}$$

3.1.1.2 Adjoint of w_e Dyad.

Now, we turn our attention to the adjoint of $\overset{\leftrightarrow}{\mathsf{w}}_e$, which is defined as the transpose of the cofactor matrix:

$$
\text{adj}\,\overset{\leftrightarrow}{\mathsf{w}}_e = \overset{\leftrightarrow}{C}{}^T \qquad \rightarrow \qquad C_{mn} = (-1)^{m+n} M_{mn}
$$

$$\tag{3.10}$$

where M_{mn} is the determinant of the minor with the mth row and n^{th} column removed. Again, this is a tediously long development, as each element of the cofactor matrix must be simplified individually. Therefore, we will bypass the details and give the individual terms of the cofactor matrix. Since we have C as

$$
\overset{\leftrightarrow}{C} = \begin{bmatrix} M_{11} & -M_{12} & M_{13} \\ -M_{21} & M_{22} & -M_{23} \\ M_{31} & -M_{32} & M_{33} \end{bmatrix}
$$

91

therefore, we have the adjoint of $\overset{\leftrightarrow}{\mathsf{w}}_e$ as:

$$\text{adj } \overset{\leftrightarrow}{\mathsf{w}}_e = \overset{\leftrightarrow}{C}^T = \begin{bmatrix} M_{11} & -M_{21} & M_{31} \\ -M_{12} & M_{22} & -M_{32} \\ M_{13} & -M_{23} & M_{33} \end{bmatrix} \tag{3.11}$$

where:

$$\begin{aligned}
M_{11} &= \left(\lambda_z{}^2 - \lambda_{z\theta}^2\right)\left(-\frac{\varepsilon_z\mu_z}{\varepsilon_t\mu_t}\lambda_{z\psi}^2\right) - \frac{\varepsilon_z}{\varepsilon_t}\lambda_y{}^2\left(\frac{\varepsilon_t\mu_z}{\varepsilon_z\mu_t}\lambda_z{}^2 - \lambda_{z\psi}^2\right) \\
M_{21} &= -\frac{\varepsilon_z}{\varepsilon_t}\lambda_x\lambda_y\left(\frac{\varepsilon_t\mu_z}{\varepsilon_z\mu_t}\lambda_z{}^2 - \lambda_{z\psi}^2\right) \\
M_{31} &= \lambda_x\lambda_z\left(\lambda_z{}^2 - \lambda_{z\theta}^2\right) \\
M_{12} &= -\frac{\varepsilon_z}{\varepsilon_t}\lambda_x\lambda_y\left(\frac{\varepsilon_t\mu_z}{\varepsilon_z\mu_t}\lambda_z{}^2 - \lambda_{z\psi}^2\right) \\
M_{22} &= \left(\lambda_z{}^2 - \lambda_{z\theta}^2\right)\left(-\frac{\varepsilon_z\mu_z}{\varepsilon_t\mu_t}\lambda_{z\psi}^2\right) - \frac{\varepsilon_z}{\varepsilon_t}\lambda_x{}^2\left(\frac{\varepsilon_t\mu_z}{\varepsilon_z\mu_t}\lambda_z{}^2 - \lambda_{z\psi}^2\right) \\
M_{32} &= \left(-\lambda_y\lambda_z\right)\left(\lambda_z{}^2 - \lambda_{z\theta}^2\right) \\
M_{13} &= \left(\lambda_z{}^2 - \lambda_{z\theta}^2\right)\left(\frac{\mu_z}{\mu_t}\lambda_x\lambda_z\right) \\
M_{23} &= \left(\lambda_z{}^2 - \lambda_{z\theta}^2\right)\left(-\frac{\mu_z}{\mu_t}\lambda_y\lambda_z\right) \\
M_{33} &= \left(\lambda_z^2 - k_t^2\right)\left(\lambda_z^2 - \lambda_{z\theta}^2\right)
\end{aligned} \tag{3.12}$$

Finally, we have the inverse of $\overset{\leftrightarrow}{\mathsf{w}}_e$ as:

$$\overset{\leftrightarrow}{\mathsf{w}}_e^{-1} = \frac{\text{adj } \overset{\leftrightarrow}{\mathsf{w}}_e}{\det \overset{\leftrightarrow}{\mathsf{w}}_e} = \frac{1}{\left(-k_z^2\right)\left(\lambda_z{}^2 - \lambda_{z\theta}^2\right)\left(\lambda_z^2 - \lambda_{z\psi}^2\right)}\begin{bmatrix} M_{11} & -M_{21} & M_{31} \\ -M_{12} & M_{22} & -M_{32} \\ M_{13} & -M_{23} & M_{33} \end{bmatrix} \tag{3.13}$$

3.1.2 *ee Green's Function.*

From (3.3), we have $\overset{\approx p}{\overset{\leftrightarrow}{G}}_{ee} = -j\omega\overset{\leftrightarrow}{\mathbf{w}}_e^{-1}\cdot\overset{\leftrightarrow}{\mu}$. Using (3.13), we can write the Green's function in terms of the *M* terms above:

$$
\begin{aligned}
\overset{\approx p}{\overset{\leftrightarrow}{G}}_{ee} &= -j\omega\overset{\leftrightarrow}{\mathbf{w}}_e^{-1}\cdot\overset{\leftrightarrow}{\mu} \\[2mm]
&= \frac{-j\omega}{\left(-k_z^2\right)\left(\lambda_z{}^2 - \lambda_{z\theta}^2\right)\left(\lambda_z^2 - \lambda_{z\psi}^2\right)}
\begin{bmatrix}
\mu_t M_{11} & -\mu_t M_{21} & \mu_z M_{31} \\
-\mu_t M_{12} & \mu_t M_{22} & -\mu_z M_{32} \\
\mu_t M_{13} & -\mu_t M_{23} & \mu_z M_{33}
\end{bmatrix} \\[2mm]
&=
\begin{bmatrix}
\widetilde{G}_{ee,xx}^{p} & \widetilde{G}_{ee,xy}^{p} & \widetilde{G}_{ee,xz}^{p} \\
\widetilde{G}_{ee,yx}^{p} & \widetilde{G}_{ee,yy}^{p} & \widetilde{G}_{ee,yz}^{p} \\
\widetilde{G}_{ee,zx}^{p} & \widetilde{G}_{ee,zy}^{p} & \widetilde{G}_{ee,zz}^{p}
\end{bmatrix}
\end{aligned}
\tag{3.14}
$$

Since we have no vectorized representation for $\overset{\leftrightarrow}{\mathbf{w}}_e^{-1}$, we must find each of the elements of the Green's function dyad individually. Following the straightforward operations indicated in (3.14), the elements of the principal electric Green's function are summarized in 3.1.2.1. It is important to note one point that would not be entirely intuitive and requires a bit of foresight. Since we are operating in a Fourier domain and will have to evaluate the λ_z integrals in the complex plane, we must take care to ensure that the contribution as $\lambda_z \to \infty$ is zero. This is true of every element in $\widetilde{G}_{ee}^{p}$, except for the $\hat{\mathbf{z}}\hat{\mathbf{z}}$ component. In fact, the limit is:

$$
\lim_{\lambda_z\to\infty}\widetilde{G}_{ee,zz}^{p} = j\omega\mu_z\frac{\left(\lambda_z^2\right)\left(\lambda_z^2\right)}{k_z^2\left(\lambda_z^2\right)\left(\lambda_z^2\right)} = -\frac{1}{j\omega\varepsilon_z}
$$

By adding and subtracting this term, we ensure $\lim_{R\to\infty} C_R \to 0$ as $\lambda_{z\theta} \to \infty$. This leads to the well-known depolarizing term.

93

3.1.2.1 Forced Electric (ee) Green's Function Summary - $(\vec{\lambda}_\rho, \lambda_z)$ Domain.

$$
\overset{\leftrightarrow}{\tilde{\tilde{G}}}_{ee}^p =
\begin{bmatrix}
\tilde{\tilde{G}}_{ee,xx}^p & \tilde{\tilde{G}}_{ee,xy}^p & \tilde{\tilde{G}}_{ee,xz}^p \\
\tilde{\tilde{G}}_{ee,yx}^p & \tilde{\tilde{G}}_{ee,yy}^p & \tilde{\tilde{G}}_{ee,yz}^p \\
\tilde{\tilde{G}}_{ee,zx}^p & \tilde{\tilde{G}}_{ee,zy}^p & \tilde{\tilde{G}}_{ee,zz}^p
\end{bmatrix}
$$

$$
\tilde{\tilde{G}}_{ee,xx}^p = -\frac{j\omega\varepsilon_z}{\varepsilon_t}\left[\frac{\mu_z\lambda_{z\psi}^2\left(\lambda_z{}^2 - \lambda_{z\theta}^2\right) + \mu_t\lambda_y{}^2\left(\frac{\varepsilon_t\mu_z}{\varepsilon_z\mu_t}\lambda_z{}^2 - \lambda_{z\psi}^2\right)}{k_z^2\left(\lambda_z{}^2 - \lambda_{z\theta}^2\right)\left(\lambda_z^2 - \lambda_{z\psi}^2\right)}\right]
$$

$$
\tilde{\tilde{G}}_{ee,xy}^p = \frac{j\omega\varepsilon_z\mu_t}{\varepsilon_t}\left[\frac{\lambda_x\lambda_y\left(\frac{\varepsilon_t\mu_z}{\varepsilon_z\mu_t}\lambda_z{}^2 - \lambda_{z\psi}^2\right)}{k_z^2\left(\lambda_z{}^2 - \lambda_{z\theta}^2\right)\left(\lambda_z^2 - \lambda_{z\psi}^2\right)}\right]
$$

$$
\tilde{\tilde{G}}_{ee,xz}^p = j\omega\mu_z\left[\frac{\lambda_x\lambda_z}{k_z^2\left(\lambda_z^2 - \lambda_{z\psi}^2\right)}\right]
$$

$$
\tilde{\tilde{G}}_{ee,yx}^p = \frac{j\omega\varepsilon_z\mu_t}{\varepsilon_t}\left[\frac{\lambda_x\lambda_y\left(\frac{\varepsilon_t\mu_z}{\varepsilon_z\mu_t}\lambda_z{}^2 - \lambda_{z\psi}^2\right)}{k_z^2\left(\lambda_z{}^2 - \lambda_{z\theta}^2\right)\left(\lambda_z^2 - \lambda_{z\psi}^2\right)}\right]
$$

$$
\tilde{\tilde{G}}_{ee,yy}^p = -\frac{j\omega\varepsilon_z}{\varepsilon_t}\left[\frac{\mu_z\lambda_{z\psi}^2\left(\lambda_z{}^2 - \lambda_{z\theta}^2\right) + \mu_t\lambda_x{}^2\left(\frac{\varepsilon_t\mu_z}{\varepsilon_z\mu_t}\lambda_z{}^2 - \lambda_{z\psi}^2\right)}{k_z^2\left(\lambda_z{}^2 - \lambda_{z\theta}^2\right)\left(\lambda_z^2 - \lambda_{z\psi}^2\right)}\right]
$$

$$
\tilde{\tilde{G}}_{ee,yz}^p = j\omega\mu_z\left[\frac{\lambda_y\lambda_z}{k_z^2\left(\lambda_z^2 - \lambda_{z\psi}^2\right)}\right]
$$

$$
\tilde{\tilde{G}}_{ee,zx}^p = j\omega\mu_z\left[\frac{\lambda_x\lambda_z}{k_z^2\left(\lambda_z^2 - \lambda_{z\psi}^2\right)}\right]
$$

$$
\tilde{\tilde{G}}_{ee,zy}^p = j\omega\mu_z\left[\frac{\lambda_y\lambda_z}{k_z^2\left(\lambda_z^2 - \lambda_{z\psi}^2\right)}\right]
$$

$$
\tilde{\tilde{G}}_{ee,zz}^p = \frac{(j\omega\mu_z)(j\omega\varepsilon_z)\left(\lambda_z^2 - k_t^2\right) + k_z^2\left(\lambda_z^2 - \lambda_{z\psi}^2\right)}{j\omega\varepsilon_z k_z^2\left(\lambda_z^2 - \lambda_{z\psi}^2\right)} - \frac{1}{j\omega\varepsilon_z}
$$

3.1.3 *eh*-type Green's Function.

From (3.3), we can also find $\overset{\leftrightarrow}{\tilde{\tilde{G}}}{}^p_{eh}$:

$$\overset{\leftrightarrow}{\tilde{\tilde{G}}}{}^p_{eh} = -j\overset{\leftrightarrow}{\mathsf{w}}{}_e^{-1} \cdot \overset{\leftrightarrow}{\mu} \cdot \overset{\leftrightarrow}{\lambda} \cdot \overset{\leftrightarrow}{\mu}{}^{-1}$$

$$= \frac{j}{k_z^2 \left(\lambda_z{}^2 - \lambda_{z\theta}^2\right) \left(\lambda_z^2 - \lambda_{z\psi}^2\right)}$$

$$\begin{bmatrix} -\lambda_z M_{21} - \frac{\lambda_y \mu_z}{\mu_t} M_{31} & \frac{\lambda_x \mu_z}{\mu_t} M_{31} - \lambda_z M_{11} & \frac{\lambda_y \mu_t}{\mu_z} M_{11} + \frac{\lambda_x \mu_t}{\mu_z} M_{21} \\[2mm] \lambda_z M_{22} + \frac{\lambda_y \mu_z}{\mu_t} M_{32} & \lambda_z M_{12} - \frac{\lambda_x \mu_z}{\mu_t} M_{32} & -\frac{\lambda_y \mu_t}{\mu_z} M_{12} - \frac{\lambda_x \mu_t}{\mu_z} M_{22} \\[2mm] -\lambda_z M_{23} - \frac{\lambda_y \mu_z}{\mu_t} M_{33} & \frac{\lambda_x \mu_z}{\mu_t} M_{33} - \lambda_z M_{13} & \frac{\lambda_y \mu_t}{\mu_z} M_{13} + \frac{\lambda_x \mu_t}{\mu_z} M_{23} \end{bmatrix}$$

$$= \begin{bmatrix} \tilde{\tilde{G}}^p_{eh,xx} & \tilde{\tilde{G}}^p_{eh,xy} & \tilde{\tilde{G}}^p_{eh,xz} \\[2mm] \tilde{\tilde{G}}^p_{eh,yx} & \tilde{\tilde{G}}^p_{eh,yy} & \tilde{\tilde{G}}^p_{eh,yz} \\[2mm] \tilde{\tilde{G}}^p_{eh,zx} & \tilde{\tilde{G}}^p_{eh,zy} & \tilde{\tilde{G}}^p_{eh,zz} \end{bmatrix}$$

$$(3.15)$$

Again, we must find each of the elements of the Green's function dyad individually. In this case, the operations are entirely straightforward. The results are summarized in 3.1.3.1.

$$
\overset{\leftrightarrow}{\tilde{\tilde{G}}}_{eh} = \left[\begin{array}{ccc} \tilde{\tilde{G}}^p_{eh,xx} & \tilde{\tilde{G}}^p_{eh,xy} & \tilde{\tilde{G}}^p_{eh,xz} \\[2mm] \tilde{\tilde{G}}^p_{eh,yx} & \tilde{\tilde{G}}^p_{eh,yy} & \tilde{\tilde{G}}^p_{eh,yz} \\[2mm] \tilde{\tilde{G}}^p_{eh,zx} & \tilde{\tilde{G}}^p_{eh,zy} & \tilde{\tilde{G}}^p_{eh,zz} \end{array} \right]
$$

$$
\tilde{\tilde{G}}^p_{eh,xx} = j\lambda_x\lambda_y\lambda_z \left[\frac{\frac{\varepsilon_z}{\varepsilon_t}\left(\frac{\varepsilon_t\mu_z}{\varepsilon_z\mu_t}\lambda_z{}^2 - \lambda^2_{z\psi}\right) - \frac{\mu_z}{\mu_t}\left(\lambda_z{}^2 - \lambda^2_{z\theta}\right)}{k_z^2\left(\lambda_z{}^2 - \lambda^2_{z\theta}\right)\left(\lambda_z^2 - \lambda^2_{z\psi}\right)} \right]
$$

$$
\tilde{\tilde{G}}^p_{eh,xy} = j\lambda_z \left[\frac{\frac{\varepsilon_z}{\varepsilon_t}\left[\left(\lambda_z{}^2 - \lambda^2_{z\theta}\right)\left(\frac{\mu_z}{\mu_t}\lambda^2_{z\psi}\right) + \lambda_y{}^2\left(\frac{\varepsilon_t\mu_z}{\varepsilon_z\mu_t}\lambda_z{}^2 - \lambda^2_{z\psi}\right)\right] + \frac{\mu_z}{\mu_t}\lambda_x^2\left(\lambda_z{}^2 - \lambda^2_{z\theta}\right)}{k_z^2\left(\lambda_z{}^2 - \lambda^2_{z\theta}\right)\left(\lambda_z^2 - \lambda^2_{z\psi}\right)} \right]
$$

$$
\tilde{\tilde{G}}^p_{eh,xz} = -j\frac{\mu_t}{\mu_z}\lambda_y \left[\frac{\left(\lambda_z{}^2 - \lambda^2_{z\theta}\right)\left(\frac{\varepsilon_z\mu_z}{\varepsilon_t\mu_t}\lambda^2_{z\psi}\right) + \frac{\varepsilon_z}{\varepsilon_t}\left(\frac{\varepsilon_t\mu_z}{\varepsilon_z\mu_t}\lambda_z{}^2 - \lambda^2_{z\psi}\right)\lambda^2_\rho}{k_z^2\left(\lambda_z{}^2 - \lambda^2_{z\theta}\right)\left(\lambda_z^2 - \lambda^2_{z\psi}\right)} \right]
$$

$$
\tilde{\tilde{G}}^p_{eh,yx} = -j\lambda_z \left[\frac{\frac{\varepsilon_z}{\varepsilon_t}\left[\left(\lambda_z{}^2 - \lambda^2_{z\theta}\right)\left(\frac{\mu_z}{\mu_t}\lambda^2_{z\psi}\right) + \lambda_x{}^2\left(\frac{\varepsilon_t\mu_z}{\varepsilon_z\mu_t}\lambda_z{}^2 - \lambda^2_{z\psi}\right)\right] + \frac{\mu_z}{\mu_t}\lambda_y{}^2\left(\lambda_z{}^2 - \lambda^2_{z\theta}\right)}{k_z^2\left(\lambda_z{}^2 - \lambda^2_{z\theta}\right)\left(\lambda_z^2 - \lambda^2_{z\psi}\right)} \right]
$$

$$
\tilde{\tilde{G}}^p_{eh,yy} = -j\lambda_x\lambda_y\lambda_z \left[\frac{\frac{\varepsilon_z}{\varepsilon_t}\left(\frac{\varepsilon_t\mu_z}{\varepsilon_z\mu_t}\lambda_z{}^2 - \lambda^2_{z\psi}\right) - \frac{\mu_z}{\mu_t}\left(\lambda_z{}^2 - \lambda^2_{z\theta}\right)}{k_z^2\left(\lambda_z{}^2 - \lambda^2_{z\theta}\right)\left(\lambda_z^2 - \lambda^2_{z\psi}\right)} \right]
$$

$$
\tilde{\tilde{G}}^p_{eh,yz} = j\frac{\mu_t}{\mu_z}\lambda_x \left[\frac{\left(\lambda_z{}^2 - \lambda^2_{z\theta}\right)\left(\frac{\varepsilon_z\mu_z}{\varepsilon_t\mu_t}\lambda^2_{z\psi}\right) + \frac{\varepsilon_z}{\varepsilon_t}\left(\frac{\varepsilon_t\mu_z}{\varepsilon_z\mu_t}\lambda_z{}^2 - \lambda^2_{z\psi}\right)\lambda^2_\rho}{k_z^2\left(\lambda_z{}^2 - \lambda^2_{z\theta}\right)\left(\lambda_z^2 - \lambda^2_{z\psi}\right)} \right]
$$

$$
\tilde{\tilde{G}}^p_{eh,zx} = j\frac{\mu_z}{\mu_t} \left[\frac{\lambda_y k_t^2}{k_z^2\left(\lambda_z^2 - \lambda^2_{z\psi}\right)} \right]
$$

$$
\tilde{\tilde{G}}^p_{eh,zy} = -j\frac{\mu_z}{\mu_t} \left[\frac{\lambda_x k_t^2}{k_z^2\left(\lambda_z^2 - \lambda^2_{z\psi}\right)} \right]
$$

$$
\tilde{\tilde{G}}^p_{eh,zz} = 0
$$

Therefore, we see a high degree of symmetry in the Green's function dyad, as expected.
Additionally, we see a depolarizing term in the electric portion of the Green's function,

but not in the magnetic portion. This agrees with our intuition about Maxwell's equations, which tells us that a $\hat{\mathbf{z}}$ directed electric current will produce no $\hat{\mathbf{z}}$ directed magnetic field. Therefore, when we perform the piecewise Principal Value integration over the entire area of interest (including the source point discontinuity) the $\overset{\leftrightarrow}{\tilde{\tilde{G}}}{}^{p}_{eh}$ Green's function will require no depolarizing term to correct for the field generated in the infinitesimal region where $z - \delta < z < z + \delta$. This depolarizing effect is shown graphically in Figure 2.2 and is well documented in previous works [3, 5, 11, 21, 23, 40, 57, 91, 93, 101, 111].

3.1.4   Evaluation of ee-type Principal Green's Function.

The principal spectral-domain dyadic Green's functions $\overset{\leftrightarrow}{\tilde{\tilde{G}}}{}^{p}_{ee}$ and $\overset{\leftrightarrow}{\tilde{\tilde{G}}}{}^{p}_{eh}$ represent the electric field maintained by the electric current density $\overset{\rightarrow}{\tilde{\tilde{J}}}_{e}$ and the magnetic current density $\overset{\rightarrow}{\tilde{\tilde{J}}}_{h}$, respectively. Now, we can use the inverse Fourier Transform from (2.40) to transform these Green's functions back to the $(\vec{\lambda}_{\rho}, z)$ domain, in much the same way as in the potential method:

$$
\begin{aligned}
\vec{\tilde{E}}{}^{p}(\vec{\lambda}_{\rho}, z) &= \frac{1}{2\pi} \int\limits_{-\infty}^{\infty} \overset{\leftrightarrow}{\tilde{\tilde{G}}}{}^{p}_{ee}(\vec{\lambda}_{\rho}, \lambda_{z}) \cdot \vec{\tilde{J}}_{e}(\vec{\lambda}_{\rho}, \lambda_{z}) e^{j\lambda_{z}z} d\lambda_{z} + \frac{1}{2\pi} \int\limits_{-\infty}^{\infty} \overset{\leftrightarrow}{\tilde{\tilde{G}}}{}^{p}_{eh}(\vec{\lambda}_{\rho}, \lambda_{z}) \cdot \vec{\tilde{J}}_{h}(\vec{\lambda}_{\rho}, \lambda_{z}) e^{j\lambda_{z}z} d\lambda_{z} \\[2mm]
&= \frac{1}{2\pi} \int\limits_{-\infty}^{\infty} \overset{\leftrightarrow}{\tilde{\tilde{G}}}{}^{p}_{ee}(\vec{\lambda}_{\rho}, \lambda_{z}) \cdot \int\limits_{z'} \vec{J}_{e}(\vec{\lambda}_{\rho}, z') e^{-j\lambda_{z}z'} dz' e^{j\lambda_{z}z} d\lambda_{z} \\[2mm]
&\quad + \frac{1}{2\pi} \int\limits_{-\infty}^{\infty} \overset{\leftrightarrow}{\tilde{\tilde{G}}}{}^{p}_{eh}(\vec{\lambda}_{\rho}, \lambda_{z}) \cdot \int\limits_{z'} \vec{J}_{h}(\vec{\lambda}_{\rho}, z') e^{-j\lambda_{z}z'} dz' e^{j\lambda_{z}z} d\lambda_{z} \\[2mm]
&= \int\limits_{z'} \underbrace{\left[\frac{1}{2\pi} \int\limits_{-\infty}^{\infty} \overset{\leftrightarrow}{\tilde{\tilde{G}}}{}^{p}_{ee}\, e^{j\lambda_{z}(z-z')} d\lambda_{z} \right]}_{\overset{\leftrightarrow}{\tilde{G}}{}^{p}_{ee}} \cdot \vec{J}_{e} dz' + \int\limits_{z'} \underbrace{\left[\frac{1}{2\pi} \int\limits_{-\infty}^{\infty} \overset{\leftrightarrow}{\tilde{\tilde{G}}}{}^{p}_{eh}\, e^{j\lambda_{z}(z-z')} d\lambda_{z} \right]}_{\overset{\leftrightarrow}{\tilde{G}}{}^{p}_{eh}} \cdot \vec{J}_{h} dz'
\end{aligned}
$$

(3.16)

Again, we recognize λ_z is complex, which means we can use the same complex analysis as in Section 2.3, where further details on the complex analysis techniques are given in Appendix A. Accordingly, we must account for the two cases ($z < z'$ and $z > z'$). Since each term must be subjected to this analysis, the details will only be shown for the $\hat{\mathbf{x}}\hat{\mathbf{x}}$ component. We can see the closure conditions are the same as in the previous chapter, which allows us to proceed directly to the two relevant cases.

3.1.4.1 UHP: $z > z'$.

Again, using Cauchy's Integral Theorem, Jordan's Lemma and Cauchy's Integral Formula, for the case of $z - z' > 0$, we have:

$$\lim_{R \to \infty} \left[\int_{-R}^{\infty} + \oint_{\sum C_p^+} + \overbrace{\int_{C_R^+}}^{0} \right] = 0$$

$$\implies \lim_{R \to \infty} \int_{-R}^{R} = -\oint_{\sum C_p^+} = \oint_{\sum C_p^+} = j2\pi \sum_{k=1}^{2} \text{Res}(\overleftrightarrow{f}, C_{p,k}^+)$$

and the Green's function is:

$$\overleftrightarrow{\tilde{G}}_{ee,eh}^{p+} = \frac{1}{2\pi} \oint_{C_{P_1}^+} \overleftrightarrow{\tilde{G}}_{ee,eh}^{p} \, e^{j\lambda_z(z-z')} d\lambda_z + \frac{1}{2\pi} \oint_{C_{P_2}^+} \overleftrightarrow{\tilde{G}}_{ee,eh}^{p} \, e^{j\lambda_z(z-z')} d\lambda_z$$

$$= \frac{1}{2\pi} \left[j2\pi \text{Res} \left(\overleftrightarrow{f}, C_{P_1}^+ \right) \right] + \frac{1}{2\pi} \left[j2\pi \text{Res} \left(\overleftrightarrow{f}, C_{P_2}^+ \right) \right]$$

$$= j\text{Res} \left(\overleftrightarrow{f}, C_{P_1}^+ \right) + j\text{Res} \left(\overleftrightarrow{f}, C_{P_2}^+ \right) \tag{3.17}$$

98

3.1.4.2 LHP: $z < z'$.

Now, we proceed similarly for the $z - z' < 0$ case:

$$\int \lim_{R \to \infty} \left[\int_{-R}^{R} + \oint_{\sum C_P^-} + \overbrace{\int_{C_R^-}}^{0} \right] = 0$$

$$\implies \int_{-\infty}^{\infty} = -\oint_{\sum C_P^-} = -j2\pi \sum_{k=1}^{2} \text{Res}(\overleftrightarrow{f}, C_{p,k}^-)$$

and the Green's function is

$$\overleftrightarrow{\tilde{G}}_{ee,eh}^{p-} = -\frac{1}{2\pi} \left[j2\pi \text{Res} \left(\overleftrightarrow{f}, C_{P_1}^- \right) \right] - \frac{1}{2\pi} \left[j2\pi \text{Res} \left(\overleftrightarrow{f}, C_{P_2}^- \right) \right]$$

$$= -j\text{Res} \left(\overleftrightarrow{f}, C_{P_1}^- \right) - j\text{Res} \left(\overleftrightarrow{f}, C_{P_2}^- \right) \tag{3.18}$$

3.1.4.3 $z > z'$ for *ee*-type Green's Function.

We are able to find the $\hat{\mathbf{x}}\hat{\mathbf{x}}$ component of the Green's function as

$$\tilde{G}_{ee,xx}^{p+} = j \left\{ -\frac{j\omega\varepsilon_z}{\varepsilon_t} \left[\frac{\mu_z \lambda_{z\psi}^2 \left(\lambda_z^2 - \lambda_{z\theta}^2 \right) + \mu_t \lambda_y^2 \left(\frac{\varepsilon_t \mu_z}{\varepsilon_z \mu_t} \lambda_z^2 - \lambda_{z\psi}^2 \right)}{k_z^2 \left(\lambda_z - \lambda_{z\theta} \right) \left(\lambda_z - \lambda_{z\psi} \right) \left(\lambda_z + \lambda_{z\psi} \right)} e^{j\lambda_z(z-z')} \right] \Bigg|_{\lambda_z = -\lambda_{z\theta}} \right.$$

$$\left. -\frac{j\omega\varepsilon_z}{\varepsilon_t} \left[\frac{\mu_z \lambda_{z\psi}^2 \left(\lambda_z^2 - \lambda_{z\theta}^2 \right) + \mu_t \lambda_y^2 \left(\frac{\varepsilon_t \mu_z}{\varepsilon_z \mu_t} \lambda_z^2 - \lambda_{z\psi}^2 \right)}{k_z^2 \left(\lambda_z - \lambda_{z\theta} \right) \left(\lambda_z + \lambda_{z\theta} \right) \left(\lambda_z - \lambda_{z\psi} \right)} e^{j\lambda_z(z-z')} \right] \Bigg|_{\lambda_z = -\lambda_{z\psi}} \right\}$$

Taking note of the following relationships

$$\frac{\varepsilon_z}{\varepsilon_t} \left[\frac{\varepsilon_t \mu_z}{\varepsilon_z \mu_t} \lambda_{z\theta}^2 - \lambda_{z\psi}^2 \right] = k_t^2 \left(\frac{\mu_z}{\mu_t} - \frac{\varepsilon_z}{\varepsilon_t} \right)$$

$$\lambda_{z\psi}^2 - \lambda_{z\theta}^2 = \lambda_\rho^2 \left(\frac{\mu_t}{\mu_z} - \frac{\varepsilon_t}{\varepsilon_z} \right)$$

$$\frac{\varepsilon_z \mu_t}{\varepsilon_t} \left(\frac{\varepsilon_t \mu_z}{\varepsilon_z \mu_t} \lambda_{z\psi}^2 - \lambda_{z\psi}^2 \right) = -\lambda_{z\psi}^2 \frac{\varepsilon_z \mu_z}{\varepsilon_t} \left(\frac{\mu_t}{\mu_z} - \frac{\varepsilon_t}{\varepsilon_z} \right) \tag{3.19}$$

$$\frac{k_t^2 \left(\frac{\mu_z}{\mu_t} - \frac{\varepsilon_z}{\varepsilon_t} \right)}{k_z^2 \left(\frac{\mu_t}{\mu_z} - \frac{\varepsilon_t}{\varepsilon_z} \right)} = -1$$

99

and simplifying, we find:

$$\boxed{\widetilde{G}^{p+}_{ee,xx} = -\frac{\omega\mu_t\lambda_y^2}{2\lambda_{z\theta}\lambda_\rho^2}e^{-j\lambda_{z\theta}(z-z')} - \frac{\lambda_{z\psi}\lambda_x^2}{2\omega\varepsilon_t\lambda_\rho^2}e^{-j\lambda_{z\psi}(z-z')}}$$ (3.20)

Before we write the final form, we also recall the depolarizing term, which is only present in $\widetilde{\widetilde{G}}^p_{ee,zz}$. It does not need to be integrated via Cauchy's Integral theorem, but can be integrated in the usual manner, where we note the appearance of a delta function:

$$\widetilde{G}^p_{ee,zz,d} = \frac{1}{2\pi}\int_{-\infty}^{\infty} -\frac{1}{j\omega\varepsilon_z}e^{j\lambda_z(z-z')}d\lambda_z = -\frac{1}{j\omega\varepsilon_z}\delta(z-z')$$ (3.21)

3.1.4.4 $z > z'$ *Summary for ee-type Green's Function.*

Performing these same calculations on the other components, we summarize the $z > z'$ case

$$\widetilde{G}^{p+}_{ee,xx} = -\frac{\omega\mu_t\lambda_y^2}{2\lambda_{z\theta}\lambda_\rho^2}e^{-j\lambda_{z\theta}(z-z')} \quad - \quad \frac{\lambda_{z\psi}\lambda_x^2}{2\omega\varepsilon_t\lambda_\rho^2}e^{-j\lambda_{z\psi}(z-z')}$$

$$\widetilde{G}^{p+}_{ee,xy} = \frac{\omega\mu_t\lambda_x\lambda_y}{2\lambda_{z\theta}\lambda_\rho^2}e^{-j\lambda_{z\theta}(z-z')} \quad - \quad \frac{\lambda_{z\psi}\lambda_x\lambda_y}{2\omega\varepsilon_t\lambda_\rho^2}e^{-j\lambda_{z\psi}(z-z')}$$

$$\widetilde{G}^{p+}_{ee,xz} = [0]\,e^{-j\lambda_{z\theta}(z-z')} \quad - \quad \frac{\omega\mu_z\lambda_x}{2k_z^2}e^{-j\lambda_{z\psi}(z-z')}$$

$$\widetilde{G}^{p+}_{ee,yx} = \frac{\omega\mu_t\lambda_x\lambda_y}{2\lambda_{z\theta}\lambda_\rho^2}e^{-j\lambda_{z\theta}(z-z')} \quad - \quad \frac{\lambda_{z\psi}\lambda_x\lambda_y}{2\omega\varepsilon_t\lambda_\rho^2}e^{-j\lambda_{z\psi}(z-z')}$$

$$\widetilde{G}^{p+}_{ee,yy} = -\frac{\omega\mu_t\lambda_x^2}{2\lambda_{z\theta}\lambda_\rho^2}e^{-j\lambda_{z\theta}(z-z')} \quad - \quad \frac{\lambda_{z\psi}\lambda_y^2}{2\omega\varepsilon_t\lambda_\rho^2}e^{-j\lambda_{z\psi}(z-z')}$$

$$\widetilde{G}^{p+}_{ee,yz} = [0]\,e^{-j\lambda_{z\theta}(z-z')} \quad - \quad \frac{\omega\mu_z\lambda_y}{2k_z^2}e^{-j\lambda_{z\psi}(z-z')}$$

$$\widetilde{G}^{p+}_{ee,zx} = [0]\,e^{-j\lambda_{z\theta}(z-z')} \quad - \quad \frac{\omega\mu_z\lambda_x}{2k_z^2}e^{-j\lambda_{z\psi}(z-z')}$$

$$\widetilde{G}^{p+}_{ee,zy} = [0]\,e^{-j\lambda_{z\theta}(z-z')} \quad - \quad \frac{\omega\mu_z\lambda_y}{2k_z^2}e^{-j\lambda_{z\psi}(z-z')}$$

$$\widetilde{G}^{p+}_{ee,zz} = [0]\,e^{j\lambda_z(z-z')} \quad - \quad \frac{\omega\varepsilon_t\mu_z\lambda_\rho^2}{2\varepsilon_z k_z^2\lambda_{z\psi}}e^{-j\lambda_{z\psi}(z-z')} \quad - \quad \frac{1}{j\omega\varepsilon_z}\delta(z-z')$$

100

3.1.4.5 $z < z'$ for *ee*-type Green's Function.

For the $z < z'$ case, we can write:

$$\widetilde{G}_{ee,xx}^{p-} = -j\left\{ -\frac{j\omega\varepsilon_z}{\varepsilon_t}\left[\frac{\mu_z\lambda_{z\psi}^2\left(\lambda_z{}^2 - \lambda_{z\theta}^2\right) + \mu_t\lambda_y{}^2\left(\frac{\varepsilon_t\mu_z}{\varepsilon_z\mu_t}\lambda_z{}^2 - \lambda_{z\psi}^2\right)}{k_z^2\left(\lambda_z + \lambda_{z\theta}\right)\left(\lambda_z - \lambda_{z\psi}\right)\left(\lambda_z + \lambda_{z\psi}\right)}e^{j\lambda_z(z-z')}\right]\Bigg|_{\lambda_z=\lambda_{z\theta}} \right.$$

$$\left. -\frac{j\omega\varepsilon_z}{\varepsilon_t}\left[\frac{\mu_z\lambda_{z\psi}^2\left(\lambda_z{}^2 - \lambda_{z\theta}^2\right) + \mu_t\lambda_y{}^2\left(\frac{\varepsilon_t\mu_z}{\varepsilon_z\mu_t}\lambda_z{}^2 - \lambda_{z\psi}^2\right)}{k_z^2\left(\lambda_z - \lambda_{z\theta}\right)\left(\lambda_z + \lambda_{z\theta}\right)\left(\lambda_z + \lambda_{z\psi}\right)}e^{j\lambda_z(z-z')}\right]\Bigg|_{\lambda_z=\lambda_{z\psi}} \right\}$$

again, using the relationships found in 3.19 and simplifying, we find the $\hat{\mathbf{x}}\hat{\mathbf{x}}$ component to be

$$\boxed{\widetilde{G}_{ee,xx}^{p-} = -\frac{\omega\mu_t\lambda_y{}^2}{2\lambda_{z\theta}\lambda_\rho^2}e^{j\lambda_{z\theta}(z-z')} - \frac{\lambda_{z\psi}\lambda_x^2}{2\omega\varepsilon_t\lambda_\rho^2}e^{j\lambda_{z\psi}(z-z')}} \tag{3.22}$$

Again, we recognize the depolarizing term will be present, integrated in the same manner as in the $z > z'$ case.

3.1.4.6 $z < z'$ Summary for *ee*-type Green's Function.

Performing these calculations on the rest of the components leads to:

$$\widetilde{G}_{ee,xx}^{p-} = -\frac{\omega\mu_t\lambda_y{}^2}{2\lambda_{z\theta}k_z^2\lambda_\rho^2}e^{j\lambda_{z\theta}(z-z')} \quad - \quad \frac{\lambda_{z\psi}\lambda_x^2}{2\omega\varepsilon_t\lambda_\rho^2}e^{j\lambda_{z\psi}(z-z')}$$

$$\widetilde{G}_{ee,xy}^{p-} = \frac{\omega\mu_t\lambda_x\lambda_y}{2\lambda_{z\theta}\lambda_\rho^2}e^{j\lambda_{z\theta}(z-z')} \quad - \quad \frac{\lambda_{z\psi}\lambda_x\lambda_y}{2\omega\varepsilon_t\lambda_\rho^2}e^{j\lambda_{z\psi}(z-z')}$$

$$\widetilde{G}_{ee,xz}^{p-} = [0]\,e^{j\lambda_{z\theta}(z-z')} \quad + \quad \frac{\omega\mu_z\lambda_x}{2k_z^2}e^{j\lambda_{z\psi}(z-z')}$$

$$\widetilde{G}_{ee,yx}^{p-} = \frac{\omega\mu_t\lambda_x\lambda_y}{2\lambda_{z\theta}\lambda_\rho^2}e^{j\lambda_{z\theta}(z-z')} \quad - \quad \frac{\lambda_x\lambda_y\lambda_{z\psi}}{2\omega\varepsilon_t\lambda_\rho^2}e^{j\lambda_{z\psi}(z-z')}$$

$$\widetilde{G}_{ee,yy}^{p-} = -\frac{\omega\mu_t\lambda_x^2}{2\lambda_{z\theta}\lambda_\rho^2}e^{j\lambda_{z\theta}(z-z')} \quad - \quad \frac{\lambda_{z\psi}\lambda_y{}^2}{2\omega\varepsilon_t\lambda_\rho^2}e^{j\lambda_{z\psi}(z-z')}$$

$$\widetilde{G}_{ee,yz}^{p-} = [0]\,e^{j\lambda_{z\theta}(z-z')} \quad + \quad \frac{\omega\mu_z\lambda_y}{2k_z^2}e^{j\lambda_{z\psi}(z-z')}$$

$$\widetilde{G}_{ee,zx}^{p-} = [0]\,e^{j\lambda_{z\theta}(z-z')} \quad + \quad \frac{\omega\mu_z\lambda_x}{2k_z^2}e^{j\lambda_{z\psi}(z-z')}$$

$$\widetilde{G}_{ee,zy}^{p-} = [0]\,e^{j\lambda_{z\theta}(z-z')} \quad + \quad \frac{\omega\mu_z\lambda_y}{2k_z^2}e^{j\lambda_{z\psi}(z-z')}$$

$$\widetilde{G}_{ee,zz}^{p-} = [0]\,e^{j\lambda_{z\theta}(z-z')} \quad - \quad \frac{\omega\varepsilon_t\mu_z\lambda_\rho^2}{2\lambda_{z\psi}\varepsilon_z k_z^2}e^{j\lambda_{z\psi}(z-z')} - \frac{1}{j\omega\varepsilon_z}\delta(z-z')$$

3.1.4.7 Grand Summary for *ee*-type Principal Green's Function .

Given the results summarized in 3.1.4.4 and 3.1.4.6, we can write $\overset{\leftrightarrow}{\tilde{G}}{}^{p}_{ee}$ as

$$\overset{\leftrightarrow}{\tilde{G}}{}^{p}_{ee}\left(\vec{\lambda}_\rho|z-z'\right) = \overset{\leftrightarrow}{\tilde{G}}{}^{p,\text{TE}}_{ee} + \overset{\leftrightarrow}{\tilde{G}}{}^{p,\text{TM}}_{ee} = \begin{bmatrix} \tilde{G}^p_{ee,xx} & \tilde{G}^p_{ee,xy} & \tilde{G}^p_{ee,xz} \\[6pt] \tilde{G}^p_{ee,yx} & \tilde{G}^p_{ee,yy} & \tilde{G}^p_{ee,yz} \\[6pt] \tilde{G}^p_{ee,zx} & \tilde{G}^p_{ee,zy} & \tilde{G}^p_{ee,zz} \end{bmatrix}$$

$$\tilde{G}^p_{ee,xx} = -\frac{\omega\mu_t\lambda_y^2}{2\lambda_{z\theta}\lambda_\rho^2}e^{-j\lambda_{z\theta}|z-z'|} \quad - \quad \frac{\lambda_{z\psi}\lambda_x^2}{2\omega\varepsilon_t\lambda_\rho^2}e^{-j\lambda_{z\psi}|z-z'|}$$

$$\tilde{G}^p_{ee,xy} = \frac{\omega\mu_t\lambda_x\lambda_y}{2\lambda_{z\theta}\lambda_\rho^2}e^{-j\lambda_{z\theta}|z-z'|} \quad - \quad \frac{\lambda_{z\psi}\lambda_x\lambda_y}{2\omega\varepsilon_t\lambda_\rho^2}e^{-j\lambda_{z\psi}|z-z'|}$$

$$\tilde{G}^p_{ee,xz} = [0]\,e^{-j\lambda_{z\theta}|z-z'|} \quad - \quad \text{sgn}\left(z-z'\right)\frac{\lambda_x}{2\omega\varepsilon_z}e^{-j\lambda_{z\psi}|z-z'|}$$

$$\tilde{G}^p_{ee,yx} = \frac{\omega\mu_t\lambda_x\lambda_y}{2\lambda_{z\theta}\lambda_\rho^2}e^{-j\lambda_{z\theta}|z-z'|} \quad - \quad \frac{\lambda_{z\psi}\lambda_x\lambda_y}{2\omega\varepsilon_t\lambda_\rho^2}e^{-j\lambda_{z\psi}|z-z'|}$$

$$\tilde{G}^p_{ee,yy} = -\frac{\omega\mu_t\lambda_x^2}{2\lambda_{z\theta}\lambda_\rho^2}e^{-j\lambda_{z\theta}|z-z'|} \quad - \quad \frac{\lambda_{z\psi}\lambda_y^2}{2\omega\varepsilon_t\lambda_\rho^2}e^{-j\lambda_{z\psi}|z-z'|}$$

$$\tilde{G}^p_{ee,yz} = [0]\,e^{-j\lambda_{z\theta}|z-z'|} \quad - \quad \text{sgn}\left(z-z'\right)\frac{\lambda_y}{2\omega\varepsilon_z}e^{-j\lambda_{z\psi}|z-z'|}$$

$$\tilde{G}^p_{ee,zx} = [0]\,e^{-j\lambda_{z\theta}|z-z'|} \quad - \quad \text{sgn}\left(z-z'\right)\frac{\lambda_x}{2\omega\varepsilon_z}e^{-j\lambda_{z\psi}|z-z'|}$$

$$\tilde{G}^p_{ee,zy} = [0]\,e^{-j\lambda_{z\theta}|z-z'|} \quad - \quad \text{sgn}\left(z-z'\right)\frac{\lambda_y}{2\omega\varepsilon_z}e^{-j\lambda_{z\psi}|z-z'|}$$

$$\tilde{G}^p_{ee,zz} = [0]\,e^{-j\lambda_{z\theta}|z-z'|} \quad - \quad \frac{\frac{\varepsilon_t}{\varepsilon_z}\lambda_\rho^2}{2\omega\varepsilon_z\lambda_{z\psi}}e^{-j\lambda_{z\psi}|z-z'|} \quad - \quad \frac{1}{j\omega\varepsilon_z}\delta(z-z')$$

3.1.5 Evaluation of *eh*-type Principal Green's Function.

We can perform similar operations on the *eh* terms found in 3.1.3.1. Avoiding the details, we write the Green's function as the combination of TE^z (terms containing $\lambda_{z\theta}$) and TM^z

(terms containing $\lambda_{z\psi}$) contributions:

$$
\overset{\leftrightarrow}{\widetilde{G}}{}_{eh}^{p}\left(\vec{\lambda}_{\rho}|z-z'\right)=\overset{\leftrightarrow}{\widetilde{G}}{}_{eh}^{p,\text{TE}}+\overset{\leftrightarrow}{\widetilde{G}}{}_{eh}^{p,\text{TM}}=
\begin{bmatrix}
\widetilde{G}_{eh,xx}^{p} & \widetilde{G}_{eh,xy}^{p} & \widetilde{G}_{eh,xz}^{p} \\[4pt]
\widetilde{G}_{eh,yx}^{p} & \widetilde{G}_{eh,yy}^{p} & \widetilde{G}_{eh,yz}^{p} \\[4pt]
\widetilde{G}_{eh,zx}^{p} & \widetilde{G}_{eh,zy}^{p} & \widetilde{G}_{eh,zz}^{p}
\end{bmatrix}
$$

$$
\begin{aligned}
\widetilde{G}_{eh,xx}^{p} &= -\operatorname{sgn}\left(z-z'\right)\frac{\lambda_{x}\lambda_{y}}{2\lambda_{\rho}^{2}}e^{-j\lambda_{z\theta}|z-z'|} & + & & \operatorname{sgn}\left(z-z'\right)\frac{\lambda_{x}\lambda_{y}}{2\lambda_{\rho}^{2}}e^{-j\lambda_{z\psi}|z-z'|} \\[4pt]
\widetilde{G}_{eh,xy}^{p} &= -\operatorname{sgn}\left(z-z'\right)\frac{\lambda_{y}^{2}}{2\lambda_{\rho}^{2}}e^{-j\lambda_{z\theta}|z-z'|} & - & & \operatorname{sgn}\left(z-z'\right)\frac{\lambda_{x}^{2}}{2\lambda_{\rho}^{2}}e^{-j\lambda_{z\psi}|z-z'|} \\[4pt]
\widetilde{G}_{eh,xz}^{p} &= -\frac{\frac{\mu_{t}}{\mu_{z}}\lambda_{y}}{2\lambda_{z\theta}}e^{-j\lambda_{z\theta}|z-z'|} & - & & [0]\,e^{-j\lambda_{z\psi}|z-z'|} \\[4pt]
\widetilde{G}_{eh,yx}^{p} &= \operatorname{sgn}\left(z-z'\right)\frac{\lambda_{x}^{2}}{2\lambda_{\rho}^{2}}e^{-j\lambda_{z\theta}|z-z'|} & + & & \operatorname{sgn}\left(z-z'\right)\frac{\lambda_{y}^{2}}{2\lambda_{\rho}^{2}}e^{-j\lambda_{z\psi}|z-z'|} \\[4pt]
\widetilde{G}_{eh,yy}^{p} &= \operatorname{sgn}\left(z-z'\right)\frac{\lambda_{x}\lambda_{y}}{2\lambda_{\rho}^{2}}e^{-j\lambda_{z\theta}|z-z'|} & - & & \operatorname{sgn}\left(z-z'\right)\frac{\lambda_{x}\lambda_{y}}{2\lambda_{\rho}^{2}}e^{-j\lambda_{z\psi}|z-z'|} \\[4pt]
\widetilde{G}_{eh,yz}^{p} &= \frac{\frac{\mu_{t}}{\mu_{z}}\lambda_{x}}{2\lambda_{z\theta}}e^{-j\lambda_{z\theta}|z-z'|} & + & & [0]\,e^{-j\lambda_{z\psi}|z-z'|} \\[4pt]
\widetilde{G}_{eh,zx}^{p} &= [0]\,e^{-j\lambda_{z\theta}|z-z'|} & + & & \frac{\frac{\varepsilon_{t}}{\varepsilon_{z}}\lambda_{y}}{2\lambda_{z\psi}}e^{-j\lambda_{z\psi}|z-z'|} \\[4pt]
\widetilde{G}_{eh,zy}^{p} &= [0]\,e^{-j\lambda_{z\theta}|z-z'|} & - & & \frac{\frac{\varepsilon_{t}}{\varepsilon_{z}}\lambda_{x}}{2\lambda_{z\psi}}e^{-j\lambda_{z\psi}|z-z'|} \\[4pt]
\widetilde{G}_{eh,zz}^{p} &= 0
\end{aligned}
$$

It is interesting to note that the $\operatorname{sgn}\left(z-z'\right)$ terms are the compliment of the terms in the *ee* Green's function, as expected by duality. These changes in sign account for the differing direction an electric field sustained by either an electric or magnetic current will be oriented, depending on whether the observation point (z') is above the source point $(z > z')$ or below the source point $(z < z')$.

Although we have not shown the development of $\overset{\leftrightarrow}{\mathsf{w}}_{h}$ and its inverse and, consequently, the principal magnetic field Green's functions ($\widetilde{G}_{he}^{p}$ and $\widetilde{G}_{hh}^{p}$), the components are given below for completeness.

103

$$\tilde{\bar{\bar{G}}}^{p}_{he}\left(\vec{\lambda}_\rho|z{-}z'\right) = \tilde{\bar{\bar{G}}}^{p,\mathrm{TE}}_{he} + \tilde{\bar{\bar{G}}}^{p,\mathrm{TM}}_{he} = \begin{bmatrix} \tilde{G}^{p}_{he,xx} & \tilde{G}^{p}_{he,xy} & \tilde{G}^{p}_{he,xz} \\[6pt] \tilde{G}^{p}_{he,yx} & \tilde{G}^{p}_{he,yy} & \tilde{G}^{p}_{he,yz} \\[6pt] \tilde{G}^{p}_{he,zx} & \tilde{G}^{p}_{he,zy} & \tilde{G}^{p}_{he,zz} \end{bmatrix}$$

$$\tilde{G}^{p}_{he,xx} = -\mathrm{sgn}\left(z-z'\right)\frac{\lambda_x\lambda_y}{2\lambda_\rho^2}e^{-j\lambda_{z\theta}|z-z'|} \quad + \quad \mathrm{sgn}\left(z-z'\right)\frac{\lambda_x\lambda_y}{2\lambda_\rho^2}e^{-j\lambda_{z\psi}|z-z'|}$$

$$\tilde{G}^{p}_{he,xy} = \mathrm{sgn}\left(z-z'\right)\frac{\lambda_x^2}{2\lambda_\rho^2}e^{-j\lambda_{z\theta}|z-z'|} \quad + \quad \mathrm{sgn}\left(z-z'\right)\frac{\lambda_y^2}{2\lambda_\rho^2}e^{-j\lambda_{z\psi}|z-z'|}$$

$$\tilde{G}^{p}_{he,xz} = [0]\,e^{-j\lambda_{z\theta}|z-z'|} \quad + \quad \frac{\frac{\varepsilon_t}{\varepsilon_z}\lambda_y}{2\lambda_{z\psi}}e^{-j\lambda_{z\psi}|z-z'|}$$

$$\tilde{G}^{p}_{he,yx} = -\mathrm{sgn}\left(z-z'\right)\frac{\lambda_y^2}{2\lambda_\rho^2}e^{-j\lambda_{z\theta}|z-z'|} \quad - \quad \mathrm{sgn}\left(z-z'\right)\frac{\lambda_x^2}{2\lambda_\rho^2}e^{-j\lambda_{z\psi}|z-z'|}$$

$$\tilde{G}^{p}_{he,yy} = \mathrm{sgn}\left(z-z'\right)\frac{\lambda_x\lambda_y}{2\lambda_\rho^2}e^{-j\lambda_{z\theta}|z-z'|} \quad - \quad \mathrm{sgn}\left(z-z'\right)\frac{\lambda_x\lambda_y}{2\lambda_\rho^2}e^{-j\lambda_{z\psi}|z-z'|}$$

$$\tilde{G}^{p}_{he,yz} = [0]\,e^{-j\lambda_{z\theta}|z-z'|} \quad - \quad \frac{\frac{\varepsilon_t}{\varepsilon_z}\lambda_x}{2\lambda_{z\psi}}e^{-j\lambda_{z\psi}|z-z'|}$$

$$\tilde{G}^{p}_{he,zx} = -\frac{\frac{\mu_t}{\mu_z}\lambda_y}{2\lambda_{z\theta}}e^{-j\lambda_{z\theta}|z-z'|} \quad - \quad [0]\,e^{-j\lambda_{z\psi}|z-z'|}$$

$$\tilde{G}^{p}_{he,zy} = \frac{\frac{\mu_t}{\mu_z}\lambda_x}{2\lambda_{z\theta}}e^{-j\lambda_{z\theta}|z-z'|} \quad + \quad [0]\,e^{-j\lambda_{z\psi}|z-z'|}$$

$$\tilde{G}^{p}_{he,zz} = 0$$

(3.23)

$$\overset{\leftrightarrow}{\tilde{G}}{}^{p}_{hh}(\vec{\lambda}_{\rho}|z-z') = \overset{\leftrightarrow}{\tilde{G}}{}^{p,\text{TE}}_{hh} + \overset{\leftrightarrow}{\tilde{G}}{}^{p,\text{TM}}_{hh} = \begin{bmatrix} \tilde{G}^{p}_{hh,xx} & \tilde{G}^{p}_{hh,xy} & \tilde{G}^{p}_{hh,xz} \\[6pt] \tilde{G}^{p}_{hh,yx} & \tilde{G}^{p}_{hh,yy} & \tilde{G}^{p}_{hh,yz} \\[6pt] \tilde{G}^{p}_{hh,zx} & \tilde{G}^{p}_{hh,zy} & \tilde{G}^{p}_{hh,zz} \end{bmatrix}$$

$$\tilde{G}^{p}_{hh,xx} = -\frac{\lambda_{z\theta}\lambda_x^2}{2\omega\mu_t\lambda_\rho^2}e^{-j\lambda_{z\theta}|z-z'|} \quad - \quad \frac{\omega\varepsilon_t\lambda_y^2}{2\lambda_{z\psi}\lambda_\rho^2}e^{-j\lambda_{z\psi}|z-z'|}$$

$$\tilde{G}^{p}_{hh,xy} = -\frac{\lambda_{z\theta}\lambda_x\lambda_y}{2\omega\mu_t\lambda_\rho^2}e^{-j\lambda_{z\theta}|z-z'|} \quad + \quad \frac{\omega\varepsilon_t\lambda_x\lambda_y}{2\lambda_{z\psi}\lambda_\rho^2}e^{-j\lambda_{z\psi}|z-z'|}$$

$$\tilde{G}^{p}_{hh,xz} = -\text{sgn}\,(z-z')\frac{\lambda_x}{2\omega\mu_z}e^{-j\lambda_{z\theta}|z-z'|} \quad - \quad [0]\,e^{-j\lambda_{z\psi}|z-z'|}$$

$$\tilde{G}^{p}_{hh,yx} = -\frac{\lambda_{z\theta}\lambda_x\lambda_y}{2\omega\mu_t\lambda_\rho^2}e^{-j\lambda_{z\theta}|z-z'|} \quad + \quad \frac{\omega\varepsilon_t\lambda_x\lambda_y}{2\lambda_{z\psi}\lambda_\rho^2}e^{-j\lambda_{z\psi}|z-z'|} \qquad (3.24)$$

$$\tilde{G}^{p}_{hh,yy} = -\frac{\lambda_{z\theta}\lambda_y^2}{2\omega\mu_t\lambda_\rho^2}e^{-j\lambda_{z\theta}|z-z'|} \quad - \quad \frac{\omega\varepsilon_t\lambda_x^2}{2\lambda_{z\psi}\lambda_\rho^2}e^{-j\lambda_{z\psi}|z-z'|}$$

$$\tilde{G}^{p}_{hh,yz} = -\text{sgn}\,(z-z')\frac{\lambda_y}{2\omega\mu_z}e^{-j\lambda_{z\theta}|z-z'|} \quad - \quad [0]\,e^{-j\lambda_{z\psi}|z-z'|}$$

$$\tilde{G}^{p}_{hh,zx} = -\text{sgn}\,(z-z')\frac{\lambda_x}{2\omega\mu_z}e^{-j\lambda_{z\theta}|z-z'|} \quad - \quad [0]\,e^{-j\lambda_{z\psi}|z-z'|}$$

$$\tilde{G}^{p}_{hh,zy} = -\text{sgn}\,(z-z')\frac{\lambda_y}{2\omega\mu_z}e^{-j\lambda_{z\theta}|z-z'|} \quad - \quad [0]\,e^{-j\lambda_{z\psi}|z-z'|}$$

$$\tilde{G}^{p}_{hh,zz} = -\frac{\frac{\mu_t}{\mu_z}\lambda_\rho^2}{2\omega\mu_z\lambda_{z\theta}}e^{-j\lambda_{z\theta}|z-z'|} \quad - \quad [0]\,e^{-j\lambda_{z\psi}|z-z'|}$$

$$\qquad\qquad -\frac{1}{j\omega\mu_z}\delta(z-z')$$

One final point of interest is, upon expanding the expressions given in [46] (which are given for a dielectric only uniaxial material) and comparing term-by-term with the expressions above, we are able to find a vectorized form. However, it is not clear to the author how such a form would be developed rigorously from the coupled solutions to Maxwell's equations. Therefore, they are not used in finding the total solution. The vectorized forms given on the following page and are again found to be combinations of TE^z and TM^z contributions.

$$\vec{\tilde{E}}^p(\vec{\lambda}_\rho, z) = \int\limits_{z'} \vec{\tilde{G}}^p_{ee}(\vec{\lambda}_\rho|z-z') \cdot \vec{\tilde{J}}_e(\vec{\lambda}_\rho|z')dz' + \int\limits_{z'} \vec{\tilde{G}}^p_{eh}(\vec{\lambda}_\rho|z-z') \cdot \vec{\tilde{J}}_h(\vec{\lambda}_\rho|z')dz'$$

$$\vec{\tilde{H}}^p(\vec{\lambda}_\rho, z) = \int\limits_{z'} \vec{\tilde{G}}^p_{he}(\vec{\lambda}_\rho|z-z') \cdot \vec{\tilde{J}}_e(\vec{\lambda}_\rho|z')dz' + \int\limits_{z'} \vec{\tilde{G}}^p_{hh}(\vec{\lambda}_\rho|z-z') \cdot \vec{\tilde{J}}_h(\vec{\lambda}_\rho|z')dz'$$

$$\vec{\tilde{G}}^p_{ee}(\vec{\lambda}_\rho|z-z') = \frac{\vec{\lambda}^e_\theta \cdot \vec{\lambda}^e_\theta - \vec{\lambda}^e_\theta \cdot \left(1 - \frac{\varepsilon_z^2 \mu_t}{\varepsilon_t^2 \mu_z}\right)\hat{\mathbf{z}}\hat{\mathbf{z}} \cdot \vec{\lambda}^e_\theta - \vec{\lambda}^e_\theta \cdot \left(\hat{\lambda}_\rho \times \hat{\mathbf{z}}\right)\left(\hat{\lambda}_\rho \times \hat{\mathbf{z}}\right) \cdot \vec{\lambda}^e_\theta}{2\omega\varepsilon_t \lambda_{z\theta}} e^{-j\lambda_{z\theta}|z-z'|}$$

$$+ \frac{\vec{\lambda}^e_\psi \cdot \left(\hat{\lambda}_\rho \times \hat{\mathbf{z}}\right)\left(\hat{\lambda}_\rho \times \hat{\mathbf{z}}\right) \cdot \vec{\lambda}^e_\psi}{2\omega\varepsilon_t \lambda_{z\psi}} e^{-j\lambda_{z\psi}|z-z'|} - \frac{\hat{\mathbf{z}}\hat{\mathbf{z}}}{j\omega\varepsilon_z}\delta\left(z - z'\right)$$

$$\vec{\tilde{G}}^p_{he}(\vec{\lambda}_\rho|z-z') = \frac{\vec{\lambda}^e_\theta - (1 - \frac{\varepsilon_z \mu_t}{\varepsilon_t \mu_z})\hat{\mathbf{z}}\hat{\mathbf{z}} \cdot \vec{\lambda}^e_\theta - \left(\hat{\lambda}_\rho \times \hat{\mathbf{z}}\right)\left(\hat{\lambda}_\rho \times \hat{\mathbf{z}}\right) \cdot \vec{\lambda}^e_\theta}{2\lambda_{z\theta}} e^{-j\lambda_{z\theta}|z-z'|}$$

$$+ \frac{\left(\hat{\lambda}_\rho \times \hat{\mathbf{z}}\right)\left(\hat{\lambda}_\rho \times \hat{\mathbf{z}}\right) \cdot \vec{\lambda}^e_\psi}{2\lambda_{z\psi}} e^{-j\lambda_{z\psi}|z-z'|}$$

$$\vec{\tilde{G}}^p_{eh}(\vec{\lambda}_\rho|z-z') = \frac{\left(\hat{\lambda}_\rho \times \hat{\mathbf{z}}\right)\left(\hat{\lambda}_\rho \times \hat{\mathbf{z}}\right) \cdot \vec{\lambda}^h_\theta}{-2\lambda_{z\theta}} e^{-j\lambda_{z\theta}|z-z'|}$$

$$+ \frac{\vec{\lambda}^h_\psi - (1 - \frac{\varepsilon_t \mu_z}{\varepsilon_z \mu_t})\hat{\mathbf{z}}\hat{\mathbf{z}} \cdot \vec{\lambda}^h_\psi - \left(\hat{\lambda}_\rho \times \hat{\mathbf{z}}\right)\left(\hat{\lambda}_\rho \times \hat{\mathbf{z}}\right) \cdot \vec{\lambda}^h_\psi}{-2\lambda_{z\psi}} e^{-j\lambda_{z\psi}|z-z'|}$$

$$\vec{\tilde{G}}^p_{hh}(\vec{\lambda}_\rho|z-z') = \frac{\vec{\lambda}^h_\theta \cdot \left(\hat{\lambda}_\rho \times \hat{\mathbf{z}}\right)\left(\hat{\lambda}_\rho \times \hat{\mathbf{z}}\right) \cdot \vec{\lambda}^h_\theta}{2\omega\mu_t \lambda_{z\theta}} e^{-j\lambda_{z\theta}|z-z'|}$$

$$+ \frac{\vec{\lambda}^h_\psi \cdot \vec{\lambda}^h_\psi - \vec{\lambda}^h_\psi \cdot \left(1 - \frac{\varepsilon_t \mu_z^2}{\varepsilon_z \mu_t^2}\right) \cdot \hat{\mathbf{z}}\hat{\mathbf{z}} \cdot \vec{\lambda}^h_\psi - \vec{\lambda}^h_\psi \cdot \left(\hat{\lambda}_\rho \times \hat{\mathbf{z}}\right)\left(\hat{\lambda}_\rho \times \hat{\mathbf{z}}\right) \cdot \vec{\lambda}^h_\psi}{2\omega\mu_t \lambda_{z\psi}} e^{-j\lambda_{z\psi}|z-z'|}$$

$$- \frac{\hat{\mathbf{z}}\hat{\mathbf{z}}}{j\omega\mu_z}\delta\left(z - z'\right)$$

$$\vec{\lambda}^e_{\theta,\psi} = \hat{\mathbf{x}}\text{sgn}\left(z - z'\right)\lambda_{z\theta,z\psi}\hat{\mathbf{y}} + \hat{\mathbf{x}}\frac{\varepsilon_t}{\varepsilon_z}\lambda_y\hat{\mathbf{z}} - \hat{\mathbf{y}}\text{sgn}\left(z - z'\right)\lambda_{z\theta,z\psi}\hat{\mathbf{x}} - \hat{\mathbf{y}}\frac{\varepsilon_t}{\varepsilon_z}\lambda_x\hat{\mathbf{z}} - \frac{\varepsilon_t}{\varepsilon_z}\hat{\mathbf{z}}\lambda_y\hat{\mathbf{x}} + \frac{\varepsilon_t}{\varepsilon_z}\hat{\mathbf{z}}\lambda_x\hat{\mathbf{y}}$$

$$\vec{\lambda}^h_{\theta,\psi} = \hat{\mathbf{x}}\text{sgn}\left(z - z'\right)\lambda_{z\theta,z\psi}\hat{\mathbf{y}} + \hat{\mathbf{x}}\frac{\mu_t}{\mu_z}\lambda_y\hat{\mathbf{z}} - \hat{\mathbf{y}}\text{sgn}\left(z - z'\right)\lambda_{z\theta,z\psi}\hat{\mathbf{x}} - \hat{\mathbf{y}}\frac{\mu_t}{\mu_z}\lambda_x\hat{\mathbf{z}} - \frac{\mu_t}{\mu_z}\hat{\mathbf{z}}\lambda_y\hat{\mathbf{x}} + \frac{\mu_t}{\mu_z}\hat{\mathbf{z}}\lambda_x\hat{\mathbf{y}}$$

3.2 Scattered Solution

Now that we have determined the principal portion of the fields for an unbounded media in the presence of electric and magnetic currents, we look for the scattered (reflected) solution in a source-free region bounded by parallel plates. From (3.1), we can write the spectral domain versions of Maxwell's equations in a source-free region:

$$j\overleftrightarrow{\lambda} \cdot \vec{\tilde{E}}^r = -j\omega\overleftrightarrow{\mu} \cdot \vec{\tilde{H}}^r \tag{3.25a}$$

$$j\overleftrightarrow{\lambda} \cdot \vec{\tilde{H}}^r = j\omega\overleftrightarrow{\varepsilon} \cdot \vec{\tilde{E}}^r \tag{3.25b}$$

Which can then be solved in a similar method as before, leading to

$$\overleftrightarrow{\mathsf{w}}_e \cdot \vec{\tilde{E}}^r = 0 \tag{3.26}$$

where $\overleftrightarrow{\mathsf{w}}_e$ takes the same form as before (3.6). For a non-trivial solution to the electric field, the determinant of $\overleftrightarrow{\mathsf{w}}_e$ must be zero. This leads to

$$\left(-k_z^2\right)\left(\lambda_z^2 - \lambda_{z\theta}^2\right)\left(\lambda_z^2 - \lambda_{z\psi}^2\right) = 0$$

$$\implies \lambda_z = \pm\lambda_{z\theta}, \pm\lambda_{z\psi}$$

These four solutions for λ_z represent the upward and downward propagating TE^z and TM^z waves. Since we are in a parallel-plate geometry, we assume a reflected solution of the form

$$\vec{\tilde{E}}^r\left(\lambda_x, \lambda_y, z\right) = \vec{\tilde{E}}_o^{r\pm}\left(\lambda_x, \lambda_y\right)e^{\mp j\lambda_z z} = \vec{\tilde{E}}_o^{r+}\left(\lambda_x, \lambda_y\right)e^{-j\lambda_z z} + \vec{\tilde{E}}_o^{r-}\left(\lambda_x, \lambda_y\right)e^{j\lambda_z z} \tag{3.27}$$

where we define the unknown scattering coefficients for $\tilde{\theta}$ to be

$$\vec{\tilde{E}}_o^{r\theta\pm} = \hat{\mathbf{x}}\tilde{E}_{ox}^{r\theta\pm} + \hat{\mathbf{y}}\tilde{E}_{oy}^{r\theta\pm} + \hat{\mathbf{z}}\tilde{E}_{oz}^{r\theta\pm} \tag{3.28}$$

and the unknown scattering coefficients for $\tilde{\psi}$ are

$$\vec{\tilde{E}}_o^{r\psi\pm} = \hat{\mathbf{x}}\tilde{E}_{ox}^{r\psi\pm} + \hat{\mathbf{y}}\tilde{E}_{oy}^{r\psi\pm} + \hat{\mathbf{z}}\tilde{E}_{oz}^{r\psi\pm} \tag{3.29}$$

Note that we are using a concise notation where the plus sign in the superscripts represent the forward-going wave and a negative sign represents the reverse-going wave.

3.2.1 TE^z wave ($\lambda_z = \mp\lambda_{z\theta}$).

Now, we seek the non-trivial TE^z solution to the scattered problem, using the assumed form of the solution (3.27)

$$\overset{\leftrightarrow}{\mathbf{w}}_e^\theta \cdot \vec{\tilde{E}}_o^{r\theta\pm}\left(\lambda_x, \lambda_y\right) e^{\mp j\lambda_{z\theta}z} = 0 \tag{3.30}$$

$$\implies \overset{\leftrightarrow}{\mathbf{w}}_e^\theta \cdot \vec{\tilde{E}}_o^{r\theta\pm} = 0 \tag{3.31}$$

Which can now be expanded to write

$$\begin{bmatrix} \lambda_{z\theta}^2 - k_t^2 + \frac{\mu_t}{\mu_z}\lambda_y^2 & -\frac{\mu_t}{\mu_z}\lambda_x\lambda_y & \pm\lambda_x\lambda_{z\theta} \\ -\frac{\mu_t}{\mu_z}\lambda_x\lambda_y & \lambda_{z\theta}^2 - k_t^2 + \frac{\mu_t}{\mu_z}\lambda_x^2 & \pm\lambda_y\lambda_{z\theta} \\ \pm\frac{\mu_z}{\mu_t}\lambda_x\lambda_{z\theta} & \pm\frac{\mu_z}{\mu_t}\lambda_y\lambda_{z\theta} & \frac{\mu_z}{\mu_t}\lambda_\rho^2 - k_z^2 \end{bmatrix} \cdot \begin{bmatrix} \tilde{E}_{ox}^{r\theta\pm} \\ \tilde{E}_{oy}^{r\theta\pm} \\ \tilde{E}_{oz}^{r\theta\pm} \end{bmatrix} = 0 \tag{3.32}$$

Recognizing that we can reduce the $\hat{\mathbf{x}}\hat{\mathbf{x}}$ and $\hat{\mathbf{y}}\hat{\mathbf{y}}$ terms by using the definition of $\lambda_{z\theta}^2$ 2.43, we write

$$\begin{bmatrix} -\frac{\mu_t}{\mu_z}\lambda_x^2 & -\frac{\mu_t}{\mu_z}\lambda_x\lambda_y & \pm\lambda_x\lambda_{z\theta} \\ -\frac{\mu_t}{\mu_z}\lambda_x\lambda_y & -\frac{\mu_t}{\mu_z}\lambda_y^2 & \pm\lambda_y\lambda_{z\theta} \\ \pm\frac{\mu_z}{\mu_t}\lambda_x\lambda_{z\theta} & \pm\frac{\mu_z}{\mu_t}\lambda_y\lambda_{z\theta} & \frac{\mu_z}{\mu_t}\lambda_\rho^2 - k_z^2 \end{bmatrix} \cdot \begin{bmatrix} \tilde{E}_{ox}^{r\theta\pm} \\ \tilde{E}_{oy}^{r\theta\pm} \\ \tilde{E}_{oz}^{r\theta\pm} \end{bmatrix} = 0 \tag{3.33}$$

from which we can extract the six equations:

$$-\frac{\mu_t}{\mu_z}\lambda_x^2\tilde{E}_{ox}^{r\theta\pm} - \frac{\mu_t}{\mu_z}\lambda_x\lambda_y\tilde{E}_{oy}^{r\theta\pm} \pm \lambda_x\lambda_{z\theta}\tilde{E}_{oz}^{r\theta\pm} = 0 \tag{3.34}$$

$$-\frac{\mu_t}{\mu_z}\lambda_x\lambda_y\tilde{E}_{ox}^{r\theta\pm} - \frac{\mu_t}{\mu_z}\lambda_y^2\tilde{E}_{oy}^{r\theta\pm} \pm \lambda_y\lambda_{z\theta}\tilde{E}_{oz}^{r\theta\pm} = 0 \tag{3.35}$$

$$\pm\frac{\mu_z}{\mu_t}\lambda_x\lambda_{z\theta}\tilde{E}_{ox}^{r\theta\pm} \pm \frac{\mu_z}{\mu_t}\lambda_y\lambda_{z\theta}\tilde{E}_{oy}^{r\theta\pm} + \left(\frac{\mu_z}{\mu_t}\lambda_\rho^2 - k_z^2\right)\tilde{E}_{oz}^{r\theta\pm} = 0 \tag{3.36}$$

Dividing out $-\frac{\mu_t}{\mu_z}\lambda_x$ from (3.34) and $-\frac{\mu_t}{\mu_z}\lambda_y$ from (3.35), we are left with identical results, leading to the equation

$$\tilde{E}_{oz}^{r\theta\pm} = \pm\left(\frac{\mu_t\lambda_x}{\mu_z\lambda_{z\theta}}\tilde{E}_{ox}^{r\theta\pm} + \frac{\mu_t\lambda_y}{\mu_z\lambda_{z\theta}}\tilde{E}_{oy}^{r\theta\pm}\right) \tag{3.37}$$

108

Now, substituting (3.37) into (3.36) and simplifying, we are able to find

$$\widetilde{E}_{oy}^{r\theta\pm} = -\frac{\lambda_x}{\lambda_y}\widetilde{E}_{ox}^{r\theta\pm} \tag{3.38}$$

Let's check to see if these results make sense. From the definition of a TE^z wave, we know the z-component of the electric field must be zero. From (3.37), we see:

$$\widetilde{E}_{oz}^{r\theta\pm} = \pm\left(\frac{\mu_t\lambda_x}{\mu_z\lambda_{z\theta}}\widetilde{E}_{ox}^{r\theta\pm} + \frac{\mu_t\lambda_y}{\mu_z\lambda_{z\theta}}\widetilde{E}_{oy}^{r\theta\pm}\right) = \pm\left[\frac{\mu_t\lambda_x}{\mu_z\lambda_{z\theta}}\widetilde{E}_{ox}^{r\theta\pm} + \frac{\mu_t\lambda_y}{\mu_z\lambda_{z\theta}}\left(-\frac{\lambda_x}{\lambda_y}\widetilde{E}_{ox}^{r\theta\pm}\right)\right] = 0$$

which is the expected result. Therefore, in summary, for a TE^z wave, we have:

$$\boxed{\vec{\widetilde{E}}^{r,\mathrm{TE}} = \left(\hat{\mathbf{x}} - \hat{\mathbf{y}}\frac{\lambda_x}{\lambda_y}\right)\widetilde{E}_{ox}^{r\theta\pm}e^{\mp j\lambda_{z\theta}z}} \tag{3.39}$$

where $\widetilde{E}_{ox}^{r\theta\pm}$ are the two unknown scattering coefficients.

3.2.2   TM^z wave ($\lambda_z = \mp\lambda_{z\psi}$).

Now, we seek the non-trivial TM^z solution to the scattered problem, using the assumed form of the solution (3.27)

$$\overleftrightarrow{\mathbf{w}}_e^\psi \cdot \vec{\widetilde{E}}_o^{r\psi\pm}\left(\lambda_x, \lambda_y\right)e^{\mp j\lambda_{z\psi}z} = 0 \tag{3.40}$$

$$\implies \overleftrightarrow{\mathbf{w}}_e^\psi \cdot \vec{\widetilde{E}}_o^{r\psi\pm} = 0 \tag{3.41}$$

Which can now be expanded to write:

$$\begin{bmatrix} \lambda_{z\psi}^2 - k_t^2 + \frac{\mu_t}{\mu_z}\lambda_y^2 & -\frac{\mu_t}{\mu_z}\lambda_x\lambda_y & \pm\lambda_x\lambda_{z\psi} \\ -\frac{\mu_t}{\mu_z}\lambda_x\lambda_y & \lambda_{z\psi}^2 - k_t^2 + \frac{\mu_t}{\mu_z}\lambda_x^2 & \pm\lambda_y\lambda_{z\psi} \\ \pm\frac{\mu_z}{\mu_t}\lambda_x\lambda_{z\psi} & \pm\frac{\mu_z}{\mu_t}\lambda_y\lambda_{z\psi} & \frac{\mu_z}{\mu_t}\lambda_\rho^2 - k_z^2 \end{bmatrix} \cdot \begin{bmatrix} \widetilde{E}_{ox}^{r\psi\pm} \\ \widetilde{E}_{oy}^{r\psi\pm} \\ \widetilde{E}_{oz}^{r\psi\pm} \end{bmatrix} = 0 \tag{3.42}$$

from which we can extract the three equations:

$$\left(\lambda_{z\psi}^2 - k_t^2 + \frac{\mu_t}{\mu_z}\lambda_y^2\right)\widetilde{E}_{ox}^{r\psi\pm} - \frac{\mu_t}{\mu_z}\lambda_x\lambda_y\widetilde{E}_{oy}^{r\psi\pm} \pm \lambda_x\lambda_{z\psi}\widetilde{E}_{oz}^{r\psi\pm} = 0 \tag{3.43}$$

$$-\frac{\mu_t}{\mu_z}\lambda_x\lambda_y\widetilde{E}_{ox}^{r\psi\pm} + \left(\lambda_{z\psi}^2 - k_t^2 + \frac{\mu_t}{\mu_z}\lambda_x^2\right)\widetilde{E}_{oy}^{r\psi\pm} \pm \lambda_y\lambda_{z\psi}\widetilde{E}_{oz}^{r\psi\pm} = 0 \tag{3.44}$$

$$\pm\frac{\mu_z}{\mu_t}\lambda_x\lambda_{z\psi}\widetilde{E}_{ox}^{r\psi\pm} \pm \frac{\mu_z}{\mu_t}\lambda_y\lambda_{z\psi}\widetilde{E}_{oy}^{r\psi\pm} + \left(\frac{\mu_z}{\mu_t}\lambda_\rho^2 - k_z^2\right)\widetilde{E}_{oz}^{r\psi\pm} = 0 \tag{3.45}$$

This time, we begin the simplification with (3.45), which can be manipulated to:

$$\widetilde{E}_{oz}^{r\psi\pm} = \pm \frac{\varepsilon_t \lambda_x}{\varepsilon_z \lambda_{z\psi}} \widetilde{E}_{ox}^{r\psi\pm} \pm \frac{\varepsilon_t \lambda_y}{\varepsilon_z \lambda_{z\psi}} \widetilde{E}_{oy}^{r\psi\pm} \tag{3.46}$$

Substituting (3.46) into (3.43) and simplifying, we have:

$$\widetilde{E}_{oy}^{r\psi\pm} = \frac{\lambda_y}{\lambda_x} \widetilde{E}_{ox}^{r\psi\pm} \tag{3.47}$$

Substituting (3.46) into (3.44) will produce the same result. In summary, then, the TM^z portion is:

$$\boxed{\begin{aligned}
\vec{\widetilde{E}}^{r,\mathrm{TM}} &= \left(\hat{\mathbf{x}} \widetilde{E}_{ox}^{r\psi\pm} + \hat{\mathbf{y}} \widetilde{E}_{oy}^{r\psi\pm} + \hat{\mathbf{z}} \widetilde{E}_{oz}^{r\psi\pm} \right) e^{\mp j\lambda_{z\psi} z} \\
\widetilde{E}_{oy}^{r\psi\pm} &= \frac{\lambda_y}{\lambda_x} \widetilde{E}_{ox}^{r\psi\pm}, \quad \widetilde{E}_{oz}^{r\psi\pm} = \pm \frac{\varepsilon_t}{\varepsilon_z} \left(\frac{\lambda_x}{\lambda_{z\psi}} \widetilde{E}_{ox}^{r\psi\pm} + \frac{\lambda_y}{\lambda_{z\psi}} \widetilde{E}_{oy}^{r\psi\pm} \right) = \pm \frac{\frac{\varepsilon_t}{\varepsilon_z} \lambda_\rho^2}{\lambda_x \lambda_{z\psi}} \widetilde{E}_{ox}^{r\psi\pm}
\end{aligned}} \tag{3.48}$$

It is noteworthy to show that both of these results satisfy Gauss's Law for source-free regions (which is the case for the scattered field). Gauss's Law states

$$\widetilde{\nabla} \cdot \vec{\widetilde{D}} = 0 \tag{3.49}$$

$$\widetilde{\nabla} \cdot \vec{\overleftrightarrow{\varepsilon}} \vec{\widetilde{E}}_o^\pm e^{\mp \lambda_z z} = 0$$

$$\left(\hat{\mathbf{x}} j\lambda_x + \hat{\mathbf{y}} j\lambda_y + \hat{\mathbf{z}} \frac{\partial}{\partial z} \right) \cdot \left(\hat{\mathbf{x}} \varepsilon_t \widetilde{E}_{ox}^{r\theta,r\psi\pm} + \hat{\mathbf{y}} \varepsilon_t \widetilde{E}_{oy}^{r\theta,r\psi\pm} + \hat{\mathbf{z}} \varepsilon_z \widetilde{E}_{oz}^{r\theta,r\psi\pm} \right) e^{\mp j\lambda_{z\theta,z\psi}} = 0$$

In the TE^z case, the left hand side becomes

$$\left(\hat{\mathbf{x}} j\lambda_x + \hat{\mathbf{y}} j\lambda_y + \hat{\mathbf{z}} \frac{\partial}{\partial z} \right) \cdot \left(\hat{\mathbf{x}} \varepsilon_t \widetilde{E}_{ox}^{r\theta\pm} + \hat{\mathbf{y}} \varepsilon_t \widetilde{E}_{oy}^{r\theta\pm} + \hat{\mathbf{z}} \varepsilon_z \widetilde{E}_{oz}^{r\theta\pm} \right) e^{\mp j\lambda_{z\theta}}$$

$$= \left(\hat{\mathbf{x}} j\lambda_x + \hat{\mathbf{y}} j\lambda_y + \hat{\mathbf{z}} \frac{\partial}{\partial z} \right) \cdot \left(\hat{\mathbf{x}} - \hat{\mathbf{y}} \frac{\lambda_x}{\lambda_y} \right) \varepsilon_t \widetilde{E}_{ox}^{r\theta\pm} e^{\mp j\lambda_{z\theta}}$$

$$= \left(j\lambda_x - j\lambda_x \right) \varepsilon_t \widetilde{E}_{ox}^{r\theta\pm} e^{\mp j\lambda_{z\theta}} = 0$$

In the TM^z case, we have

$$\left(\hat{\mathbf{x}} j\lambda_x + \hat{\mathbf{y}} j\lambda_y + \hat{\mathbf{z}} \frac{\partial}{\partial z} \right) \cdot \left(\hat{\mathbf{x}} \varepsilon_t \widetilde{E}_{ox}^{r\psi\pm} + \hat{\mathbf{y}} \varepsilon_t \widetilde{E}_{oy}^{r\psi\pm} + \hat{\mathbf{z}} \varepsilon_z \widetilde{E}_{oz}^{r\psi\pm} \right) e^{\mp j\lambda_{z\psi}} = 0$$

$$\left(\hat{\mathbf{x}} j\lambda_x + \hat{\mathbf{y}} j\lambda_y + \hat{\mathbf{z}} \frac{\partial}{\partial z} \right) \cdot \left(\hat{\mathbf{x}} \varepsilon_t \widetilde{E}_{ox}^{r\psi\pm} e^{\mp j\lambda_{z\psi}} + \hat{\mathbf{y}} \varepsilon_t \widetilde{E}_{oy}^{r\psi\pm} e^{\mp j\lambda_{z\psi}} + \varepsilon_z \hat{\mathbf{z}} \widetilde{E}_{oz}^{r\psi\pm} e^{\mp j\lambda_{z\psi}} \right) = 0$$

$$j\lambda_x \varepsilon_t \widetilde{E}_{ox}^{r\psi\pm} e^{\mp j\lambda_{z\psi}} + j\lambda_y \varepsilon_t \widetilde{E}_{oy}^{r\psi\pm} e^{\mp j\lambda_{z\psi}} \mp j\lambda_{z\psi} \varepsilon_z \widetilde{E}_{oz}^{r\psi\pm} e^{\mp j\lambda_{z\psi}} = 0$$

110

which can be manipulated to give

$$\pm j\lambda_{z\psi}\varepsilon_z \tilde{E}_{oz}^{r\psi\pm} e^{\mp j\lambda_{z\psi}} = j\lambda_x \varepsilon_t \tilde{E}_{ox}^{r\psi\pm} e^{\mp j\lambda_{z\psi}} + j\lambda_y \varepsilon_t \tilde{E}_{oy}^{r\psi\pm} e^{\mp j\lambda_{z\psi}}$$

$$\tilde{E}_{oz}^{r\psi\pm} = \pm \frac{\varepsilon_t}{\varepsilon_z} \left(\frac{\lambda_x}{\lambda_{z\psi}} \tilde{E}_{ox}^{r\psi\pm} + \frac{\lambda_y}{\lambda_{z\psi}} \tilde{E}_{oy}^{r\psi\pm} \right)$$

which is the exact result found in (3.48). Therefore, we see that our results satisfy the expected physical laws.

Now, we will find the four unknown coefficients $\tilde{E}_{ox}^{r\theta+}, \tilde{E}_{ox}^{r\theta-}, \tilde{E}_{ox}^{r\psi+}$ and $\tilde{E}_{ox}^{r\psi-}$ through enforcement of the boundary conditions on the total fields. We see that we require four boundary conditions to constitute a well-posed problem.

3.3   Total Fields and Parallel Plate Boundary Conditions

The total fields are given by

$$\vec{\tilde{E}} = \vec{\tilde{E}}^p + \vec{\tilde{E}}^r = \vec{\tilde{E}}^{p,\text{TE}} + \vec{\tilde{E}}^{p,\text{TM}} + \vec{\tilde{E}}^{r\theta} + \vec{\tilde{E}}^{r\psi}$$

$$= \int_{z'} \vec{\tilde{G}}_{ee}^{p,\text{TE}} \cdot \vec{\tilde{J}}_e dz' + \int_{z'} \vec{\tilde{G}}_{ee}^{p,\text{TM}} \cdot \vec{\tilde{J}}_e dz' + \int_{z'} \vec{\tilde{G}}_{eh}^{p,\text{TE}} \cdot \vec{\tilde{J}}_h dz' + \int_{z'} \vec{\tilde{G}}_{eh}^{p,\text{TM}} \cdot \vec{\tilde{J}}_h dz'$$

$$+ \vec{\tilde{E}}_o^{r\theta+} e^{-j\lambda_{z\theta}z} + \vec{\tilde{E}}_o^{r\theta-} e^{j\lambda_{z\theta}z} + \vec{\tilde{E}}_o^{r\psi+} e^{-j\lambda_{z\psi}z} + \vec{\tilde{E}}_o^{r\theta-} e^{j\lambda_{z\psi}z}$$

(3.50)

At this point, we are free to investigate the boundary conditions for a magnetically and electrically uniaxial material contained by parallel plates. Of course, these boundary conditions are explicitly applied to the tangential fields at the boundaries. We assume that the boundaries are located in the xy plane at $z = 0$ and $z = d$. In the course of this development, we will make use of the following convenient notation for the principal Green's function

$$\vec{\tilde{G}}_{ee,eh}^{p,\text{TE}|p,\text{TM}} = \vec{\tilde{g}}_{ee,eh}^{p,\text{TE}|p,\text{TM}} e^{-j\lambda_{z\theta,z\psi}|z-z'|}$$

(3.51)

and introduce reflection terms $R_x, \overline{R}_x, R_y$ and $R_x, \overline{R}_y$ in order to facilitate a physical interpretation later on.

- Boundary Condition #1: $\widetilde{E}_x(z{=}0) = 0$

  Applying the PEC boundary condition at $z = 0$ to the x-component of the electric field leads to

$$
\widetilde{E}_x = \overbrace{\int_{z'} \hat{\mathbf{x}} \cdot \overset{\leftrightarrow}{\widetilde{G}}{}^{p,\mathrm{TE}}_{ee} (z{=}0) \cdot \vec{\widetilde{J}}_e dz'}^{\widetilde{V}^{\theta-}_{ee,x}} + \overbrace{\int_{z'} \hat{\mathbf{x}} \cdot \overset{\leftrightarrow}{\widetilde{G}}{}^{p,\mathrm{TM}}_{ee} (z{=}0) \cdot \vec{\widetilde{J}}_e dz'}^{\widetilde{V}^{\psi-}_{ee,x}}
$$

$$
+ \overbrace{\int_{z'} \hat{\mathbf{x}} \cdot \overset{\leftrightarrow}{\widetilde{G}}{}^{p,\mathrm{TE}}_{eh} (z{=}0) \cdot \vec{\widetilde{J}}_h dz'}^{\widetilde{V}^{\theta-}_{eh,x}} + \overbrace{\int_{z'} \hat{\mathbf{x}} \cdot \overset{\leftrightarrow}{\widetilde{G}}{}^{p,\mathrm{TM}}_{eh} (z{=}0) \cdot \vec{\widetilde{J}}_h dz'}^{\widetilde{V}^{\psi-}_{eh,x}}
$$

$$
+ \widetilde{E}^{r\theta+}_{ox} e^{-j\lambda_{z\theta}(0)} + \widetilde{E}^{r\theta-}_{ox} e^{j\lambda_{z\theta}(0)} + \widetilde{E}^{r\psi+}_{ox} e^{-j\lambda_{z\psi}(0)} + \widetilde{E}^{r\psi-}_{ox} e^{j\lambda_{z\psi}(0)} = 0
$$

  which can be simplified to:

$$
\widetilde{E}^{r\theta+}_{ox} + \widetilde{E}^{r\psi+}_{ox} = R_x \widetilde{V}^{\theta-}_{ee,x} + R_x \widetilde{V}^{\psi-}_{ee,x} + R_x \widetilde{V}^{\theta-}_{eh,x} + R_x \widetilde{V}^{\psi-}_{eh,x} + R_x \widetilde{E}^{r\theta-}_{ox} + R_x \widetilde{E}^{r\psi-}_{ox} \tag{3.52}
$$

  where $R_x = -1$

- Boundary Condition #2 $\widetilde{E}_x(z{=}d) = 0$ Similarly, applying the PEC boundary condition at $z = d$ to the x-component of the electric field, we can write:

$$
\widetilde{E}_x = \overbrace{\int_{z'} \hat{\mathbf{x}} \cdot \overset{\leftrightarrow}{\widetilde{G}}{}^{p,\mathrm{TE}}_{ee} (z{=}d) \cdot \vec{\widetilde{J}}_e dz'}^{\widetilde{V}^{\theta+}_{ee,x} e^{-j\lambda_{z\theta}d}} + \overbrace{\int_{z'} \hat{\mathbf{x}} \cdot \overset{\leftrightarrow}{\widetilde{G}}{}^{p,\mathrm{TM}}_{ee} (z{=}d) \cdot \vec{\widetilde{J}}_e dz'}^{\widetilde{V}^{\psi+}_{ee,x} e^{-j\lambda_{z\psi}d}}
$$

$$
+ \overbrace{\int_{z'} \hat{\mathbf{x}} \cdot \overset{\leftrightarrow}{\widetilde{G}}{}^{p,\mathrm{TE}}_{eh} (z{=}d) \cdot \vec{\widetilde{J}}_h dz'}^{\widetilde{V}^{\theta+}_{eh,x} e^{-j\lambda_{z\theta}d}} + \overbrace{\int_{z'} \hat{\mathbf{x}} \cdot \overset{\leftrightarrow}{\widetilde{G}}{}^{p,\mathrm{TM}}_{eh} (z{=}d) \cdot \vec{\widetilde{J}}_h dz'}^{\widetilde{V}^{\psi+}_{eh,x} e^{-j\lambda_{z\psi}d}}
$$

$$
+ \widetilde{E}^{r\theta+}_{ox} e^{-j\lambda_{z\theta}d} + \widetilde{E}^{r\theta-}_{ox} e^{j\lambda_{z\theta}d} + \widetilde{E}^{r\psi+}_{ox} e^{-j\lambda_{z\psi}d} + \widetilde{E}^{r\psi-}_{ox} e^{j\lambda_{z\psi}d} = 0
$$

which simplifies to

$$\widetilde{E}_{ox}^{r\theta-} e^{j\lambda_{z\theta}d} + \widetilde{E}_{ox}^{r\psi-} e^{j\lambda_{z\psi}d} = \overline{R}_x \widetilde{V}_{ee,x}^{\theta+} e^{-j\lambda_{z\theta}d} + \overline{R}_x \widetilde{V}_{ee,x}^{\psi+} e^{-j\lambda_{z\psi}d} + \overline{R}_x \widetilde{V}_{eh,x}^{\psi+} e^{-j\lambda_{z\psi}d}$$

$$+ \overline{R}_x \widetilde{V}_{eh,x}^{\theta+} e^{-j\lambda_{z\theta}d} + \overline{R}_x \widetilde{E}_{ox}^{r\theta+} e^{-j\lambda_{z\theta}d} + \overline{R}_x \widetilde{E}_{ox}^{r\psi+} e^{-j\lambda_{z\psi}d}$$

(3.53)

where $\overline{R}_x = -1$

- Boundary Condition #3: $\widetilde{E}_y(z{=}0) = 0$

  Applying the PEC boundary condition at $z = 0$ to the y-component of the electric field allows us to write:

$$\widetilde{E}_y = \overbrace{\int_{z'} \hat{\mathbf{y}} \cdot \overleftrightarrow{\tilde{G}}_{ee}^{p,\text{TE}} (z{=}0) \cdot \vec{\tilde{J}}_e dz'}^{\widetilde{V}_{ee,y}^{\theta-}} + \overbrace{\int_{z'} \hat{\mathbf{y}} \cdot \overleftrightarrow{\tilde{G}}_{ee}^{p,\text{TM}} (z{=}0) \cdot \vec{\tilde{J}}_e dz'}^{\widetilde{V}_{ee,y}^{\psi-}}$$

$$+ \overbrace{\int_{z'} \hat{\mathbf{y}} \cdot \overleftrightarrow{\tilde{G}}_{eh}^{p,\text{TE}} (z{=}0) \cdot \vec{\tilde{J}}_h dz'}^{\widetilde{V}_{eh,y}^{\theta-}} + \overbrace{\int_{z'} \hat{\mathbf{y}} \cdot \overleftrightarrow{\tilde{G}}_{eh}^{p,\text{TM}} (z{=}0) \cdot \vec{\tilde{J}}_h dz'}^{\widetilde{V}_{eh,y}^{\psi-}}$$

$$+ \widetilde{E}_{oy}^{r\theta+} e^{-j\lambda_{z\theta}(0)} + \widetilde{E}_{oy}^{r\theta-} e^{j\lambda_{z\theta}(0)} + \widetilde{E}_{oy}^{r\psi+} e^{-j\lambda_{z\psi}(0)} + \widetilde{E}_{oy}^{r\psi-} e^{j\lambda_{z\psi}(0)} = 0$$

which simplifies to:

$$\widetilde{E}_{oy}^{r\theta+} + \widetilde{E}_{oy}^{r\psi+} = R_y \widetilde{V}_{ee,y}^{\theta-} + R_y \widetilde{V}_{ee,y}^{\psi-} + R_y \widetilde{V}_{eh,y}^{\theta-} + R_y \widetilde{V}_{eh,y}^{\psi-} + R_y \widetilde{E}_{oy}^{r\theta-} + R_y \widetilde{E}_{oy}^{r\psi-}$$

(3.54)

where $R_y = -1$. However, we recall:

$$\widetilde{E}_{oy}^{r\theta\pm} = -\frac{\lambda_x}{\lambda_y} \widetilde{E}_{ox}^{r\theta\pm} \qquad \text{and} \qquad \widetilde{E}_{oy}^{r\psi\pm} = \frac{\lambda_y}{\lambda_x} \widetilde{E}_{ox}^{r\psi\pm}$$

Therefore, (3.54) becomes:

$$-\lambda_x^2 \widetilde{E}_{ox}^{r\theta+} + \lambda_y^2 \widetilde{E}_{ox}^{r\psi+} = R_y \lambda_x \lambda_y \widetilde{V}_{ee,y}^{\theta-} + R_y \lambda_x \lambda_y \widetilde{V}_{ee,y}^{\psi-} + R_y \lambda_x \lambda_y \widetilde{V}_{eh,y}^{\theta-} + R_y \lambda_x \lambda_y \widetilde{V}_{eh,y}^{\psi-}$$

$$- R_y \lambda_x^2 \widetilde{E}_{ox}^{r\theta-} + R_y \lambda_y^2 \widetilde{E}_{ox}^{r\psi-}$$

(3.55)

113

- Boundary Condition #4 $\tilde{E}_y(z=d) = 0$

  Applying the PEC boundary condition at $z = d$ to the y-component of the electric field allows us to write:

$$\tilde{E}_y = \int\limits_{z'} \hat{\mathbf{y}} \cdot \overset{\leftrightarrow}{\tilde{G}}{}^{p,\text{TE}}_{ee}(z{=}d)\cdot\vec{\tilde{J}}_e dz' + \int\limits_{z'} \hat{\mathbf{y}} \cdot \overset{\leftrightarrow}{\tilde{G}}{}^{p,\text{TM}}_{ee}(z{=}d)\cdot\vec{\tilde{J}}_e dz'$$

where the first integral is labeled $\tilde{V}^{\theta+}_{ee,y}e^{-j\lambda_{z\theta}d}$ and the second is labeled $\tilde{V}^{\psi+}_{ee,y}e^{-j\lambda_{z\psi}d}$.

$$+ \int\limits_{z'} \hat{\mathbf{y}} \cdot \overset{\leftrightarrow}{\tilde{G}}{}^{p,\text{TE}}_{eh}(z{=}d)\cdot\vec{\tilde{J}}_h dz' + \int\limits_{z'} \hat{\mathbf{y}} \cdot \overset{\leftrightarrow}{\tilde{G}}{}^{p,\text{TM}}_{eh}(z{=}d)\cdot\vec{\tilde{J}}_h dz'$$

where the first integral is labeled $\tilde{V}^{\theta+}_{eh,y}e^{-j\lambda_{z\theta}d}$ and the second is labeled $\tilde{V}^{\psi+}_{eh,y}e^{-j\lambda_{z\psi}d}$.

$$+ \tilde{E}^{r\theta+}_{oy}e^{-j\lambda_{z\theta}d} + \tilde{E}^{r\theta-}_{oy}e^{j\lambda_{z\theta}d} + \tilde{E}^{r\psi+}_{oy}e^{-j\lambda_{z\psi}d} + \tilde{E}^{r\psi-}_{oy}e^{j\lambda_{z\psi}d} = 0$$

which simplifies to:

$$
\begin{aligned}
\tilde{E}^{r\theta-}_{oy}e^{j\lambda_{z\theta}d} + \tilde{E}^{r\psi-}_{oy}e^{j\lambda_{z\psi}d} = {}& +\overline{R}_y\tilde{V}^{\theta+}_{ee,y}e^{-j\lambda_{z\theta}d} + \overline{R}_y\tilde{V}^{\psi+}_{ee,y}e^{-j\lambda_{z\psi}d} + \overline{R}_y\tilde{V}^{\theta+}_{eh,y}e^{-j\lambda_{z\theta}d} \\
& + \overline{R}_y\tilde{V}^{\psi+}_{eh,y}e^{-j\lambda_{z\psi}d} + \overline{R}_y\tilde{E}^{r\theta+}_{oy}e^{-j\lambda_{z\theta}d} + \overline{R}_y\tilde{E}^{r\psi+}_{oy}e^{-j\lambda_{z\psi}d}
\end{aligned}
\tag{3.56}
$$

where $\overline{R}_y = -1$. However, we recall:

$$\tilde{E}^{r\theta\pm}_{oy} = -\frac{\lambda_x}{\lambda_y}\tilde{E}^{r\theta\pm}_{ox} \qquad \text{and} \qquad \tilde{E}^{r\psi\pm}_{oy} = \frac{\lambda_y}{\lambda_x}\tilde{E}^{r\psi\pm}_{ox}$$

Therefore, (3.56) becomes:

$$
\begin{aligned}
-\lambda_x^2\tilde{E}^{r\theta-}_{ox}e^{j\lambda_{z\theta}d} + \lambda_y^2\tilde{E}^{r\psi-}_{ox}e^{j\lambda_{z\psi}d} = {}& \overline{R}_y\lambda_x\lambda_y\tilde{V}^{\theta+}_{ee,y}e^{-j\lambda_{z\theta}d} + \overline{R}_y\lambda_x\lambda_y\tilde{V}^{\psi+}_{ee,y}e^{-j\lambda_{z\psi}d} \\
& + \overline{R}_y\lambda_x\lambda_y\tilde{V}^{\theta+}_{eh,y}e^{-j\lambda_{z\theta}d} + \overline{R}_y\lambda_x\lambda_y\tilde{V}^{\psi+}_{eh,y}e^{-j\lambda_{z\psi}d} \\
& - \overline{R}_y\lambda_x^2\tilde{E}^{r\theta+}_{ox}e^{-j\lambda_{z\theta}d} + \overline{R}_y\lambda_y^2\tilde{E}^{r\psi+}_{ox}e^{-j\lambda_{z\psi}d}
\end{aligned}
\tag{3.57}
$$

3.3.1 Calculation of Scattering Coefficients.

We can use (3.52)-(3.57) to solve for the unknowns $\tilde{E}^{r\theta+}_{ox}, \tilde{E}^{r\theta-}_{ox}, \tilde{E}^{r\psi+}_{ox}, \tilde{E}^{r\psi-}_{ox}$ and from the relations found in (3.48), find $\tilde{E}^{r\psi\pm}_{oy}$ and $\tilde{E}^{r\theta\pm}_{oz}$. Additionally, we collapse the reflection coefficients to $R_x = R_y = R = -1$ and $\overline{R}_x = \overline{R}_y = \overline{R} = -1$. Multiplying equation (3.55)

114

by λ_x^2 and adding the result to equation (3.55), then also multiplying (3.53) and adding the result to equation (3.57), and finally solving the resulting system of coupled equations, we find $\tilde{E}_{ox}^{r\psi+}$ and $\tilde{E}_{ox}^{r\psi-}$:

$$
\tilde{E}_{ox}^{r\psi+} = \left\{ R\tilde{V}_{1,ee}^{\theta-} + R\tilde{V}_{1,ee}^{\psi-} + R\overline{R}\tilde{V}_{1,ee}^{\theta+}e^{-j\lambda_{z\theta}d}e^{-j\lambda_{z\psi}d} \right.
$$
$$
\left. + R\overline{R}\tilde{V}_{1,ee}^{\psi+}e^{-j2\lambda_{z\psi}d} + R\tilde{V}_{1,eh}^{\theta-} + R\tilde{V}_{1,eh}^{\psi-} \right. \tag{3.58}
$$
$$
\left. + R\overline{R}\tilde{V}_{1,eh}^{\theta+}e^{-j\lambda_{z\theta}d}e^{-j\lambda_{z\psi}d} + R\overline{R}\tilde{V}_{1,eh}^{\psi+}e^{-j2\lambda_{z\psi}d} \right\} \bigg/ \left(1 - R\overline{R}e^{-j2\lambda_{z\psi}d} \right)
$$

and

$$
\tilde{E}_{ox}^{r\psi-} = \left\{ \overline{R}\tilde{V}_{1,ee}^{\theta+}e^{-j\lambda_{z\theta}d}e^{-j\lambda_{z\psi}d} + \overline{R}\tilde{V}_{1,ee}^{\psi+}e^{-j2\lambda_{z\psi}d} + R\overline{R}\tilde{V}_{1,ee}^{\theta-}e^{-j2\lambda_{z\psi}d} \right.
$$
$$
\left. + R\overline{R}\tilde{V}_{1,ee}^{\psi-}e^{-j2\lambda_{z\psi}d} + \overline{R}\tilde{V}_{1,eh}^{\theta+}e^{-j\lambda_{z\theta}d}e^{-j\lambda_{z\psi}d} + \overline{R}\tilde{V}_{1,eh}^{\psi+}e^{-j2\lambda_{z\psi}d} \right. \tag{3.59}
$$
$$
\left. + R\overline{R}\tilde{V}_{1,eh}^{\theta-}e^{-j2\lambda_{z\psi}d} + R\overline{R}\tilde{V}_{1,eh}^{\psi-}e^{-j2\lambda_{z\psi}d} \right\} \bigg/ \left(1 - R\overline{R}e^{-j2\lambda_{z\psi}d} \right)
$$

Here we have combined the x and y terms into the following representation in order to condense notation (note: the top superscript represents one equation and the bottom represents another):

$$
\tilde{V}_{1,ee}^{\theta\pm} = \frac{\lambda_x^2}{\lambda_\rho^2}\tilde{V}_{ee,x}^{\theta\pm} + \frac{\lambda_x\lambda_y}{\lambda_\rho^2}\tilde{V}_{ee,y}^{\theta\pm} \quad \text{and} \quad \tilde{V}_{1,eh}^{\theta\pm} = \frac{\lambda_x^2}{\lambda_\rho^2}\tilde{V}_{eh,x}^{\theta\pm} + \frac{\lambda_x\lambda_y}{\lambda_\rho^2}\tilde{V}_{eh,y}^{\theta\pm} \tag{3.60}
$$

and

$$
\tilde{V}_{1,ee}^{\psi\pm} = \frac{\lambda_x^2}{\lambda_\rho^2}\tilde{V}_{ee,x}^{\psi\pm} + \frac{\lambda_x\lambda_y}{\lambda_\rho^2}\tilde{V}_{ee,y}^{\psi\pm} \quad \text{and} \quad \tilde{V}_{1,eh}^{\psi\pm} = \frac{\lambda_x^2}{\lambda_\rho^2}\tilde{V}_{eh,x}^{\psi\pm} + \frac{\lambda_x\lambda_y}{\lambda_\rho^2}\tilde{V}_{eh,y}^{\psi\pm} \tag{3.61}
$$

Similarly, multiplying equation (3.52) by $-\lambda_y^2$ and adding the result to equation (3.55), then also multiplying (3.53) by $-\lambda_y^2$ and adding the result to (3.57), then finally solving the resulting set of coupled equations, we find $\tilde{E}_{ox}^{r\theta+}$ and $\tilde{E}_{ox}^{r\theta-}$:

$$
\tilde{E}_{ox}^{r\theta+} = \left\{ R\tilde{V}_{2,ee}^{\theta-} + R\tilde{V}_{2,ee}^{\psi-} + R\overline{R}\tilde{V}_{2,ee}^{\theta+}e^{-j2\lambda_{z\theta}d} \right.
$$
$$
\left. + R\overline{R}\tilde{V}_{2,ee}^{\psi+}e^{-j\lambda_{z\theta}d}e^{-j\lambda_{z\psi}d} + R\tilde{V}_{2,eh}^{\theta-} + R\tilde{V}_{2,eh}^{\psi-} \right. \tag{3.62}
$$
$$
\left. + R\overline{R}\tilde{V}_{2,eh}^{\theta+}e^{-j2\lambda_{z\theta}d} + R\overline{R}\tilde{V}_{2,eh}^{\psi+}e^{-j\lambda_{z\theta}d}e^{-j\lambda_{z\psi}d} \right\} \bigg/ \left(1 - R\overline{R}e^{-j2\lambda_{z\theta}d} \right)
$$

115

and

$$
\begin{aligned}
\widetilde{E}_{ox}^{r\theta-} = \Bigg\{ &\overline{R}\widetilde{V}_{2,ee}^{\theta+}e^{-j2\lambda_{z\theta}d} + \overline{R}\widetilde{V}_{2,ee}^{\psi+}e^{-j\lambda_{z\theta}d}e^{-j\lambda_{z\psi}d} + R\overline{R}\widetilde{V}_{2,ee}^{\theta-}e^{-j2\lambda_{z\theta}d} + R\overline{R}\widetilde{V}_{2,ee}^{\psi-}e^{-j2\lambda_{z\theta}d} \\
&+ \overline{R}\widetilde{V}_{2,eh}^{\theta+}e^{-j2\lambda_{z\theta}d} + \overline{R}\widetilde{V}_{2,eh}^{\psi+}e^{-j\lambda_{z\theta}d}e^{-j\lambda_{z\psi}d} \\
&+ R\overline{R}\widetilde{V}_{2,eh}^{\theta-}e^{-j2\lambda_{z\theta}d} + R\overline{R}\widetilde{V}_{2,eh}^{\psi-}e^{-j2\lambda_{z\theta}d} \Bigg\} \Bigg/ \left(1 - R\overline{R}e^{-j2\lambda_{z\theta}d}\right)
\end{aligned}
\tag{3.63}
$$

where, as before, we have defined consolidated terms:

$$
\widetilde{V}_{1,\text{ee}}^{\theta\pm} = \frac{\lambda_y^2}{\lambda_\rho^2}\widetilde{V}_{ee,x}^{\theta\pm} - \frac{\lambda_x\lambda_y}{\lambda_\rho^2}\widetilde{V}_{ee,y}^{\theta\pm} \quad \text{and} \quad \widetilde{V}_{1,\text{eh}}^{\theta\pm} = \frac{\lambda_y^2}{\lambda_\rho^2}\widetilde{V}_{eh,x}^{\theta\pm} - \frac{\lambda_x\lambda_y}{\lambda_\rho^2}\widetilde{V}_{eh,y}^{\theta\pm}
\tag{3.64}
$$

and

$$
\widetilde{V}_{1,\text{ee}}^{\psi\pm} = \frac{\lambda_y^2}{\lambda_\rho^2}\widetilde{V}_{ee,x}^{\psi\pm} - \frac{\lambda_x\lambda_y}{\lambda_\rho^2}\widetilde{V}_{ee,y}^{\psi\pm} \quad \text{and} \quad \widetilde{V}_{1,\text{eh}}^{\psi\pm} = \frac{\lambda_y^2}{\lambda_\rho^2}\widetilde{V}_{eh,x}^{\psi\pm} - \frac{\lambda_x\lambda_y}{\lambda_\rho^2}\widetilde{V}_{eh,y}^{\psi\pm}
\tag{3.65}
$$

3.4 Identification of Total Green's Functions

Now that we have determined the principal and scattered Green's functions, we combine the results to find the total PPWG Green's function. Recall the definition of the total electric field is given by (3.50) and is repeated here for convenience:

$$
\begin{aligned}
\vec{\tilde{E}} &= \vec{\tilde{E}}^p + \vec{\tilde{E}}^r = \vec{\tilde{E}}^{p,\text{TE}} + \vec{\tilde{E}}^{p,\text{TM}} + \vec{\tilde{E}}^{r\theta} + \vec{\tilde{E}}^{r\psi} \\
&= \int_{z'} \overset{\leftrightarrow}{\tilde{G}}_{ee}^{p,\text{TE}} \cdot \vec{\tilde{J}}_e dz' + \int_{z'} \overset{\leftrightarrow}{\tilde{G}}_{ee}^{p,\text{TM}} \cdot \vec{\tilde{J}}_e dz' + \int_{z'} \overset{\leftrightarrow}{\tilde{G}}_{eh}^{p,\text{TE}} \cdot \vec{\tilde{J}}_h dz' + \int_{z'} \overset{\leftrightarrow}{\tilde{G}}_{eh}^{p,\text{TM}} \cdot \vec{\tilde{J}}_h dz'
\end{aligned}
\tag{3.66}
$$

$$
+ \vec{\tilde{E}}_o^{r\theta+}e^{-j\lambda_{z\theta}z} + \vec{\tilde{E}}_o^{r\theta-}e^{j\lambda_{z\theta}z} + \vec{\tilde{E}}_o^{r\psi+}e^{-j\lambda_{z\psi}z} + \vec{\tilde{E}}_o^{r\theta-}e^{j\lambda_{z\psi}z}
\tag{3.67}
$$

Since we know the form of the principal Green's function, we will investigate the form of the reflected portion and combine the results.

3.4.1 Scattered Green's Function.

The reflected contribution to the electric field can be written as the combination of the TE^z and TM^z parts:

$$\vec{E}^r = \vec{E}^{r,\text{TE}} + \vec{E}^{r,\text{TM}} \tag{3.68}$$

where:

$$\vec{E}^{r,\text{TE}} = \left(\hat{\mathbf{x}} - \hat{\mathbf{y}} \frac{\lambda_x}{\lambda_y} \right) \widetilde{E}_{ox}^{r\theta+} e^{-j\lambda_{z\theta}z} + \left(\hat{\mathbf{x}} - \hat{\mathbf{y}} \frac{\lambda_x}{\lambda_y} \right) \widetilde{E}_{ox}^{r\theta-} e^{j\lambda_{z\theta}z} \tag{3.69}$$

$$\vec{E}^{r,\text{TM}} = \left(\hat{\mathbf{x}} \widetilde{E}_{ox}^{r\psi+} + \hat{\mathbf{y}} \widetilde{E}_{oy}^{r\psi+} + \hat{\mathbf{z}} \widetilde{E}_{oz}^{r\psi+} \right) e^{-j\lambda_{z\psi}z} + \left(\hat{\mathbf{x}} \widetilde{E}_{ox}^{r\psi-} + \hat{\mathbf{y}} \widetilde{E}_{oy}^{r\psi-} + \hat{\mathbf{z}} \widetilde{E}_{oz}^{r\psi-} \right) e^{j\lambda_{z\psi}z}$$

$$\widetilde{E}_{oy}^{r\psi\pm} = \frac{\lambda_y}{\lambda_x} \widetilde{E}_{ox}^{r\psi\pm} \quad \text{and} \quad \widetilde{E}_{oz}^{r\psi\pm} = \pm \frac{\frac{\varepsilon_t}{\varepsilon_z} \lambda_\rho^2}{\lambda_x \lambda_{z\psi}} \widetilde{E}_{ox}^{r\psi\pm} \tag{3.70}$$

- TE^z Contribution, x-component

    We see that both the y- and z- components can be found from the x-component, so we examine it first.

    $$\vec{E}^{r,\text{TE}} = \left(\hat{\mathbf{x}} - \hat{\mathbf{y}} \frac{\lambda_x}{\lambda_y} \right) \widetilde{E}_{ox}^{r\theta+} e^{-j\lambda_{z\theta}z} + \left(\hat{\mathbf{x}} - \hat{\mathbf{y}} \frac{\lambda_x}{\lambda_y} \right) \widetilde{E}_{ox}^{r\theta-} e^{j\lambda_{z\theta}z}$$

    $$\implies \widetilde{E}_x^{r,\text{TE}} = \widetilde{E}_{ox}^{r\theta+} e^{-j\lambda_{z\theta}z} + \widetilde{E}_{ox}^{r\theta-} e^{j\lambda_{z\theta}z}$$

    Defining the denominator term containing the $\lambda_{z\theta}$ terms as

    $$D_\theta = \left(1 - R\overline{R} e^{-j2\lambda_{z\theta}d} \right) \tag{3.71}$$

and simplifying, we find:

$$\widetilde{E}_x^{r,\text{TE}} D_\theta = \left\{ R\widetilde{V}_{2,ee}^{\theta-} e^{-j\lambda_{z\theta}z} + R\widetilde{V}_{2,ee}^{\psi-} e^{-j\lambda_{z\theta}z} \right.$$

$$+ R\overline{R}\widetilde{V}_{2,ee}^{\theta+} e^{-j\lambda_{z\theta}(2d+z)} + R\overline{R}\widetilde{V}_{2,ee}^{\psi+} e^{-j\lambda_{z\theta}(d+z)} e^{-j\lambda_{z\psi}d}$$

$$+ \overline{R}\widetilde{V}_{2,ee}^{\theta+} e^{-j\lambda_{z\theta}(2d-z)} + \overline{R}\widetilde{V}_{2,ee}^{\psi+} e^{-j\lambda_{z\theta}(d-z)} e^{-j\lambda_{z\psi}d}$$

$$+ R\overline{R}\widetilde{V}_{2,ee}^{\theta-} e^{-j\lambda_{z\theta}(2d-z)} + R\overline{R}\widetilde{V}_{2,ee}^{\psi-} e^{-j\lambda_{z\theta}(2d-z)}$$

$$+ R\widetilde{V}_{2,eh}^{\theta-} e^{-j\lambda_{z\theta}z} + R\widetilde{V}_{2,eh}^{\psi-} e^{-j\lambda_{z\theta}z} \qquad (3.72)$$

$$+ R\overline{R}\widetilde{V}_{2,eh}^{\theta+} e^{-j\lambda_{z\theta}(2d+z)} + R\overline{R}\widetilde{V}_{2,eh}^{\psi+} e^{-j\lambda_{z\theta}(d+z)} e^{-j\lambda_{z\psi}d}$$

$$+ \overline{R}\widetilde{V}_{2,eh}^{\theta+} e^{-j\lambda_{z\theta}(2d-z)} + \overline{R}\widetilde{V}_{2,eh}^{\psi+} e^{-j\lambda_{z\theta}(d-z)} e^{-j\lambda_{z\psi}d}$$

$$\left. + R\overline{R}\widetilde{V}_{2,eh}^{\theta-} e^{-j\lambda_{z\theta}(2d-z)} + R\overline{R}\widetilde{V}_{2,eh}^{\psi-} e^{-j\lambda_{z\theta}(2d-z)} \right\}$$

- TM^z Contribution, x-component

$$\vec{\widetilde{E}}^{r,\text{TM}} = \left(\hat{\mathbf{x}}\widetilde{E}_{ox}^{r\psi+} + \hat{\mathbf{y}}\widetilde{E}_{oy}^{r\psi+} + \hat{\mathbf{z}}\widetilde{E}_{oz}^{r\psi+} \right) e^{-j\lambda_{z\psi}z} + \left(\hat{\mathbf{x}}\widetilde{E}_{ox}^{r\psi-} + \hat{\mathbf{y}}\widetilde{E}_{oy}^{r\psi-} + \hat{\mathbf{z}}\widetilde{E}_{oz}^{r\psi-} \right) e^{j\lambda_{z\psi}z}$$

$$\implies \widetilde{E}_x^{r,\text{TM}} = \widetilde{E}_{ox}^{r\psi+} e^{-j\lambda_{z\psi}z} + \widetilde{E}_{ox}^{r\psi-} e^{j\lambda_{z\psi}z}$$

Defining the denominator term containing the $\lambda_{z\psi}$ terms as

$$D_\psi = \left(1 - R\overline{R}e^{-j2\lambda_{z\psi}d} \right) \qquad (3.73)$$

and simplifying, we find:

$$
\widetilde{E}_x^{r,\text{TM}} D_\psi = \left\{ R\widetilde{V}_{1,ee}^{\theta-}e^{-j\lambda_{z\psi}z} + R\widetilde{V}_{1,ee}^{\psi-}e^{-j\lambda_{z\psi}z} \right.
$$
$$
+ R\overline{R}\widetilde{V}_{1,ee}^{\theta+}e^{-j\lambda_{z\theta}d}e^{-j\lambda_{z\psi}(d+z)} + R\overline{R}\widetilde{V}_{1,ee}^{\psi+}e^{-j\lambda_{z\psi}(2d+z)}
$$
$$
+ \overline{R}\widetilde{V}_{1,ee}^{\theta+}e^{-j\lambda_{z\theta}d}e^{-j\lambda_{z\psi}(d-z)} + \overline{R}\widetilde{V}_{1,ee}^{\psi+}e^{-j\lambda_{z\psi}(2d-z)}
$$
$$
+ R\overline{R}\widetilde{V}_{1,ee}^{\theta-}e^{-j\lambda_{z\psi}(2d-z)} + R\overline{R}\widetilde{V}_{1,ee}^{\psi-}e^{-j\lambda_{z\psi}(2d-z)}
$$
$$
+ R\widetilde{V}_{1,eh}^{\theta-}e^{-j\lambda_{z\psi}z} + R\widetilde{V}_{1,eh}^{\psi-}e^{-j\lambda_{z\psi}z}
$$
$$
+ R\overline{R}\widetilde{V}_{1,eh}^{\theta+}e^{-j\lambda_{z\theta}d}e^{-j\lambda_{z\psi}(d+z)} + R\overline{R}\widetilde{V}_{1,eh}^{\psi+}e^{-j\lambda_{z\psi}(2d+z)}
$$
$$
+ \overline{R}\widetilde{V}_{1,eh}^{\theta+}e^{-j\lambda_{z\theta}d}e^{-j\lambda_{z\psi}(d-z)} + \overline{R}\widetilde{V}_{1,eh}^{\psi+}e^{-j\lambda_{z\psi}(2d-z)}
$$
$$
\left. + R\overline{R}\widetilde{V}_{1,eh}^{\theta-}e^{-j\lambda_{z\psi}(2d-z)} + R\overline{R}\widetilde{V}_{1,eh}^{\psi-}e^{-j\lambda_{z\psi}(2d-z)} \right\}
$$

(3.74)

(3.72) and (3.74) represent the *x*-component of the reflected electric field maintained by both electric and magnetic sources. Therefore, we can examine the *ee* and *eh* type Green's functions separately.

3.4.2 *Electric (ee) Reflected Green's Function, x-componenet, TE^z Field.*

From (3.72), we have the *x*-component of the TE^z portion of the reflected electric field maintained by an electric source (*ee*-type) as:

$$
\widetilde{E}_{ee,x}^{r,\text{TE}} D_\theta = R\widetilde{V}_{2,ee}^{\theta-}e^{-j\lambda_{z\theta}z} + R\widetilde{V}_{2,ee}^{\psi-}e^{-j\lambda_{z\theta}z}
$$
$$
+ R\overline{R}\widetilde{V}_{2,ee}^{\theta+}e^{-j\lambda_{z\theta}(2d+z)} + R\overline{R}\widetilde{V}_{2,ee}^{\psi+}e^{-j\lambda_{z\theta}(d+z)}e^{-j\lambda_{z\psi}d}
$$
$$
+ \overline{R}\widetilde{V}_{2,ee}^{\theta+}e^{-j\lambda_{z\theta}(2d-z)} + \overline{R}\widetilde{V}_{2,ee}^{\psi+}e^{-j\lambda_{z\theta}(d-z)}e^{-j\lambda_{z\psi}d}
$$
$$
+ R\overline{R}\widetilde{V}_{2,ee}^{\theta-}e^{-j\lambda_{z\theta}(2d-z)} + R\overline{R}\widetilde{V}_{2,ee}^{\psi-}e^{-j\lambda_{z\theta}(2d-z)}
$$

(3.75)

where:

$$\widetilde{V}_{2,ee}^{\theta+} = \frac{\lambda_y^2}{\lambda_\rho^2}\widetilde{V}_{ee,x}^{\theta+} - \frac{\lambda_x\lambda_y}{\lambda_\rho^2}\widetilde{V}_{ee,y}^{\theta+}$$

$$= \int\limits_{z'} \underbrace{\left[\frac{\lambda_y^2}{\lambda_\rho^2}\hat{\mathbf{x}}\boldsymbol{\cdot}\ \overset{\leftrightarrow}{\tilde{\mathbf{g}}}_{ee}^{p\theta}\ (z{=}d) - \frac{\lambda_x\lambda_y}{\lambda_\rho^2}\hat{\mathbf{y}}\boldsymbol{\cdot}\ \overset{\leftrightarrow}{\tilde{\mathbf{g}}}_{ee}^{p\theta}\ (z{=}d)\right]}_{\mathsf{V}_{2,ee}^{\theta+}} e^{j\lambda_{z\theta}z'}\boldsymbol{\cdot}\overset{\rightarrow}{\tilde{\mathbf{J}}}_e dz' \qquad (3.76)$$

$$\widetilde{V}_{2,ee}^{\theta-} = \frac{\lambda_y^2}{\lambda_\rho^2}\widetilde{V}_{ee,x}^{\theta-} - \frac{\lambda_x\lambda_y}{\lambda_\rho^2}\widetilde{V}_{ee,y}^{\theta-}$$

$$= \int\limits_{z'} \underbrace{\left[\frac{\lambda_y^2}{\lambda_\rho^2}\hat{\mathbf{x}}\boldsymbol{\cdot}\ \overset{\leftrightarrow}{\tilde{\mathbf{g}}}_{ee}^{p\theta}\ (z{=}0) - \frac{\lambda_x\lambda_y}{\lambda_\rho^2}\hat{\mathbf{y}}\boldsymbol{\cdot}\ \overset{\leftrightarrow}{\tilde{\mathbf{g}}}_{ee}^{p\theta}\ (z{=}0)\right]}_{\mathsf{V}_{2,ee}^{\theta-}} e^{-j\lambda_{z\theta}z'}\boldsymbol{\cdot}\overset{\rightarrow}{\tilde{\mathbf{J}}}_e dz' \qquad (3.77)$$

$$\widetilde{V}_{2,ee}^{\psi+} = \frac{\lambda_y^2}{\lambda_\rho^2}\widetilde{V}_{ee,x}^{\psi+} - \frac{\lambda_x\lambda_y}{\lambda_\rho^2}\widetilde{V}_{ee,y}^{\psi+}$$

$$= \int\limits_{z'} \underbrace{\left[\frac{\lambda_y^2}{\lambda_\rho^2}\hat{\mathbf{x}}\boldsymbol{\cdot}\ \overset{\leftrightarrow}{\tilde{\mathbf{g}}}_{ee}^{p\psi}\ (z{=}d) - \frac{\lambda_x\lambda_y}{\lambda_\rho^2}\hat{\mathbf{y}}\boldsymbol{\cdot}\ \overset{\leftrightarrow}{\tilde{\mathbf{g}}}_{ee}^{p\psi}\ (z{=}d)\right]}_{\mathsf{V}_{2,ee}^{\psi+}} e^{j\lambda_{z\psi}z'}\boldsymbol{\cdot}\overset{\rightarrow}{\tilde{\mathbf{J}}}_e dz' \qquad (3.78)$$

$$\widetilde{V}_{2,ee}^{\psi-} = \frac{\lambda_y^2}{\lambda_\rho^2}\widetilde{V}_{ee,x}^{\psi-} - \frac{\lambda_x\lambda_y}{\lambda_\rho^2}\widetilde{V}_{ee,y}^{\psi-}$$

$$= \int\limits_{z'} \underbrace{\left[\frac{\lambda_y^2}{\lambda_\rho^2}\hat{\mathbf{x}}\boldsymbol{\cdot}\ \overset{\leftrightarrow}{\tilde{\mathbf{g}}}_{ee}^{p\psi}\ (z{=}0) - \frac{\lambda_x\lambda_y}{\lambda_\rho^2}\hat{\mathbf{y}}\boldsymbol{\cdot}\ \overset{\leftrightarrow}{\tilde{\mathbf{g}}}_{ee}^{p\psi}\ (z{=}0)\right]}_{\mathsf{V}_{2,ee}^{\psi-}} e^{-j\lambda_{z\psi}z'}\boldsymbol{\cdot}\overset{\rightarrow}{\tilde{\mathbf{J}}}_e dz' \qquad (3.79)$$

120

Therefore, we can write (3.75), which is the TE^z electric field maintained by an electric current, as:

$$\widetilde{E}_{ee,x}^{r,\text{TE}} D_\theta = \int_{z'} \left\{ \underbrace{R\text{V}_{2,ee}^{\theta-}e^{-j\lambda_{z\theta}(z+z')} + R\text{V}_{2,ee}^{\psi-}e^{-j\lambda_{z\theta}z}e^{-j\lambda_{z\psi}z'}}_{(r_1)} \right.$$

$$\underbrace{+R\overline{R}\text{V}_{2,ee}^{\theta+}e^{-j\lambda_{z\theta}(2d+z-z')} + R\overline{R}\text{V}_{2,ee}^{\psi+}e^{-j\lambda_{z\theta}(d+z)}e^{-j\lambda_{z\psi}(d-z')}}_{(r_2)}$$

$$\underbrace{+\overline{R}\text{V}_{2,ee}^{\theta+}e^{-j\lambda_{z\theta}(2d-z-z')} + \overline{R}\text{V}_{2,ee}^{\psi+}e^{-j\lambda_{z\theta}(d-z)}e^{-j\lambda_{z\psi}(d-z')}}_{(r_3)}$$

$$\left. \underbrace{+R\overline{R}\text{V}_{2,ee}^{\theta-}e^{-j\lambda_{z\theta}(2d-z+z')} + R\overline{R}\text{V}_{2,ee}^{\psi-}e^{-j\lambda_{z\theta}(2d-z)}e^{-j\lambda_{z\psi}z'}}_{(r_4)} \right\} \cdot \vec{\tilde{J}}_e dz' \tag{3.80}$$
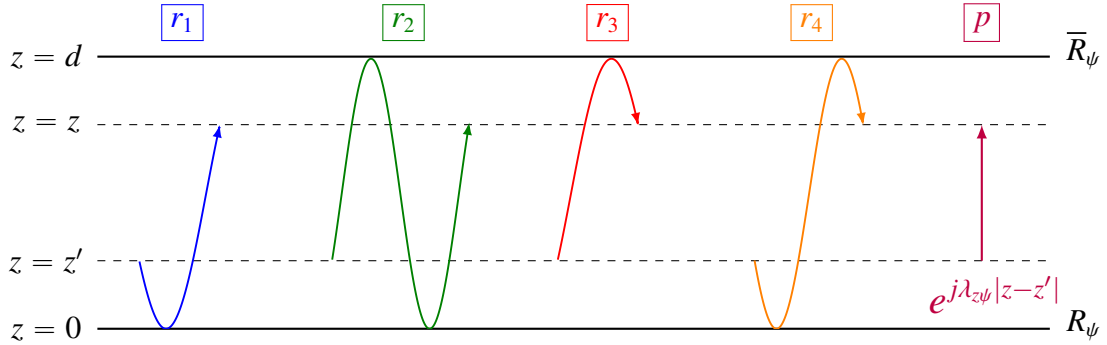
Figure 3.1: A graphical representation of the unique paths inside the waveguide structure which contribute to an observed TE^z field at a given observation point z. Clearly, both TE^z and TM^z sources contribute to an observed TE^z wave. The path r_1 represents a downward propagating wave (either TE^z or TM^z) that is reflected off the bottom wall and observed at z. The path r_2 represents an upward propagating wave that is reflected off of both walls before being observed. The path r_3 represents an upward propagating wave that is reflected off the top wall before observation. The path r_4 represents a downward propagating wave that is reflected off of both walls before observation.

We have taken great pains to develop the expressions in a manner that connect the mathematical expressions to the physical meaning of the problem. This is a more tedious process than was the case when using the potential development. Now, however, we can examine the fruits of this labor. Figure 3.1 presents a graphical interpretation of (3.80). The direction and orientation of the source wave is indicated in (3.80) by the principal source terms $V_{2,ee}^{\theta-}$, $V_{2,ee}^{\theta+}$, $V_{2,ee}^{\psi-}$ and $V_{2,ee}^{\psi+}$. The phase shift introduced by the propagation is given by the trailing exponential. Finally, the reflection coefficients R and $\overline{R}$ indicate which boundaries are impacted by the wave and the effect of this boundary in the propagation of the wave. For example, examining the first term in (3.80), we see it takes the path r_1. This represents a downward propagating TE^z wave that undergoes a phase shift of z', is reflected off the bottom boundary (R) and then undergoes a further phase shift of z. Following this same logic, we are able to find a physical correlation for each term with each path shown in Figure 3.1 - which provides further confidence in the analysis up to this point. Also note that the second set of terms in the terms a, b, c, and d imply TE^z waves (shown by the $e^{-j\lambda_{z\theta}z}$ terms) excited by TM^z sources ($e^{-j\lambda_{z\psi}z'}$ terms). We expect that these terms will reduce to zero, since no TE^z -TM^z coupling would be expected in a material with diagonal constitutive parameter dyads. Now that we have given ourselves a certain degree of confidence, we can begin the final task in this tedious process of identifying the electric Green's function. First, we will need to find the source terms. Note that we find the $\tilde{\overset{\leftrightarrow}{g}}_{ee}^{p\theta}$ terms from 3.1.4.7. The source term $V_{2,ee}^{\theta+}$ is:

$$V_{2,ee}^{\theta+} = \frac{\lambda_y^2}{\lambda_\rho^2}\hat{\mathbf{x}}\cdot\tilde{\overset{\leftrightarrow}{g}}_{ee}^{p\theta}\,(z{=}d) - \frac{\lambda_x\lambda_y}{\lambda_\rho^2}\hat{\mathbf{y}}\cdot\tilde{\overset{\leftrightarrow}{g}}_{ee}^{p\theta}\,(z{=}d) \tag{3.81}$$

$$= \frac{\lambda_y^2}{\lambda_\rho^2}\left[-\frac{\omega\mu_t\lambda_y^2}{2\lambda_{z\theta}\lambda_\rho^2}\hat{\mathbf{x}} + \frac{\omega\mu_t\lambda_x\lambda_y}{2\lambda_{z\theta}\lambda_\rho^2}\hat{\mathbf{y}}\right] - \frac{\lambda_x\lambda_y}{\lambda_\rho^2}\left[\frac{\omega\mu_t\lambda_x\lambda_y}{2\lambda_{z\theta}\lambda_\rho^2}\hat{\mathbf{x}} - \frac{\omega\mu_t\lambda_x^2}{2\lambda_{z\theta}\lambda_\rho^2}\hat{\mathbf{y}}\right] \tag{3.82}$$

which can be simplified to

$$V_{2,ee}^{\theta+} = \frac{\omega\mu_t}{2\lambda_{z\theta}\lambda_\rho^2}\left[-\lambda_y^2\hat{\mathbf{x}} + \lambda_x\lambda_y\hat{\mathbf{y}}\right] \tag{3.83}$$

We readily see that $V_{2,ee}^{\theta-} = V_{2,ee}^{\theta+}$, as neither contains a z-component. This is intuitive, as no z-component of the TE^z field is found from a z-directed electric source. Now, we can turn our attention to $V_{2,ee}^{\psi+}$ and $V_{2,ee}^{\psi-}$. They are found to be

$$V_{2,ee}^{\psi+} = V_{2,ee}^{\psi-} = 0 \tag{3.84}$$

As (3.80) represents the total TE^z field that is excited within the parallel plates, it contains source terms for both TE^z and TM^z excitations. Therefore, we can further deconstruct the TE^z electric field maintained by an electric source into two cases, based on the excitation type (TE^z or TM^z).

TE^z Wave Excited by a TE^z Source. The x-component of the TE^z contribution to an electric field maintained by a TE^z electric source is found by picking out the appropriate terms from (3.80):

$$\widetilde{E}_{ee,x}^{r,\text{TE,TE}} D_\theta = \int_{z'} \left\{ R V_{2,ee}^{\theta-} e^{-j\lambda_{z\theta}(z+z')} + R\overline{R} V_{2,ee}^{\theta+} e^{-j\lambda_{z\theta}(2d+z-z')} \right.$$
$$\left. + \overline{R} V_{2,ee}^{\theta+} e^{-j\lambda_{z\theta}(2d-z-z')} + R\overline{R} V_{2,ee}^{\theta-} e^{-j\lambda_{z\theta}(2d-z+z')} \right\} \cdot \vec{\widetilde{J}}_e dz'$$

Substituting in the expression for $V_{2,ee}^{\theta+}$ from (3.83), using $R = \overline{R} = -1$ and recognizing $V_{2,ee}^{\theta-} = V_{2,ee}^{\theta+}$, we can write:

$$\widetilde{E}_{ee,x}^{r,\text{TE,TE}} D_\theta = \int_{z'} \left\{ V_{2,ee}^{\theta+} \left[-e^{-j\lambda_{z\theta}(z+z')} + e^{-j\lambda_{z\theta}(2d+z-z')} - e^{-j\lambda_{z\theta}(2d-z-z')} + e^{-j\lambda_{z\theta}(2d-z+z')} \right] \right\} \cdot \vec{\widetilde{J}}_e dz'$$

$$= \int_{z'} \left\{ \frac{\omega\mu_t}{2\lambda_{z\theta}\lambda_\rho^2} \left[-\lambda_y^2 \hat{\mathbf{x}} + \lambda_x \lambda_y \hat{\mathbf{y}} \right] \right.$$
$$\left. \left[-e^{-j\lambda_{z\theta}(z+z')} + e^{-j\lambda_{z\theta}(2d+z-z')} - e^{-j\lambda_{z\theta}(2d-z-z')} + e^{-j\lambda_{z\theta}(2d-z+z')} \right] \right\} \cdot \vec{\widetilde{J}}_e dz'$$

Therefore, we can write the *xx*-component as $\widetilde{E}^{r\theta,\theta}_{ee,xx} = \widetilde{E}^{r\theta,\theta}_{ee,x} \cdot \hat{\mathbf{x}}$, leading to

$$\widetilde{E}^{r,\text{TE,TE}}_{ee,x} D_\theta = \int_{z'} \left\{ -\left(\frac{\omega\mu_t\lambda_y^2}{2\lambda_{z\theta}\lambda_\rho^2}\right) \right.$$
$$\left. \left[-e^{-j\lambda_{z\theta}(z+z')} + e^{-j\lambda_{z\theta}(2d+z-z')} - e^{-j\lambda_{z\theta}(2d-z-z')} + e^{-j\lambda_{z\theta}(2d-z+z')} \right] \right\} \cdot \vec{\tilde{J}}_e dz'$$

(3.85)

and the *xy*-component as $\widetilde{E}^{r\theta,\theta}_{ee,xy} = \widetilde{E}^{r\theta,\theta}_{ee,x} \cdot \hat{\mathbf{y}}$

$$\widetilde{E}^{r,\text{TE,TE}}_{ee,xy} D_\theta = \int_{z'} \left\{ \left(\frac{\omega\mu_t\lambda_x\lambda_y}{2\lambda_{z\theta}\lambda_\rho^2}\right) \right.$$
$$\left. \left[-e^{-j\lambda_{z\theta}(z+z')} + e^{-j\lambda_{z\theta}(2d+z-z')} - e^{-j\lambda_{z\theta}(2d-z-z')} + e^{-j\lambda_{z\theta}(2d-z+z')} \right] \right\} \cdot \vec{\tilde{J}}_e dz'$$

(3.86)

We will now determine the total Green's function for each component individually (which are also separated by coupling type) by combining the principal and reflected Green's function.

- TE^z -TE^z Coupling, *xx* Component

  Recall, the *xx* term of principal Green's function (from 3.1.4.7) is

  $$\widetilde{G}^{p,\text{TE}}_{ee,xx} = -\frac{\omega\mu_t\lambda_y^2}{2\lambda_{z\theta}\lambda_\rho^2} e^{-j\lambda_{z\theta}|z-z'|}$$

  Combining this with the reflected portion given in (3.85) and recalling the definition of D_θ from (3.71), the total *xx*-component of the TE^z electric field excited by a TE^z

124

source is given by

$$\widetilde{E}_{ee,x}^{r,\text{TE,TE}}D_\theta = \int_{z'}\left\{-D_\theta\frac{\omega\mu_t\lambda_y^2}{2\lambda_{z\theta}\lambda_\rho^2}e^{-j\lambda_{z\theta}|z-z'|} - \left(\frac{\omega\mu_t\lambda_y^2}{2\lambda_{z\theta}\lambda_\rho^2}\right)\right.$$

$$\left.\times\left[-e^{-j\lambda_{z\theta}(z+z')} + e^{-j\lambda_{z\theta}(2d+z-z')} - e^{-j\lambda_{z\theta}(2d-z-z')} + e^{-j\lambda_{z\theta}(2d-z+z')}\right]\right\}\cdot\vec{\widetilde{J}}_e dz'$$

which, after a considerable amount of algebraic effort and application of Euler's identities (as was previously used in the potential method), becomes

$$\boxed{\widetilde{E}_{ee,xx}^{\text{TE,TE}} = \int_{z'} -\frac{\omega\mu_t\lambda_y^2}{2\lambda_{z\theta}\lambda_\rho^2}\left\{\frac{\cos\left[\lambda_{z\theta}\left(d-|z-z'|\right)\right] - \cos\left[\lambda_{z\theta}\left(d-(z+z')\right)\right]}{j\sin\left(\lambda_{z\theta}d\right)}\right\}\cdot\vec{\widetilde{J}}_e dz'} \quad (3.87)$$

- TE^z -TE^z Coupling, xy Component

  Recall, the xy term of principal Green's function (from 3.1.4.7) is:

  $$\widetilde{G}_{ee,xy}^{p,\text{TE}} = \frac{\omega\mu_t\lambda_x\lambda_y}{2\lambda_{z\theta}\lambda_\rho^2}e^{-j\lambda_{z\theta}|z-z'|}$$

  Combining this with the reflected portion from (3.86), the total xy-component of the electric field, simplifying and converting to sinusoidal form leads to:

  $$\boxed{\widetilde{E}_{ee,xy}^{\text{TE,TE}} = \int_{z'}\frac{\omega\mu_t\lambda_x\lambda_y}{2\lambda_{z\theta}\lambda_\rho^2}\left\{\frac{\cos\left[\lambda_{z\theta}\left(d-|z-z'|\right)\right] - \cos\left[\lambda_{z\theta}\left(d-(z+z')\right)\right]}{j\sin\left(\lambda_{z\theta}d\right)}\right\}\cdot\vec{\widetilde{J}}_e dz'} \quad (3.88)$$

- TE^z -TE^z Coupling, y-Components

  All that remains to complete the analysis of the TE^z field maintained by a TE^z electric source is to find $\widetilde{E}_{ee,y}^{r\theta}$ and $\widetilde{E}_{ee,z}^{r\theta}$. Recall, from (3.39):

  $$\widetilde{E}_y^{r,\text{TE}} = -\frac{\lambda_x}{\lambda_y}\widetilde{E}_{ox}^{r\theta+}e^{-j\lambda_{z\theta}z} - \frac{\lambda_x}{\lambda_y}\widetilde{E}_{ox}^{r\theta-}e^{j\lambda_{z\theta}z} = -\frac{\lambda_x}{\lambda_y}\left[\widetilde{E}_{ox}^{r\theta+}e^{-j\lambda_{z\theta}z} + \widetilde{E}_{ox}^{r\theta-}e^{j\lambda_{z\theta}z}\right] = -\frac{\lambda_x}{\lambda_y}\widetilde{E}_x^{r\theta}$$

  Also, noting the fact that $\widetilde{G}_{ee,yx}^{p,\text{TE}} = -\frac{\lambda_x}{\lambda_y}\widetilde{G}_{ee,xx}^{p,\text{TE}}$ and $\widetilde{G}_{ee,yy}^{p,\text{TE}} = -\frac{\lambda_x}{\lambda_y}\widetilde{G}_{ee,xy}^{p,\text{TE}}$, we can readily see:

125

$$
\begin{aligned}
\widetilde{E}_{ee,yx}^{\text{TE}} &= -\frac{\lambda_x}{\lambda_y}\widetilde{E}_{xx}^{\theta} \\
&= \int\limits_{z'} \frac{\omega\mu_t\lambda_x\lambda_y}{2\lambda_{z\theta}\lambda_\rho^2}\left\{\frac{\cos\left[\lambda_{z\theta}\left(d-|z-z'|\right)\right]-\cos\left[\lambda_{z\theta}\left(d-(z+z')\right)\right]}{j\sin\left(\lambda_{z\theta}d\right)}\right\}\cdot\vec{\widetilde{J}}_e dz'
\end{aligned}
\tag{3.89}
$$

$$
\begin{aligned}
\widetilde{E}_{ee,yy}^{\text{TE}} &= -\frac{\lambda_x}{\lambda_y}\widetilde{E}_{ee,xy}^{\theta} \\
&= \int\limits_{z'} -\frac{\omega\mu_t\lambda_x^2}{2\lambda_{z\theta}\lambda_\rho^2}\left\{\frac{\cos\left[\lambda_{z\theta}\left(d-|z-z'|\right)\right]-\cos\left[\lambda_{z\theta}\left(d-(z+z')\right)\right]}{j\sin\left(\lambda_{z\theta}d\right)}\right\}\cdot\vec{\widetilde{J}}_e dz'
\end{aligned}
\tag{3.90}
$$

$$
\boxed{\widetilde{E}_{ee,yz}^{\text{TE}} = 0}
\tag{3.91}
$$

- TE^z -TE^z Coupling, z-Components

  Finally, recall from (3.39), $\widetilde{E}_{ee,z}^{r,\text{TE}} = \widetilde{E}_{ee,z}^{p,\text{TE}} = 0$, which means:

$$
\boxed{\widetilde{E}_{ee,zx}^{\text{TE}} = \widetilde{E}_{ee,zy}^{\text{TE}} = \widetilde{E}_{ee,zz}^{\text{TE}} = 0.}
\tag{3.92}
$$

TE^z Wave Excited by a TM^z Source. The TE^z contribution excited by a TM^z source is give by:

$$
\begin{aligned}
\widetilde{E}_{ee,x}^{r,\text{TE},\text{TM}}D_\theta = \int\limits_{z'} \Bigg\{ &R\mathsf{V}_{2,ee}^{\psi-}e^{-j\lambda_{z\theta}z}e^{-j\lambda_{z\psi}z'} + R\overline{R}\mathsf{V}_{2,ee}^{\psi+}e^{-j\lambda_{z\theta}(d+z)}e^{-j\lambda_{z\psi}(d-z')} \\
&+ \overline{R}\mathsf{V}_{2,ee}^{\psi+}e^{-j\lambda_{z\theta}(d-z)}e^{-j\lambda_{z\psi}(d-z')} + R\overline{R}\mathsf{V}_{2,ee}^{\psi-}e^{-j\lambda_{z\theta}(2d-z)}e^{-j\lambda_{z\psi}z'} \Bigg\}\cdot\vec{\widetilde{J}}_e dz'
\end{aligned}
$$

126

Since $V_{2,ee}^{\psi+} = V_{2,ee}^{\psi-} = 0$, we see that $\widetilde{E}_{ee,xx}^{r\theta,\psi} = \widetilde{E}_{ee,xy}^{r\theta,\psi} = \widetilde{E}_{ee,xz}^{r\theta,\psi} = 0$. This is as expected, since no TE^z field is expected to be excited in the parallel plate waveguide due to a TM^z source. Therefore, we immediately recognize $\widetilde{E}_{ee,x}^{\text{TE}} = \widetilde{E}_{ee,x}^{\text{TE,TE}}$.

3.4.3 Electric (ee) Total Green's Function, TE^z Field Summary.

$$\vec{\tilde{E}}_{ee}^{\text{TE}} = \int\limits_{z'} \overleftrightarrow{\tilde{G}}_{ee}^{\text{TE}} \cdot \vec{\tilde{J}}_e dz' \quad , \quad \overleftrightarrow{\tilde{G}}_{ee}^{\text{TE}} = \overleftrightarrow{\tilde{G}}_{ee}^{\text{TE,TE}} + \overleftrightarrow{\tilde{G}}_{ee}^{\text{TE,TM}}$$

$$\overleftrightarrow{\tilde{G}}_{ee}^{\text{TE,TE}} = \begin{bmatrix} \tilde{G}_{ee,xx}^{\text{TE}} & \tilde{G}_{ee,xy}^{\text{TE}} & \tilde{G}_{ee,xz}^{\text{TE}} \\[2mm] \tilde{G}_{ee,yx}^{\text{TE}} & \tilde{G}_{ee,yy}^{\text{TE}} & \tilde{G}_{ee,yz}^{\text{TE}} \\[2mm] \tilde{G}_{ee,zx}^{\text{TE}} & \tilde{G}_{ee,zy}^{\text{TE}} & \tilde{G}_{ee,zz}^{\text{TE}} \end{bmatrix} \quad , \quad \overleftrightarrow{\tilde{G}}_{ee}^{\text{TE,TM}} = 0$$

$$\tilde{G}_{ee,xx}^{\text{TE}} = \frac{j\omega\mu_t\lambda_y^2}{2\lambda_{z\theta}\lambda_\rho^2} \left\{ \frac{\cos\left[\lambda_{z\theta}\left(d - |z-z'|\right)\right] - \cos\left[\lambda_{z\theta}\left(d - (z+z')\right)\right]}{\sin\left(\lambda_{z\theta}d\right)} \right\}$$

$$\tilde{G}_{ee,xy}^{\text{TE}} = -\frac{j\omega\mu_t\lambda_x\lambda_y}{2\lambda_{z\theta}\lambda_\rho^2} \left\{ \frac{\cos\left[\lambda_{z\theta}\left(d - |z-z'|\right)\right] - \cos\left[\lambda_{z\theta}\left(d - (z+z')\right)\right]}{\sin\left(\lambda_{z\theta}d\right)} \right\}$$

$$\tilde{G}_{ee,xz}^{\text{TE}} = 0$$

$$\tilde{G}_{ee,yx}^{\text{TE}} = -\frac{j\omega\mu_t\lambda_x\lambda_y}{2\lambda_{z\theta}\lambda_\rho^2} \left\{ \frac{\cos\left[\lambda_{z\theta}\left(d - |z-z'|\right)\right] - \cos\left[\lambda_{z\theta}\left(d - (z+z')\right)\right]}{\sin\left(\lambda_{z\theta}d\right)} \right\}$$

$$\tilde{G}_{ee,yy}^{\text{TE}} = \frac{j\omega\mu_t\lambda_x^2}{2\lambda_{z\theta}\lambda_\rho^2} \left\{ \frac{\cos\left[\lambda_{z\theta}\left(d - |z-z'|\right)\right] - \cos\left[\lambda_{z\theta}\left(d - (z+z')\right)\right]}{\sin\left(\lambda_{z\theta}d\right)} \right\}$$

$$\tilde{G}_{ee,yz}^{\text{TE}} = 0$$

$$\tilde{G}_{ee,zx}^{\text{TE}} = \tilde{G}_{ee,zy}^{\text{TE}} = \tilde{G}_{ee,zz}^{\text{TE}} = 0$$

3.4.4 Electric (ee) Reflected Green's Function, TM^z Field.

From (3.74) and recalling the definition of D_ψ from (3.73), we have the x-component of the TM^z portion of the ee reflected field as

$$
\begin{aligned}
\tilde{E}_{ee,x}^{r,\text{TM}} D_\psi = {} & R\tilde{V}_{1,ee}^{\theta-}e^{-j\lambda_{z\psi}z} + R\tilde{V}_{1,ee}^{\psi-}e^{-j\lambda_{z\psi}z} \\
& + R\overline{R}\tilde{V}_{1,ee}^{\theta+}e^{-j\lambda_{z\theta}d}e^{-j\lambda_{z\psi}(d+z)} + R\overline{R}\tilde{V}_{1,ee}^{\psi+}e^{-j\lambda_{z\psi}(2d+z)} \\
& + \overline{R}\tilde{V}_{1,ee}^{\theta+}e^{-j\lambda_{z\theta}d}e^{-j\lambda_{z\psi}(d-z)} + \overline{R}\tilde{V}_{1,ee}^{\psi+}e^{-j\lambda_{z\psi}(2d-z)} \\
& + R\overline{R}\tilde{V}_{1,ee}^{\theta-}e^{-j\lambda_{z\psi}(2d-z)} + R\overline{R}\tilde{V}_{1,ee}^{\psi-}e^{-j\lambda_{z\psi}(2d-z)}
\end{aligned}
\tag{3.93}
$$

Using the methods of the previous section, we determine the total TM^z portion of the Green's function.

$$\vec{\tilde{E}}_{ee}^{\text{TM}} = \int_{z'} \tilde{G}_{ee}^{\text{TM}} \cdot \vec{\tilde{J}}_e dz' \qquad , \qquad \tilde{G}_{ee}^{\text{TM}} = \overset{\leftrightarrow}{\tilde{G}}_{ee}^{\text{TM,TE}} + \overset{\leftrightarrow}{\tilde{G}}_{ee}^{\text{TM,TM}}$$

$$\overset{\leftrightarrow}{\tilde{G}}_{ee}^{\text{TM,TE}} = 0 \qquad , \qquad \overset{\leftrightarrow}{\tilde{G}}_{ee}^{\text{TM,TM}} = \begin{bmatrix} \tilde{G}_{ee,xx}^{\text{TM}} & \tilde{G}_{ee,xy}^{\text{TM}} & \tilde{G}_{ee,xz}^{\text{TM}} \\ \tilde{G}_{ee,yx}^{\text{TM}} & \tilde{G}_{ee,yy}^{\text{TM}} & \tilde{G}_{ee,yz}^{\text{TM}} \\ \tilde{G}_{ee,zx}^{\text{TM}} & \tilde{G}_{ee,zy}^{\text{TM}} & \tilde{G}_{ee,zz}^{\text{TM}} \end{bmatrix}$$

$$\tilde{G}_{ee,xx}^{\text{TM}} = \frac{j\lambda_x^2 \lambda_{z\psi}}{2\omega\varepsilon_t \lambda_\rho^2} \left\{ \frac{\cos\left[\lambda_{z\psi}\left(d - |z-z'|\right)\right] - \cos\left[\lambda_{z\psi}\left(d - (z+z')\right)\right]}{\sin\left(\lambda_{z\psi}d\right)} \right\}$$

$$\tilde{G}_{ee,xy}^{\text{TM}} = \frac{j\lambda_x \lambda_y \lambda_{z\psi}}{2\omega\varepsilon_t \lambda_\rho^2} \left\{ \frac{\cos\left[\lambda_{z\psi}\left(d - |z-z'|\right)\right] - \cos\left[\lambda_{z\psi}\left(d - (z+z')\right)\right]}{\sin\left(\lambda_{z\psi}d\right)} \right\}$$

$$\tilde{G}_{ee,xz}^{\text{TM}} = -\frac{\lambda_x}{2\omega\varepsilon_z} \left\{ \frac{\text{sgn}\left(z-z'\right)\sin\left[\lambda_{z\psi}\left(d - |z-z'|\right)\right] + \sin\left[\lambda_{z\psi}\left(d - (z+z')\right)\right]}{\sin\left(\lambda_{z\psi}d\right)} \right\}$$

$$\tilde{G}_{ee,yx}^{\text{TM}} = \frac{j\lambda_x \lambda_y \lambda_{z\psi}}{2\omega\varepsilon_t \lambda_\rho^2} \left\{ \frac{\cos\left[\lambda_{z\psi}\left(d - |z-z'|\right)\right] - \cos\left[\lambda_{z\psi}\left(d - (z+z')\right)\right]}{\sin\left(\lambda_{z\psi}d\right)} \right\}$$

$$\tilde{G}_{ee,yy}^{\text{TM}} = \frac{j\lambda_y^2 \lambda_{z\psi}}{2\omega\varepsilon_t \lambda_\rho^2} \left\{ \frac{\cos\left[\lambda_{z\psi}\left(d - |z-z'|\right)\right] - \cos\left[\lambda_{z\psi}\left(d - (z+z')\right)\right]}{\sin\left(\lambda_{z\psi}d\right)} \right\}$$

$$\tilde{G}_{ee,yz}^{\text{TM}} = -\frac{\lambda_y}{2\omega\varepsilon_z} \left\{ \frac{\text{sgn}\left(z-z'\right)\sin\left[\lambda_{z\psi}\left(d - |z-z'|\right)\right] + \sin\left[\lambda_{z\psi}\left(d - (z+z')\right)\right]}{\sin\left(\lambda_{z\psi}d\right)} \right\}$$

$$\tilde{G}_{ee,zx}^{\text{TM}} = -\frac{\lambda_x}{2\omega\varepsilon_z} \left\{ \frac{\text{sgn}\left(z-z'\right)\sin\left[\lambda_{z\psi}\left(d - |z-z'|\right)\right] - \sin\left[\lambda_{z\psi}\left(d - (z+z')\right)\right]}{\sin\left(\lambda_{z\psi}d\right)} \right\}$$

$$\tilde{G}_{ee,zy}^{\text{TM}} = -\frac{\lambda_y}{2\omega\varepsilon_z} \left\{ \frac{\text{sgn}\left(z-z'\right)\sin\left[\lambda_{z\psi}\left(d - |z-z'|\right)\right] - \sin\left[\lambda_{z\psi}\left(d - (z+z')\right)\right]}{\sin\left(\lambda_{z\psi}d\right)} \right\}$$

$$\tilde{G}_{ee,zz}^{\text{TM}} = \frac{j\frac{\varepsilon_t}{\varepsilon_z}\lambda_\rho^2}{2\omega\varepsilon_z \lambda_{z\psi}} \left\{ \frac{\cos\left[\lambda_{z\psi}\left(d - |z-z'|\right)\right] + \cos\left[\lambda_{z\psi}\left(d - (z+z')\right)\right]}{\sin\left(\lambda_{z\psi}d\right)} \right\}$$

3.4.5 Electric (ee) Total Green's Function Summary.

The *ee*-type Green's functions may be written in the concise form (where the representation $\Upsilon_1^{\theta|\psi}$ represents either Υ_1^θ (which contains $\lambda_{z\theta}$ terms) or Υ_1^ψ (which contains $\lambda_{z\psi}$ terms)

$$\overset{\leftrightarrow}{\tilde{\tilde{G}}}_{ee} = \overset{\leftrightarrow}{\tilde{\tilde{G}}}_{ee}^{\text{TE}} + \overset{\leftrightarrow}{\tilde{\tilde{G}}}_{ee}^{\text{TM}} + \overset{\leftrightarrow}{\tilde{\tilde{G}}}_{ee}^{\text{d}}$$

where

$$\overset{\leftrightarrow}{\tilde{\tilde{G}}}_{ee}^{\text{TE}} = \left(\frac{j\omega\mu_t}{2\lambda_{z\theta}\lambda_\rho^2} \right) \begin{bmatrix} \lambda_y^2 & -\lambda_x\lambda_y & 0 \\ -\lambda_x\lambda_y & \lambda_x^2 & 0 \\ 0 & 0 & 0 \end{bmatrix} \Upsilon_1^\theta$$

$$\overset{\leftrightarrow}{\tilde{\tilde{G}}}_{ee}^{\text{TM}} = \left(\frac{j}{2\omega\varepsilon_t\lambda_\rho^2} \right) \begin{bmatrix} \lambda_x^2\lambda_{z\psi}\Upsilon_1^\psi & \lambda_x\lambda_y\lambda_{z\psi}\Upsilon_1^\psi & j\frac{\varepsilon_t}{\varepsilon_z}\lambda_x\lambda_\rho^2\Upsilon_4^\psi \\ \\ \lambda_x\lambda_y\lambda_{z\psi}\Upsilon_1^\psi & \lambda_y^2\lambda_{z\psi}\Upsilon_1^\psi & j\frac{\varepsilon_t}{\varepsilon_z}\lambda_y\lambda_\rho^2\Upsilon_4^\psi \\ \\ j\frac{\varepsilon_t}{\varepsilon_z}\lambda_x\Upsilon_3^\psi & j\frac{\varepsilon_t}{\varepsilon_z}\lambda_y\lambda_\rho^2\Upsilon_3^\psi & \left(\frac{j}{\lambda_{z\psi}} \right) \left(\frac{\varepsilon_t\lambda_\rho^2}{\varepsilon_z} \right)^2 \Upsilon_2^\psi \end{bmatrix}$$

$$\overset{\leftrightarrow}{\tilde{\tilde{G}}}_{ee}^{\text{d}} = -\frac{1}{j\omega\varepsilon_z}\delta(z-z')$$

$$\Upsilon_1^{\theta|\psi} = \frac{\cos\left(\lambda_{z\theta|z\psi}\left[d-|z-z'|\right]\right) -\cos\left(\lambda_{z\theta|z\psi}\left[d-(z+z')\right]\right)}{\sin\left(\lambda_{z\theta|z\psi}d\right)}$$

$$\Upsilon_2^{\theta|\psi} = \frac{\cos\left(\lambda_{z\theta|z\psi}\left[d-|z-z'|\right]\right) +\cos\left(\lambda_{z\theta|z\psi}\left[d-(z+z')\right]\right)}{\sin\left(\lambda_{z\theta|z\psi}d\right)}$$

$$\Upsilon_3^{\theta|\psi} = \frac{\text{sgn}\left(z-z'\right)\sin\left(\lambda_{z\theta|z\psi}\left[d-|z-z'|\right]\right) -\sin\left(\lambda_{z\theta|z\psi}\left[d-(z+z')\right]\right)}{\sin\left(\lambda_{z\theta|z\psi}d\right)}$$

$$\Upsilon_4^{\theta|\psi} = \frac{\text{sgn}\left(z-z'\right)\sin\left(\lambda_{z\theta|z\psi}\left[d-|z-z'|\right]\right) +\sin\left(\lambda_{z\theta|z\psi}\left[d-(z+z')\right]\right)}{\sin\left(\lambda_{z\theta|z\psi}d\right)}$$

3.4.6 *Magnetoelectric (eh) Reflected Green's Function, TE^z Field.*

From (3.72), we have the *x*-component of the TE^z portion of the reflected electric field maintained by a magnetic source as:

$$
\begin{aligned}
\widetilde{E}_{eh,x}^{r,\text{TE}} D_\theta = {} & R\widetilde{V}_{2,eh}^{\theta-}e^{-j\lambda_{z\theta}z} + R\widetilde{V}_{2,eh}^{\psi-}e^{-j\lambda_{z\theta}z} \\
& + R\overline{R}\widetilde{V}_{2,eh}^{\theta+}e^{-j\lambda_{z\theta}(2d+z)} + R\overline{R}\widetilde{V}_{2,eh}^{\psi+}e^{-j\lambda_{z\theta}(d+z)}e^{-j\lambda_{z\psi}d} \\
& + \overline{R}\widetilde{V}_{2,eh}^{\theta+}e^{-j\lambda_{z\theta}(2d-z)} + \overline{R}\widetilde{V}_{2,eh}^{\psi+}e^{-j\lambda_{z\theta}(d-z)}e^{-j\lambda_{z\psi}d} \\
& + R\overline{R}\widetilde{V}_{2,eh}^{\theta-}e^{-j\lambda_{z\theta}(2d-z)} + R\overline{R}\widetilde{V}_{2,eh}^{\psi-}e^{-j\lambda_{z\theta}(2d-z)}
\end{aligned}
\tag{3.94}
$$

Following the same procedure as with the *ee*-type Green's function, we find the total Green's function, which is summarized in the next section.

3.4.7 Magnetoelectric (eh) Green's Function Grand Summary.

$$\tilde{\tilde{\overleftrightarrow{G}}}_{eh} = \tilde{\tilde{\overleftrightarrow{G}}}_{eh}^{\text{TE}} + \tilde{\overleftrightarrow{G}}_{eh}^{\text{TM}}$$

where

$$\tilde{\tilde{\overleftrightarrow{G}}}_{eh}^{\text{TE}} = \left(\frac{1}{2\lambda_\rho^2}\right) \begin{bmatrix} -\lambda_x\lambda_y\Upsilon_4^\theta & -\lambda_y^2\Upsilon_4^\theta & \dfrac{j\mu_t\lambda_y\lambda_\rho^2}{\mu_z\lambda_{z\theta}}\Upsilon_1^\theta \\[2em] \lambda_x^2\Upsilon_4^\theta & \lambda_x\lambda_y\Upsilon_4^\theta & -\dfrac{j\mu_t\lambda_x\lambda_\rho^2}{\mu_z\lambda_{z\theta}}\Upsilon_1^\theta \\[2em] 0 & 0 & 0 \end{bmatrix}$$

$$\tilde{\overleftrightarrow{G}}_{eh}^{\text{TM}} = \left(\frac{1}{2\lambda_\rho^2}\right) \begin{bmatrix} \lambda_x\lambda_y\Upsilon_4^\psi & -\lambda_x^2\Upsilon_4^\psi & 0 \\[2em] \lambda_y^2\Upsilon_4^\psi & -\lambda_x\lambda_y\Upsilon_4^\psi & 0 \\[2em] -\dfrac{j\varepsilon_t\lambda_y\lambda_\rho^2}{\varepsilon_z\lambda_{z\psi}}\Upsilon_2^\psi & \dfrac{j\varepsilon_t\lambda_x\lambda_\rho^2}{\varepsilon_z\lambda_{z\psi}}\Upsilon_2^\psi & 0 \end{bmatrix}$$

$$\Upsilon_1^{\theta|\psi} = \frac{\cos\left(\lambda_{z_\theta|z_\psi}\left[d-|z-z'|\right]\right) - \cos\left(\lambda_{z_\theta|z_\psi}\left[d-(z+z')\right]\right)}{\sin\left(\lambda_{z_\theta|z_\psi}d\right)}$$

$$\Upsilon_2^{\theta|\psi} = \frac{\cos\left(\lambda_{z_\theta|z_\psi}\left[d-|z-z'|\right]\right) + \cos\left(\lambda_{z_\theta|z_\psi}\left[d-(z+z')\right]\right)}{\sin\left(\lambda_{z_\theta|z_\psi}d\right)}$$

$$\Upsilon_3^{\theta|\psi} = \frac{\text{sgn}\,(z-z')\sin\left(\lambda_{z_\theta|z_\psi}\left[d-|z-z'|\right]\right) - \sin\left(\lambda_{z_\theta|z_\psi}\left[d-(z+z')\right]\right)}{\sin\left(\lambda_{z_\theta|z_\psi}d\right)}$$

$$\Upsilon_4^{\theta|\psi} = \frac{\text{sgn}\,(z-z')\sin\left(\lambda_{z_\theta|z_\psi}\left[d-|z-z'|\right]\right) + \sin\left(\lambda_{z_\theta|z_\psi}\left[d-(z+z')\right]\right)}{\sin\left(\lambda_{z_\theta|z_\psi}d\right)}$$

3.4.8 Comparison of Potential Method and Direct Field Method.

In comparing the electric (ee) and magnetoelectric (eh) Green's functions obtained by the potential method in (B.9) and (B.10) and those found by the direct field method in

3.4.5 and 3.4.7, we find they agree exactly. However, we also see a substantial reduction in the amount of work required to find all the Green's functions (*ee*, *eh*, *he* and *hh*-type) through the potential-based method. In fact, we have only truly obtained the *ee*- and *eh*-type Green's functions through the direct field solution and we would have to repeat most of the work in this chapter in order to obtain the *he* and *hh* Green's function. Although it is true that we could use duality to find the *he* and *hh*-type Green's functions, there are a few points that could lead to errors, not the least of which is the change of sign in the scattered portion of the Green's function due to the change in reflection coefficient magnitude since the PEC boundary condition can't be changed to a PMC. Perhaps the most tedious part of the direct field method has been the necessity of a term-by-term calculation, whereas the potential based method allows for groups of terms to be calculated simultaneously. Therefore, since we have confidence in the agreement between the two methods in the *ee* and *eh*-type Green's functions, we will use the results from the potential-based method in the chapters to come.

IV.   Theory of the Extraction of Uniaxial Constitutive Parameters by the tFWMT

Having determined the total PPWG Green's function for uniaxial media, we now seek to apply it to a practical scenario for the extraction of the constitutive parameters. Although there are many potential geometries, we will utilize the two-flanged waveguide technique (tFWMT) of [51, 53–55]. The geometry is shown in Figure 4.1. In this configuration, the media sample is placed between two flanged waveguides, which have centered cutouts for the appropriate sized waveguide. The size and type of waveguides are chosen to best correspond to the bandwidth of interest. The flanges are sized appropriately [54], so that, when combined with time-gating, the edge reflections can be eliminated from the measurements. This development will follow the general methods of [51–54, 56, 83, 87], incorporating the required theory for a uniaxial material, rather than for isotropic materials. The amplitude of the incoming wave is given by a_1^+, which is known to be propagating in the fundamental TE_{10}^z mode. Upon encountering the discontinuity at the aperture of the waveguide, an infinite number (q) of modes will be reflected with amplitude a_q^-, while an infinite number of modes will be transmitted through the material with amplitude b_q^+. Therefore, the reflection and transmission coefficients are, in general, given by

$$ \mathrm{R}_q = \frac{a_q^-}{a_1^+} \quad \implies \quad \mathrm{R}_1 = \frac{a_1^-}{a_1^+} = \mathrm{S}_{11}^{\mathrm{thy}} \tag{4.1} $$

$$ \mathrm{T}_q = \frac{b_q^+}{a_1^+} \quad \implies \quad \mathrm{T}_1 = \frac{b_1^+}{a_1^+} = \mathrm{S}_{21}^{\mathrm{thy}} \tag{4.2} $$

Our task is to determine how to extract the values for $\overset{\leftrightarrow}{\varepsilon}$ and $\overset{\leftrightarrow}{\mu}$ from the measured transmission and reflection coefficient. We will use a combination of Love's equivalence principle, continuity of tangential fields, and the Method of Moments to arrive at a set of coupled MFIE's. Then, we will discuss, in detail, the method used for extracting the constitutive parameter dyads.
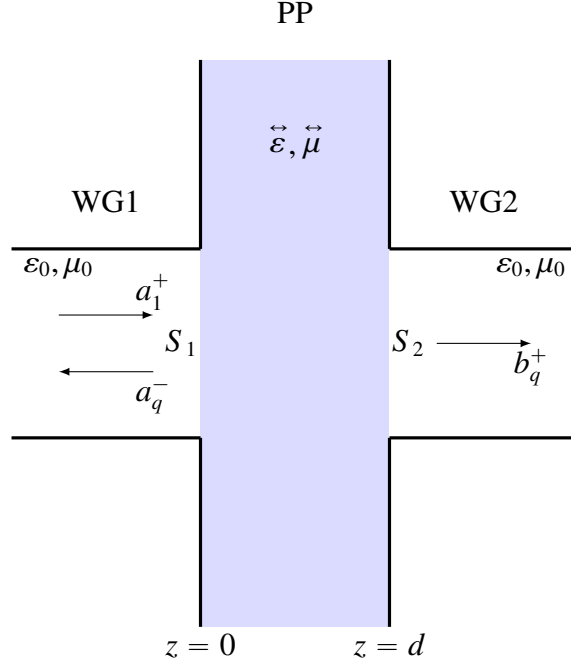
Figure 4.1: Geometry for a clamped waveguide measurement system. The two waveguide probes are fed into a clamped waveguide containing the material under test. The amplitudes of the incoming wave, the reflected modes and the transmitted modes are specified by a_1^+, a_q^- and b_q^+, respectively.

4.1 Waveguide 1 (WG1)

The tangential fields inside WG1 can be written as the sum of the dominant mode (TE$_{10}$) incident wave and the infinite number of reflected modes (which is truncated to Q modes):

$$\vec{E}_{t1} = a_1^+ \vec{e}_1 e^{-jk_z z} + \sum_{q=1}^{Q} a_q^- \vec{e}_q e^{jk_z z} \tag{4.3}$$

where the index q is used as a compact notation for the standard mode indices, incorporating all possible reflected modes (TE$_{vw}^z$ and TM$_{vw}^z$). The modes are arranged in order of increasing cutoff frequency (see Appendix D). At the junction of WG1 and the parallel plates (PP), which is $z = 0$, we can write the electric field in the aperture ($\vec{e}_{a1}$)

135

as

$$\vec{E}_{t1}(z=0) = \vec{e}_{a1} = a_1^+ \vec{e}_1 + \sum_{q=1}^{Q} a_q^- \vec{e}_q \tag{4.4}$$

Since we are using the method of moments and the unknowns are already expanded, we can test using the pth mode of the electric field:

$$\int_{S_1} \vec{e}_p \cdot \vec{e}_{a1} dS = a_1^+ \overbrace{\int_{S_1} \vec{e}_p \cdot \vec{e}_1}^{\delta_{p1}} + \sum_{q=1}^{Q} a_q^- \overbrace{\int_{S_1} \vec{e}_p \cdot \vec{e}_q dS}^{\delta_{pq}} = a_1^+ \delta_{p1} + \sum_{q=1}^{Q} a_q^- \delta_{pq}$$

$$\implies \sum_{q=1}^{Q} a_q^- \delta_{pq} = \int_{S_1} \vec{e}_p \cdot \vec{e}_{a1} dS - a_1^+ \delta_{p1}$$

$$\implies a_p^- = \int_{S_1} \vec{e}_p \cdot \vec{e}_{a1} dS - a_1^+ \delta_{p1}$$

However, p is just a dummy index value, so we let $p = q$ and easily write

$$a_q^- = \int_{S_1} \vec{e}_q \cdot \vec{e}_{a1} dS - a_1^+ \delta_{q1} \tag{4.5}$$

Now, we need to determine the magnetic field in the WG1 region. From Figure 4.1, we can write

$$\vec{H}_{t1} = a_1^+ \vec{h}_1 - \sum_{q=1}^{Q} a_q^- \vec{h}_q e^{jk_z z}$$

At the boundary ($z = 0$), we have

$$\vec{H}_{t1}(z=0) = a_1^+ \vec{h}_1 - \sum_{q=1}^{Q} a_q^- \vec{h}_q \tag{4.6}$$

136

Substituting the expression for a_q^- found in (4.5) into (4.6):

$$\vec{H}_{t1}(z=0) = a_1^+ \vec{h}_1 - \sum_{q=1}^{Q} \left[\int_{S_1} \vec{e}_q \cdot \vec{e}_{a1} dS - a_1^+ \delta_{q1} \right] \vec{h}_q$$

$$= a_1^+ \vec{h}_1 - \sum_{q=1}^{Q} \int_{S_1} \vec{e}_q \cdot \vec{e}_{a1} dS \, \vec{h}_q + \sum_{q=1}^{Q} a_1^+ \delta_{q1} \vec{h}_q$$

$$= a_1^+ \vec{h}_1 - \sum_{q=1}^{Q} \int_{S_1} \vec{e}_q \cdot \vec{e}_{a1} dS \, \vec{h}_q + a_1^+ \vec{h}_1$$

$$\implies \vec{H}_{t1}(z=0) = 2a_1^+ \vec{h}_1 - \sum_{q=1}^{Q} \int_{S_1} \vec{e}_q \cdot \vec{e}_{a1} dS \, \vec{h}_q \tag{4.7}$$

4.2   Waveguide 2 (WG2)

Again, referring to Figure 4.1, we can write the electric field in the WG2 region as

$$\vec{E}_{t2} = \sum_{q=1}^{Q} b_q^+ \vec{e}_q e^{-jk_z(z-d)}$$

At the boundary ($z = d$), we have

$$\vec{E}_{t2}(z=d) = \vec{e}_{a2} = \sum_{q=1}^{Q} b_q^+ \vec{e}_q$$

Using the method of moments (MoM), we test with the pth mode:

$$\int_{S_2} \vec{e}_p \cdot \vec{e}_{a2} dS = \sum_{q=1}^{Q} b_q^+ \int_{S_2} \vec{e}_p \cdot \vec{e}_q dS = \sum_{q=1}^{Q} b_q^+ \delta_{pq} = b_p^+$$

$$\implies b_q^+ = \int_{S_2} \vec{e}_q \cdot \vec{e}_{a2} dS \tag{4.8}$$

Similarly, we can write the magnetic field in WG2 as

$$\vec{H}_{t2} = \sum_{q=1}^{Q} b_q^+ \vec{h}_q e^{-jk_z(z-d)}$$

137

At the boundary ($z = d$), the magnetic field is

$$\vec{H}_{t2}(z = d) = \sum_{q=1}^{Q} b_q^+ \vec{h}_q$$

Substituting in the expression for b_q^+ found in (4.8), we have

$$\vec{H}_{t2}(z = d) = \left(\sum_{q=1}^{Q} \int_{S_2} \vec{e}_q \cdot \vec{e}_{a2} dS \right) \vec{h}_q \tag{4.9}$$

4.3 Parallel Plate (PP)

In order to determine the fields in the PP region, we will use Love's equivalence principle extended to a PEC to replace the fields in apertures with equivalent magnetic currents, as shown in Figure 4.2. The equivalent magnetic currents are given in [9].

$$\vec{J}_{ht1} = -\hat{n}_1 \times \vec{E}_1^{\mathrm{pp}} = -\hat{\mathbf{z}} \times \vec{E}_1^{\mathrm{pp}} \qquad \text{and} \qquad \vec{J}_{ht2} = -\hat{n}_2 \times \vec{E}_2^{\mathrm{pp}} = \hat{\mathbf{z}} \times \vec{E}_2^{\mathrm{pp}}$$

However, the boundary conditions require continuity of tangential fields, leading to

$$\vec{J}_{ht1} = -\hat{\mathbf{z}} \times \vec{E}_1^{\mathrm{pp}} = -\hat{\mathbf{z}} \times \vec{e}_{a1} \qquad \text{and} \qquad \vec{J}_{ht2} = \hat{\mathbf{z}} \times \vec{E}_2^{\mathrm{pp}} = \hat{\mathbf{z}} \times \vec{e}_{a2} \tag{4.10}$$

The magnetic fields due to these equivalent magnetic sources may be found from the Green's functions determined in previous chapters. Recall, though, that the Green's functions were determined in the spectral $(\vec{\lambda}_\rho, z)$ domain. Therefore, the spatial representation of the fields can be written as

$$\vec{H}^{\mathrm{pp}}(\vec{\rho}, z) = \frac{1}{4\pi^2} \iint_{-\infty}^{\infty} \vec{\tilde{H}}^{\mathrm{pp}} e^{j\vec{\lambda}_\rho \cdot \vec{\rho}} d\lambda_\rho^2$$

$$= \frac{1}{4\pi^2} \iint_{-\infty}^{\infty} \left[\int_0^d \overset{\leftrightarrow}{\tilde{G}}_{hh} (\vec{\lambda}_\rho, z|z') \cdot \vec{\tilde{J}}_h(\vec{\lambda}_\rho, z') dz' \right] e^{j\vec{\lambda}_\rho \cdot \vec{\rho}} d\lambda_\rho^2$$
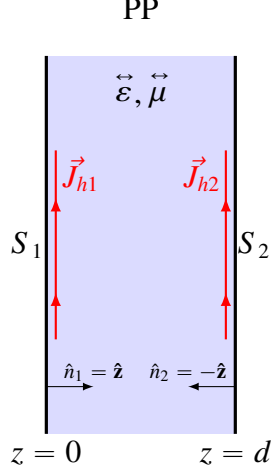
138

Figure 4.2: The geometry for the parallel plate region, where the fields at the aperture have been replaced by equivalent magnetic currents, according to Love's Equivalence Principle.

Utilizing the inverse transform of $\vec{\tilde{J}}_h$, we have:

$$\vec{H}^{\text{pp}}(\vec{\rho},z) = \frac{1}{4\pi^2}\iint\limits_{-\infty}^{\infty}\left[\int\limits_0^d \vec{\tilde{G}}_{hh}\,(\vec{\lambda}_\rho,z|z')\cdot\left(\iint\limits_S \vec{J}_h(\vec{\rho}',z')e^{-j\vec{\lambda}_\rho\cdot\vec{\rho}'}d\rho'^2\right)dz'\right]e^{j\vec{\lambda}_\rho\cdot\vec{\rho}}d\lambda_\rho^2$$

$$= \iint\limits_{-\infty}^{\infty}\left[\frac{1}{4\pi^2}\int\limits_{V'}\vec{\tilde{G}}_{hh}\,(\vec{\lambda}_\rho,z|z')\cdot\vec{J}_h(\vec{\rho}',z')e^{j\vec{\lambda}_\rho\cdot(\vec{\rho}-\vec{\rho}')}dV'\right]d\lambda_\rho^2 \tag{4.11}$$

which could also be written in the more familiar Green's function notation:

$$\vec{H}^{\text{pp}}(\vec{\rho},z) = \int\limits_{V'}\underbrace{\left[\iint\limits_{-\infty}^{\infty}\frac{1}{4\pi^2}\vec{\tilde{G}}_{hh}\,(\vec{\lambda}_\rho,z|z')\cdot e^{j\vec{\lambda}_\rho\cdot(\vec{\rho}-\vec{\rho}')}d\lambda_\rho^2\right]}_{\vec{\vec{G}}_{hh}(\vec{\rho},z)}\cdot\vec{J}_h(\vec{\rho}',z')dV' \tag{4.12}$$

We consider the magnetic fields just to the right of S_1 at the coordinates (x,y,z_1^+) and just to the left of S_2 at the coordinates (x,y,z_2^-). Clearly, a magnetic field existing anywhere in the material will be maintained by a contribution from both equivalent magnetic currents, $\vec{J}_{ht_1}$ and $\vec{J}_{ht_2}$. Therefore, using the representation from (4.11), we have the magnetic field

just to the right of S_1 as

$$\vec{H}_{t1}(\vec{r}_1^+) = \iint\limits_{-\infty}^{\infty} \left[\frac{1}{4\pi^2} \int\limits_{V_1'} \overset{\leftrightarrow}{\tilde{G}}_{hh} (\vec{\lambda}_\rho, z_1^+|z_1') \cdot \vec{J}_{ht_1}(\vec{\rho}_1') \delta(z'-z_1^+) e^{j\vec{\lambda}_\rho \cdot (\vec{\rho}_1-\vec{\rho}_1')} dV_1' \right] d\lambda_\rho^2$$

$$+ \iint\limits_{-\infty}^{\infty} \left[\frac{1}{4\pi^2} \int\limits_{V_2'} \overset{\leftrightarrow}{\tilde{G}}_{hh} (\vec{\lambda}_\rho, z_1^+|z_2') \cdot \vec{J}_{ht_2}(\vec{\rho}_2') \delta(z'-z_2^-) e^{j\vec{\lambda}_\rho \cdot (\vec{\rho}_1-\vec{\rho}_2')} dV_2' \right] d\lambda_\rho^2$$

$$= \frac{1}{4\pi^2} \iint\limits_{-\infty}^{\infty} \left[\int\limits_{S_1'} \overset{\leftrightarrow}{\tilde{G}}_{hh} (\vec{\lambda}_\rho, z_1^+|z_1') \cdot \vec{J}_{ht_1}(\vec{\rho}_1') e^{j\vec{\lambda}_\rho \cdot (\vec{\rho}_1-\vec{\rho}_1')} dS_1' \right] d\lambda_\rho^2$$

$$+ \frac{1}{4\pi^2} \iint\limits_{-\infty}^{\infty} \left[\int\limits_{S_2'} \overset{\leftrightarrow}{\tilde{G}}_{hh} (\vec{\lambda}_\rho, z_1^+|z_2') \cdot \vec{J}_{ht_2}(\vec{\rho}_2') e^{j\vec{\lambda}_\rho \cdot (\vec{\rho}_1-\vec{\rho}_2')} dS_2' \right] d\lambda_\rho^2$$

Recalling the definition of the equivalent magnetic currents, placing the origin in the corner of the waveguide aperture and assuming perfect alignment of the two apertures (e.g., $x_1 = x_2, y_1 = y_2$, etc.)[3] we write the expanded expression

$$\vec{H}_{t1}(\vec{r}_1^+) = \frac{1}{4\pi^2} \iint\limits_{-\infty}^{\infty} \left[\int\limits_0^b \int\limits_0^a \overset{\leftrightarrow}{\tilde{G}}_{hh} (\vec{\lambda}_\rho, z_1^+|z_1') \cdot [-\hat{\mathbf{z}} \times \vec{e}_{a1}(\vec{r}_1')] e^{j\vec{\lambda}_\rho \cdot (\vec{\rho}-\vec{\rho}')} dx'dy' \right] d\lambda_\rho^2$$

$$+ \frac{1}{4\pi^2} \iint\limits_{-\infty}^{\infty} \left[\int\limits_0^b \int\limits_0^a \overset{\leftrightarrow}{\tilde{G}}_{hh} (\vec{\lambda}_\rho, z_1^+|z_2') \cdot [\hat{\mathbf{z}} \times \vec{e}_{a2}(\vec{r}_2')] e^{j\vec{\lambda}_\rho \cdot (\vec{\rho}-\vec{\rho}')} dx'dy' \right] d\lambda_\rho^2 \qquad (4.13)$$

Similarly, we can write the magnetic field just to the left of S_2 as

$$\vec{H}_{t2}(\vec{r}_2^-) = \frac{1}{4\pi^2} \iint\limits_{-\infty}^{\infty} \left[\int\limits_0^b \int\limits_0^a \overset{\leftrightarrow}{\tilde{G}}_{hh} (\vec{\lambda}_\rho, z_2^-|z_1') \cdot [-\hat{\mathbf{z}} \times \vec{e}_{a1}(\vec{r}_1')] e^{j\vec{\lambda}_\rho \cdot (\vec{\rho}-\vec{\rho}')} dx'dy' \right] d\lambda_\rho^2$$

$$+ \frac{1}{4\pi^2} \iint\limits_{-\infty}^{\infty} \left[\int\limits_0^b \int\limits_0^a \overset{\leftrightarrow}{\tilde{G}}_{hh} (\vec{\lambda}_\rho, z_2^-|z_2') \cdot [\hat{\mathbf{z}} \times \vec{e}_{a2}(\vec{r}_2')] e^{j\vec{\lambda}_\rho \cdot (\vec{\rho}-\vec{\rho}')} dx'dy' \right] d\lambda_\rho^2 \qquad (4.14)$$

---

[3]The error due to slight misalignment has been previously shown to be small [51].

Enforcing continuity of tangential magnetic fields across S_1, from (4.7) and (4.13) we have

$$\vec{H}_{t1}(\vec{r}_1^-) = \vec{H}_{t1}(\vec{r}_1^+)$$

or

$$2a_1^+\vec{h}_1(\vec{r}_1^-) - \sum_{q=1}^{Q}\int_{S_1}\vec{e}_q(\vec{r}_1^-)\cdot\vec{e}_{a1}(\vec{r}_1^-)dS\,\vec{h}_q(\vec{r}_1^-) =$$

$$\frac{1}{4\pi^2}\iint_{-\infty}^{\infty}\left[\int_0^b\int_0^a \widetilde{\overset{\leftrightarrow}{G}}_{hh}\,(\vec{\lambda}_\rho, z_1^+|z_1')\cdot[-\hat{\mathbf{z}}\times\vec{e}_{a1}(\vec{r}_1')]\,e^{j\vec{\lambda}_\rho\cdot(\vec{\rho}-\vec{\rho}')}dx'dy'\right]d\lambda_\rho^2 \qquad (4.15)$$

$$+\frac{1}{4\pi^2}\iint_{-\infty}^{\infty}\left[\int_0^b\int_0^a \widetilde{\overset{\leftrightarrow}{G}}_{hh}\,(\vec{\lambda}_\rho, z_1^+|z_2')\cdot[\hat{\mathbf{z}}\times\vec{e}_{a2}(\vec{r}_2')]\,e^{j\vec{\lambda}_\rho\cdot(\vec{\rho}-\vec{\rho}')}dx'dy'\right]d\lambda_\rho^2$$

Again, employing the method of moments, we use the following expansions for the unknown electric fields across the apertures:

$$\vec{e}_{a1} = \sum_{n=1}^{N}a_1^+C_n^{(1)}\vec{e}_n \qquad \vec{e}_{a2} = \sum_{n=1}^{N}a_1^+C_n^{(2)}\vec{e}_n \qquad (4.16)$$

Transforming (4.15) to

$$2\vec{h}_1(\vec{r}_1^-) - \sum_{q=1}^{Q}\sum_{n=1}^{N}C_n^{(1)}\overbrace{\int_{S_1}\vec{e}_q(\vec{r}_1^-)\cdot\vec{e}_n(\vec{r}_1^-)dS}^{\delta_{qn}}\,\vec{h}_q(\vec{r}_1) =$$

$$-\frac{1}{4\pi^2}\iint_{-\infty}^{\infty}\left[\int_0^b\int_0^a \widetilde{\overset{\leftrightarrow}{G}}_{hh}\,(\vec{\lambda}_\rho, z_1^+|z_1')\cdot\left(\sum_{n=1}^{N}C_n^{(1)}\hat{\mathbf{z}}\times\vec{e}_n(\vec{r}_1')\right)e^{j\vec{\lambda}_\rho\cdot(\vec{\rho}-\vec{\rho}')}dx'dy'\right]d\lambda_\rho^2$$

$$+\frac{1}{4\pi^2}\iint_{-\infty}^{\infty}\left[\int_0^b\int_0^a \widetilde{\overset{\leftrightarrow}{G}}_{hh}\,(\vec{\lambda}_\rho, z_1^+|z_2')\cdot\left(\sum_{n=1}^{N}C_n^{(2)}\hat{\mathbf{z}}\times\vec{e}_n(\vec{r}_2')\right)e^{j\vec{\lambda}_\rho\cdot(\vec{\rho}-\vec{\rho}')}dx'dy'\right]d\lambda_\rho^2$$

Now, recalling $Z_n \vec{h}_n = \hat{\mathbf{z}} \times \vec{e}_n$, and simplifying:

$$2\vec{h}_1(\vec{r}_1^-) =$$

$$\sum_{n=1}^{N} \left\{ C_n^{(1)} \vec{h}_n(\vec{r}_1^-) - C_n^{(1)} \frac{Z_n}{4\pi^2} \iint_{-\infty}^{\infty} \left[\int_0^b \int_0^a \overset{\leftrightarrow}{\tilde{G}}_{hh} (\vec{\lambda}_\rho, z_1^+|z_1') \cdot \vec{h}_n(\vec{r}_1') e^{j\vec{\lambda}_\rho \cdot (\vec{\rho}-\vec{\rho}')} dx' dy' \right] d\lambda_\rho^2 \right.$$

$$\left. + C_n^{(2)} \frac{Z_n}{4\pi^2} \iint_{-\infty}^{\infty} \left[\int_0^b \int_0^a \overset{\leftrightarrow}{\tilde{G}}_{hh} (\vec{\lambda}_\rho, z_1^+|z_2') \cdot \vec{h}_n(\vec{r}_2') e^{j\vec{\lambda}_\rho \cdot (\vec{\rho}-\vec{\rho}')} dx' dy' \right] d\lambda_\rho^2 \right\}$$

We employ the following operator in the test step of the MoM (and note that, in the required limit of continuity of tangential fields, $\vec{r}_1^- = \vec{r}_1^+ = \vec{r}_1$):

$$\int_{S_1} \vec{h}_m(\vec{r}_1) \cdot \left\{ \right\} dS_1 \qquad \dots m = 1, \dots, N$$

to obtain

$$2 \sum_{m=1}^{N} \int_{S_1} \vec{h}_m(\vec{r}_1) \cdot \vec{h}_1(\vec{r}_1) dS_1 =$$

$$\sum_{n=1}^{N} \sum_{m=1}^{N} \left\{ C_n^{(1)} \int_{S_1} \vec{h}_m(\vec{r}_1) \cdot \vec{h}_n(\vec{r}_1) dS_1 \right.$$

$$- C_n^{(1)} \int_{S_1} \vec{h}_m(\vec{r}_1) \cdot \left[\frac{Z_n}{4\pi^2} \iint_{-\infty}^{\infty} \overset{\leftrightarrow}{\tilde{G}}_{hh} (\vec{\lambda}_\rho, z_1|z_1') \cdot \left(\int_0^b \int_0^a \vec{h}_n(\vec{r}_1') e^{j\vec{\lambda}_\rho \cdot (\vec{\rho}-\vec{\rho}')} dx' dy' \right) d\lambda_\rho^2 \right] dS_1$$

$$\left. + C_n^{(2)} \int_{S_1} \vec{h}_m(\vec{r}_1) \cdot \left[\frac{Z_n}{4\pi^2} \iint_{-\infty}^{\infty} \overset{\leftrightarrow}{\tilde{G}}_{hh} (\vec{\lambda}_\rho, z_1|z_2') \cdot \left(\int_0^b \int_0^a \vec{h}_n(\vec{r}_2') e^{j\vec{\lambda}_\rho \cdot (\vec{\rho}-\vec{\rho}')} dx' dy' \right) d\lambda_\rho^2 \right] dS_1 \right\}$$

(4.17)

Before we proceed, we can glean some physical insight from this form. The first term on the right side of the equation represents the dominant mode excitation at S_1. The second term represents how the nth mode excitation in the S_1 aperture maintains the mth mode

at the S_1 aperture. Similarly, the third term represents how the nth mode excitation at S_2 maintains the mth mode at S_1.

We can use the same methods to enforce the boundary conditions on S_2, using the same expansion coefficients and the test operator

$$\sum_{m=1}^{N} \int_{S_2} \vec{h}_m(\vec{r}_2) \cdot \{ \} dS_2 \qquad \ldots m = 1, ..., N$$

to obtain

$$
\begin{aligned}
0 = \sum_{n=1}^{N} \Bigg\{ & C_n^{(2)} \int_{S_2} \vec{h}_m(\vec{r}_2) \cdot \vec{h}_n(\vec{r}_2) dS_2 \\
& - C_n^{(1)} \left[\frac{Z_n}{4\pi^2} \iint_{-\infty}^{\infty} \left(\int_0^b \int_0^a \vec{h}_m(\vec{r}_2) e^{j\vec{\lambda}_\rho \cdot \vec{\rho}} \, dxdy \right) \cdot \overset{\leftrightarrow}{\tilde{G}}_{hh} \left(\vec{\lambda}_\rho, z_2 | z_1' \right) \cdot \left(\int_0^b \int_0^a \vec{h}_n(\vec{r}_1') e^{-j\vec{\lambda}_\rho \cdot \vec{\rho}'} dx' dy' \right) d\lambda_\rho^2 \right] \\
& + C_n^{(2)} \left[\frac{Z_n}{4\pi^2} \iint_{-\infty}^{\infty} \left(\int_0^b \int_0^a \vec{h}_m(\vec{r}_2) e^{j\vec{\lambda}_\rho \cdot \vec{\rho}} \, dxdy \right) \cdot \overset{\leftrightarrow}{\tilde{G}}_{hh} \left(\vec{\lambda}_\rho, z_2 | z_2' \right) \cdot \left(\int_0^b \int_0^a \vec{h}_n(\vec{r}_2') e^{-j\vec{\lambda}_\rho \cdot \vec{\rho}'} dx' dy' \right) d\lambda_\rho^2 \right] \Bigg\}
\end{aligned}
$$

(4.18)

We see that (4.17) and (4.18) can be written as a system of $2N$ equations:

$$\underbrace{\begin{bmatrix} A^{(11)} & A^{(12)} \\ A^{(21)} & A^{(22)} \end{bmatrix}}_{2N \times 2N} \underbrace{\begin{bmatrix} C^{(1)} \\ C^{(2)} \end{bmatrix}}_{2N \times 1} = \underbrace{\begin{bmatrix} B^{(1)} \\ B^{(2)} \end{bmatrix}}_{2N \times 1}$$

(4.19)

143

with

$$A_{mn}^{(11)} = \int_{S_1} \vec{h}_m(\vec{r}_1) \cdot \vec{h}_n(\vec{r}_1) dS_1$$

$$- \frac{Z_n}{4\pi^2} \iint_{-\infty}^{\infty} \left(\int_0^b \int_0^a \vec{h}_m(\vec{r}_1) e^{j\vec{\lambda}_\rho \cdot \vec{\rho}} \, dx dy \right) \cdot \overleftrightarrow{\tilde{G}}_{hh}(\vec{\lambda}_\rho, z_1|z_1') \cdot \left(\int_0^b \int_0^a \vec{h}_n(\vec{r}'_1) e^{-j\vec{\lambda}_\rho \cdot \vec{\rho}'} dx' dy' \right) d\lambda_\rho^2$$

$$A_{mn}^{(12)} = \frac{Z_n}{4\pi^2} \iint_{-\infty}^{\infty} \left(\int_0^b \int_0^a \vec{h}_m(\vec{r}_1) e^{j\vec{\lambda}_\rho \cdot \vec{\rho}} \, dx dy \right) \cdot \overleftrightarrow{\tilde{G}}_{hh}(\vec{\lambda}_\rho, z_1|z_2') \cdot \left(\int_0^b \int_0^a \vec{h}_n(\vec{r}'_2) e^{-j\vec{\lambda}_\rho \cdot \vec{\rho}'} dx' dy' \right) d\lambda_\rho^2$$

$$A_{mn}^{(21)} = \frac{Z_n}{4\pi^2} \iint_{-\infty}^{\infty} \left(\int_0^b \int_0^a \vec{h}_m(\vec{r}_2) e^{j\vec{\lambda}_\rho \cdot \vec{\rho}} \, dx dy \right) \cdot \overleftrightarrow{\tilde{G}}_{hh}(\vec{\lambda}_\rho, z_2|z_1') \cdot \left(\int_0^b \int_0^a \vec{h}_n(\vec{r}'_1) e^{-j\vec{\lambda}_\rho \cdot \vec{\rho}'} dx' dy' \right) d\lambda_\rho^2$$

$$A_{mn}^{(22)} = \int_{S_2} \vec{h}_m(\vec{r}_2) \cdot \vec{h}_n(\vec{r}_2) dS_2$$

$$- \frac{Z_n}{4\pi^2} \iint_{-\infty}^{\infty} \left(\int_0^b \int_0^a \vec{h}_m(\vec{r}_2) e^{j\vec{\lambda}_\rho \cdot \vec{\rho}} \, dx dy \right) \cdot \overleftrightarrow{\tilde{G}}_{hh}(\vec{\lambda}_\rho, z_2|z_2') \cdot \left(\int_0^b \int_0^a \vec{h}_n(\vec{r}'_2) e^{-j\vec{\lambda}_\rho \cdot \vec{\rho}'} dx' dy' \right) d\lambda_\rho^2$$

$$B^{(1)} = 2 \int_{S_1} \vec{h}_m(\vec{r}_1) \cdot \vec{h}_1(\vec{r}_1) dS_1$$

$$B^{(2)} = 0$$

The $A_{mn}^{(11)}$ and $A_{mn}^{(22)}$ terms are the "self" terms, that is, the field in the aperture at $z = 0$ or $z = d$ due to a source at the same position. The $A_{mn}^{(12)}$ and $A_{mn}^{(21)}$ terms are the "cross" terms, which represent the field at one aperture due to a source in the opposite aperture. Due to the symmetry of the system and the form of the magnetic type Green's functions in (B.12), we see that $A_{mn}^{(11)} = A_{mn}^{(22)}$. Due to reciprocity, we also find $A_{mn}^{(12)} = A_{mn}^{(21)}$. Therefore, we will only have to find two of the coefficients in order to solve the system. This will significantly reduce the required analysis and computation time.

So far, we have used the method of moments to convert what was an ill-posed system into a well-defined system of $2N$ equations, where the index N can be chosen to produce the desired convergence, based on our knowledge of the modes with the strongest contribution for this particular geometry [51]. This system can be solved using traditional linear algebra methods. The numeric subscripts on the PP magnetic fields represent, in the first case, the field at S_1 due to the source at S_1 and, in the second case, the field at S_1 due to the source at S_2. In both (4.17) and (4.18), the m index is associated with the observer (test function), whereas the n index is associated with the source (expansion function).

It is impossible to obtain a completely closed form solution of (4.17) and (4.18), but we will seek analytical solutions for all but one of the spectral integrals. The two inner source integrals may be calculated in the following manner.

$$\int_0^b \int_0^a \vec{h}_n(\vec{r}_1')e^{-j\vec{\lambda}_\rho \cdot \vec{\rho}'}dx'dy' = \int_0^b \int_0^a \vec{h}_n(x',y',z_1'=0)e^{-j\lambda_x x'}e^{-j\lambda_y y'}dx'dy'$$

Recall that $\vec{h}_n$ is the transverse electric field in the aperture, which can be written as $\vec{h}_n = \hat{\mathbf{x}}h_{nx} + \hat{\mathbf{y}}h_{ny}$. This leads to

$$\int_0^b \int_0^a \vec{h}_n(\vec{r}_1')e^{-j\vec{\lambda}_\rho \cdot \vec{\rho}'}dx'dy' = \int_0^b \int_0^a \left(\hat{\mathbf{x}}h_{nx} + \hat{\mathbf{y}}h_{ny}\right)e^{-j\lambda_x x'}e^{-j\lambda_y y'}dx'dy'$$

Using the usual field representations for TE^z and TM^z modes in a rectangular waveguide, which can be found in [9], we expand to

$$\int_0^b \int_0^a \vec{h}_n(\vec{r}_1')e^{-j\vec{\lambda}_\rho \cdot \vec{\rho}'}dx'dy' = \hat{\mathbf{x}}M_{xn}^h \int_0^b \int_0^a \sin\left(k_{xn}x'\right)\cos\left(k_{yn}y'\right)e^{-j\lambda_x x'}e^{-j\lambda_y y'}dx'dy'$$

$$+ \hat{\mathbf{y}}M_{yn}^h \int_0^b \int_0^a \cos\left(k_{xn}x'\right)\sin\left(k_{yn}y'\right)e^{-j\lambda_x x'}e^{-j\lambda_y y'}dx'dy'$$

$$(4.20)$$

145

where $M_{hx,hy}^n$ is the appropriate amplitude coefficient and depends on whether the mode n is TE^z or TM^z (in the equations below, $\alpha = m, n$):

	$M_{x\alpha}^h$	$M_{y\alpha}^h$	Z_α
TE^z	$\dfrac{k_{x\alpha}}{Z_\alpha}$	$\dfrac{k_{y\alpha}}{Z_\alpha}$	$\dfrac{\omega\mu_0}{k_{zn}}$
TM^z	$k_{y\alpha}$	$-k_{x\alpha}$	$\dfrac{k_{zn}}{\omega\varepsilon_0}$

$$\dots \text{with}$$

$$k_{x\alpha} = \frac{v_\alpha \pi}{a}$$

$$k_{y\alpha} = \frac{w_\alpha \pi}{b}$$

$$k_{c\alpha} = \sqrt{k_{x\alpha}^2 + k_{y\alpha}^2}$$

$$k_{z\alpha} = \sqrt{k_0^2 - k_{c\alpha}^2}$$

(4.21)

Again, we note that m and n are mode indices which designate the traditional modal notation, which is expressed as TE$^z_{v_n w_n}$ or TM$^z_{v_n w_n}$. We can apply a separation of variables solution to the source integrals (4.20) to write

$$\int_0^b \int_0^a \vec{h}_n(\vec{r}_1')e^{-j\vec{\lambda}_\rho \cdot \vec{\rho}'}dx'dy' = \hat{\mathbf{x}}M_{xn}^h \int_0^a \sin(k_{xn}x')\,e^{-j\lambda_x x'}dx' \int_0^b \cos(k_{yn}y')\,e^{-j\lambda_y y'}dy'$$

$$+ \hat{\mathbf{y}}M_{yn}^h \int_0^a \cos(k_{xn}x')\,e^{-j\lambda_x x'}dx' \int_0^b \sin(k_{yn}y')\,e^{-j\lambda_y y'}dy'$$

(4.22)

The solution to (4.20) can be found in closed form and is presented in detail in Appendix B of [86]. We follow this solution, noting that v values must be odd and w values must be even, due to the symmetry of the waveguide. Recalling the form of k_{xn} and k_{yn}, we find the generalized results of the integrals are (where $u = v_n, w_n$)

$$\int_0^a \sin\left(\frac{u\pi}{a}x\right)e^{\pm j\lambda_x x} = -\frac{u\pi}{a}\left[\frac{(1-(-1)^u e^{\pm j\lambda_x a})}{\left(\lambda_x + \frac{u\pi}{a}\right)\left(\lambda_x - \frac{u\pi}{a}\right)}\right]$$

$$\int_0^a \cos\left(\frac{u\pi}{a}x\right)e^{\pm j\lambda_x x} = \pm j\lambda_x\left[\frac{(1-(-1)^u e^{\pm j\lambda_x a})}{\left(\lambda_x + \frac{u\pi}{a}\right)\left(\lambda_x - \frac{u\pi}{a}\right)}\right]$$

(4.23)

146

Therefore the source integrals for the nth mode from (4.22) become

$$
\int_0^b \int_0^a \vec{h}_n(\vec{r}'_1) e^{-j\vec{\lambda}_\rho \cdot \vec{\rho}'} dx' dy'
$$

(4.24)

$$
= \left[\frac{\left(1 - (-1)^{v_n} e^{-j\lambda_x a}\right) \left(1 - (-1)^{w_n} e^{-j\lambda_y b}\right)}{(\lambda_y + k_{yn})(\lambda_y - k_{yn})(\lambda_x + k_{xn})(\lambda_x - k_{xn})} \right] \left[\hat{\mathbf{x}} j M^h_{xn} k_{xn} \lambda_y + \hat{\mathbf{y}} j M^h_{yn} k_{yn} \lambda_x \right]
$$

We note that $\vec{h}_n(\vec{r}'_1) = \vec{h}_n(\vec{r}'_2)$, since we assume the waveguides are perfectly aligned in the transverse dimensions (i.e. - $\vec{\rho}'_1 = \vec{\rho}'_2$) and there is no z-dependency. Similarly, we can write the testing functions (m^{th} modes) as

$$
\int_0^b \int_0^a \vec{h}_m(\vec{r}'_1) e^{j\vec{\lambda}_\rho \cdot \vec{\rho}} dx dy
$$

$$
= -\left[\frac{\left(1 - (-1)^{v_m} e^{j\lambda_x a}\right) \left(1 - (-1)^{w_m} e^{j\lambda_y b}\right)}{(\lambda_y + k_{ym})(\lambda_y - k_{ym})(\lambda_x + k_{xm})(\lambda_x - k_{xm})} \right] \left[\hat{\mathbf{x}} j M^h_{xm} k_{xm} \lambda_y + \hat{\mathbf{y}} j M^h_{ym} k_{ym} \lambda_x \right]
$$

(4.25)

Finally, we will simplify the excitation terms in $A^{(11)}_{mn}$, $A^{(22)}_{mn}$ and $B^{(1)}_{m1}$. Using the rectangular waveguide modes from (4.21), we write

$$
\int_{S_1} \vec{h}_m(\vec{r}_1) \cdot \vec{h}_n(\vec{r}_1) dS_1
$$

$$
= \int_{S_1} \left\{ \left[\hat{\mathbf{x}} M^h_{xm} \sin(k_{xm} x) \cos(k_{ym} y) + \hat{\mathbf{y}} M^h_{ym} \cos(k_{xm} x) \sin(k_{ym} y) \right] \cdot \right.
$$

(4.26)

$$
\left. \left[\hat{\mathbf{x}} M^h_{xm} \sin(k_{xm} x) \cos(k_{ym} y) + \hat{\mathbf{y}} M^h_{ym} \cos(k_{xm} x) \sin(k_{ym} y) \right] \right\} dS_1
$$

$$
= \int_{S_1} \left[\left(M^h_{xm}\right)^2 \sin^2(k_{xm} x) \cos^2(k_{ym} y) + \left(M^h_{ym}\right)^2 \cos^2(k_{xm} x) \sin^2(k_{ym} y) \right] dS_1 \quad (4.27)
$$

147

Assuming a separation of variables solution and making use of mode orthogonality, we can write

$$
= \delta_{m,n} \left\{ \left(M_{xm}^h\right)^2 \int_0^a \sin^2 (k_{xm}x) \, dx \int_0^b \cos^2 (k_{ym}y) \, dy \right.
$$
$$
\left. + \left(M_{ym}^h\right)^2 \int_0^a \cos^2 (k_{xm}x) \, dx \int_0^b \sin^2 (k_{ym}y) \, dy \right\}
\tag{4.28}
$$

$$
= \delta_{m,n} \left[\left(M_{xm}^h\right)^2 \left(\frac{ab}{4}\right) + \left(M_{ym}^h\right)^2 \left(\frac{ab}{4}\right) \right] (1 + \delta_{m,0})
\tag{4.29}
$$

$$
\boxed{= \delta_{m,n} \left(\frac{ab}{4}\right) \left[\left(M_{xm}^h\right)^2 + \left(M_{ym}^h\right)^2 \right] (1 + \delta_{w_m,0})}
\tag{4.30}
$$

In (4.30), the $(1 + \delta_{w_m,0})$ term is required because, in the case of $w_m = 0$, we find

$$
\int_0^b \cos^2 (k_{y1}y) \, dy = \int_0^b \cos^2 (0) \, dy = \int_0^b (1) dy = b
\tag{4.31}
$$

rather than $\frac{b}{2}$, as will be the case for higher order modes. Now, for the $B_1^{(1)}$ term, we have $w_m = w_n = 0$, which leads to $M_{ym}^h = M_{yn}^h = 0$

$$
B_1^{(1)} = 2 \int_{S_1} \vec{h}_m(\vec{r}_1) \cdot \vec{h}_1(\vec{r}_1) dS_1 = 2\delta_{1,1} \left(\frac{ab}{4}\right) \left[\left(M_{xm}^h\right)^2 + (0)^2 \right] (2)
\tag{4.32}
$$

$$
\implies B_1^{(1)} = ab \left(M_{xm}^h\right)^2 = \frac{abk_{x_1}^2}{Z_1^2}
\tag{4.33}
$$

Therefore, the excitation matrix $B^{(1)}$ may be succinctly written as

$$
\boxed{B^{(1)} = ab \left(M_{xm}^h\right)^2 \delta_{m,1} = \frac{abk_{x_1}^2}{Z_1^2} \delta_{m,1}}
\tag{4.34}
$$

We can now write the $A^{(11)}$ and $A^{(12)}$ coefficients as

$$A^{(11)} = \delta_{m,n} \left(\frac{ab}{4}\right) \left[\left(M^h_{xm}\right)^2 + \left(M^h_{ym}\right)^2\right] (1 + \delta_{w_m,0})$$

$$- \frac{Z_n}{4\pi^2} \iint\limits_{-\infty}^{\infty} \left\{ - \left[\frac{\left(1-(-1)^{v_m}e^{j\lambda_x a}\right)\left(1-(-1)^{w_m}e^{j\lambda_y b}\right)}{(\lambda_y + k_{ym})(\lambda_y - k_{ym})(\lambda_x + k_{xm})(\lambda_x - k_{xm})} \right] \right.$$

(4.35)

$$\left[\hat{\mathbf{x}}jM^h_{xm}k_{xm}\lambda_y + \hat{\mathbf{y}}M^h_{ym}k_{ym}\lambda_x\right] \cdot \overset{\leftrightarrow}{\widetilde{G}}_{hh}\left(\vec{\lambda}_\rho, z_1|z_1'\right) \cdot \left[\hat{\mathbf{x}}jM^h_{xn}k_{xn}\lambda_y + \hat{\mathbf{y}}jM^h_{yn}k_{yn}\lambda_x\right]$$

$$\left. \left[\frac{\left(1-(-1)^{v_n}e^{-j\lambda_x a}\right)\left(1-(-1)^{w_n}e^{-j\lambda_y b}\right)}{(\lambda_y + k_{yn})(\lambda_y - k_{yn})(\lambda_x + k_{xn})(\lambda_x - k_{xn})} \right] \right\} d\lambda_x d\lambda_y$$

$$A^{(12)} = \frac{Z_n}{4\pi^2} \iint\limits_{-\infty}^{\infty} \left\{ - \left[\frac{\left(1-(-1)^{v_m}e^{j\lambda_x a}\right)\left(1-(-1)^{w_m}e^{j\lambda_y b}\right)}{(\lambda_y + k_{ym})(\lambda_y - k_{ym})(\lambda_x + k_{xm})(\lambda_x - k_{xm})} \right] \right.$$

$$\left[\hat{\mathbf{x}}jM^h_{xm}k_{xm}\lambda_y + \hat{\mathbf{y}}jM^h_{ym}k_{ym}\lambda_x\right] \cdot \overset{\leftrightarrow}{\widetilde{G}}_{hh}\left(\vec{\lambda}_\rho, z_1|z_2'\right) \cdot \left[\hat{\mathbf{x}}jM^h_{xn}k_{xn}\lambda_y + \hat{\mathbf{y}}jM^h_{yn}k_{yn}\lambda_x\right]$$ (4.36)

$$\left. \left[\frac{\left(1-(-1)^{v_n}e^{-j\lambda_x a}\right)\left(1-(-1)^{w_n}e^{-j\lambda_y b}\right)}{(\lambda_y + k_{yn})(\lambda_y - k_{yn})(\lambda_x + k_{xn})(\lambda_x - k_{xn})} \right] \right\} d\lambda_x d\lambda_y$$

Recognizing that $\overset{\leftrightarrow}{\widetilde{G}}_{hh}\left(\vec{\lambda}_\rho, z_1|z_1'\right)$ is a dyad of full rank, we examine the vector portions of the A coefficients:

$$\left[\hat{\mathbf{x}}jM^h_{xm}k_{xm}\lambda_y + \hat{\mathbf{y}}jM^h_{ym}k_{ym}\lambda_x\right] \cdot \overset{\leftrightarrow}{\widetilde{G}}_{hh}\left(\vec{\lambda}_\rho, z_1|z_1'\right) \cdot \left[\hat{\mathbf{x}}jM^h_{xn}k_{xn}\lambda_y + \hat{\mathbf{y}}jM^h_{yn}k_{yn}\lambda_x\right]$$

$$= -M^h_{xm}M^h_{xn}k_{xm}k_{xn}\lambda_y^2\widetilde{G}^{11}_{hh,xx} - M^h_{xm}M^h_{yn}k_{xm}k_{yn}\lambda_x\lambda_y\widetilde{G}^{11}_{hh,xy}$$

$$- M^h_{ym}M^h_{xn}k_{xm}k_{yn}\lambda_x\lambda_y\widetilde{G}^{11}_{hh,yx} - M^h_{ym}M^h_{yn}k_{ym}k_{yn}\lambda_x^2\widetilde{G}^{11}_{hh,yy}$$

149

where $\overset{\leftrightarrow}{\tilde{G}}_{hh}\left(\vec{\lambda}_\rho, z_1|z_1'\right) = \tilde{G}^{11}_{hh,yx}$. After some algebraic manipulation, we can finally write the $A^{(11)}_{mn}$ and $A^{(12)}_{mn}$ coefficients as

$$
\begin{aligned}
A^{(11)}_{mn} = {} & \delta_{m,n}\left(\frac{ab}{4}\right)\left[\left(M^h_{xm}\right)^2 + \left(M^h_{ym}\right)^2\right](1 + \delta_{w_m,0}) \\[2mm]
& - \frac{Z_n}{4\pi^2}\int\limits_{-\infty}^{\infty}\left\{\left[\frac{\left(1-(-1)^{v_m}e^{j\lambda_x a}\right)\left(1-(-1)^{v_n}e^{-j\lambda_x a}\right)}{(\lambda_x+k_{xm})(\lambda_x-k_{xm})(\lambda_x+k_{xn})(\lambda_x-k_{xn})}\right]\right. \\[2mm]
& \int\limits_{-\infty}^{\infty}\left[M^h_{xm}M^h_{xn}k_{xm}k_{xn}\lambda_y^2\tilde{G}^{11}_{hh,xx} + M^h_{xm}M^h_{yn}k_{xm}k_{yn}\lambda_x\lambda_y\tilde{G}^{11}_{hh,xy}\right. \\[2mm]
& \left. + M^h_{ym}M^h_{xn}k_{xm}k_{yn}\lambda_x\lambda_y\tilde{G}^{11}_{hh,yx} + M^h_{ym}M^h_{yn}k_{ym}k_{yn}\lambda_x^2\tilde{G}^{11}_{hh,yy}\right] \\[2mm]
& \left.\left[\frac{\left(1-(-1)^{w_m}e^{j\lambda_y b}\right)\left(1-(-1)^{w_n}e^{-j\lambda_y b}\right)}{(\lambda_y+k_{ym})(\lambda_y-k_{ym})(\lambda_y+k_{yn})(\lambda_y-k_{yn})}\right]d\lambda_y\right\}d\lambda_x
\end{aligned}
$$
(4.37)

$$
\begin{aligned}
A^{(12)}_{mn} = {} & \frac{Z_n}{4\pi^2}\int\limits_{-\infty}^{\infty}\left\{\left[\frac{\left(1-(-1)^{v_m}e^{j\lambda_x a}\right)\left(1-(-1)^{v_n}e^{-j\lambda_x a}\right)}{(\lambda_x+k_{xm})(\lambda_x-k_{xm})(\lambda_x+k_{xn})(\lambda_x-k_{xn})}\right]\right. \\[2mm]
& \int\limits_{-\infty}^{\infty}\left[M^h_{xm}M^h_{xn}k_{xm}k_{xn}\lambda_y^2\tilde{G}^{12}_{hh,xx} + M^h_{xm}M^h_{yn}k_{xm}k_{yn}\lambda_x\lambda_y\tilde{G}^{12}_{hh,xy}\right. \\[2mm]
& \left. + M^h_{ym}M^h_{xn}k_{xm}k_{yn}\lambda_x\lambda_y\tilde{G}^{12}_{hh,yx} + M^h_{ym}M^h_{yn}k_{ym}k_{yn}\lambda_x^2\tilde{G}^{12}_{hh,yy}\right] \\[2mm]
& \left.\left[\frac{\left(1-(-1)^{w_m}e^{j\lambda_y b}\right)\left(1-(-1)^{w_n}e^{-j\lambda_y b}\right)}{(\lambda_y+k_{ym})(\lambda_y-k_{ym})(\lambda_y+k_{yn})(\lambda_y-k_{yn})}\right]d\lambda_y\right\}d\lambda_x
\end{aligned}
$$
(4.38)

4.4 Evaluation of λ_y Integral

The inner integrals of both (4.36) and (4.38) can be integrated in the complex λ_y plane, using the complex analysis techniques described in Appendix A. From the form of the integral, we see there are several cases which must be considered with regards to the y-variations of the source (n^{th} modes) and observation (m^{th} modes) fields:

- Case I: $w_m = w_n = 0$

- Case II: $w_m \neq 0, w_n = 0$

- Case III: $w_m = 0, w_n \neq 0$

- Case IV: $w_m = w_n \neq 0$

- Case V: $w_m \neq w_n \neq 0$

For the moment, we will examine Case I, which lends itself to a dominant mode analysis, where we assume that only the dominant mode is present in both the testing and observation functions. Admittedly, this is not the most accurate expansion, but will provide a sufficient foundation upon which to build. For this analysis, recall $z_1 = z_1' = 0$ and $z_2 = z_2' = d$.

4.4.1 Case I: $w_m = w_n = 0$ $(A_{mn}^{(11)})$.

In the simplest case, when both $TE_{v_m 0}^z$ (observation) and $TE_{v_n 0}^z$ (source) modes are present, we have $w_m = w_n = 0 \implies k_{ym} = k_{yn} = 0$ and the inner integral of the $A_{mn}^{(11)}$ coefficient becomes

$$\int_{-\infty}^{\infty} \frac{M_{xm}^h M_{xn}^h k_{xm} k_{xn}}{\lambda_y^2} \widetilde{G}_{hh,xx}^{11} \left[\left(1 - e^{j\lambda_y b}\right) \left(1 - e^{-j\lambda_y b}\right) \right] d\lambda_y \tag{4.39}$$

We recall from (B.12) that $\widetilde{G}_{hh,xx}$ consists of a TE^z and a TM^z portion. According to the superposition principle, we can consider each part individually.

TE^z Contribution of $\widetilde{G}_{hh,xx}$. The TE^z contribution of $\widetilde{G}_{hh,xx}$ is given by (B.12):

$$\widetilde{G}_{hh,xx}^{\text{TE}} = \left(\frac{j\lambda_{z\theta}\lambda_x^2}{2\lambda_\rho^2 \omega \mu_t} \right) \left[\frac{\cos\left(\lambda_{z\theta}\left[d - |z - z'|\right]\right) + \cos\left(\lambda_{z\theta}\left[d - (z + z')\right]\right)}{\sin\left(\lambda_{z\theta}d\right)} \right]$$

and recall $\widetilde{G}_{hh,xx}^{11} = \widetilde{G}_{hh,xx}(\vec{r}_1 | \vec{r}_1')$, which leads to

$$\widetilde{G}_{hh,xx}^{\text{TE},11} = \left(\frac{j\lambda_{z\theta}\lambda_x^2}{\lambda_\rho^2 \omega \mu_t} \right) \left[\frac{\cos\left(\lambda_{z\theta}d\right)}{\sin\left(\lambda_{z\theta}d\right)} \right]$$

Therefore, (4.39) becomes

$$
\frac{j M_{xm}^h M_{xn}^h k_{xm} k_{xn} \lambda_x^2}{\omega \mu_t} \left\{ \int\limits_{-\infty}^{\infty} \left[\frac{\lambda_{z\theta} \left(1 - e^{j\lambda_y b} \right)}{\lambda_y^2 \lambda_\rho^2} \right] \left[\frac{\cos\left(\lambda_{z\theta} d\right)}{\sin\left(\lambda_{z\theta} d\right)} \right] d\lambda_y \right.
$$
$$
\left. + \int\limits_{-\infty}^{\infty} \left[\frac{\lambda_{z\theta} \left(1 - e^{-j\lambda_y b} \right)}{\lambda_y^2 \lambda_\rho^2} \right] \left[\frac{\cos\left(\lambda_{z\theta} d\right)}{\sin\left(\lambda_{z\theta} d\right)} \right] d\lambda_y \right\}
$$

(4.40)

Recall that $\lambda_\rho^2 = \lambda_x^2 + \lambda_y^2$ and $\lambda_{z\theta}^2 = k_t^2 - \frac{\mu_t}{\mu_z} \lambda_\rho^2 = k_t^2 - \frac{\mu_t}{\mu_z} \lambda_x^2 - \frac{\mu_t}{\mu_z} \lambda_y^2$. This form reveals the need for UHP and LHP closure in the complex λ_y plane. We have simple poles at $\lambda_y = \pm j\lambda_x$ and $\lambda_y = \pm \sqrt{ \frac{\mu_z}{\mu_t} \left[k_t^2 - (\frac{\pi l}{d})^2 \right] - \lambda_x^2 }$ (where $l = 0, 1, \ldots, \infty$) and what would appear to be a double pole at $\lambda_y = 0$. However, the double pole at $\lambda_y = 0$ turns out to be a simple pole, as L'Hôspital's rule indicates one of the poles is removable:

$$
\lim_{\lambda_y \to 0} \frac{1 - e^{j\lambda_y b}}{\lambda_y} = -jb \neq 0
$$

Therefore, we find only a simple pole at $\lambda_y = 0$. We choose the appropriate closure conditions by separating λ_y into real and imaginary parts ($\lambda_y = \lambda_{y_{re}} + j\lambda_{y_{im}}$). This leads to

$$
e^{j\lambda_y b} = e^{j\lambda_{y_{re}} b} e^{-\lambda_{y_{im}} b} \implies \lambda_{y_{im}} > 0 \implies \text{UHP}
$$

$$
\implies \lambda_{y_{p1}} = j\lambda_x \quad , \quad \lambda_{y_{p2}} = -\sqrt{ \frac{\mu_z}{\mu_t} \left(k_t^2 - (\frac{\pi l}{d})^2 \right) - \lambda_x^2 }
$$

$$
e^{-j\lambda_y b} = e^{-j\lambda_{y_{re}} b} e^{\lambda_{y_{im}} b} \implies \lambda_{y_{im}} < 0 \implies \text{LHP}
$$

$$
\implies \lambda_{y_{p1}} = -j\lambda_x \quad , \quad \lambda_{y_{p2}} = \sqrt{ \frac{\mu_z}{\mu_t} \left(k_t^2 - (\frac{\pi l}{d})^2 \right) - \lambda_x^2 }
$$

Where $\lambda_{y_{p1}}$ and $\lambda_{y_{p2}}$ are the non-trivial poles, which are utilized in the next sections.
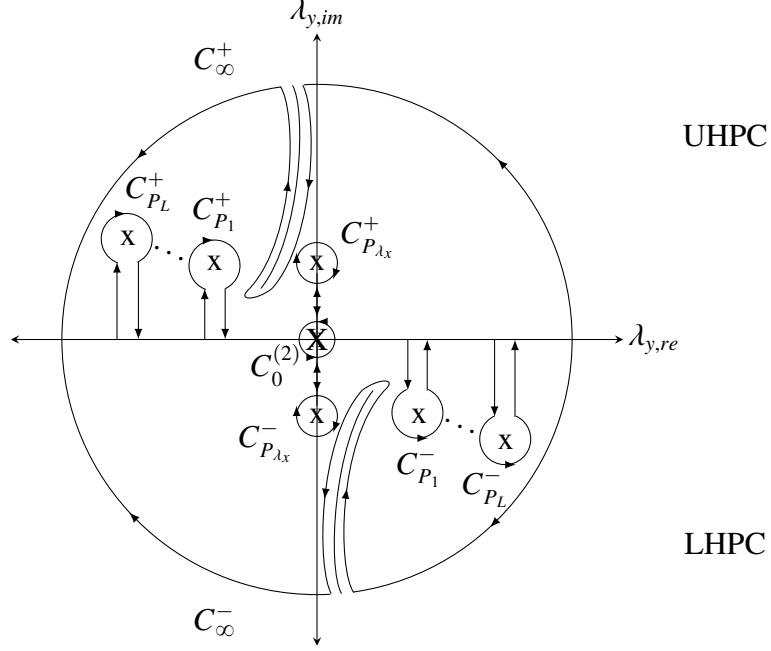
152

Figure 4.3: Complex λ_y plane integration, showing the poles at $\lambda_y = 0, \lambda_y = \pm J\lambda_x$ and $\lambda_y = \pm \sqrt{\frac{\mu_z}{\mu_t}\left[k_t^2 - \left(\frac{\pi l}{d}\right)^2\right] - \lambda_x^2}$. The branch cuts arise from the multi-valuedness of the radical in the argument of the sine term. The branch point at $l = 0$ is removable, based on the form of the numerator.

- UHP for TE^z Contribution

  We first consider the UHP. For brevity's sake, we look only at the integral and will carry the multiplicative factors through at the end.

153

For UHP, by Cauchy's Integral Theorem, Jordan's Lemma and Cauchy's Integral Formula, we have

$$\int_{-\infty}^{\infty} + \underset{C_0^+}{\oint} + \underset{C_{j\lambda_x}^+}{\oint} + \underset{\Sigma C_l^+}{\oint} + \overbrace{\int}^{0}_{C_\infty^+} = 0$$

$$\implies \int_{-\infty}^{\infty} = -\underset{C_0^+}{\oint} - \underset{C_{j\lambda_x}^+}{\oint} - \underset{\Sigma C_l^+}{\oint} = \underset{C_0^+}{\oint} + \underset{C_{j\lambda_x}^+}{\oint} + \underset{\Sigma C_l^+}{\oint}$$

$$= j\pi \mathrm{Res}(f, \lambda_y = 0) + j2\pi \mathrm{Res}(f, \lambda_y = j\lambda_x) + j2\pi \mathrm{Res}(f, \lambda_{z\theta} = \pm\frac{\pi l}{d})$$

1. C_0^+ Pole

   The contribution from the simple pole at $\lambda_y = 0$ can be found using Cauchy's Integral Formula for a semi-circular contour. The value of the pole contribution for a pole of second-order around a semi-circular contour of a function $\frac{f(z)}{g(z)}$ is given by

   $$\oint \frac{f(z)}{g(z)} = j\pi \frac{\partial f(z)}{\partial z} \tag{4.41}$$

   In this case, we have

   $$f(\lambda_y) = \left[\frac{\lambda_{z\theta}\left(1-e^{j\lambda_y b}\right)}{\left(\lambda_x^2 + \lambda_y^2\right)}\right]\left[\frac{\cos\left(\lambda_{z\theta} d\right)}{\sin\left(\lambda_{z\theta} d\right)}\right] \tag{4.42}$$

   $$g(\lambda_y) = \lambda_y^2 \tag{4.43}$$

   which leads to

   $$\underset{C_0^+}{\oint} = j\pi \lim_{\lambda_y \to 0} \frac{\partial}{\partial \lambda_y} \left\{\left[\frac{\lambda_{z\theta}\left(1-e^{j\lambda_y b}\right)}{\left(\lambda_x^2 + \lambda_y^2\right)}\right]\left[\frac{\cos\left(\lambda_{z\theta} d\right)}{\sin\left(\lambda_{z\theta} d\right)}\right]\right\} \tag{4.44}$$

   $$= j\pi \lim_{\lambda_y \to 0} \frac{\lambda_\rho^2 \sin\left(\lambda_{z\theta} d\right) \frac{\partial}{\partial \lambda_y}\left[\lambda_{z\theta}\left(1 - e^{j\lambda_y b}\right)\cos\left(\lambda_{z\theta} d\right)\right]}{\left[\lambda_\rho \sin\left(\lambda_{z\theta} d\right)\right]^2} \tag{4.45}$$

   $$- \frac{\lambda_{z\theta}\left(1 - e^{j\lambda_y b}\right)\cos\left(\lambda_{z\theta} d\right) \frac{\partial}{\partial \lambda_y}\left(\lambda_\rho^2 \sin\left(\lambda_{z\theta} d\right)\right)}{\left[\lambda_\rho \sin\left(\lambda_{z\theta} d\right)\right]^2} \tag{4.46}$$

154

However, because we are interested in the limit of $\lambda_y \rightarrow 0$, $1 - e^{j\lambda_y b} \rightarrow 0$, which means the entire second term can be neglected. Canceling one of the $\lambda_\rho \sin(\lambda_{z\theta} d)$ terms in the denominator leads to

$$
\implies j\pi \lim_{\lambda_y \rightarrow 0} \frac{\frac{\partial}{\partial \lambda_y} \left[\lambda_{z\theta} \left(1 - e^{j\lambda_y b} \right) \cos(\lambda_{z\theta} d) \right]}{\lambda_\rho \sin(\lambda_{z\theta} d)} \tag{4.47}
$$

$$
= j\pi \lim_{\lambda_y \rightarrow 0} \frac{\lambda_{z\theta} \frac{\partial}{\partial \lambda_y} \left[\left(1 - e^{j\lambda_y b} \right) \cos(\lambda_{z\theta} d) \right] + \left(1 - e^{j\lambda_y b} \right) \cos(\lambda_{z\theta} d) \frac{\partial}{\partial \lambda_y} \lambda_{z\theta}}{\lambda_\rho \sin(\lambda_{z\theta} d)} \tag{4.48}
$$

Again, the second term may be neglected due to the limit

$$
\implies j\pi \lim_{\lambda_y \rightarrow 0} \frac{\lambda_{z\theta} \frac{\partial}{\partial \lambda_y} \left[\left(1 - e^{j\lambda_y b} \right) \cos(\lambda_{z\theta} d) \right]}{\lambda_\rho \sin(\lambda_{z\theta} d)} \tag{4.49}
$$

$$
= j\pi \lim_{\lambda_y \rightarrow 0} \frac{\lambda_{z\theta} \left[\left(1 - e^{j\lambda_y b} \right) \frac{\partial}{\partial \lambda_y} \cos(\lambda_{z\theta} d) + \cos(\lambda_{z\theta} d) \left(-jb e^{j\lambda_y b} \right) \right]}{\lambda_\rho \sin(\lambda_{z\theta} d)} \tag{4.50}
$$

Again, the first term is cancelled due to the required limit, leading to a final solution:

$$
\oint_{C_0^+} = \frac{\pi b \lambda_{z\theta}^*}{\lambda_x^2} \left[\frac{\cos(\lambda_{z\theta}^* d)}{\sin(\lambda_{z\theta}^* d)} \right] \quad , \quad \lambda_{z\theta}^* = \sqrt{k_t^2 - \frac{\mu_t}{\mu_z} \lambda_x^2} \tag{4.51}
$$

2. $C_{j\lambda_x}^+$ Pole The contribution from the simple pole at $\lambda_y = j\lambda_x$ can be calculated by

$$
\oint_{C_{j\lambda_x}^+} = j2\pi \text{Res}(f, \lambda_y = j\lambda_x)
$$

$$
= j2\pi \lim_{\lambda_y \rightarrow j\lambda_x} \left\{ (\lambda_y - j\lambda_x) \left[\frac{\lambda_{z\theta} \left(1 - e^{j\lambda_y b} \right)}{\lambda_y^2 \left(\lambda_y + j\lambda_x \right) \left(\lambda_y - j\lambda_x \right)} \right] \left[\frac{\cos(\lambda_{z\theta} d)}{\sin(\lambda_{z\theta} d)} \right] \right\}
$$

$$
= - \left[\frac{\pi \left(1 - e^{-\lambda_x b} \right)}{\lambda_x^3} \right] \left[\frac{k_t \cos(k_t d)}{\sin(k_t d)} \right]
$$

155

where we have used the relationship $\lambda_{z\theta} = \sqrt{k_t^2 - \frac{\mu_t}{\mu_z}\lambda_x^2 - \frac{\mu_t}{\mu_z}(j\lambda_x)^2} = \pm k_t$. A further examination shows that the sign of k_t is unimportant, since $\frac{k_t\cos(k_t d)}{\sin(k_t d)}$ is seen to be even in k_t.

3. C_l^+ Pole

Finally, the contribution from the poles when $\lambda_{z\theta} = \pm\frac{\pi l}{d}$ ($l = 0, 1, 2..., \infty$) can be found. This pole leads to a series of special values of λ_y:

$$\lambda_{yl\theta} = \pm\sqrt{\frac{\mu_z}{\mu_t}\left[k_t^2 - \left(\frac{\pi l}{d}\right)^2\right] - \lambda_x^2} \qquad (4.52)$$

Due to the form of the integrand, we use the formula

$$\text{Res}\left(\frac{f(x)}{g(x)}, x_0\right) = \frac{f(x_0)}{g'(x_0)} \qquad (4.53)$$

and, from (4.40)

$$f(\lambda_y) = \frac{\lambda_{z\theta}\left(1 - e^{j\lambda_y b}\right)\cos\left(\lambda_{z\theta}d\right)}{\lambda_y^2\left(\lambda_y^2 + \lambda_x^2\right)}$$

$$g(\lambda_y) = \sin\left(\lambda_{z\theta}d\right)$$

Recalling $\lambda_{z\theta} = \sqrt{k_t^2 - \frac{\mu_t}{\mu_z}\lambda_x^2 - \frac{\mu_t}{\mu_z}\lambda_y^2}$, we can find g' by the chain rule:

$$g'(\lambda_y) = \frac{\partial}{\partial\lambda_y}\sin\left(\lambda_{z\theta}d\right) = d\cos\left(\lambda_{z\theta}d\right)\left(\frac{1}{2\lambda_{z\theta}}\right)\left(-2\frac{\mu_t}{\mu_z}\lambda_y\right) = -\frac{\mu_t d\lambda_y}{\mu_z\lambda_{z\theta}}\cos\left(\lambda_{z\theta}d\right)$$

Which allows us to finally write (using the $-\lambda_{yl\theta}$ root):

$$j2\pi\text{Res}(f, \lambda_{z\theta} = \pm\frac{\pi l}{d}) = j2\pi\frac{f(-\lambda_{yl\theta})}{g'(-\lambda_{yl\theta})}$$

The contribution is found to be the sum over all possible values of l:

$$\oint_{\Sigma C_l^+} = \frac{j2\pi\mu_z}{\mu_t d}\sum_{l=0}^{\infty}\left(\frac{\pi l}{d}\right)^2\left[\frac{\left(1 - e^{-j\lambda_{yl\theta}b}\right)}{\lambda_{yl\theta}^3\left(\lambda_{yl\theta}^2 + \lambda_x^2\right)}\right] \qquad (4.54)$$

156

- LHP for TE^z Contribution

For the LHP, Cauchy's Integral Theorem, Jordan's Lemma and Cauchy's Integral Formula allow us to write

$$\int_{-\infty}^{\infty} + \oint_{C_0^-} + \oint_{C_{j\lambda_x}^-} + \oint_{\Sigma C_l^-} + \overbrace{\int_{C_\infty^-}}^{0} = 0$$

$$\implies \int_{-\infty}^{\infty} = -\oint_{C_0^-} - \oint_{C_{-j\lambda_x}^-} - \oint_{\Sigma C_l^-}$$

$$= -j2\pi\text{Res}(f, \lambda_y = 0) - j2\pi\text{Res}(f, \lambda_y = j\lambda_x) - j2\pi\text{Res}(f, \lambda_{z\theta} = \pm\frac{\pi l}{d})$$

Due to the similarities in the terms in (4.40), we find similar forms of the residue contributions, using $\lambda_{y_{p1}} = -j\lambda_x$ and $\lambda_{y_{p2}} = \sqrt{\frac{\mu_z}{\mu_t}\left[k_t^2 - \left(\frac{\pi l}{d}\right)^2\right] - \lambda_x^2}$:

$$-\oint_{C_0^-} = \frac{\pi b\lambda_{z\theta}^*}{\lambda_x^2}\frac{\cos\left(\lambda_{z\theta}^* d\right)}{\sin\left(\lambda_{z\theta}^* d\right)} \tag{4.55}$$

$$-\oint_{j\lambda_x^-} = -\left[\frac{\pi\left(1-e^{-\lambda_x b}\right)}{\lambda_x^3}\right]\left[\frac{k_t\cos\left(k_t d\right)}{\sin\left(k_t d\right)}\right] \tag{4.56}$$

$$-\oint_{\Sigma C_l^-} = \frac{j2\pi\mu_z}{\mu_t d}\sum_{l=0}^{\infty}\left(\frac{\pi^2 l^2}{d^2}\right)\left[\frac{\left(1 - e^{-j\lambda_{yl\theta}b}\right)}{\lambda_{yl\theta}^3\left(\lambda_{yl\theta}^2 + \lambda_x^2\right)}\right] \tag{4.57}$$

The total integral from (4.40) for the TE^z contribution in this case is the combination of these contributions and can be written as

$$\Omega_{\text{TE}}^{(11)} = M_{xm}^h M_{xn}^h k_{xm} k_{xn} \left\{ \frac{j2\pi b\lambda_{z\theta}^*}{\omega\mu_t}\left[\frac{\cos\left(\lambda_{z\theta}^* d\right)}{\sin\left(\lambda_{z\theta}^* d\right)}\right] - \frac{j2\pi\left(1-e^{-\lambda_x b}\right)}{\lambda_x}\left[\frac{k_t\cos\left(k_t d\right)}{\omega\mu_t\sin\left(k_t d\right)}\right] \right.$$

$$\left. - \frac{4\pi\mu_z\lambda_x^2}{\omega\mu_t^2 d}\sum_{l=0}^{\infty}\left(\frac{\pi l}{d}\right)^2\left[\frac{\left(1 - e^{-j\lambda_{yl\theta}b}\right)}{\lambda_{yl\theta}^3\left(\lambda_{yl\theta}^2 + \lambda_x^2\right)}\right]\right\}$$

where

$$\lambda_{z\theta}^* = \sqrt{k_t^2 - \frac{\mu_t}{\mu_z}\lambda_x^2} \quad , \quad \lambda_{yl\theta} = \sqrt{\frac{\mu_z}{\mu_t}\left[k_t^2 - \left(\frac{\pi l}{d}\right)^2\right] - \lambda_x^2}$$

157

TM^z (ψ) Contribution of $\widetilde{G}_{hh,xx}$. The TM^z portion of $\widetilde{G}_{hh,xx}$ is given by (B.12):

$$\widetilde{G}^{\psi}_{hh,xx} = \left(\frac{j\omega\varepsilon_t\lambda_y^2}{2\lambda_{z\psi}\lambda_\rho^2}\right)\left[\frac{\cos\left(\lambda_{z\psi}\left[d-|z-z'|\right]\right) + \cos\left(\lambda_{z\psi}\left[d-(z+z')\right]\right)}{\sin\left(\lambda_{z\psi}d\right)}\right]$$

and recall $\widetilde{G}^{(11)}_{hh,xx} = \widetilde{G}_{hh,xx}(\vec{r}_1|\vec{r}'_1)$, which leads to

$$\widetilde{G}^{\psi(11)}_{hh,xx} = \left(\frac{j\omega\varepsilon_t\lambda_y^2}{\lambda_{z\psi}\lambda_\rho^2}\right)\left[\frac{\cos\left(\lambda_{z\psi}d\right)}{\sin\left(\lambda_{z\psi}d\right)}\right]$$

Therefore, (4.39) becomes

$$j\omega\varepsilon_t M^h_{xm}M^h_{xn}k_{xm}k_{xn}\left\{\int_{-\infty}^{\infty}\left[\frac{\left(1-e^{j\lambda_y b}\right)}{\lambda_y^2+\lambda_x^2}\right]\left[\frac{\cos\left(\lambda_{z\psi}d\right)}{\lambda_{z\psi}\sin\left(\lambda_{z\psi}d\right)}\right]d\lambda_y\right.$$
$$\left.+\int_{-\infty}^{\infty}\left[\frac{\left(1-e^{-j\lambda_y b}\right)}{\lambda_y^2+\lambda_x^2}\right]\left[\frac{\cos\left(\lambda_{z\psi}d\right)}{\lambda_{z\psi}\sin\left(\lambda_{z\psi}d\right)}\right]d\lambda_y\right\} \tag{4.58}$$

with $\lambda_{z\psi} = \sqrt{k_t^2 - \frac{\varepsilon_t}{\varepsilon_z}\lambda_x^2 - \frac{\varepsilon_t}{\varepsilon_z}\lambda_y^2}$, which again shows the need for upper and lower half plane closure. In this case, we need only consider the two poles, $\lambda_y = \pm j\lambda_x$ and $\lambda_{z\psi}\sin\left(\lambda_{z\psi}d\right) = 0$.
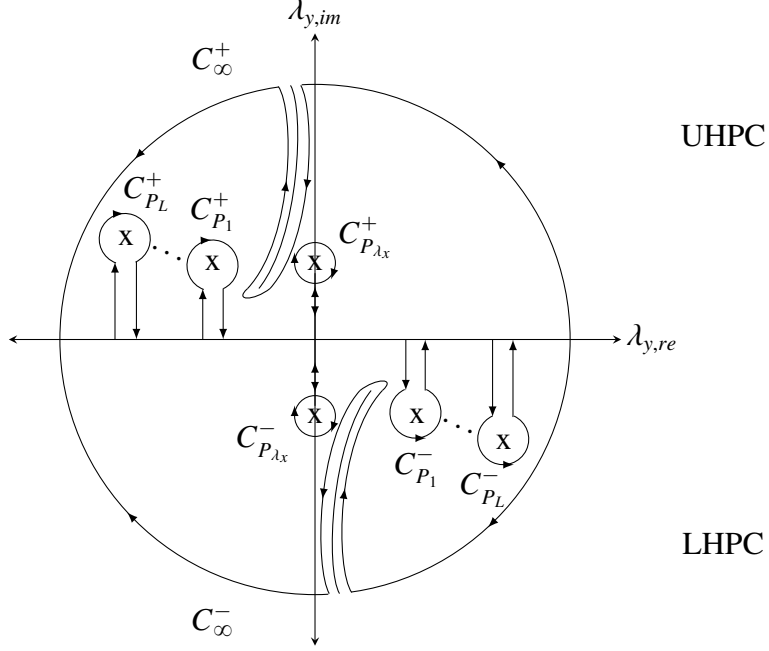
158

Figure 4.4: Complex λ_y plane integration, showing the singularities at $\lambda_y = \pm J\lambda_x$ and $\lambda_y = \pm\sqrt{\frac{\mu_z}{\mu_t}\left[k_t^2 - \left(\frac{\pi l}{d}\right)^2\right] - \lambda_x^2}$. The branch cuts arise from the multi-valuedness of the radical in the argument of the sine term. The branch point at $l = 0$ is removable, based on the form of the numerator.

- UHP for TM^z Contribtion

  For the UHP, according to Cauchy's Integral Theorem and Cauchy's Integral Formula, we have

$$\int\limits_{-\infty}^{\infty} + \oint\limits_{C_{j\lambda_x}^+} + \oint\limits_{\Sigma C_l^+} + \overbrace{\int\limits_{C_\infty^+}}^{0} = 0$$

$$\implies \int\limits_{-\infty}^{\infty} = -\oint\limits_{C_{j\lambda_x}^+} - \oint\limits_{\Sigma C_l^+} = \oint\limits_{j\lambda_x^+} \oint\limits_{\Sigma C_l^+}$$

$$= j2\pi\text{Res}(f, \lambda_y = j\lambda_x) + j2\pi\text{Res}(f, \lambda_{z\psi} = -\lambda_{y_{l\psi}})$$

159

1. $C^+_{j\lambda_x}$ Pole

For the simple pole at $\lambda_y = j\lambda_x$, we have

$$j2\pi\text{Res}(f, \lambda_y{=}j\lambda_x) = \lim_{\lambda_y \to j\lambda_x} j2\pi\,(\lambda_y - j\lambda_x) \left[\frac{\left(1 - e^{j\lambda_y b}\right)}{(\lambda_y + j\lambda_x)\,(\lambda_y - j\lambda_x)} \right] \left[\frac{\cos(\lambda_{z\psi}d)}{\lambda_{z\psi}\sin(\lambda_{z\psi}d)} \right]$$

$$= \left[\frac{\pi\left(1 - e^{-\lambda_x b}\right)}{\lambda_x} \right] \left[\frac{\cos(k_t d)}{k_t \sin(k_t d)} \right] \tag{4.59}$$

where, again, $\lambda_{z\psi}$ reduces to k_t.

2. C^+_l Poles

In order to determine the residue for the second contribution, we again use (4.53), with $\lambda_{y_{l\psi}} = \pm\sqrt{\frac{\varepsilon_z}{\varepsilon_t}\left[k_t^2 - \left(\frac{\pi l}{d}\right)^2\right] - \lambda_x^2}$.

$$j2\pi\text{Res}(f, -\lambda_{y_{l\psi}}) = j2\pi\frac{f(-\lambda_{y_{l\psi}})}{g'(-\lambda_{y_{l\psi}})}$$

where

$$f(\lambda_y) = \frac{\left(1 - e^{j\lambda_y b}\right)\cos(\lambda_{z\psi}d)}{\lambda_y^2 + \lambda_x^2}$$

$$g(\lambda_y) = \lambda_{z\psi}\sin(\lambda_{z\psi}d)$$

Recalling $\lambda_{z\psi} = \sqrt{k_t^2 - \frac{\varepsilon_t}{\varepsilon_z}\lambda_x^2 - \frac{\varepsilon_t}{\varepsilon_z}\lambda_y^2}$, we can find g' using the chain rule and the product rule.

$$g'(\lambda_y) = \frac{\partial}{\partial\lambda_y}\lambda_{z\psi}\sin(\lambda_{z\psi}d) = \lambda_{z\psi}\frac{\partial}{\partial\lambda_y}\sin(\lambda_{z\psi}d) + \sin(\lambda_{z\psi}d)\frac{\partial}{\partial\lambda_y}\lambda_{z\psi}$$

Evaluating at $\lambda_y = -\lambda_{y_{l\psi}}$, we have

$$g'(-\lambda_{y_{l\psi}}) = \frac{\varepsilon_t\lambda_{y_{l\psi}}}{\varepsilon_z}\left[d\cos(\pi l) + \frac{\sin(\pi l)}{\frac{\pi l}{d}} \right] = \frac{d\varepsilon_t\lambda_{y_{l\psi}}}{\varepsilon_z}\left[(-1)^l + \delta_{0,l} \right] \tag{4.60}$$

160

Therefore, the residue contribution to the integral is

$$j2\pi \text{Res}(f, -\lambda_{y_{l\psi}}) = \frac{j2\pi\varepsilon_z}{d\varepsilon_t} \sum_{l=0}^{\infty} \frac{\left(1 - e^{-j\lambda_{y_{l\psi}}b}\right)}{\lambda_{y_{l\psi}} \left(\lambda_{y_{l\psi}}^2 + \lambda_x^2\right) [1 + \delta_{0,l}]}$$

$$\lambda_{y_{l\psi}} = \sqrt{\frac{\varepsilon_z}{\varepsilon_t}\left[k_t^2 - \left(\frac{\pi l}{d}\right)^2\right] - \lambda_x^2} \quad , \qquad \delta_{0,l} = \begin{cases} 1 & l = 0 \\ 0 & l \neq 0 \end{cases}$$

$$(4.61)$$

- LHP for TM^z Contribution

For the LHP, we have

$$\int_{-\infty}^{\infty} + \oint_{C_{j\lambda_x}^+} + \oint_{\Sigma C_l^+} + \overbrace{\int_{C_\infty^+}}^{0} = 0$$

$$\implies \int_{-\infty}^{\infty} = -\oint_{C_{j\lambda_x}^+} - \oint_{\Sigma C_l^+}$$

$$= -j2\pi\text{Res}(f, \lambda_y = j\lambda_x) - j2\pi\text{Res}(f, \lambda_{z\psi} = \lambda_{y_{l\psi}})$$

Due to the similar forms of the terms of (4.58), we easily see the LHP contributions to be

$$\int_{-\infty}^{\infty} = \pi\left[\frac{\left(1 - e^{-\lambda_x b}\right)}{\lambda_x}\right]\left[\frac{\cos(k_t d)}{k_t \sin(k_t d)}\right] + \frac{j2\pi\varepsilon_z}{d\varepsilon_t}\sum_{l=0}^{\infty}(-1)^l\frac{\left(1 - e^{-j\lambda_{y_{l\psi}}b}\right)}{\lambda_{y_{l\psi}}\left(\lambda_{y_{l\psi}}^2 + \lambda_x^2\right)[(-1)^l + \delta_{0,l}]}$$

$$\lambda_{y_{l\psi}} = \sqrt{\frac{\varepsilon_z}{\varepsilon_t}\left[k_t^2 - \left(\frac{\pi l}{d}\right)^2\right] - \lambda_x^2} \quad , \qquad \delta_{0,l} = \begin{cases} 1 & l = 0 \\ 0 & l \neq 0 \end{cases}$$

$$(4.62)$$

161

Therefore, the total integral for the TM^z contribution from (4.58) is given as

$$
\Omega_{\text{TM}}^{(11)} = M_{xm}^h M_{xn}^h k_{xm} k_{xn} \left\{ \left[\frac{j2\pi \left(1 - e^{-\lambda_x b}\right)}{\lambda_x} \right] \left[\frac{\omega \varepsilon_t \cos\left(k_t d\right)}{k_t \sin\left(k_t d\right)} \right] \right.
$$

$$
\left. - \frac{4\pi \omega \varepsilon_z}{d} \sum_{l=0}^{\infty} \frac{\left(1 - e^{-j\lambda_{y_{l\psi}} b}\right)}{\lambda_{y_{l\psi}} \left(\lambda_{y_{l\psi}}^2 + \lambda_x^2\right) \left[1 + \delta_{0,l}\right]} \right\}
$$

$$
\lambda_{y_{l\psi}} = \sqrt{\frac{\varepsilon_z}{\varepsilon_t} \left[k_t^2 - \left(\frac{\pi l}{d}\right)^2\right] - \lambda_x^2} \quad , \qquad \delta_{0,l} = \begin{cases} 1 & l = 0 \\ \\ 0 & l \neq 0 \end{cases}
$$

Noting that $\frac{\omega \varepsilon_t}{k_t} = \frac{k_t}{\omega \mu_t} = \frac{1}{\eta_t}$, we see the terms originating from the $\lambda_y = \pm j\lambda_x$ cancel out.

Therefore, for $w_m = w_n = 0 \implies k_{xm} = k_{xn} = 0$, $A_{mn}^{(11)}$ becomes

162

$$A_{mn}^{(11)} = \frac{1}{Z_m Z_n} \delta_{m,n} - \frac{Z_n M_{xm}^h M_{xn}^h k_{xm} k_{xn}}{4\pi^2} \int\limits_{-\infty}^{\infty} C^{\lambda_x} \left(\Omega_{\text{TE}}^{(11)} + \Omega_{\text{TM}}^{(11)} \right) d\lambda_x$$

where:

$$C^{\lambda_x} = \left[\frac{\left(1 - (-1)^{v_m} e^{j\lambda_x a}\right)\left(1 - (-1)^{v_n} e^{-j\lambda_x a}\right)}{\left(\lambda_x + k_{xm}\right)\left(\lambda_x - k_{xm}\right)\left(\lambda_x + k_{xn}\right)\left(\lambda_x - k_{xn}\right)} \right]$$

$$\Omega_{\text{TE}}^{(11)} = \frac{j 2\pi b \lambda_{z\theta}^*}{\omega \mu_t} \left[\frac{\cos\left(\lambda_{z\theta}^* d\right)}{\sin\left(\lambda_{z\theta}^* d\right)} \right] - \frac{4\pi \mu_z \lambda_x^2}{\omega \mu_t^2 d} \sum_{l=0}^{\infty} \left(\frac{\pi l}{d} \right)^2 \frac{\left(1 - e^{-j\lambda_{y_{l\theta}} b}\right)}{\lambda_{y_{l\theta}}^3 \left(\lambda_{y_{l\theta}}^2 + \lambda_x^2\right)}$$

$$\Omega_{\text{TM}}^{(11)} = -\frac{4\pi \omega \varepsilon_z}{d} \sum_{l=0}^{\infty} \frac{\left(1 - e^{-j\lambda_{y_{l\psi}} b}\right)}{\lambda_{y_{l\psi}} \left(\lambda_{y_{l\psi}}^2 + \lambda_x^2\right) \left[1 + \delta_{0,l}\right]}$$

(4.63)

with:

$$\lambda_{z\theta}^* = \sqrt{k_t^2 - \frac{\mu_t}{\mu_z} \lambda_x^2} \qquad\qquad k_{x\alpha} = \frac{\pi v_\alpha}{a} \dots \alpha = m, n$$

$$\lambda_{y_{l\theta}} = \sqrt{\frac{\mu_z}{\mu_t}\left[k_t^2 - \left(\frac{\pi l}{d}\right)^2\right] - \lambda_x^2} \qquad\qquad k_{y\alpha} = \frac{\pi w_\alpha}{b} \dots \alpha = m, n$$

$$\lambda_{y_{l\psi}} = \sqrt{\frac{\varepsilon_z}{\varepsilon_t}\left[k_t^2 - \left(\frac{\pi l}{d}\right)^2\right] - \lambda_x^2}$$

The values for the $M_{hx,hy}^{m,n}$ and $Z_{m,n}$ terms can be found in (4.21).

4.4.2   Case I: $w_m = w_n = 0$ ($A_{mn}^{(12)}$).

In the simplest case, when both $\text{TE}_{v_m 0}^z$ (observation) and $\text{TE}_{v_n 0}^z$ (source) modes are present, we have $w_m = w_n = 0 \implies k_{xm} = k_{xn} = 0$ and the inner integral of the $A_{mn}^{(12)}$ coefficient becomes very similar to (4.39):

$$\int\limits_{-\infty}^{\infty} \frac{M_{xm}^h M_{xn}^h k_{xm} k_{xn}}{\lambda_y^2} \widetilde{G}_{hh,xx}^{12} \left[\left(1 - e^{j\lambda_y b}\right)\left(1 - e^{-j\lambda_y b}\right) \right] d\lambda_y \qquad (4.64)$$

163

Following the same methods as above, we find the $A_{mn}^{(12)}$ coefficient to be:

$$A_{mn}^{(12)} = \frac{Z_n M_{xm}^h M_{xn}^h k_{xm} k_{xn}}{4\pi^2} \int\limits_{-\infty}^{\infty} C^{\lambda_x} \left(\Omega_{\text{TE}}^{(12)} + \Omega_{\text{TM}}^{(12)} \right) d\lambda_x$$

where:

$$C^{\lambda_x} = \left[\frac{\left(1-(-1)^{v_m} e^{j\lambda_x a}\right)\left(1-(-1)^{v_n} e^{-j\lambda_x a}\right)}{(\lambda_x+k_{xm})(\lambda_x-k_{xm})(\lambda_x+k_{xn})(\lambda_x-k_{xn})} \right]$$

$$\Omega_{\text{TE}}^{(12)} = \frac{j2\pi b \lambda_{z\theta}^*}{\omega\mu_t} \left[\frac{1}{\sin\left(\lambda_{z\theta}^* d\right)} \right]$$
$$- \frac{4\pi\mu_z \lambda_x^2}{\omega\mu_t^2 d} \sum_{l=0}^{\infty} (-1)^l \left(\frac{\pi l}{d}\right)^2 \left[\frac{1-e^{-j\lambda_{y l\theta} b}}{\lambda_{y l\theta}^3 \left(\lambda_{y l\theta}^2 + \lambda_x^2\right)} \right]$$

$$\Omega_{\text{TM}}^{(12)} = -\frac{4\pi\omega\varepsilon_z}{d} \sum_{l=0}^{\infty} \frac{\left(1-e^{-j\lambda_{y l\psi} b}\right)}{\lambda_{y l\psi} \left(\lambda_{y l\psi}^2 + \lambda_x^2\right) \left[(-1)^l + \delta_{0,l}\right]}$$

with

$$\lambda_{z\theta}^* = \sqrt{k_t^2 - \frac{\mu_t}{\mu_z}\lambda_x^2} \qquad\qquad k_{x\alpha} = \frac{\pi v_\alpha}{a} \dots \alpha = m, n$$

$$\lambda_{y l\theta} = \sqrt{\frac{\mu_z}{\mu_t}\left[k_t^2 - \left(\frac{\pi l}{d}\right)^2\right] - \lambda_x^2} \qquad k_{y\alpha} = \frac{\pi v_\alpha}{b} \dots \alpha = m, n$$

$$\lambda_{y l\psi} = \sqrt{\frac{\varepsilon_z}{\varepsilon_t}\left[k_t^2 - \left(\frac{\pi l}{d}\right)^2\right] - \lambda_x^2}$$

(4.65)

Again, we recall that the values for the $M_{hx,hy}^{m,n}$ and $Z_{m,n}$ terms can be found in (4.21). Note that the λ_x integrals cannot be evaluated analytically, as the $\lambda_{y l\theta}$ or $\lambda_{y l\psi}$ points become non-removable branch points in the λ_x plane, as the integrands are not even with respect to $\lambda_{y l\theta}$ or $\lambda_{y l\psi}$. Therefore, we will evaluate the λ_x integrals numerically.

Now that we have obtained expressions for the 2N x 2N system of (4.19), we must determine the theoretical reflection and transmission coefficients. Recall, they are given by (4.1) and (4.2), respectively. The reflection coefficient (S_{11}) is (where a_q^- is given by

(4.5) and $\vec{e}_{a1}$ is the MoM expansion term of (4.16)):

$$S_{11}^{\text{thy}} = R_1 = \frac{a_1^-}{a_1^+} = C_1^{(1)} - 1 \tag{4.66}$$

Similarly, the transmission coefficient (S_{21}) is (with b_q^+ given by (4.8) and $\vec{e}_{a2}$ is the MoM expansion term of (4.16)):

$$S_{21}^{\text{thy}} = T_1 = \frac{b_1^+}{a_1^+} = C_1^{(2)} \tag{4.67}$$

Therefore, we see that, even though we consider N modes through the MoM solution, the theoretical reflection and transmission coefficients depend only on the first C_1 terms. At this point, all that remains of the extraction is to minimize the difference between the theoretical scattering terms and the measured data:

$$\arg\min_{\varepsilon_t, \varepsilon_z, \mu_t, \mu_z \in \mathbb{C}} \left\| \begin{bmatrix} S_{11}^{\text{thy}}(f, d; \varepsilon_t, \varepsilon_z, \mu_t, \mu_z) - S_{11}^{\text{exp}}(f) \\ S_{21}^{\text{thy}}(f, d; \varepsilon_t, \varepsilon_z, \mu_t, \mu_z) - S_{21}^{\text{exp}}(f) \\ S_{12}^{\text{thy}}(f, d; \varepsilon_t, \varepsilon_z, \mu_t, \mu_z) - S_{12}^{\text{exp}}(f) \\ S_{22}^{\text{thy}}(f, d; \varepsilon_t, \varepsilon_z, \mu_t, \mu_z) - S_{22}^{\text{exp}}(f) \end{bmatrix} \right\|_2 \tag{4.68}$$

which can be performed on a point-by-point basis using a non-linear least-squares method, such as the Levenberg-Marquardt or Trust Region Reflective (TRR) method [63]. We note here, that the above development is only valid for extracting two complex parameters. Therefore, we could use it to extract the permittivity from a dielectric uniaxial, magnetically isotropic material (where the permeability is known). An additional independent measurement would be required to extract all four uniaxial constitutive parameters. The two-thickness method (TTM) could be used in such a case.

This chapter has demonstrated the computation of the dominant mode scattering parameters (Case I). These computations have been repeated for Cases II-V and the relevant expressions are found in Appendix E.

V.   Measurement of Uniaxial Media by the tFWMT

Now that we have developed the MFIE's which describe the scattering parameters for a uniaxial media in the tFWMT configuration, we must determine a suitable method by which we may solve the reverse problem. This reverse problem consists of minimizing the difference between the theoretical scattering parameters and the experimentally measured scattering parameters. This chapter describes the computational method (which has been implemented in MATLAB®), the laboratory configuration and results for a variety of materials.

5.1   Computational Method

This section will discuss the structure and flow of the computational method used to solve the minimization problem, detailing some of the complications that arise by virtue of the complexity of the problem. To the knowledge of the author, such a detailed description of the code has not been given in any previous literature. Therefore, the present section represents a significant contribution to the measurement community in two ways: it allows the current results to be reproduced for a wide variety of research applications and it allows for future codes to be built based on the current code, rather than from scratch. The full code is available in Appendix F. MATLAB® was used extensively in the extraction of the constitutive parameters. The least squares routine is an iterative process that calculates numerical values for functions with dependencies on the unknown constitutive parameters. Therefore, the problem can be written in the forward sense, creating functions depending on values for $\varepsilon_t, \varepsilon_z, \mu_t$ and μ_z and the least squares program will iteratively solve this function for the values which best minimize the problem at hand (4.68). The program is widely configurable across the scope of our problem, allowing

the user to choose downsampling, the modes which are used for the MoM solution, the type of problem under consideration (uniaxial or isotropic; dielectric, magnetic or both) and the specific type of LSQ algorithm to use (TRR or L-M). Furthermore, the program contains the ability to utilize the TTM to extract both the permittivity and permeability from a dielectric and magnetic uniaxial material. For this more general type of material, we require two independent measurement sets (transmission and reflection for each set), obtained by measuring two different thicknesses of the same material. A basic flowchart of the program is given in Figure 5.1. Each block will be discussed in detail in the following subsections.
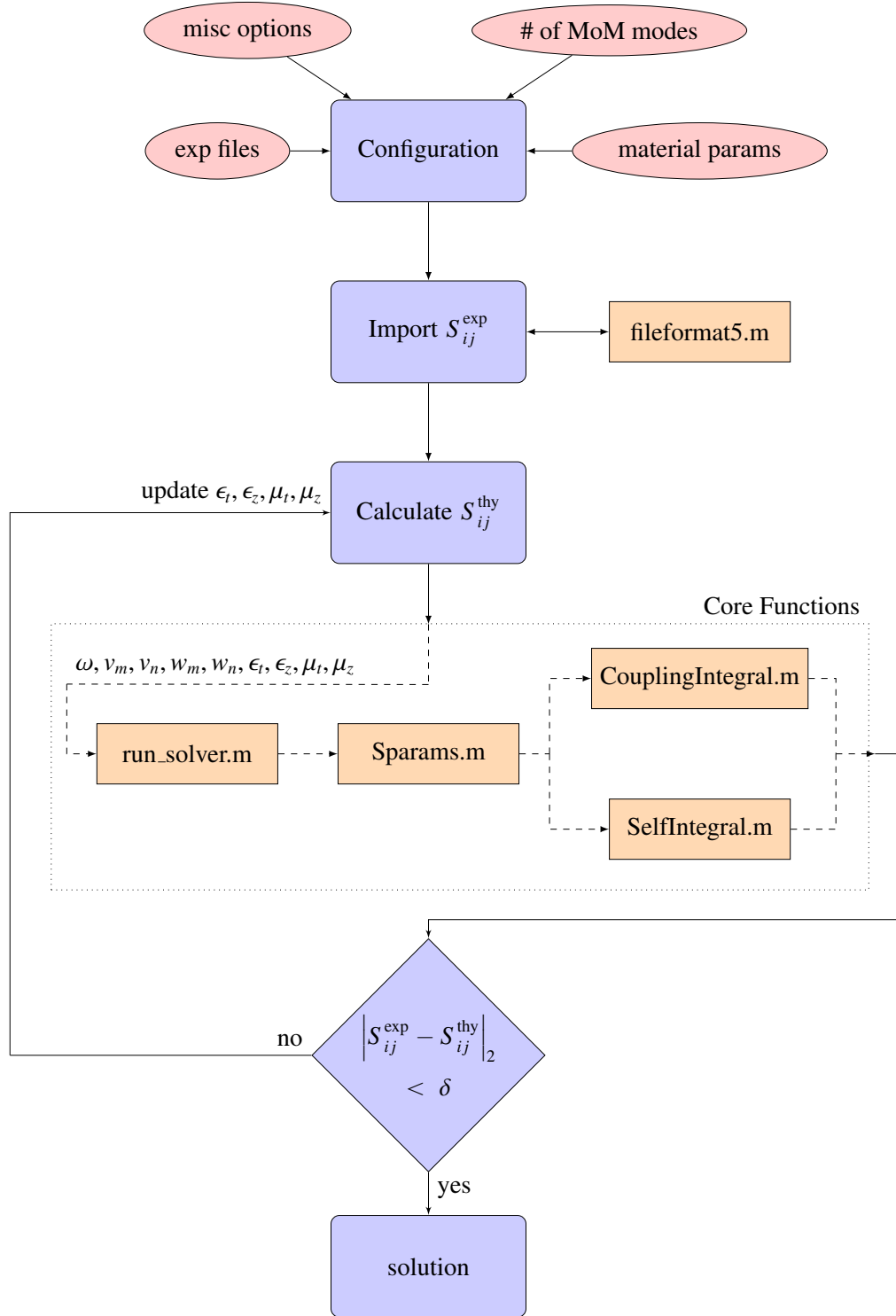
Figure 5.1: A basic flowchart describing the extraction program in MATLAB® . The orange blocks represent the critical functions required by the program. Note that the lower half of the flowchart is repeated for each frequency point.

5.1.1 Configuration.

This portion of the program allows the user to define many of the required parameters and options for the program to run. The required parameters are:

- Input file: the input file string is assembled by combining the material type, measurement method, version and thickness (d1 or d2). The selected naming convention is: fgm125_tfwmt_v1_d1.txt, where the *.cti files from the VNA have been renamed to *.txt files. The first term (fgm125) specifies the material name, the second (tfwmt) refers to the measurement technique, the third (v1) specification represents the version of the measurement and the final term (d1) gives the thickness (when more than one thickness is required).

- Downsampling: since the measured data may contain as many as 1600 points, the program downsamples to `numds` points using a standard 1D linear interpolation.

- Solver options

  - TRR or L-M algorithm: The program uses MATLAB®'s `lsqcurvefit` as the iterative least squares solver. As such, either a Trust Region Reflective (TRR) or Levenburg-Marquardt (L-M) algorithm is available. The TRR is selected by default, due to the fact that it allows for upper and lower bounds to be set on the search region. Since we are assuming non-negative constitutive parameters, this allows us to confine the root search for the real part of the constitutive parameters to values above zero and below some large value (50, for example) and also to confine the search for the imaginary part to below zero.

  - Initial guess method: Although least squares methods are not terribly sensitive to the initial guess, the program allows for selection of 3 methods of providing initial guesses across the band: a single initial guess value for each frequency point (`initone`); initial guess for the first frequency point and update the next

guess based on the solution (`initup`); or known values, from NRW or other measurements (`nrw`).

- Number of modes to consider (*m* and *n*): the indices *m* and *n* determine which modes are considered in the MoM solution. Recall that the index *m* refers to the observation modes, while the index *n* refers to the source modes. Also, recall that the indices $m, n = 1, 2, \ldots, \infty$ and correspond to a list of modes organized from lowest cutoff frequency to highest cutoff frequency. The first 20 of these modes are given in Appendix D.

- The desired parameters which are sought (from the set of $\varepsilon_t, \varepsilon_z, \mu_t, \mu_z$) and whether the material is treated as uniaxial or isotropic. It has already been shown that the uniaxial Green's function easily reduces to the isotropic case when $\varepsilon_t = \varepsilon_z = \varepsilon$ and $\mu_t = \mu_z = \mu$, therefore, it is useful to have a code which incorporates both cases. It will be shown later that the results for a well-characterized isotropic material, such as ECCOSORB® FGM125 agree well with those published in the previous literature.

- Known material parameters (such as thicknesses, $\vec{d} = \begin{bmatrix} d_1 \\ d_2 \end{bmatrix}$).

- The parameter `porttouse` allows the specification of whether to use port 1 excited S-parameters (S_{11} and S_{21}), port 2 excited S-parameters (S_{22} and S_{12}) or all four.

- Miscellaneous options are available, which make batch running of the program slightly easier, as well as allowing for debugging or testing of new materials.

5.1.2   Import Experimental Data.

The VNA outputs data files in a *.cti format, which include the frequency points followed by a column list of S-parameter values in *real,imag* format. This is a bit more difficult than a standard format, such as *.csv. Therefore, the fileformat5.m function has been written to parse the *.cti files. It provides an output cell array [*S*, *svarnames*], where the first

column of S represents the frequency points and the subsequent columns are the real and imaginary parts of S_{ij} (the scattering parameters). Each corresponding position in the cell array *svarnames* provides a string of the S-parameter name (S_{11}, S_{21}, S_{12} and S_{22}), so that the appropriate values may be associated with the correct S-parameter. Finally, the data is downsampled, parsed and formatted in a way that is appropriate for the LSQ solver.

5.1.3 Calculation of Theoretical Scattering Parameters.

The calculation of the theoretical S-parameters is at the core of the program. The MATLAB® command `lsqcurvefit` only allows as inputs the variables to be solved for. Therefore, some parameters, which are frequency dependent and yet are required for the integrals of (4.63) and (4.65) are declared as global at the beginning of each frequency loop. Additionally, some frequency independent parameters, such as $d1, d2, a, b, \mu_0, \varepsilon_0$, etc. are maintained at the global level for ease of access to the integral functions.

5.1.3.1 run_solver.m function.

The run_solver.m function controls what parameters are passed to the integral calculations. This primarily depends on the configuration parameter `solveCase`, which determines how the material is being treated. The available options are:

1. Isotropic, dielectric, non-magnetic ($\varepsilon_t = \varepsilon_z = \varepsilon_r$ and $\mu_t = \mu_z = \mu_0$)

2. Isotropic, non-dielectric, magnetic ($\varepsilon_t = \varepsilon_z = \varepsilon_0$ and $\mu_t = \mu_z = \mu_r$)

3. Isotropic, dielectric, magnetic ($\varepsilon_t = \varepsilon_z = \varepsilon_r$ and $\mu_t = \mu_z = \mu_r$)

4. Uniaxial, dielectric, non-magnetic ($\varepsilon_t \neq \varepsilon_z$ and $\mu_t = \mu_z = \mu_0$)

5. Uniaxial, non-dielectric, magnetic ($\varepsilon_t = \varepsilon_z = \varepsilon_0$ and $\mu_t \neq \mu_z$)

6. Uniaxial, dielectric, magnetic ($\varepsilon_t \neq \varepsilon_z$ and $\mu_t \neq \mu_z$)

171

7. Uniaxial with known et and mut (ε_t and μ_t set to known values, then solve for ε_z and μ_z).

5.1.3.2   *Sparams.m function.*

The Sparams.m function calculates values for the constitutive parameters and calculates the theoretical S-parameters based on (4.66) and (4.67). The function is able to calculate these theoretical parameters for either one thickness or two, based on the number of values provided for $\vec{d}$ in the configuration. As a part of this function, we have included the logic required to account for all possible values of m and n and building the complete A dyad. The Sparams.m function calls the CouplingIntegral.m and SelfIntegral.m functions in order to calculate the numerical values of the integrals. The final output of this function is given in the same form into which the measured data is parsed, corresponding to (4.68):

$$\vec{S}^{\text{thy}} = \begin{bmatrix} S_{11}^{\text{thy},d_1} \\ S_{21}^{\text{thy},d_1} \\ S_{12}^{\text{thy},d_1} \\ S_{22}^{\text{thy},d_1} \\ S_{11}^{\text{thy},d_2} \\ S_{21}^{\text{thy},d_2} \\ S_{12}^{\text{thy},d_2} \\ S_{22}^{\text{thy},d_2} \end{bmatrix} \tag{5.1}$$

5.1.3.3   *CouplingIntegral.m and SelfIntegral.m functions.*

The CouplingIntegral.m and SelfIntegral.m functions are written to calculate the scattering parameters from the coefficients $A_{mn}^{(11)}$ and $A_{mn}^{(12)}$, given inputs of the sample thickness(es) ($\vec{d}$), frequency (f), mode indices under consideration (m, n) and, of course, the constitutive parameters ($\varepsilon_t, \varepsilon_z, \mu_t, \mu_z$). Within the A coefficients, it is clear that we must calculate the numerical integral in the λ_x plane. This is accomplished using the command `quadgk` in

MATLAB®. This particular command is able to handle the singularities of the integral and integrate over infinite limits.

A second complexity faced during the calculation of the $A_{mn}^{(ik)}$ coefficients is determining the number of l values over which the sums converge. Consider, for example, the sum found in the $\Omega_{\mathrm{TE}}^{(11)}$ term:

$$\sum_{l=0}^{\infty} \left(\frac{\pi l}{d}\right)^2 \frac{\left(1 - e^{-j\lambda_{yl\theta}b}\right)}{\lambda_{yl\theta}^3 \left(\lambda_{yl\theta}^2 + \lambda_x^2\right)} \tag{5.2}$$

For a given value of λ_x, this term is seen to approach superlinear convergence for values above $l = 100$. Figure 5.2 clearly demonstrates this convergence, regardless of the value of λ_x (since the sum is contained in an integral over the λ_x plane). In this figure, the linear convergence is defined as $\mu = \dfrac{\Omega_{\mathrm{TE}l}^{(11)}}{\Omega_{\mathrm{TE}l-1}^{(11)}}$. In order to balance computational time with accuracy, we choose $l_{max} = 100$. The same behavior can be shown for the other sum terms in $A_{mn}^{(11)}$ and $A_{mn}^{(12)}$.

A third and unexpected difficulty in translating the theory to a numerical application is found in the calculation of $\lambda_{yl\theta}$ and $\lambda_{yl\psi}$. When $|\mathrm{Im}(\mu_t)| < |\mathrm{Im}(\mu_z)|$ or $|\mathrm{Im}(\varepsilon_t)| < |\mathrm{Im}(\varepsilon_z)|$, MATLAB® allows the phase to cross over the branch point of the complex plane (which is typically defined at $\theta = -\pi$) and $\lambda_{yl\theta}$ diverges, causing the sum term of $\Omega_{\mathrm{TE}}^{(11)}$ to also diverge. Since this is a non-physical behavior, the least squares solver is unable to converge to a solution. We hypothesized that this crossing of the branch point, which is not allowed, is due to the simultaneous multiplication/division of three complex quantities. Therefore, in order to reduce the number of simultaneous operations, we can algebraically manipulate the original forms and re-write $\lambda_{yl\theta}$ and $\lambda_{yl\psi}$ as:

$$\begin{aligned}
\lambda_{yl\theta} &= k_{tz} \sqrt{1 - \left(\frac{\pi l}{dk_t}\right)^2 - \left(\frac{\lambda_x}{k_{tz}}\right)^2} \\
\lambda_{yl\psi} &= k_{zt} \sqrt{1 - \left(\frac{\pi l}{dk_t}\right)^2 - \left(\frac{\lambda_x}{k_{zt}}\right)^2}
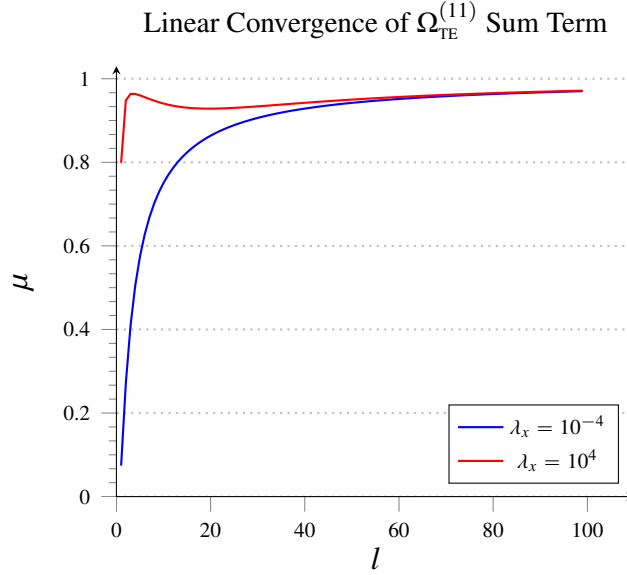\end{aligned} \tag{5.3}$$

173

Figure 5.2: The linear convergence of the $\Omega_{\text{TE}}^{(11)}$ sum term, defined as $\mu = \dfrac{\Omega_{\text{TE}l}^{(11)}}{\Omega_{\text{TE}l-1}^{(11)}}$. Since the term is contained in an integral over λ_x, the sum is computed for two extreme values of λ_x. Clearly, for both values, the sum approaches superlinear convergence by the value $l = 100$.

where

$$k_{tz} = \sqrt{\omega^2 \varepsilon_t \mu_z} \quad \text{and} \quad k_{zt} = \sqrt{\omega^2 \varepsilon_z \mu_t} \tag{5.4}$$

This leads to a stable computation of the sum terms, which in turn, leads to a stable solution from the least squares solver.

5.2 Validation of Code

Now that we have given a general overview of the code which has been constructed to extract the uniaxial constitutive parameters, we would like to establish that it works properly. To that end, we will start by comparing the theoretical scattering parameters calculated by letting $\varepsilon_z = \varepsilon_t$ and $\mu_z = \mu_t$ with a set of measured data for an isotropic

174

material, FGM125. Then, we will compare the extracted parameters of FGM 125 with an established method.

Figure 5.3 shows a comparison of the theoretical, calculated scattering parameters and the experimentally measured ones. This calculation uses only the dominant mode assumption. The values for ε_r and μ_r were determined from Nicholson-Ross-Weir (NRW) analysis of data obtained from rectangular waveguide measurements. Even when using only the dominant mode solution, the theoretical scattering parameters are in good agreement with the measured ones. Therefore, we conclude that the Sparams.m function has been correctly implemented for the isotropic case.
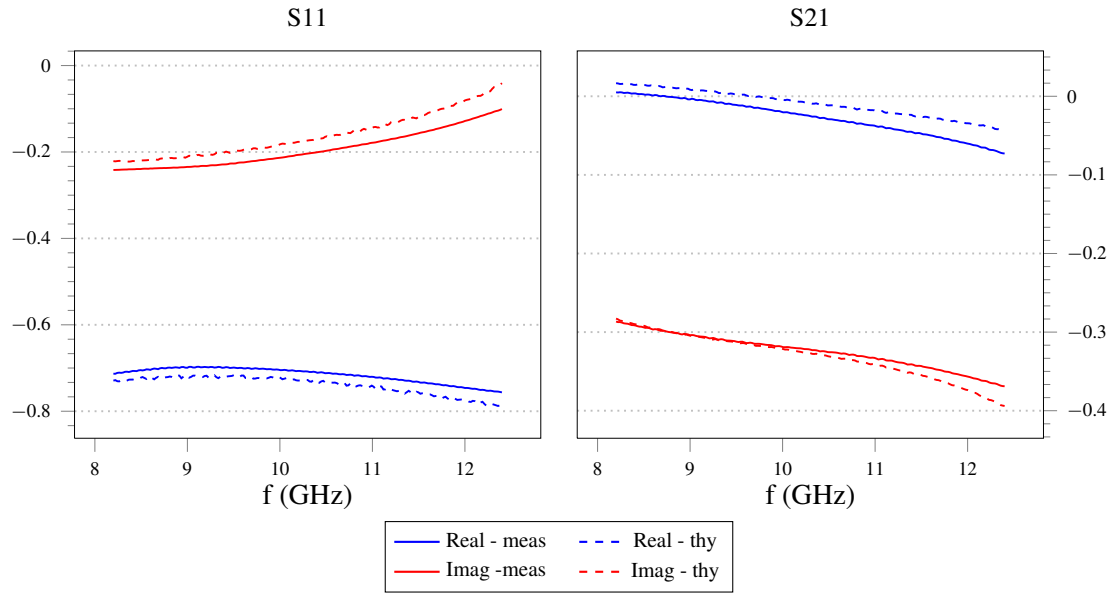

Figure 5.3: A comparison of theoretical parameters calculated using the Sparams.m function and those measured using the tFWMT for FGM125. The theoretical calculations used only the dominant mode.

At this point, we would like to compare the results of extractions performed on isotropic media using this code with a well-known method, such as the NRW method. FGM125 is

well characterized in previous publications and can therefore be used as a benchmark for validating this code. Even though FGM 125 is a magnetic material, we are able to use the TTM to extract both the permittivity and permeability. Figure 5.4 demonstrates extractions on FGM125 material where the material was assumed to be isotropic and only the dominant mode was used in the extraction process. Although the results are close, we expect a greater accuracy may be achieved by incorporating higher order modes.
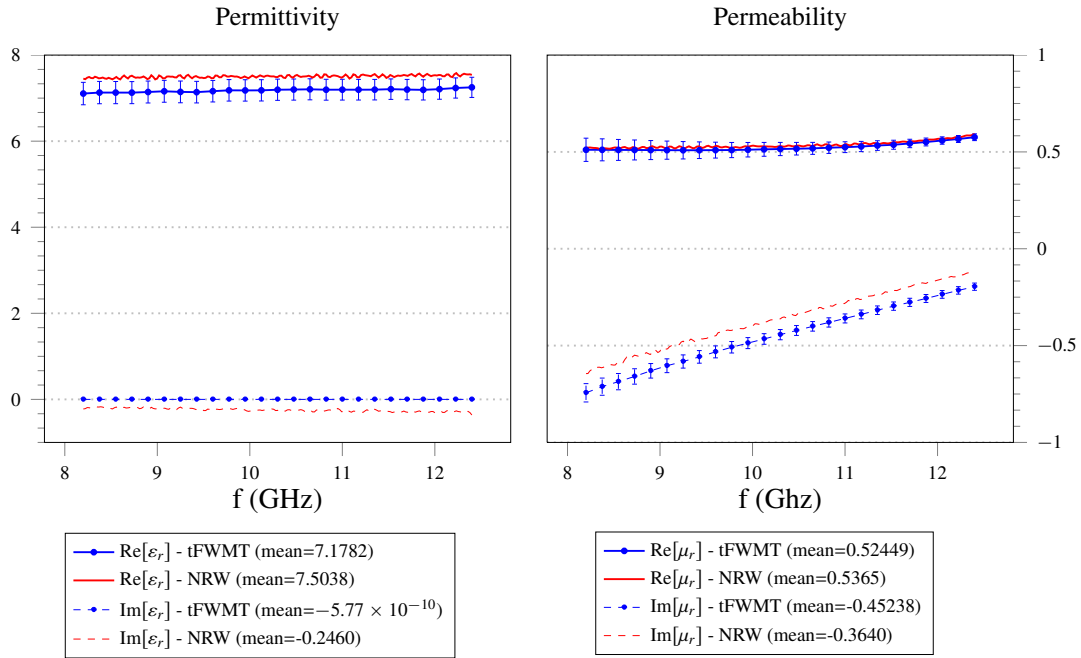

Figure 5.4: A comparison of tFWGT and NRW FGM125 measurements, where the parameters were extracted by treating the material as isotropic (i.e. - $\varepsilon_t = \varepsilon_z$ and $\mu_t = \mu_z$). This extraction was performed using only the dominant mode.

Finally, it should be noted that applying the full uniaxial extraction method, whereby $\varepsilon_t \neq \varepsilon_z$ and $\mu_t \neq \mu_z$ to an isotropic media produces poor results in the longitudinal (z) direction, assuming the material is indeed isotropic. Figure 5.5 clearly demonstrates this phenomenon. At first, this would appear to be a result of the lack of a $\hat{\mathbf{z}}-$directed electric

field component, which precludes the fields in the system from physically interrogating ε_z. However, we also see the results for μ_z are equally unstable. Therefore, we defer on making a conclusion until further measurements can be performed, but note that considering higher order modes in the MoM solution should improve these results.
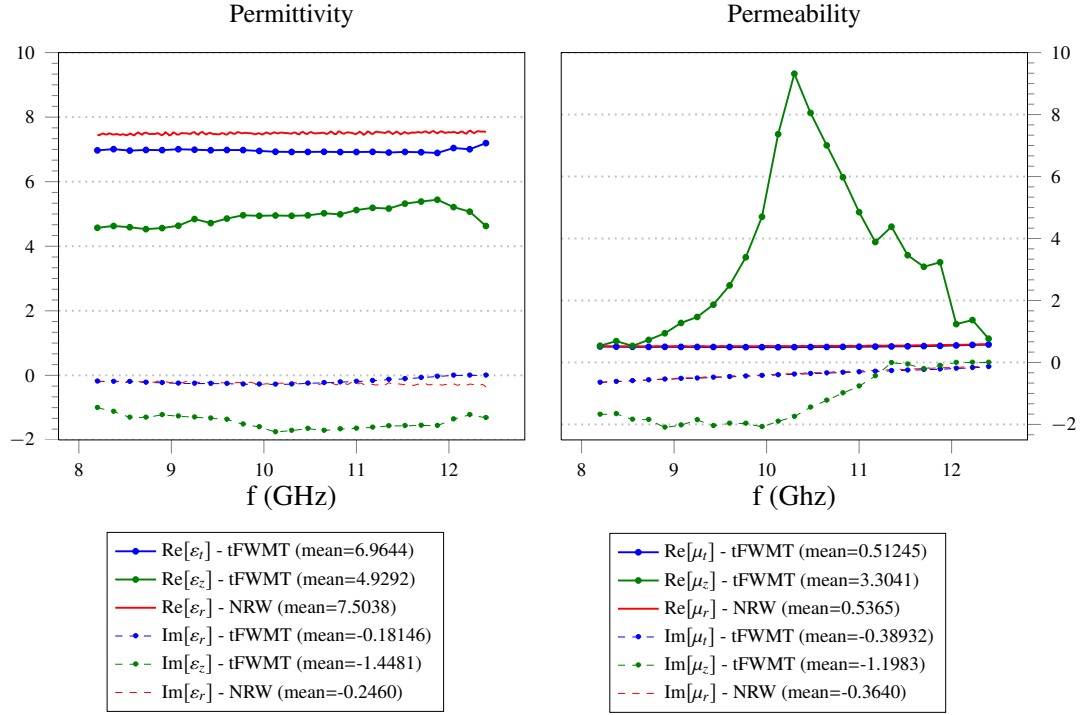

Figure 5.5: A comparison of tFWGT and NRW FGM125 measurements, where the parameters ($\sigma = \varepsilon, \mu$) were extracted by treating the material as fully uniaxial. This extraction was performed using only the dominant mode.

5.2.1 *Uncertainty Analysis.*

There are two primary source of measurement uncertainty: material thickness and scattering parameters. Therefore, we have the uncertainty for a given solution at a single

frequency value as:

$$\sigma_\alpha^2 = \sum_{i=1}^{2}\sum_{j=1}^{2}\left[\sigma_{S_{ij,\text{real}}}\left(\frac{\partial\alpha}{\partial S_{ij,\text{real}}}\right)\right]^2 + \sum_{i=1}^{2}\sum_{j=1}^{2}\left[\sigma_{S_{ij,\text{imag}}}\left(\frac{\partial\alpha}{\partial S_{ij,\text{imag}}}\right)\right]^2$$
$$+ \sum_{k=1}^{2}\left[\sigma_{d_k}\left(\frac{\partial\alpha}{\partial d_k}\right)\right]^2 \quad \ldots \alpha = \varepsilon_t, \varepsilon_z \mu_t, \mu_z \tag{5.5}$$

In the absence of analytical expressions for the required partial derivatives, we compute the approximate numerical derivatives using the finite difference formula:

$$\frac{\partial f(x)}{\partial x} = \frac{f(x+h) - f(x)}{h} \tag{5.6}$$

Note that the error bars are given as $2\sigma_\alpha$. Finally, we must determine the standard deviations for both the measured S-parameters and the measured thicknesses. The variance for the thicknesses is taken to be the square of the standard deviation of the calipers, which is found to be $\sigma_d = 5.0800e - 05$. The uncertainties (σ) for the transmission and reflection measurements are found in Table 31 of [1] (which are reproduced below) and are dependent upon the magnitude of the measured parameter. The function s_uncertainties.m implements a spline function as a means of looking up the appropriate uncertainty for the current value of the measured S-parameter. The reflected scattering parameters are given in terms of linear magnitude, however the uncertainties for transmitted scattering parameters are given in terms of dB. The transmission parameters are converted to dB in the usual way:

$$S_{\text{tx,dB}} = 20\log_{10}\left|S_{\text{tx,meas,linear}}\right| \tag{5.7}$$

and they must be converted back to linear units for uncertainty calculation by means of the following non-standard formula:

$$\sigma_{\text{tx,linear}} = 1 - 10^{\sigma_{\text{tx,dB}}/20} \tag{5.8}$$
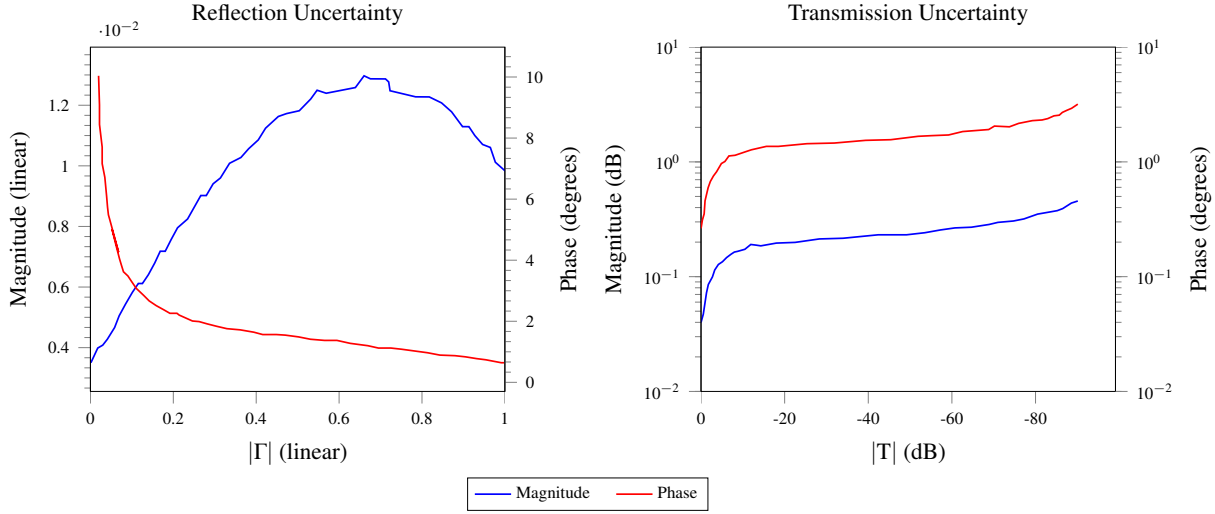
178

Figure 5.6: The uncertainties for reflection and transmission measurements made on the E8362B VNA. Reproduced from [1].

5.3 Laboratory Configuration and Validation Methods

Material measurements are made using the configuration shown in Figures 5.7-5.10, capturing both the transmission and reflection measurements from an Agilent Technologies E8362B Vector Network Analyzer (VNA). The clamped waveguide configuration consisted of 6" x 6" x 0.250" aluminum flanges attached using precision alignment pins and securing screws to Maury Microwave precision X-band waveguides. The waveguides are mounted on a newly devised stable platform using optical table components and custom machined waveguide clamps, significantly enhancing the repeatability, accuracy and precision of the measurements. The system is calibrated using the well-known Thru-Reflect-Line [38] calibration technique. Here, the thru measurement is made with the rectangular waveguides connected to the flange plates, which are then clamped together. For the reflect measurement, a highly reflective brass plate is placed between the flanges. The normal $\lambda/4$ line standard is replaced with a modified measurement, in which the two rectangular waveguides are directly connected and a phase delay of -43.730 ps for two 0.25"

flange plates is used (the phase delay is negative because the line standard is "shorter" than the thru standard). Additionally, the following settings were used in setting up the VNA:

Table 5.1: The E8362B PNA settings.

Channel Start	7GHz
Channel Stop	13GHz
step dwell time	50ms
IF Bandwidth	50Hz
System Z_0	1 Ω

The start and stop frequency values are outside of the range of the band under consideration (X-band is from 8.2GHz to 12.4GHz), to minimize band edge effects in the measurements; the data is then restricted to the X-band in post-processing. Furthermore, although a large number of points is used in data collection (up to 1601), the data is frequently downsampled to a more computationally efficient number (such as 25 points). This is especially helpful when incorporating more modes, as the computational time increases not only due to the larger number of integrals that must be computed, but also due to the complexity of these additional integrals.

5.3.1 Validation Methods.

The design, manufacture and measurement of complex media are still areas of active research which are highly developmental, especially over the bandwidth of interest. As such, no one validation method can be selected as the absolute standard to which the current results may be compared. Therefore, we utilized a number of material
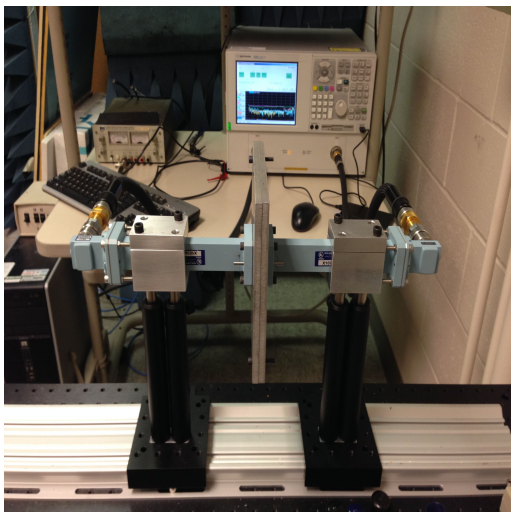
180

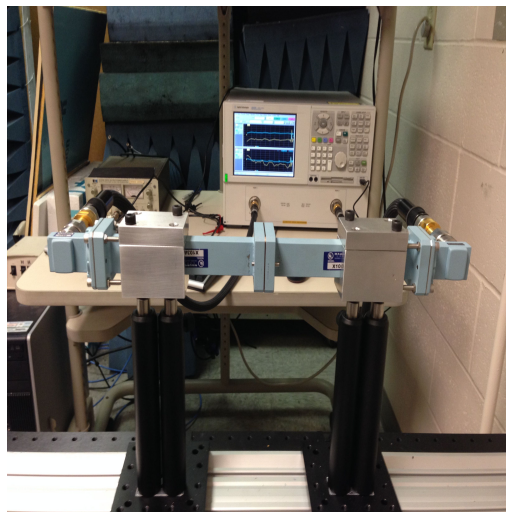Figure 5.7: The thru calibration measurement.

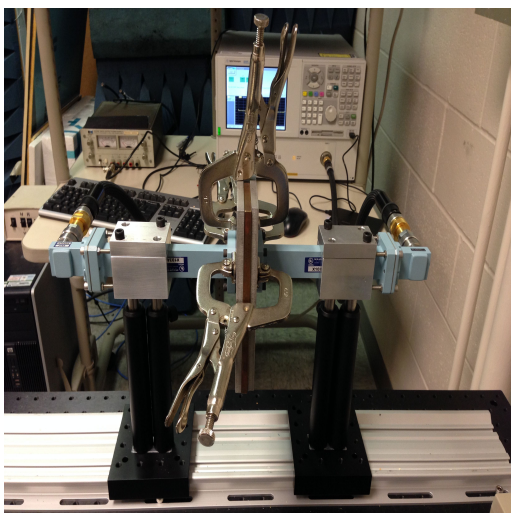Figure 5.8: The modified line calibration measurement.
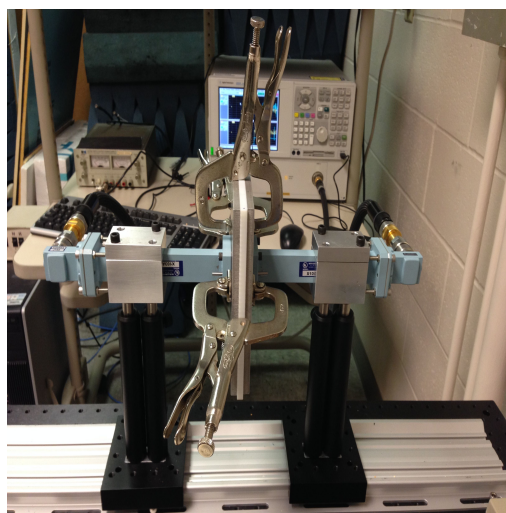

Figure 5.9: The reflect calibration measurement.

Figure 5.10: The tFWMT material measurement using a solid sheet of the white nylon material.

measurement methods, which can be viewed as reference points for the various materials under test.

5.3.1.1 *Waveguide Rectangular to Waveguide Square Technique.*

The Waveguide Rectangular to Waveguide Square Technique (WRWST) is a novel method of extracting the diagonal elements of the constitutive parameters of materials with uniaxial or biaxial anisotropy, similar to the reduced aperture method of [29]. However, instead of using a reduced aperture, the interior of the waveguide is slowly tapered in order to minimize the excitation of higher order modes and ensure only the dominant mode (TE_{10}) is supported at the square end of the waveguide. Furthermore, the sample holder is 0.9" thick, allowing for a single cube sample to be measured at any of 6 orthogonal orientations and thus enabling extraction of the diagonal elements of the constitutive parameter dyads. This method is similar to the work performed in the S-band in [29], although the tapered waveguide transition of the WRWS apparatus reduces the mode matching technique to a single mode. Similar to other waveguide measurement techniques, an iterative solver method (such as Newton's method) is used to solve the minimization problem and extract the constitutive parameters. The theory and efficacy of this method is still under study and will be discussed in more detail in future publications. We note, though, that a resonance was found in the reflection measurements, which corrupts the extraction results around those points. However, since the white nylon polymer is non-magnetic, extractions may be performed on a cube of the white nylon polymer using only the transmission data. The results are given in Figure 5.12 and shown to correspond very well to the NRW extractions given in Figure 5.18. Therefore, we assume for non-magnetic materials, we can confidently use WRWST measurements to help validate our tFWMT results.

We have already identified the presence of the resonance frequencies, which corrupt extractions made using both transmission and reflection measurments. However, it is noteworthy that it may be possible to remedy the problem points if both transmission and reflection measurements are required (for a dielectric, magnetic material). If the iterative
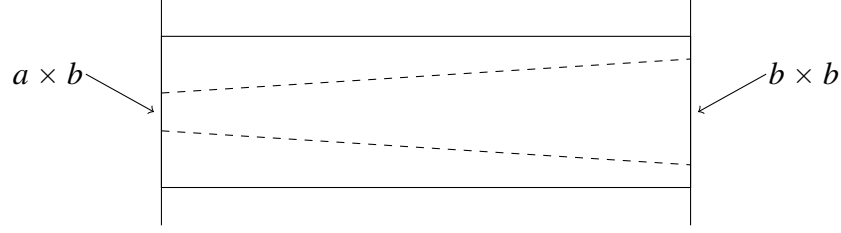
Figure 5.11: A side-view of the WRWST waveguide. The waveguiding region is tapered from normal X-band waveguide dimensions ($0.4'' \times 0.9''$) to a square waveguide region ($0.9'' \times 0.9''$).
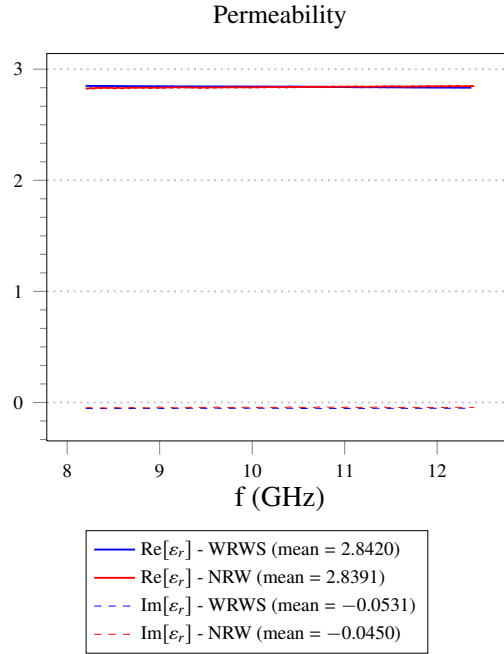
Figure 5.12: Extraction of the permittivity of the white nylon polymer from the 3D printer using the WRWST compared with the results obtained via NRW extraction.

solver evaluates to NaN, then we assume the parameter under consideration is locally linear and replace the value at that frequency with the finite value at the previous frequency. Although, as Figure 5.13 shows, there are still some "bumps" in the area of the resonant

183

frequencies, the results are considerably more stable. It should be noted that there were only a small number of "problem" frequencies, for this case, less than 5% of the total measured spectrum.
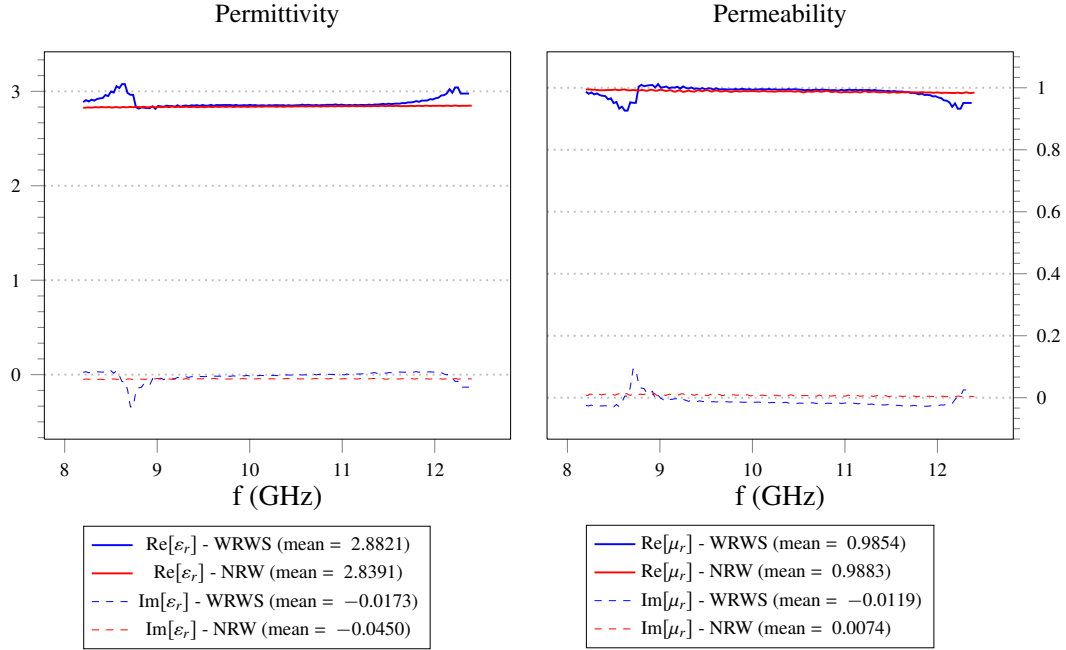
Figure 5.13: Extraction of the permittivity of the white nylon polymer from the 3D printer using the WRWST compared with the results obtained via NRW extraction.

5.3.1.2 *Focused Beam Measurement Technique.*

The Focused Beam Measurement Technique (FBMT) can also be used for validation of results, if larger samples are available. Typically, samples of at least 12" × 12" are required for proper illumination. The theory behind FBMT measurements for isotropic media is well documented elsewhere [81]. However, we expect the theoretical S-parameters to take a different form for uniaxial dielectric media. A cursory derivation will now be presented for completeness. The geometry for the FBMT is given in Figure 5.14. We will determine the fields in each region, then enforce boundary conditions in order to

determine the transmission coefficient. Since the system is limited in its bistatic capability, only the transmission coefficients (S_{21} and S_{12}) will be determined. We also note that only h-polarization is used, since the electric field in this case has a component in both the $\hat{\mathbf{x}}$ and $\hat{\mathbf{z}}$ direction, whereas the electric field v-polarization has only a $\hat{\mathbf{y}}$ component. Using the h-polarization allows us to interrogate the relevant components of the permittivity (the materials for which this method are used are assumed to be non-magnetic). It also simplifies our analysis.

Figure 5.14: The geometry for a slab illuminated by an arbitrarily polarized field at the angle of incidence θ_i.

The equation we will need to minimize is the same as we have seen with other methods:
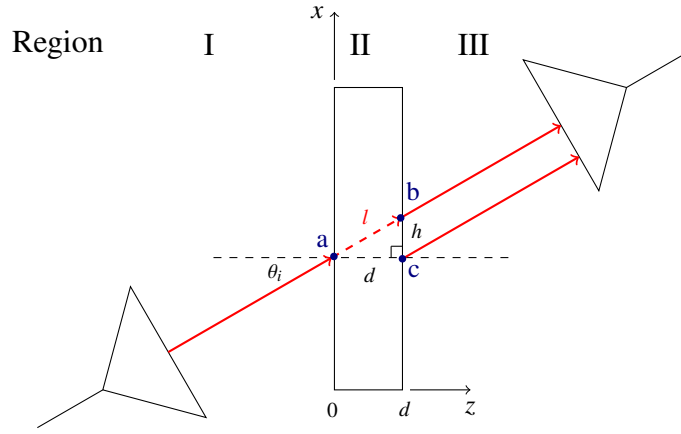
$$\underset{\varepsilon_t,\varepsilon_z,\mu_t,\mu_z\in\mathbb{C}}{\arg\min} \left\| S^{\text{thy}} - S^{\text{exp}} \right\|_2 \tag{5.9}$$

Expressions for the theoretical scattering coefficients will now be developed. The general fields for anisotropic media are found from Maxwell's equations:

$$\nabla \times \vec{E} = \nabla \times \overleftrightarrow{I} \cdot \vec{E} = -j\omega\overleftrightarrow{\mu} \cdot \vec{H} \tag{5.10}$$

$$\nabla \times \vec{H} = \nabla \times \overleftrightarrow{I} \cdot \vec{H} = j\omega\overleftrightarrow{\varepsilon} \cdot \vec{E} \tag{5.11}$$

Using assumed solutions of the form $\vec{E} = \vec{E}_0 e^{-j\vec{k}\vec{r}}$ and $\vec{H} = \vec{H}_0 e^{-j\vec{k}\vec{r}}$ and solving the decoupled equations, we find:

$$\vec{H} = \frac{1}{\omega} \cdot \overleftrightarrow{\mu}^{-1} \cdot \overleftrightarrow{k} \cdot \vec{E} \tag{5.12}$$

$$\overleftrightarrow{w}_e \cdot \vec{E} = 0 \tag{5.13}$$

$$\overleftrightarrow{w}_e = -\left(\overleftrightarrow{\mu} \cdot \overleftrightarrow{k} \cdot \overleftrightarrow{\mu}^{-1} \cdot \overleftrightarrow{k} + \omega^2 \overleftrightarrow{\mu} \cdot \overleftrightarrow{\varepsilon} \right) \tag{5.14}$$

$$\overleftrightarrow{k} = \vec{k} \times \overleftrightarrow{I} = \begin{bmatrix} 0 & -k_z & k_y \\ k_z & 0 & -k_x \\ -k_y & k_x & 0 \end{bmatrix} \tag{5.15}$$

- Region I

    Region I is assumed to be isotropic media with $\overleftrightarrow{\varepsilon} = \varepsilon_1 \overleftrightarrow{I}$, $\overleftrightarrow{\mu} = \mu_1 \overleftrightarrow{I}$ and $\vec{k} = \hat{\mathbf{x}} k_{x1} + \hat{\mathbf{z}} k_{z1}$. This leads to

    $$\overleftrightarrow{w}_e = -\left(\overleftrightarrow{k} \cdot \overleftrightarrow{k} + \omega^2 \mu_1 \varepsilon_1 \overleftrightarrow{I} \right) \tag{5.16}$$

    The eigenvalues of $\overleftrightarrow{w}_e$ represent the propagation vectors for the forward and reverse traveling waves. They are found from the determinant of $\overleftrightarrow{w}_e$

    $$\begin{aligned} k_{z1}^+ &= k_{z1}^i = +\sqrt{\omega^2 \mu_1 \varepsilon_1 - \left(k_{x1}^i\right)^2} \\ k_{z1}^- &= k_{z1}^r = -\sqrt{\omega^2 \mu_1 \varepsilon_1 - \left(k_{x1}^r\right)^2} \end{aligned} \tag{5.17}$$

186

Solving (5.13) using these eigenvalues and using the result in (5.12) , we find the expression for the fields in Region I:

$$
\begin{aligned}
\vec{E}_1^{i,r} &= \left(\hat{\mathbf{x}} - \hat{\mathbf{z}} \frac{k_{x1}^{i,r}}{k_{z1}^{i,r}} \right) E_{x1,0}^{i,r} e^{-j\left(k_{x1}^{i,r}x + k_{z1}^{i,r}z\right)} \\
\vec{H}_1^{i,r} &= \hat{\mathbf{y}} \frac{E_{x1,0}^{i,r}}{Z_1^{i,r}} e^{-j\left(k_{x1}^{i,r}x + k_{z1}^{i,r}z\right)} \\
k_{z1}^{i,r} &= \pm \sqrt{\omega^2 \mu_1 \varepsilon_1 - \left(k_{x1}^{i,r}\right)^2} \qquad , \qquad k_{x1}^{i,r} = k_1 \sin\left(\theta_i\right) \\
Z_1^{i,r} &= \frac{k_{z1}^{i,r}}{\omega \varepsilon_1}
\end{aligned}
\tag{5.18}
$$

- Region II

Region II is assumed to be uniaxial media, therefore $\overleftrightarrow{\mathbf{w}}_e$ is found to be:

$$
\overleftrightarrow{\mathbf{w}}_{e2} = - \left(\overleftrightarrow{\mu}_2 \cdot \overleftrightarrow{k}_2 \cdot \overleftrightarrow{\mu}_2^{-1} \cdot \overleftrightarrow{k}_2 + \omega^2 \overleftrightarrow{\mu}_2 \cdot \overleftrightarrow{\varepsilon}_2 \right)
\tag{5.19}
$$

and the eigenvalues for the h-polarization case are found to be:

$$
k_{z2}^{i,r} = \pm \sqrt{\omega^2 \mu_{t2} \varepsilon_{t2} - \frac{\varepsilon_{t2}}{\varepsilon_{z2}} \left(k_{x2}^{i,r}\right)}
\tag{5.20}
$$

Again, using these eigenvectors, (5.13) and (5.12), we find the fields in the uniaxial region to be

$$
\begin{aligned}
\vec{E}_2^{i,r} &= \left(\hat{\mathbf{x}} - \hat{\mathbf{z}} \frac{\varepsilon_{t2} k_{x2}^{i,r}}{\varepsilon_{z2} k_{z2}^{i,r}} \right) E_{x2,0}^{i,r} e^{-j\left(k_{x2}^{i,r}x + k_{z2}^{i,r}z\right)} \\
\vec{H}_2^{i,r} &= \hat{\mathbf{y}} \frac{E_{x2,0}^{i,r}}{Z_2^{i,r}} e^{-j\left(k_{x2}^{i,r}x + k_{z2}^{i,r}z\right)} \\
k_{z2}^{i,r} &= \pm \sqrt{\omega^2 \mu_{t2} \varepsilon_{t2} - \frac{\varepsilon_{t2}}{\varepsilon_{z2}} \left(k_{x2}^{i,r}\right)} \\
Z_2^{i,r} &= \frac{k_{z2}^{i,r}}{\omega \varepsilon_{t1}}
\end{aligned}
\tag{5.21}
$$

- Region III

187

Region III is assumed to be the same as Region I, therefore, the fields are given as (note that the reference plane has been set at $z = d$)

$$\vec{E}_3^{i,r} = \left(\hat{\mathbf{x}} - \hat{\mathbf{z}} \frac{k_{x1}^{i,r}}{k_{z1}^{i,r}} \right) E_{x3,0}^{i,r} e^{-j\left[k_{x3}^{i,r} x + k_{z3}^{i,r}(z-d) \right]}$$

$$\vec{H}_3^{i,r} = \hat{\mathbf{y}} \frac{E_{x3,0}^{i,r}}{Z_1^{i,r}} e^{-j\left[k_{x3}^{i,r} x + k_{z3}^{i,r}(z-d) \right]}$$

$$k_{z3}^{i,r} = \pm \sqrt{\omega^2 \mu_1 \varepsilon_1 - \left(k_{x3}^{i,r} \right)^2}$$
(5.22)

$$Z_3^{i,r} = Z_1^{i,r} = \frac{k_{z1}^{i,r}}{\omega \varepsilon_1}$$

All that remains is to enforce the boundary conditions on the total tangential fields in order to determine the transmission (T) and reflection (Γ) coefficients.

- $\vec{E}_{t1}(z = 0) = \vec{E}_{t1}(z = 0)$

  By considering the total fields (which is the sum of the incident and reflected fields) at $z = 0^-$ and $z = 0^+$, we find

$$\vec{E}_t(z = 0^-) = \vec{E}_t(z = 0^+) \implies e^{-jk_{x1}^i x} + \Gamma e^{-jk_{x1}^r x} = te^{-jk_{x2}^i x} + re^{-jk_{x2}^r x} \quad (5.23)$$

  where $\Gamma = \dfrac{E_{x1,0}^r}{E_{x1,0}^i}$ is the reflection coefficient, $t = \dfrac{E_{x2,0}^i}{E_{x1,0}^i}$ and $r = \dfrac{E_{x2,0}^r}{E_{x1,0}^i}$. We know that (5.23) must be true for all values of x, therefore, we immediately see that $k_{x1}^i = k_{x1}^r = k_{x2}^i = k_{x1}^r$. Once enforcing this requirement, we obtain

$$1 + \Gamma = t + r \quad (5.24)$$

- $\vec{H}_{t1}(z = 0) = \vec{H}_{t1}(z = 0)$

  Following a similar procedure for the magnetic field at the $z = 0$ boundary, we find

$$1 - \Gamma = \frac{Z_1}{Z_2} (t - r) \quad (5.25)$$

- $\vec{E}_{t1}(z = d) = \vec{E}_{t1}(z = d)$

  Similarly, from the electric field at the $z = d$ boundary gives:

$$tP + rP^{-1} = T \tag{5.26}$$

  where $P = e^{-jk_{z2}d}$ is the one-way phase delay through the slab and $T = \dfrac{E^r_{x3,0}}{E^i_{x1,0}}$ is the transmission coefficient.

- $\vec{H}_{t1}(z = d) = \vec{H}_{t1}(z = d)$

  Finally, from the tangential magnetic fields at the $z = d$ boundary, we find:

$$\frac{Z_1}{Z_2}\left(tP - rP^{-1}\right) = T \tag{5.27}$$

We can solve (5.24) - (5.27) for the theoretical transmission and reflection coefficients (assuming that $\varepsilon_1 = \varepsilon_0$ and $\mu_1 = \mu_0$ in Region I and Region III):

$$
\boxed{
\begin{aligned}
T &= S_{21} = \frac{P\left(1 - R^2\right)}{1 - R^2 P^2} \\[4pt]
\Gamma &= S_{11} = \frac{R\left(1 - P^2\right)}{1 - R^2 P^2} \\[4pt]
P &= e^{-jk_{z2}d} \quad , \quad R = \frac{Z_2 - Z_1}{Z_2 + Z_1} \\[4pt]
k_{z1} &= k_{z0} = \sqrt{k_0^2 - k_x^2} = \sqrt{k_0^2 - k_0^2 \sin^2(\theta_i)} = k_0 \cos(\theta_i) \\[4pt]
k_{z2} &= \sqrt{k_t^2 - \frac{\varepsilon_t}{\varepsilon_z}k_x^2} \qquad k_t = \omega\sqrt{\varepsilon_t \mu_t} \qquad k_x = k_0 \sin(\theta_i) \\[4pt]
Z_1 &= Z_0 = \frac{k_{z0}}{\omega\varepsilon_0} \qquad Z_2 = \frac{k_{z2}}{\omega\varepsilon_{t1}} = \eta_0 \cos(\theta_i)
\end{aligned}
}
\tag{5.28}
$$

We have now determined the theoretical parameters and turn our attention to calibration of the system and correction for the angle of incidence. The system is calibrated using the response-only method. From Figure 5.14, we can see the measured time-gated S-parameters (S^{ms}) are the multiplication of the responses from each region, which allows

189

us to find the S-parameter response for only the sample as follows:

$$S_{21}^{ms} = S_{21}^{I} S_{21}^{s} S_{21}^{III} \implies S_{21}^{s} = \frac{S_{21}^{ms}}{S_{21}^{I} S_{21}^{III}} \tag{5.29}$$

Consequently, we require the responses from Regions I and III, which can be found from the empty measurements at each angle (S^{me})

$$S_{21}^{me} = S_{21}^{I} \overbrace{S_{21}^{e}}^{e^{-jk_0 l}} S_{21}^{III} \implies S_{21}^{I} S_{21}^{III} = S_{21}^{me} e^{jk_0 l} = S_{21}^{me} e^{jk_0 \frac{d}{\cos(\theta_i)}} \tag{5.30}$$

Using the relationships found in (5.29) and (5.30), we find the response from the sample as referenced from point "a" to point "b" (in Figure 5.14) to be

$$\boxed{S_{21}^{exp} = S_{21}^{s} = \frac{S_{21}^{ms}}{S_{21}^{me}} e^{-jk_0 \frac{d}{\cos(\theta_i)}}} \tag{5.31}$$

There is one further noteworthy area with regards to oblique angle measurements in a focused beam system, which has been given very little attention. When calculating the theoretical scattering parameters for off-normal angles of incidence, an additional angular correction term is necessary to ensure proper extraction of the constitutive parameters. In Figure 5.14, we note that the theoretical parameters are referenced from point "a" to point "c". Therefore, it is necessary to correct the phase of the theoretical S-parameters so that they will be referenced to the same points as the measured parameters. This is accomplished by multiplying the theoretical the phase term by $e^{-jk_x h} = e^{-jk_x d \tan(\theta_i)} = e^{-jk_0 d \frac{\sin^2(\theta_i)}{\cos(\theta_i)}}$. Since we are only measuring the transmission parameters, we have the

190

argument of (5.9) as:

$$\begin{aligned}
S_{21}^{\text{thy}} - S_{21}^{\text{exp}} &= S^{\text{thy}} e^{-jk_0 d \frac{\sin^2(\theta_i)}{\cos(\theta_i)}} - \frac{S_{21}^{\text{ms}}}{S_{21}^{\text{me}}} e^{-jk_0 \frac{d}{\cos(\theta_i)}} \\
&= S^{\text{thy}} - \frac{S_{21}^{\text{ms}}}{S_{21}^{\text{me}}} e^{-jk_0 \frac{d}{\cos(\theta_i)}} e^{jk_0 d \frac{\sin^2(\theta_i)}{\cos(\theta_i)}} \\
&= S^{\text{thy}} - \frac{S_{21}^{\text{ms}}}{S_{21}^{\text{me}}} e^{-jk_0 \frac{d}{\cos(\theta_i)} \left[1 - \sin^2(\theta_i)\right]} \\
&= S^{\text{thy}} - \frac{S_{21}^{\text{ms}}}{S_{21}^{\text{me}}} e^{-jk_0 \frac{d\cos^2(\theta_i)}{\cos(\theta_i)}} \\
&= S^{\text{thy}} - \frac{S_{21}^{\text{ms}}}{S_{21}^{\text{me}}} e^{-jk_0 \cos(\theta_i) d} \\
&= S^{\text{thy}} - \frac{S_{21}^{\text{ms}}}{S_{21}^{\text{me}}} e^{-jk_{z0} d}
\end{aligned}$$

and the minimization problem becomes:

$$\underset{\varepsilon_t, \varepsilon_z, \mu_t, \mu_z \in \mathbb{C}}{\arg \min} \left\| S^{\text{thy}} - \frac{S_{21}^{\text{ms}}}{S_{21}^{\text{me}}} e^{-jk_{z0} d} \right\|_2 \tag{5.32}$$

It should be mentioned that this method requires measurements at 2 independent angles of incidence. A normal incidence angle of measurement ensures $k_x = 0$, which reduces k_{z2} to k_t. Therefore, no ε_z term exists in the equations and ε_t can be found using an iterative solver method. Then, the results from ε_t are used along with a set of measurements collected at a non-normal angle of incidence in order to extract ε_z.

5.3.1.3 *Rectangular Waveguide Measurement Technique.*

The Rectangular Waveguide Measurement Technique (RWMT) is a well-known destructive characterization technique. Using the NRW extraction technique, closed-form solutions are available for the permittivity and permeability, making it a computationally efficient method. Additionally, as long as the sample fits tightly in the rectangular waveguide, the results are precise and repeatable. In a RWG, the dominant mode electric field is oriented in the $\hat{\mathbf{y}}$ direction (the short dimension of the aperture), thus we may extract permittivity and permeability in only that direction. Therefore, we require 2 independent measurements

at different orientations. Figure 5.15 demonstrates which component of the constitutive parameter dyad is extracted for a given orientation. Unfortunately, it can be difficult to achieve a precise, uniform fit inside the RWG and across the aperture, leading to some experimental error.
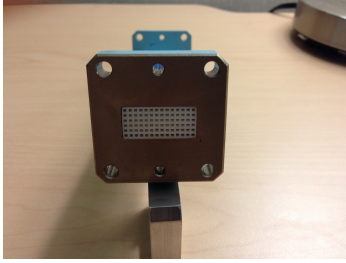
(a) The orientation used for extracting ε_t
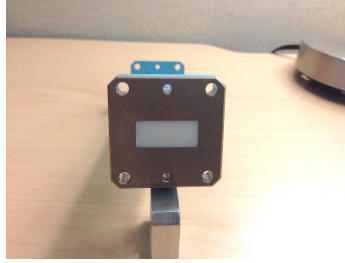
(b) The orientation used for extracting ε_z - the sample has been rotated $90°$ in the direction of the small pre-vision alignment hole.
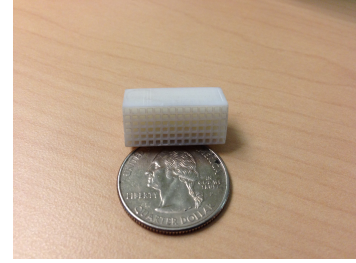
(c) The sample shown with a quarter for perspective.

Figure 5.15: The orientations used for extracting ε_t and ε_z. The displayed sample is the square lattice type material with $d_1 = 0.5315$mm and $d_2 = 1.063$mm The outer dimensions are 0.4" $\times$ 0.9" $\times$ 0.4". Recall that the dominant mode electric field is polarized in the $\hat{\mathbf{y}}$ direction, which is the guiding principle in determining the correct orientation for a given element of the constitutive parameter dyad.

5.3.1.4 *Equivalent Transmission Line Theory.*

For the square lattice material shown in Figure 5.19, a basic transmission line theory can be used to compare with the measured values. This theory utilizes the equivalent capacitance of a parallel plate capacitor of area A, filled with a material of permittivity ε_r and separated
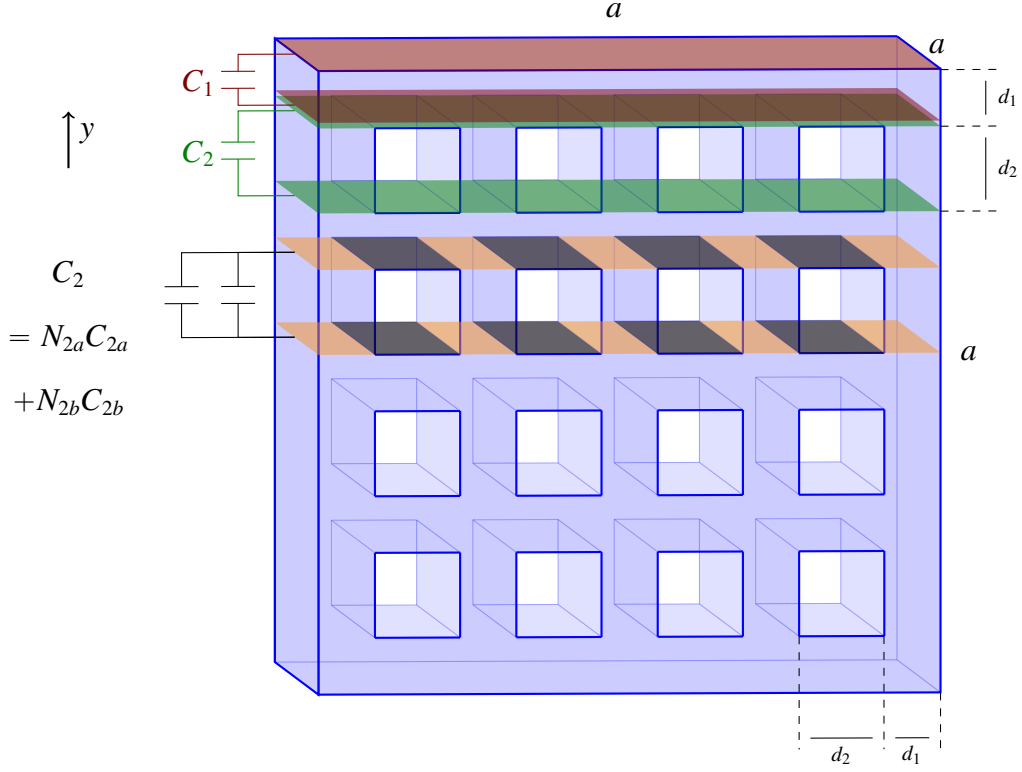
Figure 5.16: Transmission line theory for a uniaxial media based on a square lattice. The incident wave is assumed to be propagating in the $\hat{\mathbf{z}}$ direction and polarized in the $\hat{\mathbf{y}}$ direction, therefore this orientation would be used for computing ε_t. Note that the material is cubical and the inclusions are equally spaced throughout the material. The material is described by the number of lattice intervals across a row or column of the material (given by N_{2a}), and the number of inclusions across a row or column (given by N_{2b}). The material is designed for mechanical stability such that $N_{2a} = N_{2b}+1$. The lattice material is assumed to have a permittivity of ε_1 and the inclusions are assumed to have a permittivity of ε_2. The parallel plates of the equivalent capacitors are drawn in different colors so as to demonstrate their orientation with respect to the polarization of the incident field.

by distance d

$$C = \frac{\varepsilon_r A}{d} \tag{5.33}$$

The physics of the problem require the electric field to be normal to the parallel plates of the equivalent capacitors, otherwise no field would be generated within the equivalent capacitors. Since the electric field in this case is assumed to be oriented only in the $\hat{\mathbf{y}}$-direction, this basic theory requires us to consider two separate orientations - one for ε_t and one for ε_z.

Transverse case (ε_t). Figure 5.16 illustrates the configuration required to compute ε_t. In this case, we view the material as a composed of alternating layers. Layer 1 is composed of solid lattice material ($\varepsilon_r = \varepsilon_1$). Layer 2 is a mixed layer containing alternating sublayers of lattice material ($\varepsilon_r = \varepsilon_1$) and inclusion material ($\varepsilon_r = \varepsilon_2$). Due to the $\hat{\mathbf{y}}$-directed polarization of the electric field, an equiphase plane of the impinging wave "sees" the capacitances of the main layers in series, leading to an effective capacitance (C_{eff}) of

$$\frac{1}{C_{\text{eff}}} = \frac{1}{C_1} + \frac{1}{C_2} + \frac{1}{C_1} + \frac{1}{C_2} + \ldots + \frac{1}{C_1} = \frac{N_1}{C_1} + \frac{N_2}{C_2} \tag{5.34}$$

where N_1 and N_2 are the number of each layer (note $N_1 = N_2 + 1$, by design). Taking note of the geometry of the "plates" shown in Figure 5.16, we see the equivalent capacitance of layer 1 is simply

$$C_1 = \frac{\varepsilon_1 a^2}{d_1} \tag{5.35}$$

Since layer 2 is a mixed layer of the lattice material and the inclusion material, each seen at the same time by an equiphase plane of the incident wave, the equivalent capacitances are taken to be in parallel, leading to an equivalent capacitance of

$$C_2 = C_{2a} + C_{2b} + C_{2a} + C_{2b} + \ldots + C_{2a} = N_{2a} C_{2a} + N_{2b} C_{2b} \tag{5.36}$$

where, again, N_{2a} and N_{2b} are the number of each sublayer and $N_{2a} = N_{2b} + 1$. The capacitances C_{2a} and C_{2b} are seen to be

$$C_{2a} = \frac{\varepsilon_1 d_1 a}{d_2} \qquad C_{2b} = \frac{\varepsilon_2 d_2 a}{d_2} \tag{5.37}$$

Therefore, we have C_2 as

$$C_2 = N_{2a}C_{2a} + N_{2b}C_{2b} = N_{2a}\left(\frac{\varepsilon_1 d_1 a}{d_2}\right) + N_{2b}\left(\frac{\varepsilon_2 d_2 a}{d_2}\right)$$

$$\implies \frac{1}{C_2} = \frac{d_2}{N_{2a}\varepsilon_1 d_1 a + N_{2b}\varepsilon_2 d_2 a} \tag{5.38}$$

Notice that the effective capacitance of the cube is equivalent to parallel plates of area a^2 and separated by distance a. Also, the relative permittivities are given by $\varepsilon_k = \varepsilon_{kr}\varepsilon_0$. This leads to

$$\frac{1}{C_{\text{eff}}} = \frac{a}{\varepsilon_{t,\text{eff}r}\varepsilon_0 a^2} = \frac{N_1}{C_1} + \frac{N_2}{C_2}$$

$$= N_1\left(\frac{d_1}{\varepsilon_{1r}\varepsilon_0 a^2}\right) + N_2\left(\frac{d_2}{N_{2a}\varepsilon_{1r}\varepsilon_0 d_1 a + N_{2b}\varepsilon_{2r}\varepsilon_0 d_2 a}\right) \tag{5.39}$$

Because the material is cubic and symmetric, we are able to set $N_2 = N_{2b} = N$ and $N_1 = N_{2a} = N + 1$.

$$\frac{1}{\varepsilon_{t,\text{eff}r}\cancel{\varepsilon_0}\cancel{a}} = (N+1)\left(\frac{d_1}{\varepsilon_{1r}\cancel{\varepsilon_0}\cancel{a^2}}\cancel{a}\right) + N\left(\frac{d_2}{(N+1)\,\varepsilon_{1r}\cancel{\varepsilon_0}d_1\cancel{a} + N\varepsilon_{2r}\cancel{\varepsilon_0}d_2\cancel{a}}\right)$$

$$\implies \frac{1}{\varepsilon_{t,\text{eff}r}} = (N+1)\left(\frac{d_1}{\varepsilon_{1r}a}\right) + N\left(\frac{d_2}{(N+1)\,\varepsilon_{1r}d_1 + N\varepsilon_{2r}d_2}\right) \tag{5.40}$$

Cross-multiplying, simplifying and replacing $\varepsilon_{t,\text{eff}r}$ with ε_{tr}, we have:

$$\boxed{\varepsilon_{tr} = \frac{(N+1)\,ad_1\varepsilon_{1r}^2 + Nad_2\varepsilon_{1r}\varepsilon_{2r}}{(N+1)^2\,d_1^2\varepsilon_{1r} + N(N+1)\,d_1d_2\varepsilon_{2r} + Nad_2\varepsilon_{1r}}} \tag{5.41}$$

Longitudinal Case (ε_z). Figure 5.17 demonstrates the orientation for computing ε_z. In this case, because the inclusions are now parallel to the polarization of the electric field, the parallel plates are oriented along the empty (outer) face of the inclusions, rather than the top and bottom (inner) faces. This leads to parallel plates that are separated by a, rather

195
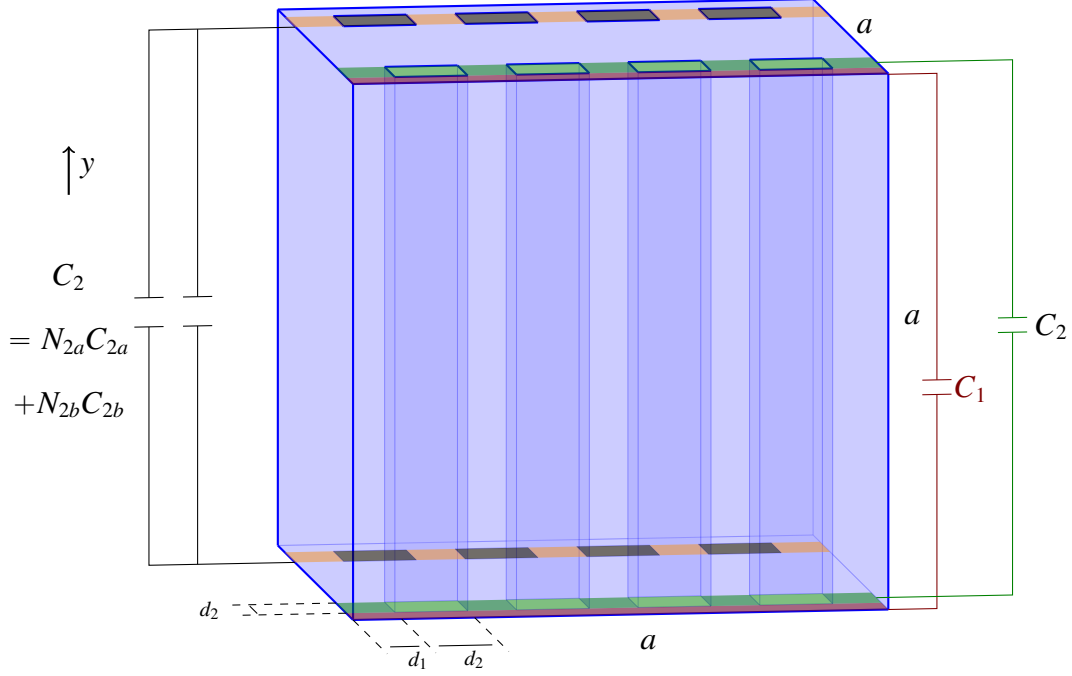
Figure 5.17: Transmission line theory for a uniaxial media based on a square lattice. The incident wave is assumed to be propagating in the $\hat{\mathbf{z}}$ direction and polarized in the $\hat{\mathbf{y}}$ direction, therefore this orientation would be used for computing ε_z. Note that the material is cube and the inclusions are equally spaced throughout the material. The material is described by the number of lattice intervals across a row or column of the material (given by N_{2a}), and the number of inclusions across a row or column (given by N_{2b}). The material is designed for mechanical stability such that $N_{2a} = N_{2b} + 1$. As before, the lattice material is assumed to have a permittivity of ε_1 and the inclusions are assumed to have a permittivity of ε_2.

than d_1 and d_2. As a result, the equivalent capacitances are given by

$$
\begin{aligned}
C_{\text{eff}} &= N_1 C_1 + N_2 C_2 \\
C_1 &= \frac{\varepsilon_1 d_1 a}{a} \\
C_2 &= N_{2a} C_{2a} + N_{2b} C_{2b} \rightarrow C_{2a} = \frac{\varepsilon_1 d_1 d_2}{a} \quad , \quad C_{2b} = \frac{\varepsilon_2 d_2^2}{a} \\
N_2 &= N_{2b} = N \qquad N_1 = N_{2a} = N + 1
\end{aligned}
\tag{5.42}
$$

Combining these equations and simplifying as in the previous case, we find the expression for ε_z

$$\varepsilon_z = (N+1)\frac{d_1\varepsilon_{1r}}{a} + \frac{N(N+1)d_1d_2\varepsilon_{1r} + N^2d_2^2}{a^2} \tag{5.43}$$

5.4 tFWMT Measurement of Uniaxial Media

Now that we have established a good measure of confidence in the extraction code, the next step is to apply it to a number of uniaxial media. However, while some naturally occurring materials (such as sapphire, ruby and calcite) are uniaxial in the optical frequency spectrum, materials that are uniaxial in the microwave regime are more difficult to find. Collin [26] theorized that one could quickly and cheaply manufacture a uniaxial media from several alternating layers of isotropic media with contrasting dielectric constants. In light of the simplicity of this approach, it was the first approach we tried. However, in spite of attempting several types of materials, this method did not produce the expected uniaxial results. This could be due to the relatively large thicknesses of the sample layers with respect to the wavelengths of interest. Therefore, alternative means of constructing a uniaxial material were sought.

Materials with inclusions arranged in a lattice structure (such as honeycomb) can also be expected to demonstrated uniaxial characteristics. Fortunately, with the recent advances to 3D printing technology and ease of access to such devices which patterned materials can be generated in Computer-aided Design (CAD) software, such as SolidWorks, rapid prototyping a number of different types of materials becomes a fairly simple matter. In the course of our work, a Connex 500 was used for producing prototype materials. The "ink" used in this printer is a nylon polymer. The constitutive parameters of this material have been extracted using a solid, homogeneous X-band rectangular waveguide sample using the well-known NRW method and are shown in Figure 5.18. This will help serve as a baseline when exploring different lattice structures. Unfortunately, due to resource limitations, the

197

white nylon polymer is the only material available at the time. Therefore, for the prototype materials, the "inclusions" will consist of air pockets.
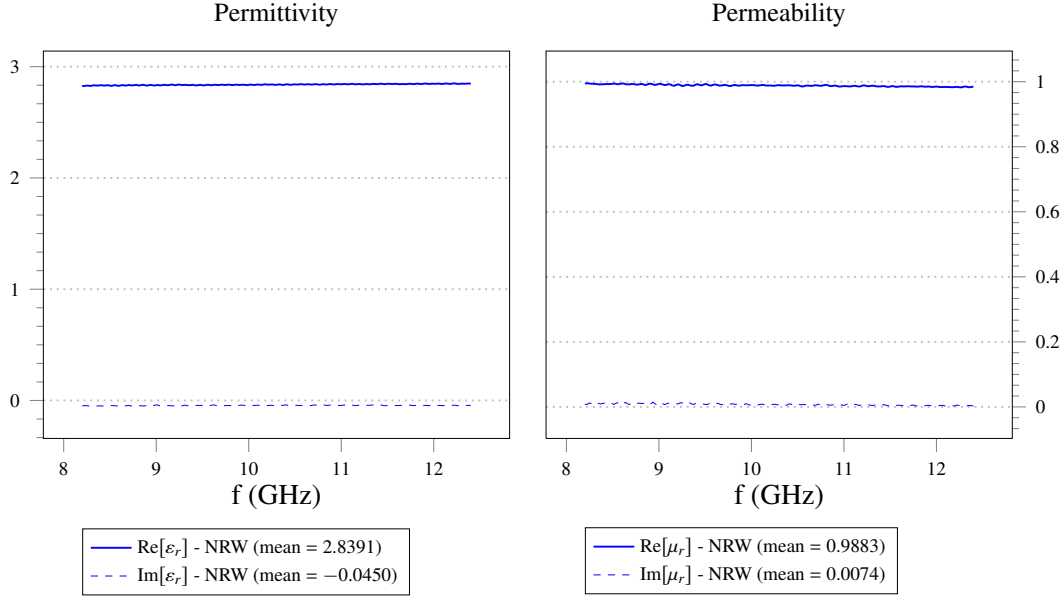
Figure 5.18: The constitutive parameters of the (isotropic) white nylon polymer used by the 3D printer. This material will be used to construct various lattice materials.

Clearly, there are any number of ways to construct a 6"x6" sample simply by altering various dimensions and by altering the shape of the lattice structure. Since the samples are required to have uniaxial properties, we will use inclusion shapes which possess twofold rotational symmetry (or a single mirror plane). Two simple choices are squares and hexagons. The lattice structures and the dimensions which drive designs incorporating these two types of inclusions are shown in Figure 5.23 and Figure 5.19.

5.4.1 *Square Lattice.*

In order to obtain a good sampling of the material by the interrogating field, the inclusions should be at least $\lambda/4$ (with $\lambda/10$ preferred) at the highest frequency in the band. At

12.4GHz, this equates to $d_1 = 2.4$mm. Due to the resolution of the 3D printer, though, we choose $d_1 = 0.53$mm and $d_2 = 1.06$mm. These numbers allow symmetry to be maintained within the smaller samples used for the validation techniques. One of the main benefits of using this type of lattice structure is the relative ease in our ability to compute a theoretical value for both ε_t and ε_z, as shown in Section 5.3.1.4. The geometry for the samples is shown in Figure 5.19 and the actual material samples are shown in Figure 5.20. When measuring these samples, it is important to note that the S-parameters were time-gated [54] using the center/span gate centered at $t = 0$s with a half-width of $t = 1.04$ns. Since the materials are printed using a 3D printer and the inclusions are relatively small, the RWG method was chosen for comparison. Additionally, the theoretical values obtained using the transmission line theory of Section 5.3.1.4 are included.

From Figure 5.21, we take note of several salient characteristics of the tFWMT results. First, measurements were taken in a number of orientations, equivalent to $90°$ rotations around the z-axis. All orientations provided nearly equivalent results, within numerical and experimental error. Therefore, we conclude that the material is in fact uniaxial. Next, we note that the RWG and theoretical values trend in the same manner (i.e., $\text{Re}[\varepsilon_z] > \text{Re}[\varepsilon_t]$). However, the dominant mode tFWMT results indicate the opposite trend (i.e., $\text{Re}[\varepsilon_z] < \text{Re}[\varepsilon_t]$). Additionally, the dominant mode results indicate the material is artificially lossy in the longitudinal dimension. This could be due to either numerical instabilities within the solver, standing waves in the material structure which lead to higher than expected loss or inherent shortcomings in the method.

Finally, we observe that $\text{Re}[\varepsilon_z]$ and $\text{Re}[\varepsilon_t]$ are essentially within each other's error bars. Since the validation methods show very little contrast between the transverse and longitudinal permittivities, it is difficult to draw a conclusion as to the accuracy of the tFWMT from these measurements. It is reasonable to expect that a material with a higher
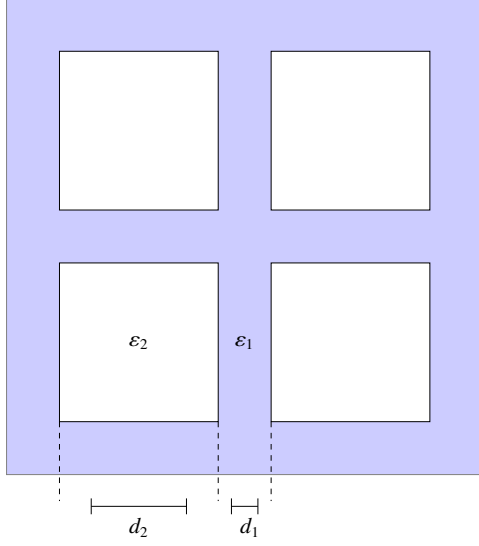
Figure 5.19: The variable dimensions of a unit cell of the upright square lattice material, which can be used to generate a variety of structures. Here, d_1 is the width of the lattice structure (which will be composed of the white nylon polymer) and d_2 is the width of the square inclusions.
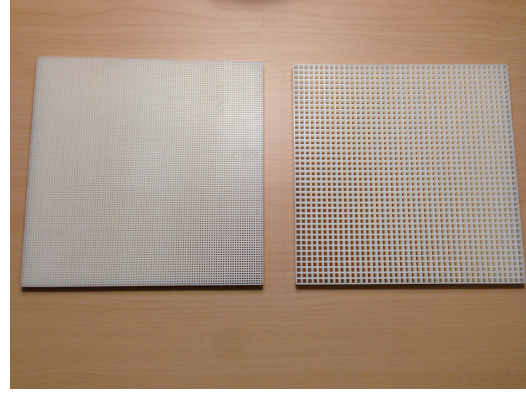
Figure 5.20: Samples of the square lattice material used for tFWGT measurement. Referencing the geometry of Figure 5.19, the dimensions of the sample on the left are $d_1 = 0.53$mm and $d_2 = 1.06$mm and the dimensions of the right sample are $d_1 = 0.91$mm and $d_2 = 2.75$mm, with a thickness of 0.25".

contrast between the two elements of the constitutive parameter dyads would provide more reasonable results.

5.4.2 Hexagonal Honeycomb.

Hexagonal honeycomb materials are used in many commercial, industrial and military applications. Additionally, if the honeycomb cells are perfectly hexagonal, it is seen to have uniaxial characteristics. The precision of 3D printing allows for this reasonable assumption. Therefore, it is a natural choice for this type of measurement. Again, due to the low-loss

Transverse

Longitudinal

Legend (left):
- Re[ε_t] - tFWMT (mean =2.0484)
- Re[ε_t] - RWG (mean=1.7324)
- Re[ε_t] - Theory (mean=1.9249)
- Im[ε_t] - tFWMT (mean=-0.0032896)
- Im[ε_t] - RWG (mean=-0.036197)
- Im[ε_t] - Theory (mean=-0.021258)

Legend (right):
- Re[ε_z] - tFWMT (mean =1.906)
- Re[ε_z] - RWG (mean=1.8797)
- Re[ε_z] - Theory (mean=2.0585)
- Im[ε_z] - tFWMT (mean=-0.36465)
- Im[ε_z] - RWG (mean=-0.032044)
- Im[ε_z] - Theory (mean=-0.025898)
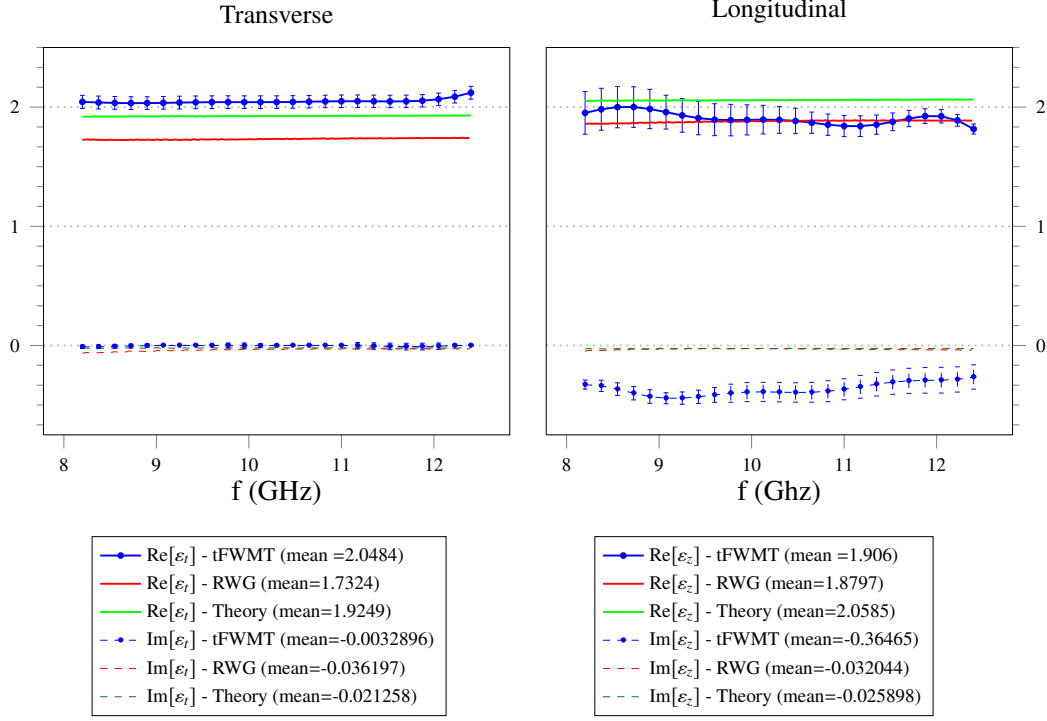
Figure 5.21: The results from the tFWMT extraction performed on the square lattice material with $d_1 = 0.53$mm and $d_2 = 1$mm using only the dominant mode.

nature of the lattice material and the hexagonal cells, the S-parameters are time-gated using the same settings as were used for the square lattice material. As with the previous material, various rotations with respect to the *z*-axis provided nearly equivalent results. In this case, due to the larger size of the inclusions, the WRWS method was chosen for comparison values.

Many of the observations from the square lattice material apply to the hexagonal honeycomb, as can be seen in Figure 5.25, except we see a much better agreement between the two methods in the dominant mode case.
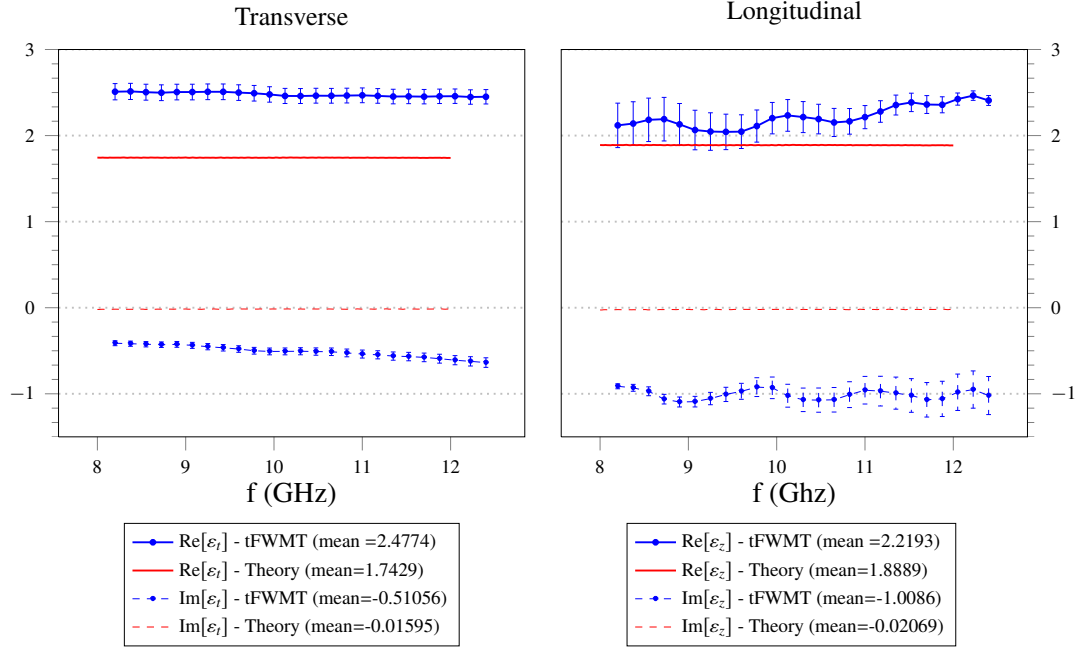
Figure 5.22: The results from the tFWMT extraction performed on the square lattice material with $d_1 = 0.91$mm and $d_2 = 2.75$mm using only the dominant mode. The transmission line theory is used as a comparison method, because RWG data was unavailable.

5.4.3 Cuming Microwave Lossy Honeycomb.

A lossy material alleviates the need for time-gating and retain all phase information, a uniform insertion loss carbon-loaded honeycomb core was ordered from Cuming Microwave. The cells were manufactured at $0.125''$ width and the core is loaded with a proprietary lossy coating rated at 10dBi/inch. Since the material is not structurally suited for a WRWS or RWG measurement and the samples are provided in $12'' \times 12'' \times 0.4''$ sheets, a free-space measurement was determined to be most effective comparison method. The results from the FBMT were obtained from measurements made at $\theta_i = 0$ and $\theta_i = 60$. Additionally, a Coaxial measurement was used to obtain another set of validation data.

202
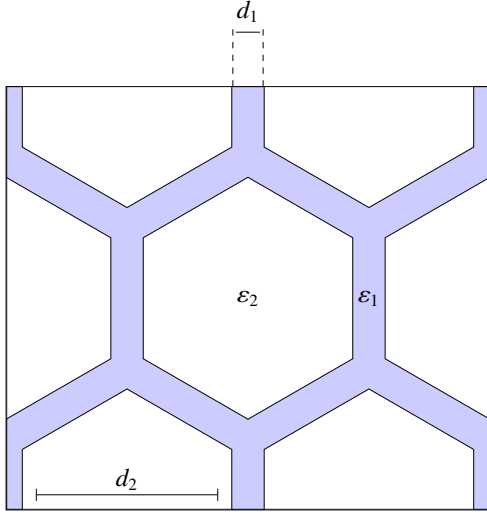
Figure 5.23: The variable dimensions of a unit cell of the honeycomb lattice material, which can be used to generate a variety of structures. Here, d_1 is the width of the lattice structure (which is composed of the white nylon polymer) and d_2 is the width of the hexagonal inclusions. The hexagons are regular polygons, with equal side lengths and inner angles.
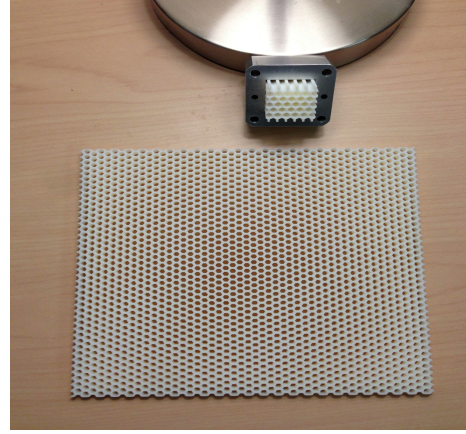

Figure 5.24: Samples of the honeycomb material used for tFWMT and WRWS measurement. Referencing the geometry in Figure 5.23, $d_2 = $ 3mm and $d_1 = $ 1mm.

Figures 5.26 presents the results of the extractions. Again, we see a reasonable correlation between $\text{Re}[\varepsilon_t]$ for the dominant mode case. However, the correlation between $\text{Im}[\varepsilon_t]$, $\text{Re}[\varepsilon_z]$ and $\text{Im}[\varepsilon_z]$ varies too much to conclude that any of the methods provide a precise answer. One complication that was experienced is the inhomogeneity of the material with respect to both the transverse and longitudinal dimensions, which was found by experience and a number of measurements. Inhomogeneity in the transverse plane can

203
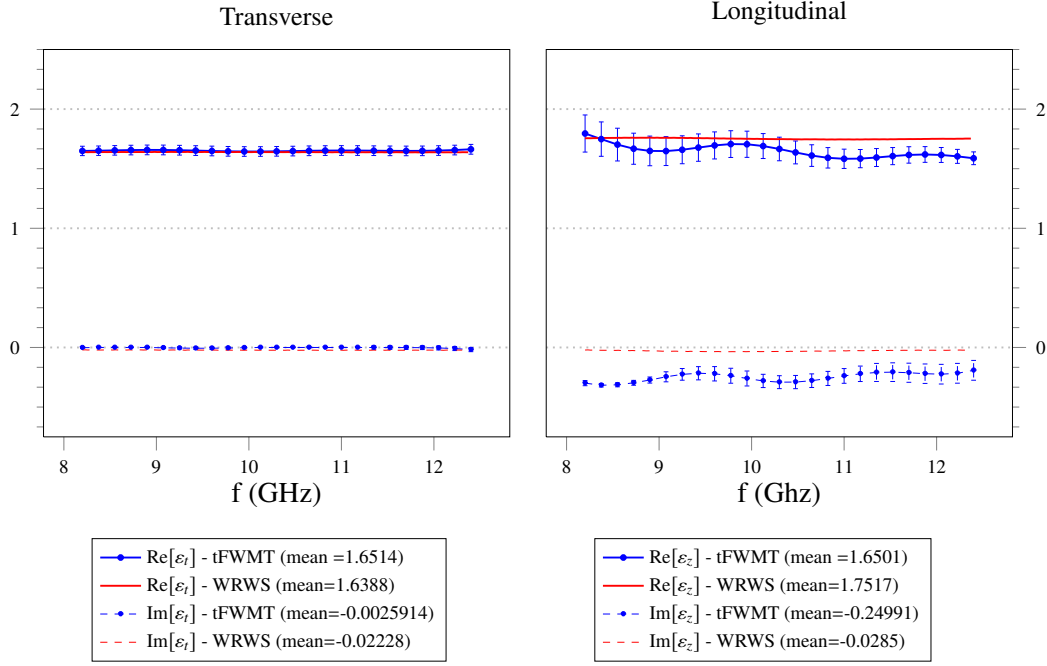
Figure 5.25: The results from the tFWMT extraction performed on the hexagonal honeycomb material using only the dominant mode.

only be accounted for by making an effective medium assumption. However, in extracting the constitutive parameters for the lossy honeycomb, we can utilize either the port 1-excited parameters (S_{11}/S_{21}) or the port 2-excited parameters (S_{22}/S_{12}). This minimizes the impact of the z-directed inhomogeneity.

5.5 General Remarks on Results

Now that several materials have been examined, we can make some observations about the results as a whole. Before doing so, it is worth emphasizing that the comparison methods are provided as reference points, not as precision results. In the following discussion, then, results are referred to as "reasonable" when the numerical values agree within 10% or when the results trend in similar ways across the band of interest.
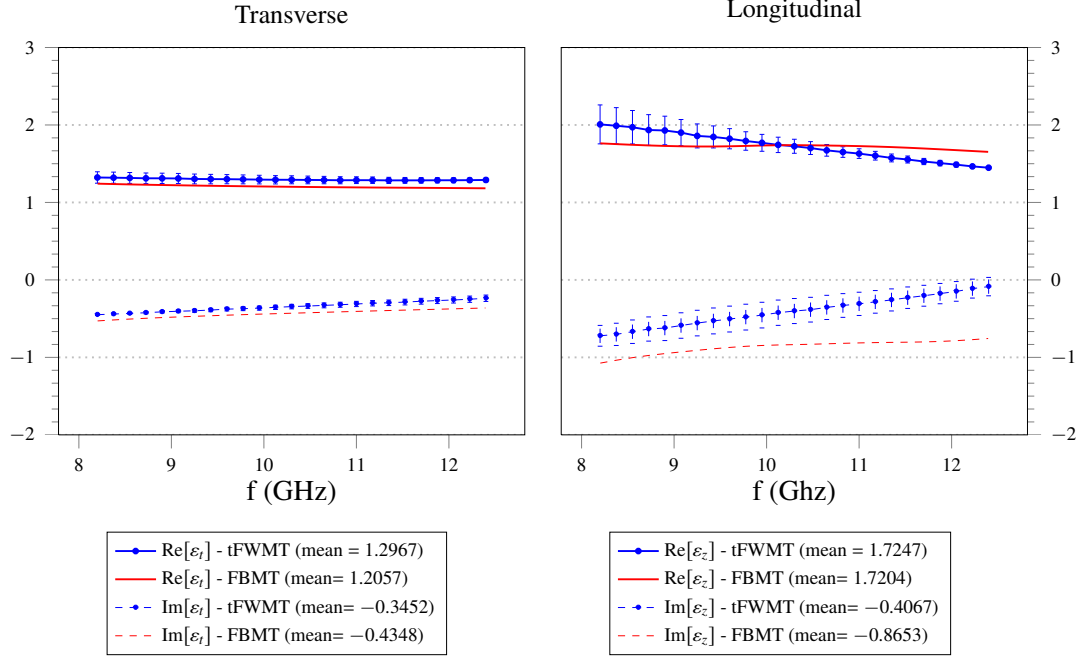
Figure 5.26: The results from the tFWMT extraction performed on the lossy honeycomb core using only the dominant mode utilizing the port 1 excited scattering parameters.

First, we note that the ε_t values agree very well in most cases, using both the dominant mode solutions. Even in cases where the values disagree, the trends match over the frequency band. This provides a measure of confidence in the tFWMT. The results for the ε_z values are much more difficult to characterize, as a whole. In most cases, the dominant mode solution provides reasonable results for ε_z. Even though the extracted values for ε_z using the dominant mode (especially $\text{Im}[\varepsilon_z]$) are numerically different from the comparison method, they trend in the same way. When qualitatively comparing the results presented in this work with those published in [17] (where the results for ε_z are not even given, as they vary between 10 and 10,000), the tFWMT is shown to provide considerably better results.

One final note on code efficiency is in order. By creating verification codes in which the integrals over the λ_ρ plane are calculated numerically, the efficiency of the method utilizing analytical solutions for the λ_y integral becomes readily apparent. The code in which the

λ_y integrals are solved analytically runs exponentially faster, since only one numerical integration is required, as opposed to two for the verification cases. Therefore, we see the benefit of the extra work which was required to find the analytical solutions to the λ_y integrals.

VI.   Conclusions and Future Work

This primary focus of this work has been on developing and demonstrating a method for the simultaneous non-destructive extraction of the permittivity and permeability of a uniaxial anisotropic media. The method utilizes a single fixture in which the MUT is clamped between two rectangular waveguides with 6" × 6" PEC flanges. The transmission and reflection coefficients are measured, then compared with theoretically calculated coefficients to find a least squares solution to the minimization problem.

One of the keys to solving the minimization problem is to correctly calculate the theoretical scattering parameters. Love's equivalence principle was used in conjunction with the total parallel plate Green's function and the Method of Moments (MoM) in order to generate a discretized system of coupled Magnetic Field Integral Equations (MFIE's), which may then be used to determine the theoretical scattering parameters. A great deal of attention was given to determining the total parallel-plate Green's function for the apparatus. One of the primary contributions of this work is the derivation of the total spectral-domain Green's function for uniaxial media contained in a parallel plate apparatus using two independent methods: the potentials method and the direct field method. In both methods, a Fourier technique was used to determine the Green's function, which greatly simplifies the analysis. In order to inverse transform the MFIE, a double integral over the spectral plane (λ_ρ) is required. This integral could be computed numerically by MATLAB®; however, double numerical integration is significantly less efficient than single numerical integration. Therefore, another significant contribution of this work is the closed-form solution of one of the inverse transform integrals (λ_y) using complex plane analysis and careful application of Cauchy's Integral Theorem and Jordan's lemma. These calculations are detailed for the dominant mode solution and the results for all modes are given in Appendix E.

Uniaxial materials in the X-band are more difficult to construct than in other bands with longer wavelengths, due to the smaller size of the unit cell. Therefore, rapid prototyping construction of a number of uniaxial materials using 3D printing methods was described.

A third significant contribution of this work is the demonstration of non-destructive measurements of complex media which are greatly improved from previous research efforts. In the course of making measurements in the laboratory, an improved measurement platform was devised in order to enhance accuracy, precision and repeatability of measurements, as well as prolong the effectiveness of a given TRL calibration. A number of uniaxial materials were measured using this configuration. The results utilizing the dominant mode (TE_{10}) to extract the transverse constitutive parameters were reasonable when compared with various validation methods (rectangular waveguide probe method, free-space measurement, etc.). However, the method is mildly numerically unstable when extracting the longitudinal parameters. This may be due to the lack of a primary field component in the longitudinal dimension, which would represent an inherent limitation of the method. Although the results in this work are not as accurate or stable as the results utilizing the same technique on isotropic media, they serve as a new benchmark for the non-destructive electromagnetic evaluation of complex media.

A secondary contribution of this work that warrants mention is the inclusion of a flexible, complete, working code for the extraction process. Although such codes have been written before, they have not been published in the literature for broader use.

6.1 Future Work

One area of further research that would immediately build on the efforts described in this work is to investigate methods of improving the stability of the longitudinal parameter extraction. Several methods are envisioned to accomplish this goal. Firstly, incorporating

208

higher modes has been shown in previous research to help stabilize the solutions for the extracted parameters. Another possibility is to investigate the possibility of biasing the flange plates with a constant electric field across the thickness of the MUT. This would produce a z-directed electric field component which would potentially provide enhanced interrogation of ε_z. Alternatively, since the dominant mode in a coaxial waveguide is TEM, this method could be extended for such a fixture. A final possible method for improving the stability of the longitudinal permittivity is to provide a rigorous analysis of an optimal thickness for the MUT. In the course of this work, a cursory investigation of the thickness was conducted, whereby three thicknesses of the 3D printed materials were measured $(0.125'', 0.25'', 0.5'')$. It was found the $1/4''$ material gave the most stable results, but a more rigorous investigation is warranted. It is possible that fringing fields from the edges of the apertures would constructively interfere across the material gap at specific thicknesses, thereby presenting a z-directed electric field component and improving the interrogation of ε_z by the system. Such a rigorous analysis could be performed using full wave solutions such as CST Microwave Studio®, ANSYS HFSS® or COMSOL Multiphysics®.

Another area of research that warrants exploration is that of applying the tFWMT to additional materials. The materials described in this work are a small subset of the possible materials. Because the method is seen to produce good results with lossy materials, any additional materials with a higher loss tangent would be ideal for future measurements. In fact, such a material could potentially be constructed using the square lattice material, where the inclusions are filled with a two-part iron-loaded, silicone base resin manufactured by Cuming microwave. Using an assumed dielectric constant of $\varepsilon_r = 7.8 - 0.06$ for the resin (non-dispersive), the potential contrast between the transverse and longitudinal permittivity is shown to be much greater than when air inclusions are used. In addition to being more lossy, this type of material could potentially provide the solver with better numerical

209

stability. Since the resin is magnetic and dielectric, a new transmission line model would be required to more accurately calculate theoretical constitutive parameters.
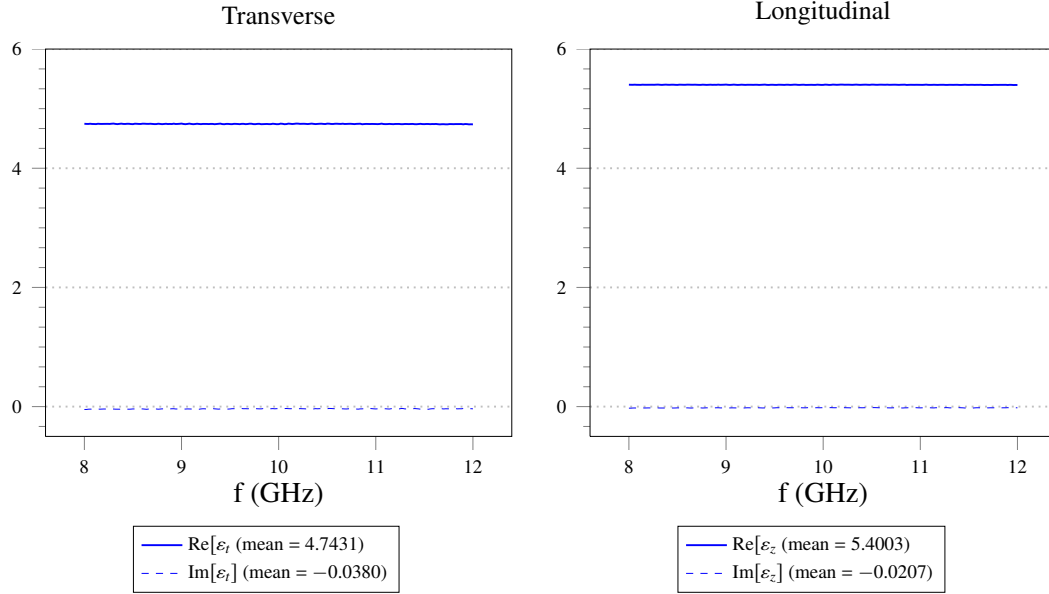
Figure 6.1: Theoretical permittivity for a uniaxial square lattice material with FGM125 representative inclusions. The theoretical permittivities were obtained using a transmission line theoretical model.

Finally, uniaxial media is known to be the simplest class of anisotropic media. An area of great interest would include extending the present theory to account for gyrotropic media. In fact, the principal Green's function for unbounded gyrotropic media has already been determined and work is in progress on the scattered solution. Determining the scattered and total Green's function and incorporating it into the tFMWT theory could provide the means to move into materials of even greater complexity.

Appendix A: Complex Plane Analysis

In the course of this work, we are often interested in analytic solutions to complicated integrations of functions which contain singularities. This process may be significantly simplified by the principles of complex plane analysis. Consider the general function

$$f(\lambda_z) = \frac{g(\lambda_z)}{h(\lambda_z)} = \frac{e^{j\lambda_z(z-z')}}{(\lambda_z - \lambda_{z\psi})(\lambda_z + \lambda_{z\psi})} \tag{A.1}$$

where $\lambda_{z\psi}$ is assumed to be a complex constant. In the case of this complex-valued function, the variable λ_z is assumed to be complex. Decomposing it into real and imaginary parts, such that $\lambda_z = \lambda_{z,\mathrm{re}} + j\lambda_{z,\mathrm{im}}$, the function becomes

$$
\begin{aligned}
f(\lambda_z) &= \frac{e^{j(\lambda_{z,\mathrm{re}} + j\lambda_{z,\mathrm{im}})(z-z')}}{(\lambda_z - \lambda_{z\psi})(\lambda_z + \lambda_{z\psi})} \\
&= \frac{e^{j\lambda_{z,\mathrm{re}}(z-z')}e^{-\lambda_{z,\mathrm{im}}(z-z')}}{(\lambda_z - \lambda_{z\psi})(\lambda_z + \lambda_{z\psi})}
\end{aligned}
\tag{A.2}
$$

Now, Jordan's Lemma [58] states that, for a semicircular contour C_R of radius R centered on the origin in the upper half plane (UHP), if the function $f(z)$ is analytic in the UHP (except for a finite number of singularities) and if $|f(z)| \rightarrow 0$ uniformly as $|z| \rightarrow \infty$ for $0 \leqslant \mathrm{Arg}(z) \leqslant \pi$, then, for $m > 0$:

$$\lim_{R \to \infty} \int_{C_R} e^{jmz} f(z) dz = 0 \tag{A.3}$$

For functions that are analytic in same manner in the lower half plane (LHP) and satisfy the same uniformly decaying conditions, Jordan's Lemma can also be applied in the LHP, as long as the contour is drawn in the counter-clockwise sense.

From (A.2), we see that, in order to satisfy the conditions of Jordan's Lemma in the UHP (where $\lambda_{z,\mathrm{im}} > 0$), then $z - z' > 0$ in order to insure the exponential will decay to zero as $\lambda_z \rightarrow \infty$. This is the closure condition required by Jordan's Lemma.

Figure A.1: The complex plane and associated contours for the function given in (A.1).

Cauchy's Integral Theorem [58] states that for a function $f(z)$, which is analytic in a simply connected domain D and also on its boundary C, which is a piecewise smooth closed simple curve, the value of the integral of the function around the contour C is given by

$$\oint_C f(z)dz = 0 \tag{A.4}$$

Since the contour may be drawn piecewise, we see that it may by the concatenation of the different contours. For the case of our function given in (A.1), Figure A.1 shows how the piecewise contour may be drawn. Therefore, we have the following equation in the UHP

$$\lim_{R \to \infty} \left[\int_{-R}^{R} + \int_{C_R} - \oint_{C_{P_1}^+} \right] = 0 \tag{A.5}$$

where the negative sign in the last term accounts for the fact that the contour is drawn in the clockwise direction, but integration is in the counter-clockwise direction. Also note that we have not included the straight pieces of the contours which lead from the real axis to the contour around the singularity and back. Since these lines point in opposite directions,

they will cancel each other out and have no contribution. Now, applying Jordan's Lemma to (A.5), since we have satisfied the appropriate closure conditions, we see that the second integral is zero. Therefore, we see that we can calculate the integral over the real plane, which is our desired value, by calculating the integral over the contour $C_{P_1}^+$ drawn around the singularity at $\lambda_z = -\lambda_{z\psi}$:

$$\lim_{R \to \infty} \int_{-R}^{R} = \oint_{C_{P_1}^+} \tag{A.6}$$

In general, Cauchy's integral formula allows us to calculate the value of the integral around a contour C_P, which contains the singularity of order n at the point $z = z_0$ [58]:

$$\oint_{C_P} = j2\pi \text{Res}(f, z_0) = \frac{j2\pi}{(n-1)!} \lim_{z \to z_0} \left\{ \frac{\partial^{n-1}}{\partial z^{n-1}} \left[(z-z_0)^n f(z) \right] \right\} \tag{A.7}$$

Similarly, the Cauchy Integral formula for derivatives states that, for an analytic function $f(z)$ in a simply connected domain D, with C being a simply closed contour within D, so long as the singularity z_0 lies within C:

$$f^{(n-1)}(z_0) = \frac{(n-1)!}{j2\pi} \int_C \frac{f(z)}{(z-z_0)^n} \tag{A.8}$$

For a more general expression, consider a function $f(z) = \frac{g(z)}{h(z)}$, where $h(z)$ contains a pole of order n at the value z_0. We want to determine the residue of this function (where the contour C_ε around the singularity has a radius ε):

$$\oint_{C_\varepsilon} \frac{g(z)}{h(z)} dz \tag{A.9}$$

The denominator $h(z)$ may be expanded into a Taylor series about the point z_0:

$$\begin{aligned}
h(z) = h(z_0) &+ \frac{(z-z_0)}{1!} \left. \frac{\partial h(z)}{\partial z} \right|_{z_0} + \frac{(z-z_0)^2}{2!} \left. \frac{\partial^2 h(z)}{\partial z^2} \right|_{z_0} + \dots \\
&+ \frac{(z-z_0)^n}{n!} \left. \frac{\partial^n h(z)}{\partial z^n} \right|_{z_0} + \frac{(z-z_0)^{n+1}}{(n+1)!} \left. \frac{\partial^{n+1} h(z)}{\partial z^{n+1}} \right|_{z_0} + \dots
\end{aligned} \tag{A.10}$$

213

Now, note that, for a pole of order n, the nth derivative will be the first non-zero term. Therefore, the expansion may be now be written (with $|z - z_0| = \varepsilon$) as:

$$h(z) = \frac{(z - z_0)^n}{n!} \left.\frac{\partial^n h(z)}{\partial z^n}\right|_{z_0} + \mathbb{O}(\varepsilon) \tag{A.11}$$

where $\mathbb{O}(\varepsilon)$ represents the higher order terms which will become non-contributing factors in the limit as $\varepsilon \to 0$. Therefore, in this limit, (A.9) becomes

$$\oint_{C_\varepsilon} \frac{g(z)}{h(z)} dz = \left[\left(\frac{n!}{\frac{\partial^n h(z)}{\partial z^n}}\right)\Bigg|_{z=z_0}\right] \oint_{C_\varepsilon} \frac{g(z)}{(z - z_0)^n} dz \tag{A.12}$$

The contour integral for $g(z)$ is given by (A.8), which transforms (A.12) to

$$\oint_{C_\varepsilon} \frac{g(z)}{h(z)} dz = \left[\left(\frac{n!}{\frac{\partial^n h(z_0)}{\partial z_0^n}}\right)\left(\frac{j2\pi}{(n-1)!}\right)\left(\frac{\partial^{n-1} g(z)}{\partial z^{n-1}}\right)\right]\Bigg|_{z=z_0} = j2\pi n \frac{\frac{\partial^{n-1} g(z)}{\partial z^{n-1}}}{\frac{\partial^n h(z)}{\partial z^n}}\Bigg|_{z=z_0}$$

$$= j2\pi n \frac{D_z^{n-1} g(z)}{D_z^n h(z)}\Bigg|_{z=z_0} \tag{A.13}$$

This clearly reduces to the well-known form for a simple pole:

$$\oint_{z_0} \frac{g(z)}{h(z)} dz = j2\pi \frac{g(z)}{h'(z)}\Bigg|_{z=z_0} \tag{A.14}$$

Using these expressions for our original example (which contains a simple pole at $\lambda_z = -\lambda_{z\psi}$ in the UHP), we define

$$g(\lambda_z) = \frac{e^{j\lambda_z(z-z')}}{(\lambda_z - \lambda_{z\psi})} \quad \text{and} \quad h(\lambda_z) = (\lambda_z + \lambda_{z\psi}) \tag{A.15}$$

Therefore, the right side of (A.6) becomes

$$\oint_{C_{P_1}^+} f(\lambda_z) dz = j2\pi \text{Res}(f, -\lambda_{z\psi}) = j2\pi \frac{g(\lambda_z)}{h'(\lambda_z)}\Bigg|_{\lambda_z=-\lambda_{z\psi}} \tag{A.16}$$

which, after recognizing $h' = 1$, leads to the desired result:

$$\lim_{R\to\infty} \int_{-R}^{R} \oint_{C_{P_1}^+} \frac{g(z)}{h(z)} dz = j2\pi \frac{e^{-j\lambda_{z\psi}(z-z')}}{-2\lambda_{z\psi}} \tag{A.17}$$

214

In the LHP, we note that Cauchy's Integral Theorem gives

$$\lim_{R\to\infty}\left[\int_{-R}^{R}+\int_{C_R}+\oint_{C_{P_1}^-}\right]=0 \qquad (A.18)$$

which, after ensuring the correct closure conditions are satisfied (thus satisfying Jordan's Lemma) implies the desired value of the integral may be found from

$$\lim_{R\to\infty}\int_{-R}^{R}=-\oint_{C_{P_1}^-} \qquad (A.19)$$

Using Cauchy's Integral Formula and the positive value of $\lambda_{z\psi}$ in the LHP leads to the expression

$$\oint_{C_{P_1}^-}\frac{g(z)}{h(z)}dz=-j2\pi\frac{e^{j\lambda_{z\psi}(z-z')}}{2\lambda_{z\psi}} \qquad (A.20)$$

In the UHP, we see that the terms in the exponential will always be negative (since $z-z'>0$) and, conversely, in the LHP, the exponential will always be positive (since $z-z'<0$). This leads to the final result

$$\boxed{\int_{-\infty}^{\infty}f(\lambda_z)d\lambda_z=j\pi\frac{e^{-j\lambda_{z\psi}|z-z'|}}{\lambda_{z\psi}}} \qquad (A.21)$$

215

Appendix B: Component Expansion of Green's Functions from Potential-Based Method

We can expand the Green's functions obtained from the potential-based method in Chapter 2 into individual components, which will be useful in comparing these results with the direct field solutions.

B.1 Expansion of Electric (*ee*) Green's Function

We have the following expression for $\overset{\leftrightarrow}{\tilde{G}}_{ee}$:

$$\overset{\leftrightarrow}{\tilde{G}}_{ee} = j\vec{\lambda}_\rho \vec{\tilde{G}}_{\Phi_{et}} + j\vec{\lambda}_\rho \vec{\tilde{G}}_{\Phi_{ez}} - \hat{\mathbf{z}} \times j\vec{\lambda}_\rho \vec{\tilde{G}}_{\theta_e} + \hat{\mathbf{z}}\frac{\lambda_\rho^2}{j\omega\varepsilon_z}\vec{\tilde{G}}_{\psi_{et}} + \hat{\mathbf{z}}\frac{\lambda_\rho^2}{j\omega\varepsilon_z}\vec{\tilde{G}}_{\psi_{ez}} - \hat{\mathbf{z}}\hat{\mathbf{z}}\frac{1}{j\omega\varepsilon_z} \qquad \text{(B.1)}$$

The first term in (B.1) is:

$$j\vec{\lambda}_\rho \vec{\tilde{G}}_{\Phi_{et}} = j\left(\hat{\mathbf{x}}\lambda_x + \hat{\mathbf{y}}\lambda_y\right)\left(\vec{\lambda}_\rho \frac{\lambda_{z\psi}}{2\lambda_\rho^2 \omega\varepsilon_t}\right)\left[\frac{\cos\left(\lambda_{z\psi}\left[d-|z-z'|\right]\right) - \cos\left(\lambda_{z\psi}\left[d-(z+z')\right]\right)}{\sin\left(\lambda_{z\psi}d\right)}\right]$$

$$= j\left(\frac{\lambda_{z\psi}}{2\lambda_\rho^2 \omega\varepsilon_t}\right)\begin{bmatrix} \lambda_x^2 & \lambda_x\lambda_y & 0 \\ \lambda_x\lambda_y & \lambda_y^2 & 0 \\ 0 & 0 & 0 \end{bmatrix}\left[\frac{\cos\left(\lambda_{z\psi}\left[d-|z-z'|\right]\right) - \cos\left(\lambda_{z\psi}\left[d-(z+z')\right]\right)}{\sin\left(\lambda_{z\psi}d\right)}\right]$$

$$\text{(B.2)}$$

The second term is:

$$j\vec{\lambda}_\rho \vec{\tilde{G}}_{\Phi_{ez}} = j\left(\hat{\mathbf{x}}\lambda_x + \hat{\mathbf{y}}\lambda_y\right)\left(\hat{\mathbf{z}}\frac{j}{2\omega\varepsilon_z}\right)\left[\frac{\text{sgn}\left(z-z'\right)\sin\left(\lambda_{z\psi}\left[d-|z-z'|\right]\right) + \sin\left(\lambda_{z\psi}\left[d-(z+z')\right]\right)}{\sin\left(\lambda_{z\psi}d\right)}\right]$$

$$= -\frac{1}{2\omega\varepsilon_z}\begin{bmatrix} 0 & 0 & \lambda_x \\ 0 & 0 & \lambda_y \\ 0 & 0 & 0 \end{bmatrix}\left[\frac{\text{sgn}\left(z-z'\right)\sin\left(\lambda_{z\psi}\left[d-|z-z'|\right]\right) + \sin\left(\lambda_{z\psi}\left[d-(z+z')\right]\right)}{\sin\left(\lambda_{z\psi}d\right)}\right]$$

$$\text{(B.3)}$$

The third term is:

$$-\hat{\mathbf{z}} \times j\vec{\lambda}_\rho \ddot{\vec{G}}_{\theta_e} = -j\left(-\hat{\mathbf{x}}\lambda_y + \hat{\mathbf{y}}\lambda_x\right)\left(-\frac{\hat{\mathbf{z}} \times \vec{\lambda}_\rho \omega \mu_t}{2\lambda_{z\theta}\lambda_\rho^2}\right)\left[\frac{\cos\left(\lambda_{z\theta}\left[d - |z-z'|\right]\right) - \cos\left(\lambda_{z\theta}\left[d - (z+z')\right]\right)}{\sin\left(\lambda_{z\theta}d\right)}\right]$$

$$= \left(\frac{j\omega\mu_t}{2\lambda_{z\theta}\lambda_\rho^2}\right)\begin{bmatrix} \lambda_y^2 & -\lambda_x\lambda_y & 0 \\ -\lambda_x\lambda_y & \lambda_x^2 & 0 \\ 0 & 0 & 0 \end{bmatrix}\left[\frac{\cos\left(\lambda_{z\theta}\left[d - |z-z'|\right]\right) - \cos\left(\lambda_{z\theta}\left[d - (z+z')\right]\right)}{\sin\left(\lambda_{z\theta}d\right)}\right]$$

$$(B.4)$$

The fourth term is:

$$\hat{\mathbf{z}}\frac{\lambda_\rho^2}{j\omega\varepsilon_z}\ddot{\vec{G}}_{\psi_{et}} = \hat{\mathbf{z}}\frac{\lambda_\rho^2}{j\omega\varepsilon_z}\left(-\vec{\lambda}_\rho\frac{j}{2\lambda_\rho^2}\right)\left[\frac{\mathrm{sgn}\left(z-z'\right)\sin\left(\lambda_{z\psi}\left[d - |z-z'|\right]\right) - \sin\left(\lambda_{z\psi}\left[d - (z+z')\right]\right)}{\sin\left(\lambda_{z\psi}d\right)}\right]$$

$$= -\left(\frac{1}{2\omega\varepsilon_z}\right)\begin{bmatrix} 0 & 0 & 0 \\ 0 & 0 & 0 \\ \lambda_x & \lambda_y & 0 \end{bmatrix}\left[\frac{\mathrm{sgn}\left(z-z'\right)\sin\left(\lambda_{z\psi}\left[d - |z-z'|\right]\right) - \sin\left(\lambda_{z\psi}\left[d - (z+z')\right]\right)}{\sin\left(\lambda_{z\psi}d\right)}\right]$$

$$(B.5)$$

The fifth term is:

$$\hat{\mathbf{z}}\frac{\lambda_\rho^2}{j\omega\varepsilon_z}\ddot{\vec{G}}_{\psi_{ez}} = \hat{\mathbf{z}}\frac{\lambda_\rho^2}{j\omega\varepsilon_z}\left(-\hat{\mathbf{z}}\frac{\varepsilon_t}{2\lambda_{z\psi}\varepsilon_z}\right)\left[\frac{\cos\left(\lambda_{z\psi}\left[d - |z-z'|\right]\right) + \cos\left(\lambda_{z\psi}\left[d - (z+z')\right]\right)}{\sin\left(\lambda_{z\psi}d\right)}\right]$$

$$= \left(\frac{j\frac{\varepsilon_t}{\varepsilon_z}\lambda_\rho^2}{2\omega\lambda_{z\psi}\varepsilon_z}\right)\begin{bmatrix} 0 & 0 & 0 \\ 0 & 0 & 0 \\ 0 & 0 & 1 \end{bmatrix}\left[\frac{\cos\left(\lambda_{z\psi}\left[d - |z-z'|\right]\right) + \cos\left(\lambda_{z\psi}\left[d - (z+z')\right]\right)}{\sin\left(\lambda_{z\psi}d\right)}\right]$$

$$(B.6)$$

And the sixth term is the depolarizing term:

$$-\hat{\mathbf{z}}\hat{\mathbf{z}}\frac{1}{j\omega\varepsilon_z} = -\frac{1}{j\omega\varepsilon_z}\begin{bmatrix} 0 & 0 & 0 \\ 0 & 0 & 0 \\ 0 & 0 & 1 \end{bmatrix} \qquad (B.7)$$

217

By examining the form, we note the $\vec{\bar{G}}_{\theta_e}$ term only contributes to the transverse fields. Therefore, we see that the terms which contain $\lambda_{z\theta}$ are TE^z, since the requirement for TE^z is $E_z = 0$. The TE^z and TM^z portions are given in the following pages, making use of the following relationships for brevity, where the representation $\Upsilon_1^{\theta|\psi}$ represents either Υ_1^θ (which contains $\lambda_{z\theta}$ terms) or Υ_1^ψ (which contains $\lambda_{z\psi}$ terms):

$$
\begin{aligned}
\Upsilon_1^{\theta|\psi} &= \frac{\cos\left(\lambda_{z_\theta|z_\psi}\left[d-|z-z'|\right]\right) - \cos\left(\lambda_{z_\theta|z_\psi}\left[d-(z+z')\right]\right)}{\sin\left(\lambda_{z_\theta|z_\psi}d\right)} \\
\Upsilon_2^{\theta|\psi} &= \frac{\cos\left(\lambda_{z_\theta|z_\psi}\left[d-|z-z'|\right]\right) + \cos\left(\lambda_{z_\theta|z_\psi}\left[d-(z+z')\right]\right)}{\sin\left(\lambda_{z_\theta|z_\psi}d\right)} \\
\Upsilon_3^{\theta|\psi} &= \frac{\operatorname{sgn}(z-z')\sin\left(\lambda_{z_\theta|z_\psi}\left[d-|z-z'|\right]\right) - \sin\left(\lambda_{z_\theta|z_\psi}\left[d-(z+z')\right]\right)}{\sin\left(\lambda_{z_\theta|z_\psi}d\right)} \\
\Upsilon_4^{\theta|\psi} &= \frac{\operatorname{sgn}(z-z')\sin\left(\lambda_{z_\theta|z_\psi}\left[d-|z-z'|\right]\right) + \sin\left(\lambda_{z_\theta|z_\psi}\left[d-(z+z')\right]\right)}{\sin\left(\lambda_{z_\theta|z_\psi}d\right)}
\end{aligned}
\tag{B.8}
$$

B.2   Electric (*ee*) Green's Function Summary

The TE^z field may be found from (B.4), the TM^z field may be found from (B.2),(B.3),(B.5) and (B.6) and the depolarizing term from (B.7):

$$\tilde{\tilde{\overleftrightarrow{G}}}_{ee}=\tilde{\tilde{\overleftrightarrow{G}}}_{ee}^{\text{TE}} + \tilde{\tilde{\overleftrightarrow{G}}}_{ee}^{\text{TM}} + \tilde{\tilde{\overleftrightarrow{G}}}_{ee}^{\text{d}}$$

$$\tilde{\tilde{\overleftrightarrow{G}}}_{ee}^{\text{TE}} = \left(\frac{j\omega\mu_t}{2\lambda_{z\theta}\lambda_\rho^2}\right)\begin{bmatrix} \lambda_y^2 & -\lambda_x\lambda_y & 0 \\[2mm] -\lambda_x\lambda_y & \lambda_x^2 & 0 \\[2mm] 0 & 0 & 0 \end{bmatrix}\Upsilon_1^\theta$$

$$\tilde{\tilde{\overleftrightarrow{G}}}_{ee}^{\text{TM}} = \left(\frac{j}{2\omega\varepsilon_t\lambda_\rho^2}\right)\begin{bmatrix} \lambda_x^2\lambda_{z\psi}\Upsilon_1^\psi & \lambda_x\lambda_y\lambda_{z\psi}\Upsilon_1^\psi & j\frac{\varepsilon_t}{\varepsilon_z}\lambda_x\lambda_\rho^2\Upsilon_4^\psi \\[4mm] \lambda_x\lambda_y\lambda_{z\psi}\Upsilon_1^\psi & \lambda_y^2\lambda_{z\psi}\Upsilon_1^\psi & j\frac{\varepsilon_t}{\varepsilon_z}\lambda_y\lambda_\rho^2\Upsilon_4^\psi \\[4mm] j\frac{\varepsilon_t}{\varepsilon_z}\lambda_x\Upsilon_3^\psi & j\frac{\varepsilon_t}{\varepsilon_z}\lambda_y\lambda_\rho^2\Upsilon_3^\psi & \left(\frac{j}{\lambda_{z\psi}}\right)\left(\frac{\varepsilon_t\lambda_\rho^2}{\varepsilon_z}\right)^2\Upsilon_2^\psi \end{bmatrix} \qquad \text{(B.9)}$$

$$\tilde{\tilde{\overleftrightarrow{G}}}_{ee}^{\text{d}} = -\frac{1}{j\omega\varepsilon_z}\delta(z-z')$$

219

B.3 Magnetoelectric (*eh*) Green's Function Summary

The components of the *eh*-type Green's function are found using the same expansion method.

$$\overset{\leftrightarrow}{\tilde{G}}_{eh} = \overset{\leftrightarrow}{\tilde{G}}_{eh}^{\text{TE}} + \overset{\leftrightarrow}{\tilde{G}}_{eh}^{\text{TM}}$$

$$\overset{\leftrightarrow}{\tilde{G}}_{eh}^{\text{TE}} = \left(\frac{1}{2\lambda_\rho^2}\right) \begin{bmatrix} -\lambda_x\lambda_y\Upsilon_4^\theta & -\lambda_y^2\Upsilon_4^\theta & \dfrac{j\mu_t\lambda_y\lambda_\rho^2}{\mu_z\lambda_{z\theta}}\Upsilon_1^\theta \\[2ex] \lambda_x^2\Upsilon_4^\theta & \lambda_x\lambda_y\Upsilon_4^\theta & -\dfrac{j\mu_t\lambda_x\lambda_\rho^2}{\mu_z\lambda_{z\theta}}\Upsilon_1^\theta \\[2ex] 0 & 0 & 0 \end{bmatrix} \tag{B.10}$$

$$\overset{\leftrightarrow}{\tilde{G}}_{eh}^{\text{TM}} = \left(\frac{1}{2\lambda_\rho^2}\right) \begin{bmatrix} \lambda_x\lambda_y\Upsilon_4^\psi & -\lambda_x^2\Upsilon_4^\psi & 0 \\[2ex] \lambda_y^2\Upsilon_4^\psi & -\lambda_x\lambda_y\Upsilon_4^\psi & 0 \\[2ex] -\dfrac{j\varepsilon_t\lambda_y\lambda_\rho^2}{\varepsilon_z\lambda_{z\psi}}\Upsilon_2^\psi & \dfrac{j\varepsilon_t\lambda_x\lambda_\rho^2}{\varepsilon_z\lambda_{z\psi}}\Upsilon_2^\psi & 0 \end{bmatrix}$$

B.4 Magnetoelectric (*he*) Green's Function Summary

The components of the *he*-type Green's function are found to be:

$$\tilde{\tilde{G}}_{he} = \tilde{\tilde{G}}_{he}^{TE} + \tilde{\tilde{G}}_{he}^{TM}$$

$$\tilde{\tilde{G}}_{he}^{TE} = \left(\frac{1}{2\lambda_\rho^2}\right) \begin{bmatrix} -\lambda_x\lambda_y\Upsilon_3^\theta & \lambda_x^2\Upsilon_3^\theta & 0 \\ & & \\ -\lambda_y^2\Upsilon_3^\theta & \lambda_x\lambda_y\Upsilon_3^\theta & 0 \\ & & \\ \dfrac{j\mu_t\lambda_y\lambda_\rho^2}{\mu_z\lambda_{z\theta}}\Upsilon_1^\theta & -\dfrac{j\mu_t\lambda_x\lambda_\rho^2}{\mu_z\lambda_{z\theta}}\Upsilon_1^\theta & 0 \end{bmatrix}$$

(B.11)

$$\tilde{\tilde{G}}_{he}^{TM} = \left(\frac{1}{2\lambda_\rho^2}\right) \begin{bmatrix} \lambda_x\lambda_y\Upsilon_3^\psi & \lambda_y^2\Upsilon_3^\psi & -\dfrac{j\varepsilon_t\lambda_y\lambda_\rho^2}{\varepsilon_z\lambda_{z\psi}}\Upsilon_2^\psi \\ & & \\ -\lambda_x^2\Upsilon_4^\psi & -\lambda_x\lambda_y\Upsilon_3^\psi & \dfrac{j\mu_t\lambda_x\lambda_\rho^2}{\mu_z\lambda_{z\psi}}\Upsilon_2^\psi \\ & & \\ 0 & 0 & 0 \end{bmatrix}$$

221

B.5 Magnetic (*hh*) Green's Function Summary

Finally, the components of the magnetic Green's function are found to be:

$$\overleftrightarrow{\tilde{G}}_{hh} = \overleftrightarrow{\tilde{G}}_{hh}^{\text{TE}} + \overleftrightarrow{\tilde{G}}_{hh}^{\text{TM}} + \overleftrightarrow{\tilde{G}}_{hh}^{\text{d}}$$

$$\overleftrightarrow{\tilde{G}}_{hh}^{\text{TE}} = \left(\frac{j}{2\omega\mu_t\lambda_\rho^2} \right) \begin{bmatrix} \lambda_x^2\lambda_{z\theta}\Upsilon_2^\theta & \lambda_x\lambda_y\lambda_{z\psi}\Upsilon_2^\theta & j\frac{\mu_t}{\mu_z}\lambda_x\lambda_\rho^2\Upsilon_3^\theta \\[3mm] \lambda_x\lambda_y\lambda_{z\theta}\Upsilon_2^\theta & \lambda_y^2\lambda_{z\theta}\Upsilon_2^\theta & j\frac{\mu_t}{\mu_z}\lambda_y\lambda_\rho^2\Upsilon_3^\theta \\[5mm] j\frac{\mu_t}{\mu_z}\lambda_x\Upsilon_4^\theta & j\frac{\mu_t}{\mu_z}\lambda_y\lambda_\rho^2\Upsilon_4^\theta & \left(\frac{j}{\lambda_{z\psi}}\right)\left(\frac{\mu_t\lambda_\rho^2}{\mu_z}\right)^2\Upsilon_1^\theta \end{bmatrix} \tag{B.12}$$

$$\overleftrightarrow{\tilde{G}}_{hh}^{\text{TM}} = \left(\frac{j\omega\varepsilon_t}{2\lambda_{z\psi}\lambda_\rho^2} \right) \begin{bmatrix} \lambda_y^2 & -\lambda_x\lambda_y & 0 \\[2mm] -\lambda_x\lambda_y & \lambda_x^2 & 0 \\[2mm] 0 & 0 & 0 \end{bmatrix} \Upsilon_2^\psi$$

$$\overleftrightarrow{\tilde{G}}_{hh}^{\text{d}} = -\frac{1}{j\omega\mu_z}\delta(z-z')$$

Appendix C: PPWG Green's Function for Isotropic Media

In this appendix, a cursory development of $\widetilde{G}_{hh}$ will be given, using a potential development. Since we are looking for the magnetic field, we will work with the F potential. Note the parallel plates are separated by a distance d. The governing equation for the F_α ($\alpha = x, y$) potential is [9] is:

$$\nabla^2 F_\alpha(\rho, z) + k^2 F_\alpha(\rho, z) = -\varepsilon J_{h\alpha}(\rho, z) \tag{C.1}$$

Using the standard Fourier transform pairs of (2.36) and (2.39), we can write:

$$(-\lambda_z^2 + \lambda_{z0}^2)\widetilde{\widetilde{F}}_\alpha(\lambda_\rho, \lambda_z) = -\varepsilon \widetilde{\widetilde{J}}_{h\alpha} \tag{C.2}$$

where $\lambda_{z0} = k^2 - \lambda_\rho^2$. The spectral domain solution is easily found to be:

$$\widetilde{\widetilde{F}}_\alpha(\lambda_\rho, \lambda_z) = \frac{\varepsilon \widetilde{\widetilde{J}}_{h\alpha}}{(\lambda_z^2 - \lambda_{z0}^2)} \tag{C.3}$$

Reverse transforming on the λ_z variable and noting the definition of $\widetilde{\widetilde{J}}_{h\alpha}$ leads to:

$$\widetilde{F}_\alpha(\lambda_\rho, z) = \int\limits_{z'} \left[\frac{1}{2\pi} \int\limits_{-\infty}^{\infty} \frac{e^{j\lambda_z(z-z')}}{(\lambda_z + \lambda_{z0})(\lambda_z - \lambda_{z0})} d\lambda_z \right] \varepsilon \widetilde{J}_{h\alpha}(\lambda_\rho, z') dz' \tag{C.4}$$

Using the same complex plane analysis as in Chapters 2 and 3, we find the principal solution:

$$\widetilde{F}_\alpha^p(\lambda_\rho, z) = \int\limits_{z'} \frac{e^{-j\lambda_{z0}|z-z'|}}{j2\lambda_{z0}} \cdot \varepsilon \widetilde{J}_{h\alpha}(\lambda_\rho, z) dz' \tag{C.5}$$

In order to find the scattered solution, we must determine the appropriate boundary conditions on $\vec{F}$. Recall, the electric field descriibed by $\vec{F}$ is:

$$\vec{E} = -\frac{\nabla \times \vec{F}}{\varepsilon} = -\frac{1}{\varepsilon}\hat{\mathbf{x}}\left(\frac{\partial F_z}{\partial y} - \frac{\partial F_y}{\partial z}\right) + \hat{\mathbf{y}}\left(\frac{\partial F_x}{\partial z} - \frac{\partial F_z}{\partial x}\right) + \hat{\mathbf{z}}\left(\frac{\partial F_y}{\partial x} - \frac{\partial F_x}{\partial y}\right) \tag{C.6}$$

Therefore, the PEC boundary condistions $E_x = E_y = 0$ lead to:

$$\frac{\partial F_z}{\partial y} - \frac{\partial F_y}{\partial z} = 0 \tag{C.7}$$

$$\frac{\partial F_x}{\partial z} - \frac{\partial F_z}{\partial x} = 0 \tag{C.8}$$

Considering the possible sources, if $\vec{J_h} = \hat{\mathbf{x}} J_{hx}$, then $\vec{F} = \hat{\mathbf{x}} F_x$. In order to fulfill the boundary conditions, we have $\frac{\partial F_x}{\partial z} = F_y = F_z = 0$. Next, if $\vec{J_h} = \hat{\mathbf{y}} J_{hy}$, then $\vec{F} = \hat{\mathbf{y}} F_y$. In order to fulfill the boundary conditions, we have $\frac{\partial F_y}{\partial z} = F_x = F_z = 0$. Finally, if $\vec{J_h} = \hat{\mathbf{z}} J_{hz}$, then $\vec{F} = \hat{\mathbf{z}} F_z$. In order to fulfill the boundary conditions, we have $\frac{\partial F_z}{\partial x} = \frac{\partial F_z}{\partial y} = F_x = F_y = F_z = 0$. By superposition, this leads to the total boundary condition on $\vec{F}$:

$$\frac{\partial F_\alpha}{\partial z} = F_z = 0 \tag{C.9}$$

Now, as before, we assume a reflected solution of the form

$$\tilde{F}^r_\alpha(\lambda_\rho, z) = \tilde{w}^+_\alpha e^{-j\lambda_{z0}z} + \tilde{w}^-_\alpha e^{j\lambda_{z0}z} \tag{C.10}$$

where $\tilde{w}^+_\alpha$ and $\tilde{w}^-_\alpha$ are the unknown scattering coefficients to be found by application of the boundary conditions. The total potential $\tilde{F}_\alpha$ is now given by the superposition of the principal and reflected solutions:

$$\tilde{F}_\alpha(\lambda_\rho, z) = \int\limits_{z'} \frac{e^{-j\lambda_{z0}|z-z'|}}{j2\lambda_{z0}} \varepsilon \tilde{J}_{h\alpha}(\lambda_\rho, z) dz' + \tilde{w}^+_\alpha e^{-j\lambda_{z0}z} + \tilde{w}^-_\alpha e^{j\lambda_{z0}z} \tag{C.11}$$

and the partial derivative with respect to z is given by:

$$\frac{\partial \tilde{F}_\alpha}{\partial z}(\lambda_\rho, z) = -j\lambda_{z0}\mathrm{sgn}\,(z-z') \int\limits_{z'} \frac{e^{-j\lambda_{z0}|z-z'|}}{j2\lambda_{z0}} \varepsilon \tilde{J}_{h\alpha}(\lambda_\rho, z) dz' - j\lambda_{z0}\tilde{w}^+_\alpha e^{-j\lambda_{z0}z} + j\lambda_{z0}\tilde{w}^-_\alpha e^{j\lambda_{z0}z}$$

$$\tag{C.12}$$

Application of the boundary conditions $\frac{\partial \widetilde{F}_\alpha}{\partial z} = 0$ leads to the solution for the scattered coefficients

$$\widetilde{w}_\alpha^+ = \frac{R_\alpha v_\alpha^- + R_\alpha \overline{R}_\alpha e^{-j\lambda_{z0}2d} v_\alpha^+}{1 - R_\alpha \overline{R}_\alpha e^{-j\lambda_{z0}2d}}$$

$$\widetilde{w}_\alpha^- = \frac{\overline{R}_\alpha v_\alpha^+ + R_\alpha \overline{R}_\alpha e^{-j\lambda_{z0}2d} v_\alpha^-}{1 - R_\alpha \overline{R}_\alpha e^{-j\lambda_{z0}2d}} \tag{C.13}$$

$$R_\alpha = \overline{R}_\alpha = 1 \qquad v_\alpha^\pm = \int\limits_{z'} \frac{e^{-j\lambda_{z0}|z-z'|}}{j2\lambda_{z0}} \cdot \varepsilon \widetilde{J}_{h\alpha}(\lambda_\rho, z) dz'$$

which, when plugged back into (C.11) and simplified, leads to:

$$\widetilde{F}_\alpha = \int\limits_{z'} \frac{\cos\left[\lambda_{z0}\left(d - |z-z'|\right)\right] + \cos\left[\lambda_{z0}\left(d - (z+z')\right)\right]}{-2\lambda_{z0}\sin\left(\lambda_{z0}d\right)} \varepsilon \widetilde{J}_{h\alpha} dz' \tag{C.14}$$

Now, the final boundary condition leads to:

$$\widetilde{F}_z = \int\limits_{z'} \frac{\cos\left[\lambda_{z0}\left(d - |z-z'|\right)\right] - \cos\left[\lambda_{z0}\left(d - (z+z')\right)\right]}{-2\lambda_{z0}\sin\left(\lambda_{z0}d\right)} \varepsilon \widetilde{J}_{h\alpha} dz' \tag{C.15}$$

Recognizing that the potential Green's function for an isotropic material will be diagonal, we write:

$$\widetilde{G}_{\alpha\alpha} = \frac{\cos\left[\lambda_{z0}\left(d - |z-z'|\right)\right] \pm \cos\left[\lambda_{z0}\left(d - (z+z')\right)\right]}{-2\lambda_{z0}\sin\left(\lambda_{z0}d\right)} \qquad \begin{cases} + & \text{for} \quad \alpha = x, y \\ \\ - & \text{for} \quad \alpha = z \end{cases} \tag{C.16}$$

The magnetic field described by $\vec{F}$ is

$$\vec{H}(\rho, z) = \frac{1}{j\omega\varepsilon\mu}\left(k^2 + \nabla\nabla\cdot\right)\vec{F} \tag{C.17}$$

$$\implies \widetilde{\vec{H}}(\lambda_\rho, z) = \frac{k^2}{j\omega\varepsilon\mu}\widetilde{\vec{F}} + \frac{1}{j\omega\varepsilon\mu}\widetilde{\nabla}\widetilde{\nabla}\cdot\widetilde{\vec{F}} \tag{C.18}$$

225

which, noting $\widetilde{\nabla} \cdot \vec{\widetilde{F}} = j\lambda_x \widetilde{F}_x + j\lambda_y \widetilde{F}_y + \frac{\partial \widetilde{F}_z}{\partial z}$, can be expanded to:

$$
\begin{aligned}
\vec{\widetilde{H}}(\lambda_\rho, z) = & \; \hat{\mathbf{x}} \left(\frac{k^2}{j\omega\varepsilon\mu} - \frac{\lambda_x^2}{j\omega\varepsilon\mu} \right) \widetilde{F}_x - \hat{\mathbf{x}} \left(\frac{\lambda_x\lambda_y}{j\omega\varepsilon\mu} \widetilde{F}_y \right) + \hat{\mathbf{x}} \frac{j\lambda_x}{j\omega\varepsilon\mu} \frac{\partial \widetilde{F}_z}{\partial z} \\
& - \hat{\mathbf{y}} \frac{\lambda_x\lambda_y}{j\omega\varepsilon\mu} \widetilde{F}_x + \hat{\mathbf{y}} \frac{k^2 - \lambda_y^2}{j\omega\varepsilon\mu} \widetilde{F}_y + \hat{\mathbf{y}} \frac{j\lambda_y}{j\omega\varepsilon\mu} \frac{\partial \widetilde{F}_z}{\partial z} \\
& + \hat{\mathbf{z}} \frac{j\lambda_x}{j\omega\varepsilon\mu} \frac{\partial \widetilde{F}_x}{\partial z} + \hat{\mathbf{z}} \frac{j\lambda_y}{j\omega\varepsilon\mu} \frac{\partial \widetilde{F}_y}{\partial z} + \hat{\mathbf{z}} \left(\frac{1}{j\omega\varepsilon\mu} \frac{\partial^2 \widetilde{F}_z}{\partial z^2} + \frac{k^2 \widetilde{F}_z}{j\omega\varepsilon\mu} \right)
\end{aligned} \tag{C.19}
$$

Using this form and the solutions for the components of $\vec{F}$, we can write all of the components of the Green's function dyad, except for the $\hat{\mathbf{z}}\hat{\mathbf{z}}$ component. For this, we use Leibnitz's rule (twice) to reverse the order of the integral and differential operator. This leads to the appearance of the well-known depolarizing term. Therefore, the Green's function dyad is given by:

$$
\vec{\widetilde{G}}_{hh} = \frac{1}{j\omega\mu}
\begin{bmatrix}
\left(k^2 - \lambda_x^2\right) \widetilde{G}_{xx} & -\lambda_x\lambda_y \widetilde{G}_{yy} & j\lambda_x \frac{\partial \widetilde{G}_{zz}}{\partial z} \\
-\lambda_x\lambda_y \widetilde{G}_{xx} & \left(k^2 - \lambda_y^2\right) \widetilde{G}_{yy} & j\lambda_y \frac{\partial \widetilde{G}_{zz}}{\partial z} \\
j\lambda_x \frac{\partial \widetilde{G}_{xx}}{\partial z} & j\lambda_y \frac{\partial \widetilde{G}_{yy}}{\partial z} & \left(k^2 + \frac{\partial^2}{\partial z^2}\right) \widetilde{G}_{zz} - \delta(z{-}z')
\end{bmatrix} \tag{C.20}
$$

$$
\widetilde{G}_{\alpha\alpha} = \frac{\cos\left[\lambda_{z0}\left(d - |z{-}z'|\right)\right] \pm \cos\left[\lambda_{z0}\left(d - (z{+}z')\right)\right]}{-2\lambda_{z0}\sin\left(\lambda_{z0}d\right)} \qquad
\begin{cases}
+ & \text{for} \quad \alpha = x, y \\
\\
- & \text{for} \quad \alpha = z
\end{cases}
$$

Appendix D: Index of TE_{uv}^z and TM_{uv}^z Modes

The index q represents the list of TE_{uv}^z and TM_{uv}^z modes arranged in order of increasing cutoff frequency. Only odd values of u and even values of v are allowed to be excited at the aperture, due to the physical symmetry of the system.

Index (q)	Mode	f_{cq} (GHz)
1	TE_{10}	6.56
2	TE_{30}	19.67
3	TE_{12}	30.22
4	TM_{12}	30.22
5	TE_{50}	32.78
6	TE_{32}	35.46
7	TM_{32}	35.46
8	TE_{52}	44.10
9	TM_{52}	44.10
10	TE_{70}	45.89
11	TE_{72}	54.56
12	TM_{72}	54.56
13	TE_{90}	59.01
14	TE_{14}	59.37
15	TM_{14}	59.37
16	TE_{34}	62.20
17	TM_{34}	62.20
18	TE_{92}	65.97
19	TM_{92}	65.97
20	TE_{54}	67.50

Appendix E: $A_{mn}^{(11)}$ and $A_{mn}^{(12)}$ Coefficients

Recall, the equation that must be solved to find the theoretical scattering coefficients is given by (4.19):

$$\begin{bmatrix} A^{(11)} & A^{(12)} \\ A^{(21)} & A^{(22)} \end{bmatrix} \begin{bmatrix} C^{(1)} \\ C^{(2)} \end{bmatrix} = \begin{bmatrix} B^{(1)} \\ B^{(2)} \end{bmatrix}$$

The A-coefficients are of the form:

$$A_{mn}^{(11)} = \frac{\delta_{mn}}{Z_m Z_n} - \frac{Z_n}{4} \int_{-\infty}^{\infty} C_{\lambda_x} \left[A_{\lambda_y}^{(11)} + B_{\lambda_y}^{(11)} + C_{\lambda_y}^{(11)} + D_{\lambda_y}^{(11)} \right] d\lambda_x$$

$$A_{mn}^{(12)} = \frac{Z_n}{4} \int_{-\infty}^{\infty} C_{\lambda_x} \left[A_{\lambda_y}^{(12)} + B_{\lambda_y}^{(12)} + C_{\lambda_y}^{(12)} + D_{\lambda_y}^{(12)} \right] d\lambda_x$$

where:

$$C_{\lambda_x} = \left[\frac{\left(1-(-1)^{\nu_m}e^{j\lambda_x a}\right)\left(1-(-1)^{\nu_n}e^{-j\lambda_x a}\right)}{(\lambda_x + k_{xm})(\lambda_x - k_{xm})(\lambda_x + k_{xn})(\lambda_x - k_{xn})} \right]$$

and the terms denoted by $A_{\lambda_y}^{(1k)}$, $B_{\lambda_y}^{(1k)}$, $C_{\lambda_y}^{(1k)}$, and $D_{\lambda_y}^{(1k)}$ $(k = 1, 2)$ are complex integrals in the λ_y plane. Because they are integrated in the complex plane, the λ_y integrals for the $A_{mn}^{(11)}$ and $A_{mn}^{(12)}$ coefficients must be computed for 5 different combinations of values for w_m and w_n (which determine the locations of the poles that contribute to the integral values):

- Case I: $w_m = w_n = 0$

- Case II: $w_m \neq 0, w_n = 0$

- Case III: $w_m = 0, w_n \neq 0$

- Case IV: $w_m = w_n \neq 0$

- Case V: $w_m \neq w_n \neq 0$

The details of the method for computing the analytical forms of the integrals for Case I were given in 4.4. The coefficients for the remainder of the cases have been determined and are now given for reference. The following values are used throughout:

$$\lambda_{y_{l\theta}} = \sqrt{\frac{\mu_z}{\mu_t}\left[k_t^2 - \left(\frac{\pi l}{d}\right)^2\right] - \lambda_x^2} \qquad \lambda_{z\theta}^* = \sqrt{k_t^2 - \frac{\mu_t}{\mu_z}\lambda_x^2} \qquad \lambda_{z\theta}^\dagger = \sqrt{k_t^2 - \frac{\mu_t}{\mu_z}\left(\lambda_x^2 + k_{y\alpha}^2\right)}$$

$$\lambda_{y_{l\psi}} = \sqrt{\frac{\varepsilon_z}{\varepsilon_t}\left[k_t^2 - \left(\frac{\pi l}{d}\right)^2\right] - \lambda_x^2} \qquad \lambda_{z\psi}^* = \sqrt{k_t^2 - \frac{\varepsilon_t}{\varepsilon_z}\lambda_x^2} \qquad \lambda_{z\psi}^\dagger = \sqrt{k_t^2 - \frac{\varepsilon_t}{\varepsilon_z}\left(\lambda_x^2 + k_{y\alpha}^2\right)}$$

$$k_{xm} = \frac{v_m\pi}{a} \qquad k_{xn} = \frac{v_n\pi}{a} \qquad k_{ym} = \frac{w_m\pi}{b} \qquad k_{yn} = \frac{w_n\pi}{b} \qquad k_{y\alpha} = \frac{w_\alpha\pi}{b}$$

E.1 Case I ($w_m = w_n = 0$)

E.1.1 Case I - $A_{mn}^{(11)}$.

$$A_{\lambda_y}^{(11)} = \left(\frac{M_{hx}^m M_{hx}^n v_m v_n}{a^2}\right)\left\{\frac{j2\pi b\lambda_{z\theta}^*}{\omega\mu_t}\left[\frac{\cos\left(\lambda_{z\theta}^* d\right)}{\sin\left(\lambda_{z\theta}^* d\right)}\right] - \frac{4\pi\mu_z\lambda_x^2}{\omega\mu_t^2 d}\sum_{l=0}^{\infty}\left(\frac{\pi l}{d}\right)^2\frac{\left(1 - e^{-j\lambda_{y_{l\theta}}b}\right)}{\lambda_{y_{l\theta}}^3\left(\lambda_{y_{l\theta}}^2 + \lambda_x^2\right)}\right.$$

$$\left. -\frac{4\pi\omega\varepsilon_z}{d}\sum_{l=0}^{\infty}\frac{\left(1 - e^{-j\lambda_{y_{l\psi}}b}\right)}{\lambda_{y_{l\psi}}\left(\lambda_{y_{l\psi}}^2 + \lambda_x^2\right)[1 + \delta_{0,l}]}\right\}$$

$$B_{\lambda_y}^{(11)} = 0$$

$$C_{\lambda_y}^{(11)} = 0$$

$$D_{\lambda_y}^{(11)} = 0$$

E.1.2 Case I - $A_{mn}^{(12)}$.

$$A_{\lambda_y}^{(12)} = \left(\frac{M_{hx}^m M_{hx}^n v_m v_n}{a^2} \right) \left\{ \frac{j2\pi b \lambda_{z\theta}^*}{\omega \mu_t} \left[\frac{1}{\sin\left(\lambda_{z\theta}^* d\right)} \right] - \frac{4\pi \mu_z \lambda_x^2}{\omega \mu_t^2 d} \sum_{l=0}^{\infty} \left(\frac{\pi l}{d} \right)^2 \frac{(-1)^l \left(1 - e^{-j\lambda_{y l\theta} b}\right)}{\lambda_{y l\theta}^3 \left(\lambda_{y l\theta}^2 + \lambda_x^2 \right)} \right. $$

$$\left. - \frac{4\pi \omega \varepsilon_z}{d} \sum_{l=0}^{\infty} \frac{\left(1 - e^{-j\lambda_{y l\psi} b}\right)}{\lambda_{y l\psi} \left(\lambda_{y l\psi}^2 + \lambda_x^2 \right) \left[(-1)^l + \delta_{0,l}\right]} \right\}$$

$$B_{\lambda_y}^{(12)} = 0$$

$$C_{\lambda_y}^{(12)} = 0$$

$$D_{\lambda_y}^{(12)} = 0$$

E.2 Case II ($w_m \neq 0, w_n = 0$)

E.2.1 Case II - $A_{mn}^{(11)}$.

$$A_{\lambda_y}^{(11)} = - \left(\frac{4\pi M_{hx}^m M_{hx}^n v_m v_n}{a^2 d} \right)$$

$$\left\{ \left(\frac{\mu_z \lambda_x^2}{\omega \mu_t^2} \right) \sum_{l=0}^{\infty} \left(\frac{\pi l}{d} \right)^2 \left(\frac{\left(1 - e^{-j\lambda_{y l\theta} b}\right)}{\lambda_{y l\theta} \left(\lambda_x^2 + \lambda_{y l\theta}^2 \right) \left(\lambda_{y l\theta}^2 - k_{ym}^2 \right)} \right) \right.$$

$$\left. + \left(\omega \varepsilon_z \right) \sum_{l=0}^{\infty} \left[\frac{\lambda_{y l\psi} \left(1 - e^{-j\lambda_{y l\psi} b}\right)}{\left(\lambda_{y l\psi}^2 + \lambda_x^2 \right) \left(\lambda_{y l\psi}^2 - k_{ym}^2 \right) \left(1 + \delta_{0,l}\right)} \right] \right\}$$

$$B_{\lambda_y}^{(11)} = \left(\frac{4\pi M_{hy}^m M_{hx}^n w_m v_n \lambda_x^2}{abd} \right)$$

$$\left\{ - \left(\frac{\mu_z}{\omega \mu_t^2} \right) \sum_{l=0}^{\infty} \left(\frac{\pi l}{d} \right)^2 \left[\frac{\left(1 - e^{-j\lambda_{y l\theta} b}\right)}{\lambda_{y l\theta} \left(\lambda_x^2 + \lambda_{y l\theta}^2 \right) \left(\lambda_{y l\theta}^2 - k_{ym}^2 \right)} \right] \right.$$

$$\left. + \left(\omega \varepsilon_z \right) \sum_{l=0}^{\infty} \left[\frac{\left(1 - e^{-j\lambda_{y l\psi} b}\right)}{\lambda_{y l\psi} \left(\lambda_{y l\psi}^2 + \lambda_x^2 \right) \left(\lambda_{y l\psi}^2 - k_{ym}^2 \right) \left(1 + \delta_{0,l}\right)} \right] \right\}$$

$$C_{\lambda_y}^{(11)} = 0$$

$$D_{\lambda_y}^{(11)} = 0$$

E.2.2 Case II - $A_{mn}^{(12)}$.

$$A_{\lambda_y}^{(12)} = - \left(\frac{4\pi M_{hx}^m M_{hx}^n v_m v_n}{a^2 d} \right)$$

$$\left[\left(\frac{\mu_z \lambda_x^2}{\omega \mu_t^2} \right) \sum_{l=0}^{\infty} \left(\frac{\pi l}{d} \right)^2 \left\{ \frac{(-1)^l \left(1 - e^{-j\lambda_{yl\theta} b} \right)}{\lambda_{yl\theta} \left(\lambda_x^2 + \lambda_{yl\theta}^2 \right) \left(\lambda_{yl\theta}^2 - k_{ym}^2 \right)} \right\} \right.$$

$$\left. + (\omega \varepsilon_z) \sum_{l=0}^{\infty} \left\{ \frac{\lambda_{yl\psi} \left(1 - e^{-j\lambda_{yl\psi} b} \right)}{\left(\lambda_{yl\psi}^2 + \lambda_x^2 \right) \left(\lambda_{yl\psi}^2 - k_{ym}^2 \right) \left[(-1)^l + \delta_{0,l} \right]} \right\} \right]$$

$$B_{\lambda_y}^{(12)} = \left(\frac{4\pi M_{hy}^m M_{hx}^n w_m v_n \lambda_x^2}{abd} \right)$$

$$\left[- \left(\frac{\mu_z}{\omega \mu_t^2} \right) \sum_{l=0}^{\infty} \left(\frac{\pi l}{d} \right)^2 \left[\frac{(-1)^l \left(1 - e^{-j\lambda_{yl\theta} b} \right)}{\lambda_{yl\theta} \left(\lambda_x^2 + \lambda_{yl\theta}^2 \right) \left(\lambda_{yl\theta}^2 - k_{ym}^2 \right)} \right] \right.$$

$$\left. + (\omega \varepsilon_z) \sum_{l=0}^{\infty} \left\{ \frac{\left(1 - e^{-j\lambda_{yl\psi} b} \right)}{\lambda_{yl\psi} \left(\lambda_{yl\psi}^2 + \lambda_x^2 \right) \left(\lambda_{yl\psi}^2 - k_{ym}^2 \right) \left[(-1)^l + \delta_{0,l} \right]} \right\} \right]$$

$$C_{\lambda_y}^{(12)} = 0$$

$$D_{\lambda_y}^{(12)} = 0$$

231

E.3 Case III $(w_m = 0, w_n \neq 0)$

E.3.1 Case III - $A_{mn}^{(11)}$**.**

$$A_{\lambda_y}^{(11)} = -\left(\frac{4\pi M_{hx}^m M_{hx}^n v_m v_n}{a^2 d}\right)$$

$$\left\{\left(\frac{\mu_z \lambda_x^2}{\omega \mu_t^2}\right) \sum_{l=0}^{\infty} \left(\frac{\pi l}{d}\right)^2 \left(\frac{\left(1 - e^{-j\lambda_{yl\theta}b}\right)}{\lambda_{yl\theta} \left(\lambda_x^2 + \lambda_{yl\theta}^2\right) \left(\lambda_{yl\theta}^2 - k_{yn}^2\right)}\right)\right.$$

$$\left. + (\omega \varepsilon_z) \sum_{l=0}^{\infty} \left[\frac{\lambda_{yl\psi} \left(1 - e^{-j\lambda_{yl\psi}b}\right)}{\left(\lambda_{yl\psi}^2 + \lambda_x^2\right) \left(\lambda_{yl\psi}^2 - k_{yn}^2\right) (1 + \delta_{0,l})}\right]\right\}$$

$$B_{\lambda_y}^{(11)} = \left(\frac{4\pi M_{hx}^m M_{hy}^n v_m w_n \lambda_x^2}{abd}\right)$$

$$\left\{-\left(\frac{\mu_z}{\omega \mu_t^2}\right) \sum_{l=0}^{\infty} \left(\frac{\pi l}{d}\right)^2 \left[\frac{\left(1 - e^{-j\lambda_{yl\theta}b}\right)}{\lambda_{yl\theta} \left(\lambda_x^2 + \lambda_{yl\theta}^2\right) \left(\lambda_{yl\theta}^2 - k_{yn}^2\right)}\right]\right.$$

$$\left. + (\omega \varepsilon_z) \sum_{l=0}^{\infty} \left[\frac{\left(1 - e^{-j\lambda_{yl\psi}b}\right)}{\lambda_{yl\psi} \left(\lambda_{yl\psi}^2 + \lambda_x^2\right) \left(\lambda_{yl\psi}^2 - k_{yn}^2\right) (1 + \delta_{0,l})}\right]\right\}$$

$$C_{\lambda_y}^{(11)} = 0$$

$$D_{\lambda_y}^{(11)} = 0$$

E.3.2   Case III - $A_{mn}^{(12)}$.

$$A_{\lambda_y}^{(12)} = -\left(\frac{4\pi M_{hx}^m M_{hx}^n v_m v_n}{a^2 d}\right)$$

$$\left[\left(\frac{\mu_z \lambda_x^2}{\omega \mu_t^2}\right) \sum_{l=0}^{\infty} \left(\frac{\pi l}{d}\right)^2 \left\{\frac{(-1)^l \left(1 - e^{-j\lambda_{y_{l\theta}} b}\right)}{\lambda_{y_{l\theta}} \left(\lambda_x^2 + \lambda_{y_{l\theta}}^2\right) \left(\lambda_{y_{l\theta}}^2 - k_{yn}^2\right)}\right\}\right.$$

$$\left.+ (\omega \varepsilon_z) \sum_{l=0}^{\infty} \left\{\frac{\lambda_{y_{l\psi}} \left(1 - e^{-j\lambda_{y_{l\psi}} b}\right)}{\left(\lambda_{y_{l\psi}}^2 + \lambda_x^2\right) \left(\lambda_{y_{l\psi}}^2 - k_{yn}^2\right) \left[(-1)^l + \delta_{0,l}\right]}\right\}\right]$$

$$B_{\lambda_y}^{(12)} = \left(\frac{4\pi M_{hx}^m M_{hy}^n v_m w_n \lambda_x^2}{abd}\right)$$

$$\left[-\left(\frac{\mu_z}{\omega \mu_t^2}\right) \sum_{l=0}^{\infty} \left(\frac{\pi l}{d}\right)^2 \left[\frac{(-1)^l \left(1 - e^{-j\lambda_{y_{l\theta}} b}\right)}{\lambda_{y_{l\theta}} \left(\lambda_x^2 + \lambda_{y_{l\theta}}^2\right) \left(\lambda_{y_{l\theta}}^2 - k_{yn}^2\right)}\right]\right.$$

$$\left.+ (\omega \varepsilon_z) \sum_{l=0}^{\infty} \left\{\frac{\left(1 - e^{-j\lambda_{y_{l\psi}} b}\right)}{\lambda_{y_{l\psi}} \left(\lambda_{y_{l\psi}}^2 + \lambda_x^2\right) \left(\lambda_{y_{l\psi}}^2 - k_{yn}^2\right) \left[(-1)^l + \delta_{0,l}\right]}\right\}\right]$$

$$C_{\lambda_y}^{(12)} = 0$$

$$D_{\lambda_y}^{(12)} = 0$$

E.4 Case IV $(w_m = w_n = w_\alpha \neq 0)$

E.4.1 *Case IV - $A_{mn}^{(11)}$.*

$$
\begin{aligned}
A_{\lambda_y}^{(11)} = \frac{M_{hx}^m M_{hx}^n v_m v_n}{a^2} &\left\{ -\left(\frac{4\pi\mu_z\lambda_x^2}{\omega\mu_t^2 d}\right) \sum_{l=0}^{\infty} \left(\frac{\pi l}{d}\right)^2 \left[\frac{\lambda_{y_{l\theta}}\left(1 - e^{-j\lambda_{y_{l\theta}}b}\right)}{\left(\lambda_x^2 + \lambda_{y_{l\theta}}^2\right)\left(\lambda_{y_{l\theta}}^2 - k_{y\alpha}^2\right)^2} \right] \right. \\
&+ \left(\frac{j\pi b}{\omega\mu_t}\right)\left(\frac{\lambda_{z\theta}^\dagger \lambda_x^2}{\lambda_x^2 + k_{y\alpha}^2}\right) \left[\frac{\cos\left(\lambda_{z\theta}^\dagger d\right)}{\sin\left(\lambda_{z\theta}^\dagger d\right)} \right] \\
&- \left(\frac{4\pi\omega\varepsilon_z}{d}\right) \sum_{l=0}^{\infty} \left[\frac{\lambda_{y_{l\psi}}^3 \left(1 - e^{-j\lambda_{y_{l\psi}}b}\right)}{\left(\lambda_{y_{l\psi}}^2 + \lambda_x^2\right)\left(\lambda_{y_{l\psi}}^2 - k_{y\alpha}^2\right)^2 (1 + \delta_{0,l})} \right] \\
&\left. + (j\pi b\omega\varepsilon_t)\left(\frac{k_{y\alpha}^2}{\lambda_x^2 + k_{y\alpha}^2}\right) \left[\frac{\cos\left(\lambda_{z\psi}^\dagger d\right)}{\lambda_{z\psi}^\dagger \sin\left(\lambda_{z\psi}^\dagger d\right)} \right] \right\}
\end{aligned}
$$

$$
\begin{aligned}
B_{\lambda_y}^{(11)} = \frac{M_{hx}^m M_{hy}^n w_\alpha v_m}{ab} &\left\{ -\left(\frac{4\pi\mu_z\lambda_x^2}{\omega\mu_t^2 d}\right) \sum_{l=0}^{\infty} \left(\frac{\pi l}{d}\right)^2 \left[\frac{\lambda_{y_{l\theta}}\left(1 - e^{-j\lambda_{y_{l\theta}}b}\right)}{\left(\lambda_x^2 + \lambda_{y_{l\theta}}^2\right)\left(\lambda_{y_{l\theta}}^2 - k_{y\alpha}^2\right)^2} \right] \right. \\
&+ \left(\frac{j\pi b}{\omega\mu_t}\right)\left(\frac{\lambda_{z\theta}^\dagger \lambda_x^2}{\lambda_x^2 + k_{y\alpha}^2}\right) \left[\frac{\cos\left(\lambda_{z\theta}^\dagger d\right)}{\sin\left(\lambda_{z\theta}^\dagger d\right)} \right] \\
&+ \left(\frac{4\pi\omega\varepsilon_z\lambda_x^2}{d}\right) \sum_{l=0}^{\infty} \left[\frac{\lambda_{y_{l\psi}}\left(1 - e^{-j\lambda_{y_{l\psi}}b}\right)}{\left(\lambda_{y_{l\psi}}^2 + \lambda_x^2\right)\left(\lambda_{y_{l\psi}}^2 - k_{y\alpha}^2\right)^2 (1 + \delta_{0,l})} \right] \\
&\left. - (j\pi b\omega\varepsilon_t)\left(\frac{\lambda_x^2}{\lambda_x^2 + k_{y\alpha}^2}\right) \left[\frac{\cos\left(\lambda_{z\psi}^\dagger d\right)}{\lambda_{z\psi}^\dagger \sin\left(\lambda_{z\psi}^\dagger d\right)} \right] \right\}
\end{aligned}
$$

$$C_{\lambda_y}^{(11)} = \frac{M_{hy}^m M_{hx}^n w_\alpha v_n}{ab} \left\{ -\left(\frac{4\pi\mu_z\lambda_x^2}{\omega\mu_t^2 d}\right) \sum_{l=0}^{\infty} \left(\frac{\pi l}{d}\right)^2 \left[\frac{\lambda_{y_{l\theta}}\left(1 - e^{-j\lambda_{y_{l\theta}}b}\right)}{\left(\lambda_x^2 + \lambda_{y_{l\theta}}^2\right)\left(\lambda_{y_{l\theta}}^2 - k_{y\alpha}^2\right)^2}\right] \right.$$

$$+ \left(\frac{j\pi b}{\omega\mu_t}\right)\left(\frac{\lambda_{z\theta}^\dagger \lambda_x^2}{\lambda_x^2 + k_{y\alpha}^2}\right)\left[\frac{\cos\left(\lambda_{z\theta}^\dagger d\right)}{\sin\left(\lambda_{z\theta}^\dagger d\right)}\right]$$

$$+ \left(\frac{4\pi\omega\varepsilon_z\lambda_x^2}{d}\right) \sum_{l=0}^{\infty} \left[\frac{\lambda_{y_{l\psi}}\left(1 - e^{-j\lambda_{y_{l\psi}}b}\right)}{\left(\lambda_{y_{l\psi}}^2 + \lambda_x^2\right)\left(\lambda_{y_{l\psi}}^2 - k_{y\alpha}^2\right)^2 (1 + \delta_{0,l})}\right]$$

$$\left. - (j\pi b\omega\varepsilon_t)\left(\frac{\lambda_x^2}{\lambda_x^2 + k_{y\alpha}^2}\right)\left[\frac{\cos\left(\lambda_{z\psi}^\dagger d\right)}{\lambda_{z\psi}^\dagger \sin\left(\lambda_{z\psi}^\dagger d\right)}\right] \right\}$$

$$D_{\lambda_y}^{(11)} = \frac{M_{hy}^m M_{hy}^n w_\alpha^2}{b^2} \left\{ -\left(\frac{4\pi\mu_z\lambda_x^2}{\omega\mu_t^2 d}\right) \sum_{l=0}^{\infty} \left(\frac{\pi l}{d}\right)^2 \left[\frac{\lambda_{y_{l\theta}}\left(1 - e^{-j\lambda_{y_{l\theta}}b}\right)}{\left(\lambda_x^2 + \lambda_{y_{l\theta}}^2\right)\left(\lambda_{y_{l\theta}}^2 - k_{y\alpha}^2\right)^2}\right] \right.$$

$$+ \left(\frac{j\pi b}{\omega\mu_t}\right)\left(\frac{\lambda_{z\theta}^\dagger \lambda_x^2}{\lambda_x^2 + k_{y\alpha}^2}\right)\left[\frac{\cos\left(\lambda_{z\theta}^\dagger d\right)}{\sin\left(\lambda_{z\theta}^\dagger d\right)}\right]$$

$$- \left(\frac{4\pi\omega\varepsilon_z\lambda_x^4}{d}\right) \sum_{l=0}^{\infty} \left[\frac{\left(1 - e^{-j\lambda_{y_{l\psi}}b}\right)}{\lambda_{y_{l\psi}}\left(\lambda_{y_{l\psi}}^2 + \lambda_x^2\right)\left(\lambda_{y_{l\psi}}^2 - k_{y\alpha}^2\right)^2 (1 + \delta_{0,l})}\right]$$

$$\left. + (j\pi b\omega\varepsilon_t)\left[\frac{\lambda_x^4}{k_{y\alpha}^2\left(\lambda_x^2 + k_{y\alpha}^2\right)}\right]\left[\frac{\cos\left(\lambda_{z\psi}^\dagger d\right)}{\lambda_{z\psi}^\dagger \sin\left(\lambda_{z\psi}^\dagger d\right)}\right] \right\}$$

E.4.2   Case IV - $A_{mn}^{(12)}$.

$$A_{\lambda_y}^{(12)} = \frac{M_{hx}^m M_{hx}^n v_m v_n}{a^2} \left\{ - \left(\frac{4\pi\mu_z\lambda_x^2}{\omega\mu_t^2 d} \right) \sum_{l=0}^{\infty} (-1)^l \left(\frac{\pi l}{d} \right)^2 \left[\frac{\lambda_{y_{l\theta}} \left(1 - e^{-j\lambda_{y_{l\theta}} b} \right)}{\left(\lambda_x^2 + \lambda_{y_{l\theta}}^2 \right) \left(\lambda_{y_{l\theta}}^2 - k_{y\alpha}^2 \right)^2} \right] \right.$$

$$+ \left(\frac{j\pi b}{\omega\mu_t} \right) \left(\frac{\lambda_{z\theta}^\dagger \lambda_x^2}{\lambda_x^2 + k_{y\alpha}^2} \right) \left[\frac{1}{\sin\left(\lambda_{z\theta}^\dagger d \right)} \right]$$

$$- \left(\frac{4\pi\omega\varepsilon_z}{d} \right) \sum_{l=0}^{\infty} \left[\frac{\lambda_{y_{l\psi}}^3 \left(1 - e^{-j\lambda_{y_{l\psi}} b} \right)}{\left(\lambda_{y_{l\psi}}^2 + \lambda_x^2 \right) \left(\lambda_{y_{l\psi}}^2 - k_{y\alpha}^2 \right)^2 \left[(-1)^l + \delta_{0,l} \right]} \right]$$

$$\left. + (j\pi b\omega\varepsilon_t) \left(\frac{k_{y\alpha}^2}{\lambda_x^2 + k_{y\alpha}^2} \right) \left[\frac{1}{\lambda_{z\psi}^\dagger \sin\left(\lambda_{z\psi}^\dagger d \right)} \right] \right\}$$

$$B_{\lambda_y}^{(12)} = \frac{M_{hx}^m M_{hy}^n w_\alpha v_m}{ab} \left\{ - \left(\frac{4\pi\mu_z\lambda_x^2}{\omega\mu_t^2 d} \right) \sum_{l=0}^{\infty} (-1)^l \left(\frac{\pi l}{d} \right)^2 \left[\frac{\lambda_{y_{l\theta}} \left(1 - e^{-j\lambda_{y_{l\theta}} b} \right)}{\left(\lambda_x^2 + \lambda_{y_{l\theta}}^2 \right) \left(\lambda_{y_{l\theta}}^2 - k_{y\alpha}^2 \right)^2} \right] \right.$$

$$+ \left(\frac{j\pi b}{\omega\mu_t} \right) \left(\frac{\lambda_{z\theta}^\dagger \lambda_x^2}{\lambda_x^2 + k_{y\alpha}^2} \right) \left[\frac{1}{\sin\left(\lambda_{z\theta}^\dagger d \right)} \right]$$

$$+ \left(\frac{4\pi\omega\varepsilon_z\lambda_x^2}{d} \right) \sum_{l=0}^{\infty} \left[\frac{\lambda_{y_{l\psi}} \left(1 - e^{-j\lambda_{y_{l\psi}} b} \right)}{\left(\lambda_{y_{l\psi}}^2 + \lambda_x^2 \right) \left(\lambda_{y_{l\psi}}^2 - k_{y\alpha}^2 \right)^2 \left[(-1)^l + \delta_{0,l} \right]} \right]$$

$$\left. - (j\pi b\omega\varepsilon_t) \left(\frac{\lambda_x^2}{\lambda_x^2 + k_{y\alpha}^2} \right) \left[\frac{1}{\lambda_{z\psi}^\dagger \sin\left(\lambda_{z\psi}^\dagger d \right)} \right] \right\}$$

$$C_{\lambda_y}^{(12)} = \frac{M_{hy}^m M_{hx}^n w_\alpha v_n}{ab} \left\{ -\left(\frac{4\pi\mu_z\lambda_x^2}{\omega\mu_t^2 d}\right) \sum_{l=0}^{\infty} (-1)^l \left(\frac{\pi l}{d}\right)^2 \left[\frac{\lambda_{y_{l\theta}}\left(1 - e^{-j\lambda_{y_{l\theta}}b}\right)}{\left(\lambda_x^2 + \lambda_{y_{l\theta}}^2\right)\left(\lambda_{y_{l\theta}}^2 - k_{y\alpha}^2\right)^2} \right] \right.$$

$$+ \left(\frac{j\pi b}{\omega\mu_t}\right)\left(\frac{\lambda_{z\theta}^\dagger \lambda_x^2}{\lambda_x^2 + k_{y\alpha}^2}\right)\left[\frac{1}{\sin\left(\lambda_{z\theta}^\dagger d\right)}\right]$$

$$+ \left(\frac{4\pi\omega\varepsilon_z\lambda_x^2}{d}\right)\sum_{l=0}^{\infty}\left[\frac{\lambda_{y_{l\psi}}\left(1 - e^{-j\lambda_{y_{l\psi}}b}\right)}{\left(\lambda_{y_{l\psi}}^2 + \lambda_x^2\right)\left(\lambda_{y_{l\psi}}^2 - k_{y\alpha}^2\right)^2\left[(-1)^l + \delta_{0,l}\right]}\right]$$

$$\left. - (j\pi b\omega\varepsilon_t)\left(\frac{\lambda_x^2}{k_{y\alpha}^2 + \lambda_x^2}\right)\left[\frac{1}{\lambda_{z\psi}^\dagger \sin\left(\lambda_{z\psi}^\dagger d\right)}\right]\right\}$$

$$D_{\lambda_y}^{(12)} = \frac{M_{hy}^m M_{hy}^n w_\alpha^2}{b^2}\left\{ -\left(\frac{4\pi\mu_z\lambda_x^2}{\omega\mu_t^2 d}\right)\sum_{l=0}^{\infty}(-1)^l\left(\frac{\pi l}{d}\right)^2\left[\frac{\lambda_{y_{l\theta}}\left(1 - e^{-j\lambda_{y_{l\theta}}b}\right)}{\left(\lambda_x^2 + \lambda_{y_{l\theta}}^2\right)\left(\lambda_{y_{l\theta}}^2 - k_{y\alpha}^2\right)^2}\right]\right.$$

$$+ \left(\frac{j\pi b}{\omega\mu_t}\right)\left(\frac{\lambda_{z\theta}^\dagger \lambda_x^2}{\lambda_x^2 + k_{y\alpha}^2}\right)\left[\frac{1}{\sin\left(\lambda_{z\theta}^\dagger d\right)}\right]$$

$$- \left(\frac{4\pi\omega\varepsilon_z\lambda_x^4}{d}\right)\sum_{l=0}^{\infty}\left[\frac{\left(1 - e^{-j\lambda_{y_{l\psi}}b}\right)}{\lambda_{y_{l\psi}}\left(\lambda_{y_{l\psi}}^2 + \lambda_x^2\right)\left(\lambda_{y_{l\psi}}^2 - k_{y\alpha}^2\right)^2\left[(-1)^l + \delta_{0,l}\right]}\right]$$

$$\left. + (j\pi b\omega\varepsilon_t)\left[\frac{\lambda_x^4}{k_{y\alpha}^2\left(\lambda_x^2 + k_{y\alpha}^2\right)}\right]\left[\frac{1}{\lambda_{z\psi}^\dagger \sin\left(\lambda_{z\psi}^\dagger d\right)}\right]\right\}$$

E.5 Case V ($w_m \neq w_n \neq 0$)

E.5.1 Case V - $A_{mn}^{(11)}$.

$$A_{\lambda_y}^{(11)} = -\left(\frac{M_{hx}^m M_{hx}^n v_m v_n}{a^2}\right) \left\{ \left(\frac{4\pi\mu_z \lambda_x^2}{\omega\mu_t^2 d}\right) \sum_{l=0}^{\infty} \left(\frac{\pi l}{d}\right)^2 \left[\frac{\lambda_{y_{l\theta}} \left(1 - e^{-j\lambda_{y_{l\theta}}b}\right)}{\left(\lambda_x^2 + \lambda_{y_{l\theta}}^2\right)\left(\lambda_{y_{l\theta}}^2 - k_{ym}^2\right)\left(\lambda_{y_{l\theta}}^2 - k_{yn}^2\right)} \right] \right.$$
$$\left. + \left(\frac{4\pi\omega\varepsilon_z}{d}\right) \sum_{l=0}^{\infty} \frac{\lambda_{y_{l\psi}}^3 \left(1 - e^{-j\lambda_{y_{l\psi}}b}\right)}{\left(\lambda_{y_{l\psi}}^2 + \lambda_x^2\right)\left(\lambda_{y_{l\psi}}^2 - k_{ym}^2\right)\left(\lambda_{y_{l\psi}}^2 - k_{yn}^2\right)(1 + \delta_{0,l})} \right\}$$

$$B_{\lambda_y}^{(11)} = \left(\frac{M_{hx}^m M_{hy}^n w_n v_m}{ab}\right) \left\{ -\left(\frac{4\pi\mu_z \lambda_x^2}{\omega\mu_t^2 d}\right) \sum_{l=0}^{\infty} \left(\frac{\pi l}{d}\right)^2 \left[\frac{\lambda_{y_{l\theta}} \left(1 - e^{-j\lambda_{y_{l\theta}}b}\right)}{\left(\lambda_x^2 + \lambda_{y_{l\theta}}^2\right)\left(\lambda_{y_{l\theta}}^2 - k_{ym}^2\right)\left(\lambda_{y_{l\theta}}^2 - k_{yn}^2\right)} \right] \right.$$
$$\left. + \left(\frac{4\pi\omega\varepsilon_z \lambda_x^2}{d}\right) \sum_{l=0}^{\infty} \frac{\lambda_{y_{l\psi}} \left(1 - e^{-j\lambda_{y_{l\psi}}b}\right)}{\left(\lambda_{y_{l\psi}}^2 + \lambda_x^2\right)\left(\lambda_{y_{l\psi}}^2 - k_{ym}^2\right)\left(\lambda_{y_{l\psi}}^2 - k_{yn}^2\right)(1 + \delta_{0,l})} \right\}$$

$$C_{\lambda_y}^{(11)} = \left(\frac{M_{hy}^m M_{hx}^n w_m v_n}{ab}\right) \left\{ -\left(\frac{4\pi\mu_z \lambda_x^2}{\omega\mu_t^2 d}\right) \sum_{l=0}^{\infty} \left(\frac{\pi l}{d}\right)^2 \left[\frac{\lambda_{y_{l\theta}} \left(1 - e^{-j\lambda_{y_{l\theta}}b}\right)}{\left(\lambda_x^2 + \lambda_{y_{l\theta}}^2\right)\left(\lambda_{y_{l\theta}}^2 - k_{ym}^2\right)\left(\lambda_{y_{l\theta}}^2 - k_{yn}^2\right)} \right] \right.$$
$$\left. + \left(\frac{4\pi\omega\varepsilon_z \lambda_x^2}{d}\right) \sum_{l=0}^{\infty} \frac{\lambda_{y_{l\psi}} \left(1 - e^{-j\lambda_{y_{l\psi}}b}\right)}{\left(\lambda_{y_{l\psi}}^2 + \lambda_x^2\right)\left(\lambda_{y_{l\psi}}^2 - k_{ym}^2\right)\left(\lambda_{y_{l\psi}}^2 - k_{yn}^2\right)(1 + \delta_{0,l})} \right\}$$

$$D_{\lambda_y}^{(11)} = -\left(\frac{M_{hy}^m M_{hy}^n w_m w_n}{b^2}\right) \left\{ \left(\frac{4\pi\mu_z \lambda_x^2}{\omega\mu_t^2 d}\right) \sum_{l=0}^{\infty} \left(\frac{\pi l}{d}\right)^2 \left[\frac{\lambda_{y_{l\theta}} \left(1 - e^{-j\lambda_{y_{l\theta}}b}\right)}{\left(\lambda_x^2 + \lambda_{y_{l\theta}}^2\right)\left(\lambda_{y_{l\theta}}^2 - k_{ym}^2\right)\left(\lambda_{y_{l\theta}}^2 - k_{yn}^2\right)} \right] \right.$$
$$\left. + \left(\frac{4\pi\omega\varepsilon_z \lambda_x^4}{d}\right) \sum_{l=0}^{\infty} \frac{\left(1 - e^{-j\lambda_{y_{l\psi}}b}\right)}{\lambda_{y_{l\psi}}\left(\lambda_{y_{l\psi}}^2 + \lambda_x^2\right)\left(\lambda_{y_{l\psi}}^2 - k_{ym}^2\right)\left(\lambda_{y_{l\psi}}^2 - k_{yn}^2\right)(1 + \delta_{0,l})} \right\}$$

E.5.2 Case V - $A_{mn}^{(12)}$.

$$A_{\lambda_y}^{(12)} = -\left(\frac{M_{hx}^m M_{hx}^n v_m v_n}{a^2}\right)\left\{\left(\frac{4\pi\mu_z\lambda_x^2}{\omega\mu_t^2 d}\right)\sum_{l=0}^{\infty}(-1)^l\left(\frac{\pi l}{d}\right)^2\left[\frac{\lambda_{y_{l\theta}}\left(1 - e^{-j\lambda_{y_{l\theta}}b}\right)}{\left(\lambda_x^2 + \lambda_{y_{l\theta}}^2\right)\left(\lambda_{y_{l\theta}}^2 - k_{ym}^2\right)\left(\lambda_{y_{l\theta}}^2 - k_{yn}^2\right)}\right]\right.$$
$$\left. + \left(\frac{4\pi\omega\varepsilon_z}{d}\right)\sum_{l=0}^{\infty}\frac{\lambda_{y_{l\psi}}^3\left(1 - e^{-j\lambda_{y_{l\psi}}b}\right)}{\left(\lambda_{y_{l\psi}}^2 + \lambda_x^2\right)\left(\lambda_{y_{l\psi}}^2 - k_{ym}^2\right)\left(\lambda_{y_{l\psi}}^2 - k_{yn}^2\right)\left[(-1)^l + \delta_{0,l}\right]}\right\}$$

$$B_{\lambda_y}^{(12)} = \left(\frac{M_{hx}^m M_{hy}^n w_n v_m}{ab}\right)\left\{-\left(\frac{4\pi\mu_z\lambda_x^2}{\omega\mu_t^2 d}\right)\sum_{l=0}^{\infty}(-1)^l\left(\frac{\pi l}{d}\right)^2\left[\frac{\lambda_{y_{l\theta}}\left(1 - e^{-j\lambda_{y_{l\theta}}b}\right)}{\left(\lambda_x^2 + \lambda_{y_{l\theta}}^2\right)\left(\lambda_{y_{l\theta}}^2 - k_{ym}^2\right)\left(\lambda_{y_{l\theta}}^2 - k_{yn}^2\right)}\right]\right.$$
$$\left. + \left(\frac{4\pi\omega\varepsilon_z\lambda_x^2}{d}\right)\sum_{l=0}^{\infty}\frac{\lambda_{y_{l\psi}}\left(1 - e^{-j\lambda_{y_{l\psi}}b}\right)}{\left(\lambda_{y_{l\psi}}^2 + \lambda_x^2\right)\left(\lambda_{y_{l\psi}}^2 - k_{ym}^2\right)\left(\lambda_{y_{l\psi}}^2 - k_{yn}^2\right)\left[(-1)^l + \delta_{0,l}\right]}\right\}$$

$$C_{\lambda_y}^{(12)} = \left(\frac{M_{hy}^m M_{hx}^n w_m v_n}{ab}\right)\left\{-\left(\frac{4\pi\mu_z\lambda_x^2}{\omega\mu_t^2 d}\right)\sum_{l=0}^{\infty}(-1)^l\left(\frac{\pi l}{d}\right)^2\left[\frac{\lambda_{y_{l\theta}}\left(1 - e^{-j\lambda_{y_{l\theta}}b}\right)}{\left(\lambda_x^2 + \lambda_{y_{l\theta}}^2\right)\left(\lambda_{y_{l\theta}}^2 - k_{ym}^2\right)\left(\lambda_{y_{l\theta}}^2 - k_{yn}^2\right)}\right]\right.$$
$$\left. + \left(\frac{4\pi\omega\varepsilon_z\lambda_x^2}{d}\right)\sum_{l=0}^{\infty}\frac{\lambda_{y_{l\psi}}\left(1 - e^{-j\lambda_{y_{l\psi}}b}\right)}{\left(\lambda_{y_{l\psi}}^2 + \lambda_x^2\right)\left(\lambda_{y_{l\psi}}^2 - k_{ym}^2\right)\left(\lambda_{y_{l\psi}}^2 - k_{yn}^2\right)\left[(-1)^l + \delta_{0,l}\right]}\right\}$$

$$D_{\lambda_y}^{(12)} = -\left(\frac{M_{hy}^m M_{hy}^n w_m w_n}{b^2}\right)\left\{\left(\frac{4\pi\mu_z\lambda_x^2}{\omega\mu_t^2 d}\right)\sum_{l=0}^{\infty}(-1)^l\left(\frac{\pi l}{d}\right)^2\left[\frac{\lambda_{y_{l\theta}}\left(1 - e^{-j\lambda_{y_{l\theta}}b}\right)}{\left(\lambda_x^2 + \lambda_{y_{l\theta}}^2\right)\left(\lambda_{y_{l\theta}}^2 - k_{ym}^2\right)\left(\lambda_{y_{l\theta}}^2 - k_{yn}^2\right)}\right]\right.$$
$$\left. + \left(\frac{4\pi\omega\varepsilon_z\lambda_x^4}{d}\right)\sum_{l=0}^{\infty}\frac{\left(1 - e^{-j\lambda_{y_{l\psi}}b}\right)}{\lambda_{y_{l\psi}}\left(\lambda_{y_{l\psi}}^2 + \lambda_x^2\right)\left(\lambda_{y_{l\psi}}^2 - k_{ym}^2\right)\left(\lambda_{y_{l\psi}}^2 - k_{yn}^2\right)\left[(-1)^l + \delta_{0,l}\right]}\right\}$$

Appendix F: tFWMT Constitutive Parameter Extraction Code

F.1 uniaxial_full.m - Top Level Code

This code controls the configuration parameters, parses the experimental data and sets up the LSQ solver.

```matlab
%%% full mode uniaxial constitutive parameter extraction
%% configuration/constants

clear all;
% clc;
close all;

global widx v wi a b dmat eps0 mu0 numModes includeModes solveCase ...
    porttouse alg ket kmut num_int;

% % % % % % % % % % % % % % % % % % % % % % %
% % constants & global parameters
% % % % % % % % % % % % % % % % % % % % % % %

v=[1 3 1 1 5 3 3 5 5 7 7 7 9 1 1 3 3 9 9 5]; % the first 20 modes
wi=[0 0 2 2 0 2 2 2 2 0 2 2 0 4 4 4 4 2 2 4];
c=3.0e8;
eps0=8.854e-12;
mu0=pi*4e-7;
ket=[];
kmut=[];
a=0.9*2.54/100;  % inches to m
b=0.4*2.54/100;  % inches to m
```

```matlab
24  wmin=8.2e9*2*pi;

25  wmax=12.4e9*2*pi;

26

27

28  % % % % % % % % % % % % % % % % % % % % %

29  % % user flags & config options

30  % % % % % % % % % % % % % % % % % % % % %

31

32  material='ui_honeycomb';

33  vers='v3'; % the version of the measurement

34  orientation=''; % needs the preceeding '_'

35  methd='tfwgt'; % tfwgt or nrw

36  add2casedesc='_multimode_test_numerical_unbounded';  % a string to add

37                                          % to the case description

38  porttouse=1; % 1=use S11 & S21, 2=use S22 & S12, 3=use all

39  % includeModes=1; % dominant mode only

40  % includeModes=[1 3 4 14 15]; % indices of the top 5 modes - 99% of the solution

41  includeModes=[1 3 4];

42  self_cal=0; % 1=provide your own TRL cal files, 0=use VNA cal'd data

43  errchk=0;    % error bar routine? 1=yes, 0=no

44

45  % % solver options

46  numds=5;  % downsample the data to this number of points, 0 = no downsampling

47  init_method='initup'; % 'nrw','nrwTruth','initone', or 'initup'

48  nrwvers='v6'; % version of nrw measurements, if using them

49  solveCase=4; % this is a switch to test some different cases, where we force

50              %  certain symmetries or conditions on eps & mu

51              % 1 - isotropic, dielectric, non-magnetic (et=ez=er)

52              %          & (mut=muz=mu0)

53              % 2 - isotropic, non-dielectric, magnetic (et=ez=eps0)

54              %          & (mut=muz=mur)

55              % 3 - isotropic, dielectric, magnetic (et=ez=er) & (mut=muz=mur)
```

241

```matlab
56              % 4 - uniaxial, dielectric, non-magnetic (et,ez) & (mut=muz=mu0)
57              % 5 - uniaxial, non-dielectric, magnetic (et=ez=eps0) & (mut,muz)
58              % 6 - uniaxial, dielectric, magnetic (et,ez) & (mut,muz)
59              % 7 - uniaxial with known et and mut (et and mut set to
60              %        etguess and mutguess, then solve for ez and muz)
61 alg='TRR';  % LM=levenburg-marquardt, TRR=Trust-region-reflective
62 num_int=1;  % use numerical integration for lamx and lamy
63
64 % % post-processing options
65 makeFile=0;  % output the results to a csv (*.dat) file? 1=yes, 0=no
66 print=1;
67 smooth_zvals=0;
68 smooth_tvals=0;
69 smeth='sgolay';
70 sspan=201;
71
72 % % % % % % % % % % % % % % % % % % % % % % % % % % % % % % % % % % % % % %
73 % % get details for the material specified above
74 % % % % % % % % % % % % % % % % % % % % % % % % % % % % % % % % % % % % % %
75
76 %% pick the correct thicknesses and initial guess based on the material
77 [myret,myiet,myrmut,myimut,myrez,myiez,myrmuz,myimuz,dmat]=...
78     material_opts(material);
79
80 display('%%%%%%%%%%%%%%%%%%%%%%%%%%%%%%%%%%%%')
81 display(['Material is: ' material]);
82 dmat
83 display('(in m)')
84 display('%%%%%%%%%%%%%%%%%%%%%%%%%%%%%%%%%%%%')
85
86
87 % check solveCase and dmat length and import relevant files
```

242

```matlab
88   if ismember(solveCase,[3 6])==0
89       inputFile=[material orientation '_' methd '_' vers '.txt'];
90       dmat=dmat(1);
91   else
92       if length(dmat)==1
93           display('Error - dmat not long enough');
94           return
95       end
96       inputFile=[material orientation '_' methd '_' vers '_d1.txt'];
97       inputFile2=[material orientation '_' methd '_' vers '_d2.txt'];
98   end
99
100  numModes=length(includeModes); % number of modes to include
101
102  % % % % % % % % % % % % % % % % % % % % % %
103  % % setup for NRW analysis
104  % % % % % % % % % % % % % % % % % % % % % %
105
106  if strcmp(init_method,'nrw')==1
107      nrwInput=[material '_nrw_' nrwvers '.txt'];
108  end
109
110  % % % % % % % % % % % % % % % % % % % % % %
111  % % other misc setup
112  % % % % % % % % % % % % % % % % % % % % % %
113
114  % the truth data i have for this init method reqires a slight adjustment
115  % to the frequency values
116  if (strcmp(init_method,'nrwTruth')==1) && (regexp(material,'white_stuff')==1)
117      wmax=12e9*2*pi;
118  end
119
```

```matlab
120
121  % names for output files
122  if numModes==1
123      casedesc=[material orientation '_' methd '_' vers '_' upper(init_method)...
124          'Init_' num2str(numds) ' points_' num2str(numModes) ' mode_solveCase'...
125          num2str(solveCase) '_port' num2str(porttouse) add2casedesc];
126      diary([upper(init_method) 'Init_' num2str(numds) 'points_' num2str(numModes)...
127          'mode_solveCase_' num2str(solveCase) '_port' num2str(porttouse) ...
128          add2casedesc '_log.txt']);
129  else
130      casedesc=[material orientation '_' methd '_' vers '_' upper(init_method)...
131          'Init_' num2str(numds) ' points_' num2str(numModes) ' modes_solveCase'...
132          num2str(solveCase) '_port' num2str(porttouse) add2casedesc];
133      diary([upper(init_method) 'Init_' num2str(numds) 'points_' ...
134          num2str(numModes) ' modes_solveCase_' num2str(solveCase) '_port'...
135          num2str(porttouse) add2casedesc '_log.txt']);
136  end
137
138  diary on;
139
140  %% get input data & setup initial guesses
141
142  % % % % % % % % % % % % % % % % % % % % % %
143  % %   Grab the input data & format it correctly
144  % % % % % % % % % % % % % % % % % % % % % %
145
146  if self_cal==0
147
148      [A,svarnames]=fileformat5(inputFile);
149      f=A(:,1);
150
151      % use the svarnames to assign the correct name to the sparams
```

244

```matlab
152        eval(['real' cell2mat(svarnames(1)) 'meas1=A(:,2);']);
153        eval(['imag' cell2mat(svarnames(1)) 'meas1=A(:,3);']);
154        eval(['real' cell2mat(svarnames(2)) 'meas1=A(:,4);']);
155        eval(['imag' cell2mat(svarnames(2)) 'meas1=A(:,5);']);
156        eval(['real' cell2mat(svarnames(3)) 'meas1=A(:,6);']);
157        eval(['imag' cell2mat(svarnames(3)) 'meas1=A(:,7);']);
158        eval(['real' cell2mat(svarnames(4)) 'meas1=A(:,8);']);
159        eval(['imag' cell2mat(svarnames(4)) 'meas1=A(:,9);']);
160
161 elseif self_cal==1
162        % if you want to do your own TRL cal
163        [f,S11meas1,S21meas1,S12meas1,S22meas1]=TRL('thru.txt','line.txt',...
164            'reflect.txt',inputFile);
165        realS11meas1=real(S11meas1);
166        imagS11meas1=imag(S11meas1);
167        realS21meas1=real(S21meas1);
168        imagS21meas1=imag(S21meas1);
169        realS12meas1=real(S12meas1);
170        imagS12meas1=imag(S12meas1);
171        realS22meas1=real(S22meas1);
172        imagS22meas1=imag(S22meas1);
173   end
174
175 wf=2*pi*f;   % for all freq's
176
177 % in case the data is outside of normal freq range, truncate it
178 minidx=find(wf>=wmin,1,'first');
179 maxidx=find(wf>=wmax,1,'first');
180 wf=wf(minidx:maxidx);
181 realS11meas1=realS11meas1(minidx:maxidx);
182 imagS11meas1=imagS11meas1(minidx:maxidx);
183 realS21meas1=realS21meas1(minidx:maxidx);
```

```matlab
184  imagS21meas1=imagS21meas1(minidx:maxidx);

185  realS12meas1=realS12meas1(minidx:maxidx);

186  imagS12meas1=imagS12meas1(minidx:maxidx);

187  realS22meas1=realS22meas1(minidx:maxidx);

188  imagS22meas1=imagS22meas1(minidx:maxidx);

189

190  % downsample the measured data, combine real & imag, transpose to columnns

191  if numds==0

192      numds=length(wf);

193  end

194

195  wfds=linspace(wf(1),wf(end),numds);

196  S11meas1=realS11meas1+1j.*imagS11meas1;

197  S11m1ds=interp1(wf,S11meas1,wfds);   % downsample

198  S11m1ds=S11m1ds(:);   % i like column vectors

199  S21meas1=realS21meas1+1j.*imagS21meas1;

200  S21m1ds=interp1(wf,S21meas1,wfds);

201  S21m1ds=S21m1ds(:);

202  S12meas1=realS12meas1+1j.*imagS12meas1;

203  S12m1ds=interp1(wf,S12meas1,wfds);

204  S12m1ds=S12m1ds(:);

205  S22meas1=realS22meas1+1j.*imagS22meas1;

206  S22m1ds=interp1(wf,S22meas1,wfds);

207  S22m1ds=S22m1ds(:);

208

209  % if using the two-thickness method, get second set of measurements

210  % if length(dmat)==2

211  if ismember(solveCase,[3 6])==1

212      if self_cal==0  % use VNA cal'd data

213  %        % original import code - needs to have sparams in a specific order

214  %           [f,realS11meas2,imagS11meas2,realS21meas2,imagS21meas2,...

215  %              realS12meas2,imagS12meas2,realS22meas2,imagS22meas2]...
```

246

```matlab
216 %            =fileformat4(inputFile2); % grab data from input file
217        [A,svarnames]=fileformat5(inputFile2);
218        % use the svarnames to assign the correct name to the sparams
219        eval(['real' cell2mat(svarnames(1)) 'meas2=A(:,2);']);
220        eval(['imag' cell2mat(svarnames(1)) 'meas2=A(:,3);']);
221        eval(['real' cell2mat(svarnames(2)) 'meas2=A(:,4);']);
222        eval(['imag' cell2mat(svarnames(2)) 'meas2=A(:,5);']);
223        eval(['real' cell2mat(svarnames(3)) 'meas2=A(:,6);']);
224        eval(['imag' cell2mat(svarnames(3)) 'meas2=A(:,7);']);
225        eval(['real' cell2mat(svarnames(4)) 'meas2=A(:,8);']);
226        eval(['imag' cell2mat(svarnames(4)) 'meas2=A(:,9);']);
227    elseif self_cal==1 % if you want to do your own TRL cal
228        [f,S11meas2,S21meas2,S12meas2,S22meas2]=TRL('thru.txt','line.txt',...
229            'reflect.txt',inputFile2);
230        realS11meas2=real(S11meas2);
231        imagS11meas2=imag(S11meas2);
232        realS21meas2=real(S21meas2);
233        imagS21meas2=imag(S21meas2);
234        realS12meas2=real(S12meas2);
235        imagS12meas2=imag(S12meas2);
236        realS22meas2=real(S22meas2);
237        imagS22meas2=imag(S22meas2);
238    end
239
240    % in case the data is outside of normal freq range, truncate it
241    realS11meas2=realS11meas2(minidx:maxidx);
242    imagS11meas2=imagS11meas2(minidx:maxidx);
243    realS21meas2=realS21meas2(minidx:maxidx);
244    imagS21meas2=imagS21meas2(minidx:maxidx);
245    realS12meas2=realS12meas2(minidx:maxidx);
246    imagS12meas2=imagS12meas2(minidx:maxidx);
247    realS22meas2=realS22meas2(minidx:maxidx);
```

```matlab
248         imagS22meas2=imagS22meas2(minidx:maxidx);

249

250     % Combine real and imaginary parts, transpose to column vector
251         S11meas2=realS11meas2+1j.*imagS11meas2;
252         S11m2ds=interp1(wf,S11meas2,wfds);
253         S11m2ds=S11m2ds(:);
254         S21meas2=realS21meas2+1j.*imagS21meas2;
255         S21m2ds=interp1(wf,S21meas2,wfds);
256         S21m2ds=S21m2ds(:);
257         S12meas2=realS12meas2+1j.*imagS12meas2;
258         S12m2ds=interp1(wf,S12meas2,wfds);
259         S12m2ds=S12m2ds(:);
260         S22meas2=realS22meas2+1j.*imagS22meas2;
261         S22m2ds=interp1(wf,S22meas2,wfds);
262         S22m2ds=S22m2ds(:);
263 end

264

265

266 % % % % % % % % % % % % % % % % % % % % % % %
267 % %   choose init guess method for LSQCurvefit
268 % % % % % % % % % % % % % % % % % % % % % % %

269

270 if strcmp(init_method,'nrw')==1

271

272     % NRW analysis
273         [fnrw,realS11ex,imagS11ex,realS21ex,imagS21ex,...
274             realS12ex,imagS12ex,realS22ex,imagS22ex]=fileformat4(nrwInput);
275         wnrw=2*pi*fnrw;
276         [epsfwd,epsbw,mufwd,mubw]=waveguide_nrw(fnrw,realS11ex,imagS11ex,...
277             realS21ex,imagS21ex,realS12ex,imagS12ex,realS22ex,imagS22ex,ls);
278         epsNRW=epsbw;
279         muNRW=mubw;
```

248

```matlab
280    % display the NRW results
281    display('%%%%%%%%%%%%%%%%%%%%%%%%%%%%%%%%%%%%%%')
282    display('NRW processing finished')
283    display(['Mean forward eps = ' num2str(mean(epsNRW))])
284    display(['Mean forward mu = ' num2str(mean(muNRW))])
285    display(['Mean backward eps = ' num2str(mean(epsbw))])
286    display(['Mean backward mu = ' num2str(mean(mubw))])
287    display('%%%%%%%%%%%%%%%%%%%%%%%%%%%%%%%%%%%%%%')
288    display(' ')
289
290    % initial guesses based on NRW
291    etguess=interp1(wnrw,epsNRW,wfds);
292    ezguess=interp1(wnrw,epsNRW,wfds);
293    mutguess=interp1(wnrw,muNRW,wfds);
294    muzguess=interp1(wnrw,muNRW,wfds);
295    etguess=etguess(:);
296    ezguess=ezguess(:);
297    mutguess=mutguess(:);
298    muzguess=muzguess(:);
299
300 elseif strcmp(init_method,'nrwTruth')==1 % load initial values from .mat file
301
302    load('NRW_vals.mat');
303
304    % initial guesses based on NRW
305    etguess=interp1(wnrw,epsNRW,wfds);
306    ezguess=interp1(wnrw,epsNRW,wfds);
307    mutguess=interp1(wnrw,muNRW,wfds);
308    muzguess=interp1(wnrw,muNRW,wfds);
309    etguess=etguess(:);
310    ezguess=ezguess(:);
311    mutguess=mutguess(:);
```

```matlab
312    muzguess=muzguess(:);

313

314  elseif strcmp(init_method,'initup')==1 % one initial guess + update as we go

315

316      etguess=zeros(length(wfds)+1,1);

317      ezguess=zeros(length(wfds)+1,1);

318      mutguess=zeros(length(wfds)+1,1);

319      muzguess=zeros(length(wfds)+1,1);

320      etguess(1)=(myret+1j*myiet);

321      ezguess(1)=(myrez+1j*myiez);

322      mutguess(1)=(myrmut+1j*myimut);

323      muzguess(1)=(myrmuz+1j*myimuz);

324

325  elseif strcmp(init_method,'initone')==1 % same initial guess every time

326

327      etguess=(myret+1j*myiet)*ones(length(wfds),1);

328      ezguess=(myrez+1j*myiez)*ones(length(wfds),1);

329      mutguess=(myrmut+1j*myimut)*ones(length(wfds),1);

330      muzguess=(myrmuz+1j*myimuz)*ones(length(wfds),1);

331

332  end

333

334  %%  solution routine

335

336  % % % % % % % % % % % % % % % % % % % % %

337  % % Calculation of A coefficients and scattering parameters

338  % % % % % % % % % % % % % % % % % % % % %

339

340  % pre-allocate the solution vectors

341  etsol=zeros(length(wfds),1);

342  ezsol=zeros(length(wfds),1);

343  mutsol=zeros(length(wfds),1);
```

```matlab
344  muzsol=zeros(length(wfds),1);
345  tsolve=zeros(length(wfds),1);
346  eigerror=zeros(length(wfds)+1,1);
347  Y=0;  % initialize the solution array
348  if errchk==1
349      stddeltaetreal=zeros(length(wfds),1);
350      stddeltaetimag=zeros(length(wfds),1);
351      stddeltaezreal=zeros(length(wfds),1);
352      stddeltaezimag=zeros(length(wfds),1);
353      stddeltamutreal=zeros(length(wfds),1);
354      stddeltamutimag=zeros(length(wfds),1);
355      stddeltamuzreal=zeros(length(wfds),1);
356      stddeltamuzimag=zeros(length(wfds),1);
357  end
358
359  for widx=1:length(wfds) % solve at each frequency
360      tic;
361      wval=wfds(widx);
362
363      % sometimes NRW routine gives positive imag eps or mu...
364      if imag(etguess(widx))>=0
365          etguess(widx)=etguess(widx)';
366          ezguess(widx)=ezguess(widx)';
367      end
368      if imag(mutguess(widx))>=0
369          mutguess(widx)=mutguess(widx)';
370          muzguess(widx)=muzguess(widx)';
371      end
372
373      if solveCase==7 % set the transverse values to known values
374          ket=etguess(widx);
375          kmut=mutguess(widx);
```

```matlab
376        end
377
378        display(sprintf('%%%%%%%%%%%%%%%%%%%%%%%%%%%%%%%%%%%%'))
379        display(sprintf(['Now processing point ' num2str(widx) '/' ...
380             num2str(length(wfds))]))
381        display(sprintf(['Frequency = ' num2str(wval/2/pi) 'GHz']))
382        display(sprintf(['Initial et =' num2str(etguess(widx)) ]))
383        display(sprintf(['Initial ez =' num2str(ezguess(widx)) ]))
384        display(sprintf(['Initial mut =' num2str(mutguess(widx)) ]))
385        display(sprintf(['Initial muz =' num2str(muzguess(widx)) ]))
386        display(sprintf('%%%%%%%%%%%%%%%%%%%%%%%%%%%%%%%%%%%%'))
387        display(sprintf(' \n'))
388
389    % construct the measured s-parameter matrices and downsample
390        if porttouse==1 % Use only S11 and S21
391            Smeas=cat(1,real(S11m1ds(widx)),imag(S11m1ds(widx)),...
392                real(S21m1ds(widx)),imag(S21m1ds(widx)));
393        elseif porttouse==2 % use only S22 and S12
394            Smeas=cat(1,real(S12m1ds(widx)),imag(S12m1ds(widx)),...
395                real(S22m1ds(widx)),imag(S22m1ds(widx)));
396        elseif porttouse==3  % use both
397            Smeas=cat(1,real(S11m1ds(widx)),imag(S11m1ds(widx)),...
398                real(S21m1ds(widx)),imag(S21m1ds(widx)),...
399                 real(S12m1ds(widx)),imag(S12m1ds(widx)),...
400                real(S22m1ds(widx)),imag(S22m1ds(widx)));
401        end
402
403        if (length(dmat)==2) && (porttouse==1)   % two thickness method
404                Smeas=cat(1,Smeas,real(S11m2ds(widx)),imag(S11m2ds(widx)),...
405                    real(S21m2ds(widx)),imag(S21m2ds(widx)));
406        elseif (length(dmat)==2) && (porttouse==2)
407                Smeas=cat(1,Smeas,real(S12m2ds(widx)),imag(S12m2ds(widx)),...
```

252

```matlab
408                  real(S22m2ds(widx)),imag(S22m2ds(widx)));
409       elseif (length(dmat)==2) && (porttouse==3)   % use both
410              Smeas=cat(1,Smeas,real(S11m2ds(widx)),imag(S11m2ds(widx)),...
411                  real(S21m2ds(widx)),imag(S21m2ds(widx)),...
412                  real(S12m2ds(widx)),imag(S12m2ds(widx)),...
413                  real(S22m2ds(widx)),imag(S22m2ds(widx)));
414       end
415
416   % % % % % % % % % % % % % % % % % % % % % % %
417   % % Solve using lsqcurvefit - unknowns are [ret iet rez iez rmut imut rmuz imuz]
418   % % % % % % % % % % % % % % % % % % % % % % %
419
420       [etsol(widx), ezsol(widx), mutsol(widx), muzsol(widx)] ...
421           = runSolver(Smeas,wval,etguess(widx),ezguess(widx),...
422               mutguess(widx),muzguess(widx));
423
424   % % % % % % % % % % % % % % % % % % % % % % %
425   % % error bars routine
426   % % % % % % % % % % % % % % % % % % % % % % %
427
428       if errchk==1
429              [stddeltaetreal(widx), stddeltaetimag(widx), stddeltaezreal(widx),...
430                  stddeltaezimag(widx),stddeltamutreal(widx), ...
431                  stddeltamutimag(widx), stddeltamuzreal(widx), ...
432                  stddeltamuzimag(widx)] ...
433                  = getErrorTerms(etsol(widx),ezsol(widx),...
434                  mutsol(widx),muzsol(widx),Smeas,wval,...
435                  etguess(widx),ezguess(widx),mutguess(widx),muzguess(widx));
436
437       end
438
439     % update initial guesses, if needed
```

253

```matlab
440        if strcmp(init_method,'initup')==1
441            etguess(widx+1)=etsol(widx);
442            ezguess(widx+1)=ezsol(widx);
443            mutguess(widx+1)=mutsol(widx);
444            muzguess(widx+1)=muzsol(widx);
445        end
446
447        tsolve(widx)=toc;
448
449    % output the final values
450        display(sprintf('%%%%%%%%%%%%%%%%%%%%%%%%%%%%%%%%%%%%'))
451        display(sprintf(['Final values for Frequency = ' num2str(wval/2/pi)...
452            'GHz']))
453        display(sprintf(['et = ' num2str(etsol(widx)) ]))
454        display(sprintf(['ez = ' num2str(ezsol(widx)) ]))
455        display(sprintf(['mut = ' num2str(mutsol(widx)) ]))
456        display(sprintf(['muz = ' num2str(muzsol(widx)) ]))
457        display(sprintf(['Time to solution = ' num2str(tsolve(widx)) 's']))
458        display(sprintf('%%%%%%%%%%%%%%%%%%%%%%%%%%%%%%%%%%%%'))
459        display(sprintf(' \n'));
460 end % end of w loop
461
462 %% final diagnostics
463 % % % % % % % % % % % % % % % % % % % % % % %
464 % all done - print some diagnostics
465 % % % % % % % % % % % % % % % % % % % % % % %
466
467 ttsolve=sum(tsolve);
468 hrs=floor(ttsolve/3600);
469 mins=floor((ttsolve-hrs*3600)/60);
470 secs=floor(ttsolve-hrs*3600-mins*60);
471 tstring=[num2str(hrs) ' hours, ' num2str(mins) ' mins, '...
```

254

```matlab
472       num2str(secs) ' secs' ];
473 meanet=mean(etsol);
474 meanez=mean(ezsol);
475 meanmut=mean(mutsol);
476 meanmuz=mean(muzsol);
477
478 display(sprintf(['Finished - total solution time = ' tstring]))
479 display(sprintf(['Avg et = ' num2str(meanet) ]))
480 display(sprintf(['Avg ez = ' num2str(meanez) ]))
481 display(sprintf(['Avg mut = ' num2str(meanmut) ]))
482 display(sprintf(['Avg muz = ' num2str(meanmuz) ]))
483
484
485 close all; % close the LSQ diagnostics
486
487 % if we want to smooth out the data
488 if smooth_zvals==1
489     ezsolbak=ezsol;
490     ezsol=smooth(ezsol,sspan,smeth);
491 end
492 if smooth_tvals==1
493     etsolbak=etsol;
494     etsol=smooth(etsol,sspan,smeth);
495 end
496
497
498 % % generate pretty pictures
499
500 % figure out the best limits, according to solution values
501 pad=0.2;
502
503 etminval=round(10*( (1+pad)*min(imag(etsol) ) ) )/10;
```

255

```
504  ezminval=round(10*( (1+pad)*min(imag(ezsol) ) ) )/10;

505  etmaxval=round(10*( (1+pad)*max(real(etsol) ) ) )/10;

506  ezmaxval=round(10*( (1+pad)*max(real(ezsol) ) ) )/10;

507  epslims=[min([etminval ezminval]) max([etmaxval ezmaxval])];

508

509  mutminval=round(10*( (1+pad)*min(imag(mutsol) ) ) )/10;

510  muzminval=round(10*( (1+pad)*min(imag(muzsol) ) ) )/10;

511  mutmaxval=round(10*( (1+pad)*max(real(mutsol) ) ) )/10;

512  muzmaxval=round(10*( (1+pad)*max(real(muzsol) ) ) )/10;

513  mulims=[min([mutminval muzminval]) max([mutmaxval muzmaxval])];

514

515  if errchk==1

516      etminval=round(10*( (1+pad)*(epslims(1)-(2*min(stddeltaetimag ))) ) )/10;

517      ezminval=round(10*( (1+pad)*(epslims(1)-(2*min(stddeltaezimag ))) ) )/10;

518      etmaxval=round(10*( (1+pad)*(epslims(2)+(2*max(stddeltaetreal ))) ) )/10;

519      ezmaxval=round(10*( (1+pad)*(epslims(2)+(2*max(stddeltaezreal ))) ) )/10;

520      epslims_err=[min([etminval ezminval]) max([etmaxval ezmaxval])];

521

522      mutminval=round(10*( (1+pad)*(mulims(1)-(2*min(stddeltamutimag ))) ) )/10;

523      muzminval=round(10*( (1+pad)*(mulims(1)-(2*min(stddeltamuzimag ))) ) )/10;

524      mutmaxval=round(10*( (1+pad)*(mulims(2)+(2*max(stddeltamutreal ))) ) )/10;

525      muzmaxval=round(10*( (1+pad)*(mulims(2)+(2*max(stddeltamuzreal ))) ) )/10;

526      mulims_err=[min([mutminval muzminval]) max([mutmaxval muzmaxval])];

527  end

528

529  sidebyside_pos_1=[0.1344    0.4    0.3319    0.4290];

530  sidebyside_pos_2=[0.5267    0.4    0.3319    0.4290];

531  sidebyside_annotation=[ 0.3184    0.1894    0.1336    0.0833];

532  sidebyside_leg=[0.4991    0.1239    0.1461    0.1935];

533

534  if strcmp(init_method,'nrw')==1 || strcmp(init_method,'nrwTruth')==1

535      myfigure;
```

```matlab
536    orient landscape;
537    subplot('Position',[0.0999    0.5514    0.3347    0.3412]);
538    plot(wfds/2/pi/1e9,real(etsol),'-o',wfds/2/pi/1e9,imag(etsol),'-o',...
539        wfds/2/pi/1e9,real(ezsol),'-o',wfds/2/pi/1e9,imag(ezsol),'-o');
540    title('Extracted \epsilon_r Values')
541    leg1=legend('Re(\sigma_t)','Imag(\sigma_t)','Re(\sigma_z)','Imag(\sigma_z)');
542    xlabel('f (GHz)');
543    ylim(epslims);
544    set(leg1,'Position',[0.4619    0.6417    0.0994    0.1835])
545
546    subplot('Position',[0.5891    0.5514    0.3347    0.3412]);
547    plot(wfds/2/pi/1e9,real(mutsol),'-o',wfds/2/pi/1e9,imag(mutsol),'-o',...
548        wfds/2/pi/1e9,real(muzsol),'-o',wfds/2/pi/1e9,imag(muzsol),'-o');
549    title('Extracted \mu_r Values')
550    xlabel('f (GHz)');
551    ylim(mulims);
552
553    subplot('Position',[0.0988    0.0776    0.3347    0.3412]);
554    plot(wfds/2/pi/1e9,real(etsol),'-o',wfds/2/pi/1e9,imag(etsol),'-o',...
555        wnrw/2/pi/1e9,real(epsNRW),'-o',wnrw/2/pi/1e9,imag(epsNRW),'-o');
556    title('Comparison of \epsilon_t Values')
557    leg2=legend('Re - tFWGT','Im - tFWGT','Re - NRW','Im - NRW');
558    xlabel('f (GHz)');
559    ylim(epslims);
560    set(leg2,'Position',[0.4409    0.2032    0.1250    0.1324])
561
562    subplot('Position',[0.5914    0.0776    0.3347    0.3412]);
563    plot(wfds/2/pi/1e9,real(mutsol),'-o',wfds/2/pi/1e9,imag(mutsol),'-o',...
564        wnrw/2/pi/1e9,real(muNRW),'-o',wnrw/2/pi/1e9,imag(muNRW),'-o');
565    title('Comparison of \mu_t Values')
566    ylim(mulims);
567    xlabel('f (GHz)');
```

```matlab
568
569     mtit(gcf,regexprep(casedesc,'_',' '),'FontSize',14,'yoff',0.06,'xoff',-0.02);
570
571 % dielectric, magnetic
572 elseif strcmp(init_method,'nrw')==0 && (solveCase==3 || solveCase==6)
573
574     myfigure;
575     orient landscape;
576
577     subplot('Position',sidebyside_pos_1);
578     plot(wfds/2/pi/1e9,real(etsol),'-o',wfds/2/pi/1e9,real(ezsol),'-o',...
579         wfds/2/pi/1e9,imag(etsol),'-o',wfds/2/pi/1e9,imag(ezsol),'-o');
580     title('Extracted \epsilon Values')
581     leg1=legend('Real - \sigma_t','Real - \sigma_z','Imag - \sigma_t',...
582         'Imag - \sigma_z');
583     xlabel('f (GHz)');
584     ylim(epslims);
585
586     subplot('Position',sidebyside_pos_2);
587     plot(wfds/2/pi/1e9,real(mutsol),'-o',wfds/2/pi/1e9,real(muzsol),'-o',...
588         wfds/2/pi/1e9,imag(mutsol),'-o',wfds/2/pi/1e9,imag(muzsol),'-o');
589     title('Extracted \mu Values')
590     ylim(mulims);
591     xlabel('f (GHz)');
592
593     set(leg1,'Position',sidebyside_annotation)
594     annotation('textbox',sidebyside_leg,'string',{['Avg \epsilon_t = ' ...
595         num2str(meanet)], ['Avg \epsilon_z = ' num2str(meanez)],...
596         ['Avg \epsilon_t = ' num2str(meanmut)], ['Avg \mu_z = ' ...
597         num2str(meanmuz)]},'FitBoxToText','on','VerticalAlignment',...
598         'middle','BackgroundColor','w');
599     mtit(gcf,regexprep(casedesc,'_',' '),'FontSize',14,'yoff',0.1,'xoff',-0.02);
```

```matlab
600    if errchk==1
601        % one figure for permittivity
602        myfigure;
603        orient landscape;
604
605        subplot('Position',sidebyside_pos_1);
606        errorbar(wfds/2/pi/1e9,real(etsol),2*stddeltaetreal,'b');
607        errorbar(wfds/2/pi/1e9,imag(etsol),2*stddeltaetimag,'Color',[0 0.4 0]);
608        title('Extracted \epsilon_t Values')
609        leg1=legend('Real','Imag ');
610        xlabel('f (GHz)');
611        ylim(epslims_err);
612
613        subplot('Position',sidebyside_pos_2);
614        errorbar(wfds/2/pi/1e9,real(ezsol),2*stddeltaezreal,'b');
615        errorbar(wfds/2/pi/1e9,imag(ezsol),2*stddeltaezimag,'Color',[0 0.4 0]);
616        title('Extracted \epsilon_z Values')
617        ylim(epslims_err);
618        xlabel('f (GHz)');
619
620        set(leg1,'Position',sidebyside_leg)
621        annotation('textbox',sidebyside_annotation,'string',...
622            {['Avg \epsilon_t = ' num2str(meanet)], ...
623            ['Avg \epsilon_z = ' num2str(meanez)]},'FitBoxToText',...
624            'on','VerticalAlignment','middle','BackgroundColor','w');
625        mtit(gcf,[regexprep(casedesc,'_',' ') ' eps uncertainty'],...
626            'FontSize',14,'yoff',0.1,'xoff',-0.02);
627
628        % another figure for permeability
629        myfigure;
630        orient landscape;
631
```

259

```matlab
632             subplot('Position',sidebyside_pos_1);
633             errorbar(wfds/2/pi/1e9,real(mutsol),2*stddeltamutreal,'b');
634             errorbar(wfds/2/pi/1e9,imag(mutsol),2*stddeltamutimag,'Color',[0 0.4 0]);
635             title('Extracted \mu_t Values')
636             leg1=legend('Real','Imag ');
637             xlabel('f (GHz)');
638             ylim(mulims_err);
639
640             subplot('Position',sidebyside_pos_2);
641             errorbar(wfds/2/pi/1e9,real(muzsol),2*stddeltamuzreal,'b');
642             errorbar(wfds/2/pi/1e9,imag(muzsol),2*stddeltamuzimag,'Color',[0 0.4 0]);
643             title('Extracted \mu_z Values')
644             ylim(mulims_err);
645             xlabel('f (GHz)');
646
647             set(leg1,'Position',sidebyside_leg)
648             annotation('textbox',sidebyside_annotation,'string',{['Avg \mu_t = ' ...
649                 num2str(meanmut)], ['Avg \mu_z = ' num2str(meanmuz)]},'FitBoxToText',...
650                 'on','VerticalAlignment','middle','BackgroundColor','w');
651         mtit(gcf,[regexprep(casedesc,'_',' ') ' mu uncertainty'],...
652             'FontSize',14,'yoff',0.1,'xoff',-0.02);
653     end
654
655 % non-dielectric, magnetic
656 elseif strcmp(init_method,'nrw')==0 && (solveCase==2 || solveCase==5)
657     myfigure;
658     orient landscape;
659
660     subplot('Position',sidebyside_pos_1);
661     plot(wfds/2/pi/1e9,real(mutsol),'-o',wfds/2/pi/1e9,imag(mutsol),'-o');
662     title('Extracted \mu_t Values')
663     leg1=legend('Real','Imag');
```

```matlab
664    xlabel('f (GHz)');
665    ylim(mulims);
666
667
668    subplot('Position',sidebyside_pos_2);
669    plot(wfds/2/pi/1e9,real(muzsol),'-o',wfds/2/pi/1e9,imag(muzsol),'-o');
670    title('Extracted \mu_z Values')
671    ylim(mulims);
672    xlabel('f (GHz)');
673
674    annotation('textbox',sidebyside_annotation,'string',{['Avg \mu_t = ' ...
675        num2str(meanmut)], ['Avg \mu_z = ' num2str(meanmuz)]},'FitBoxToText',...
676        'on','VerticalAlignment','middle','BackgroundColor','w');
677    set(leg1,'Position',sidebyside_leg)
678    mtit(gcf,regexprep(casedesc,'_',' '),'FontSize',14,'yoff',0.1,'xoff',-0.02);
679    if errchk==1
680        myfigure;
681        orient landscape;
682
683        subplot('Position',sidebyside_pos_1);
684        errorbar(wfds/2/pi/1e9,real(mutsol),2*stddeltamutreal,'b');
685        errorbar(wfds/2/pi/1e9,imag(mutsol),2*stddeltamutimag,'Color',[0 0.4 0]);
686        title('Extracted \mu_t Values')
687        leg1=legend('Real','Imag');
688        xlabel('f (GHz)');
689        ylim(mulims_err);
690
691        subplot('Position',sidebyside_pos_2);
692        errorbar(wfds/2/pi/1e9,real(muzsol),2*stddeltamuzreal,'b');
693        errorbar(wfds/2/pi/1e9,imag(muzsol),2*stddeltamuzimag,'Color',[0 0.4 0]);
694        title('Extracted \mu_z Values')
695        ylim(mulims_err);
```

261

```matlab
696            xlabel('f (GHz)');
697
698            annotation('textbox',sidebyside_annotation,'string',{['Avg \mu_t = ' ...
699                num2str(meanmut)], ['Avg \mu_z = ' num2str(meanmuz)]},'FitBoxToText',...
700                'on','VerticalAlignment','middle','BackgroundColor','w');
701            set(leg1,'Position',sidebyside_leg)
702            mtit(gcf,[regexprep(casedesc,'_',' ') ' uncertainty'],'FontSize',...
703                14,'yoff',0.1,'xoff',-0.02);
704        end
705
706
707    % dielectric, non-magnetic
708    elseif strcmp(init_method,'nrw')==0 && (solveCase==1 || solveCase==4)
709        myfigure;
710        orient landscape;
711
712        subplot('Position',sidebyside_pos_1);
713        plot(wfds/2/pi/1e9,real(etsol),'-o',wfds/2/pi/1e9,imag(etsol),'-o');
714        title('Extracted \epsilon_t Values')
715        leg1=legend('Real','Imag');
716        xlabel('f (GHz)');
717        ylim(epslims);
718
719        subplot('Position',sidebyside_pos_2);
720        plot(wfds/2/pi/1e9,real(ezsol),'-o',wfds/2/pi/1e9,imag(ezsol),'-o');
721        title('Extracted \epsilon_z Values')
722        ylim(epslims);
723        xlabel('f (GHz)');
724
725        annotation('textbox',sidebyside_annotation,'string',{['Avg \epsilon_t = ' ...
726            num2str(meanet)], ['Avg \epsilon_z = ' num2str(meanez)]},'FitBoxToText','on',...
727            'VerticalAlignment','middle','BackgroundColor','w');
```

262

```matlab
728        set(leg1,'Position',sidebyside_leg)
729        mtit(gcf,regexprep(casedesc,'_',' '),'FontSize',14,'yoff',-0.06,'xoff',-0.02);
730
731        if errchk==1
732            myfigure;
733            orient landscape;
734
735            subplot('Position',sidebyside_pos_1);
736            hold on;
737            errorbar(wfds/2/pi/1e9,real(etsol),2*stddeltaetreal,'b');
738            errorbar(wfds/2/pi/1e9,imag(etsol),2*stddeltaetimag,'Color',[0 0.4 0]);
739            title('Extracted \epsilon_t Values')
740            leg1=legend('Real','Imag');
741            xlabel('f (GHz)');
742            ylim(epslims_err);
743
744            subplot('Position',sidebyside_pos_2);
745            hold on;
746            errorbar(wfds/2/pi/1e9,real(ezsol),2*stddeltaezreal,'b');
747            errorbar(wfds/2/pi/1e9,imag(ezsol),2*stddeltaezimag,'Color',[0 0.4 0]);
748            title('Extracted \epsilon_z Values')
749            ylim(epslims_err);
750            xlabel('f (GHz)');
751
752            annotation('textbox',sidebyside_annotation,'string',...
753                {['Avg \epsilon_t = ' num2str(meanet)],...
754                ['Avg \epsilon_z = ' num2str(meanez)]},'FitBoxToText','on',...
755              'VerticalAlignment','middle','BackgroundColor','w');
756            set(leg1,'Position',sidebyside_leg)
757            mtit(gcf,[regexprep(casedesc,'_',' ') ' uncertainty'],'FontSize',...
758                14,'yoff',-0.06,'xoff',-0.02);
759        end
```

```matlab
760  end
761
762  fds=wfds(:)/2/pi/1e9;
763
764  if print==1
765      printfigs;
766  end
767
768  if makeFile==1
769      if ismember(solveCase,[1 3 4 6])==1 && errchk==0
770          M=[fds, real(etsol)];
771          csvwrite(['et_vals_real_' num2str(numModes) 'mode' add2casedesc '.dat'],M)
772          M=[fds, imag(etsol)];
773          csvwrite(['et_vals_imag_' num2str(numModes) 'mode' add2casedesc '.dat'],M)
774          M=[fds, real(ezsol)];
775          csvwrite(['ez_vals_real_' num2str(numModes) 'mode' add2casedesc '.dat'],M)
776          M=[fds, imag(ezsol)];
777          csvwrite(['ez_vals_imag_' num2str(numModes) 'mode' add2casedesc '.dat'],M)
778      elseif ismember(solveCase,[1 3 4 6])==1 && errchk==1
779          M=[fds, real(etsol), stddeltaetreal];
780          csvwrite(['et_vals_real_' num2str(numModes) 'mode' add2casedesc '.dat'],M)
781          M=[fds, imag(etsol), stddeltaetimag];
782          csvwrite(['et_vals_imag_' num2str(numModes) 'mode' add2casedesc '.dat'],M)
783          M=[fds, real(ezsol), stddeltaezreal];
784          csvwrite(['ez_vals_real_' num2str(numModes) 'mode' add2casedesc '.dat'],M)
785          M=[fds, imag(ezsol), stddeltaezimag];
786          csvwrite(['ez_vals_imag_' num2str(numModes) 'mode' add2casedesc '.dat'],M)
787      end
788      if ismember(solveCase,[2 3 5 6])==1 && errchk==0
789          M=[fds, real(mutsol)];
790          csvwrite(['mut_vals_real_' num2str(numModes) 'mode' add2casedesc '.dat'],M)
791          M=[fds, imag(mutsol)];
```

264

```matlab
792        csvwrite(['mut_vals_imag_' num2str(numModes) 'mode' add2casedesc '.dat'],M)
793        M=[fds, real(muzsol)];
794        csvwrite(['muz_vals_real_' num2str(numModes) 'mode' add2casedesc '.dat'],M)
795        M=[fds, imag(muzsol)];
796        csvwrite(['muz_vals_imag_' num2str(numModes) 'mode' add2casedesc '.dat'],M)
797    elseif ismember(solveCase,[2 3 5 6])==1 && errchk==1
798        M=[fds, real(mutsol), stddeltamutreal];
799        csvwrite(['mut_vals_real_' num2str(numModes) 'mode' add2casedesc '.dat'],M)
800        M=[fds, imag(mutsol), stddeltamutimag];
801        csvwrite(['mut_vals_imag_' num2str(numModes) 'mode' add2casedesc '.dat'],M)
802        M=[fds, real(muzsol), stddeltamuzreal];
803        csvwrite(['muz_vals_real_' num2str(numModes) 'mode' add2casedesc '.dat'],M)
804        M=[fds, imag(muzsol), stddeltamuzimag];
805        csvwrite(['muz_vals_imag_' num2str(numModes) 'mode' add2casedesc '.dat'],M)
806    end
807 end
808
809
810 % save the workspace
811 save([casedesc '_workspace.mat']);
812
813 diary off;
814
815 % % % % % % % % % % % % % % % % % % % % % %
816 % change log
817 % % % % % % % % % % % % % % % % % % % % % %
818 % 20140516
819 %      - fixed a couple of errors in Sparams case 5 integrals (11 and 12)
820 %      - added logic to output *.dat files
821 %      - limits for errorbar plots are now calculated separately from normal plots
822 %          (helps with large error bars)
823 % 20140415
```

```
824 %       - changed logic for errchk plots
825 %       - made error bars 2*sigma
826 %
827 % 20140225:
828 %       - updated S-parameters import to account for any order in the
829 %               cti file
830 %       - added print switch
831 %       - reorganized options to be a little more intuitive
832 %       - started the change log
833 %       - added ylimits to make the plots on the same scale
834 %       - added the average dotted line
835 %       - added the numds=0 option for no downsampling (requires no knowledge
836 %       of number of input points)
837 % 20140107:
838 %       - finally fixed the errorbars code!!!!
```

F.2   runSolver.m

This function determines the appropriate number of inputs for the LSQ solver to pass to the Sparams.m function (which calculates the theoretical scattering parameters.

```
1  function [etsol,ezsol,mutsol,muzsol] = runSolver(Smeas,wval,etguess,ezguess...
2      ,mutguess,muzguess)
3
4  global eps0 mu0 solveCase alg ket kmut;
5
6  % set the options for the solver
7  % options=optimset('Display','off','PlotFcns',...
8  %           {@optimplotfunccount @optimplotx @optimplotfval @optimplotstepsize});
9  if strcmp(alg,'LM')==1
10     options=optimset('Display','iter','Algorithm',{'levenberg-marquardt',1e-6});
```

266

```matlab
11   elseif strcmp(alg,'TRR')==1
12       options=optimset('Display','iter');
13       lb=-50;
14       ub=50;
15   end
16
17
18
19   % eval the solveCase flag
20   switch solveCase
21       case 1 % isotropic, dielectric, non-mag -> ez=et and muz=mut=mu0
22           if strcmp(alg,'LM')==1
23               Y=lsqcurvefit(@Sparams,[real(etguess) imag(etguess)],...
24                   wval,Smeas,[],[],options);
25           elseif strcmp(alg,'TRR')==1
26               Y=lsqcurvefit(@Sparams,[real(etguess) imag(etguess)],...
27                   wval,Smeas,[0 lb],[ub 0],options);
28           end
29       etsol=Y(1)+1j*Y(2);
30       ezsol=Y(1)+1j*Y(2);
31       mutsol=1;
32       muzsol=1;
33
34
35       case 2 % isotropic, non-dielectric, mag -> ez=et=eps0 and muz=mut
36           if strcmp(alg,'LM')==1
37               Y=lsqcurvefit(@Sparams,[real(mutguess) imag(mutguess)],...
38                   wval,Smeas,[],[],options);
39           elseif strcmp(alg,'TRR')==1
40               Y=lsqcurvefit(@Sparams,[real(mutguess) imag(mutguess)],...
41                   wval,Smeas,[0 lb],[ub 0],options);
42           end
```

267

```matlab
43        etsol=1;

44        ezsol=1;

45     mutsol=Y(1)+1j*Y(2);

46     muzsol=Y(1)+1j*Y(2);


48     case 3 % isotropic, dielectric, mag -> ez=et and muz=mut
49         if strcmp(alg,'LM')==1
50             Y=lsqcurvefit(@Sparams,[real(etguess) imag(etguess) ...
51                 real(mutguess) imag(mutguess)],...
52                 wval,Smeas,[],[],options);
53         elseif strcmp(alg,'TRR')==1
54         Y=lsqcurvefit(@Sparams,[real(etguess) imag(etguess) ...
55             real(mutguess) imag(mutguess)],...
56             wval,Smeas,[0 lb 0 lb],[ub 0 ub 0],options);
57         end
58     etsol=Y(1)+1j*Y(2);
59     ezsol=Y(1)+1j*Y(2);
60     mutsol=Y(3)+1j*Y(4);
61     muzsol=Y(3)+1j*Y(4);


63     case 4 % uniaxial, dielectric, non-mag -> ez,et and muz=mut=mu0
64         if strcmp(alg,'LM')==1
65             Y=lsqcurvefit(@Sparams,[real(etguess) imag(etguess)...
66                 real(ezguess) imag(ezguess)],...
67                 wval,Smeas,[],[],options);
68         elseif strcmp(alg,'TRR')==1
69 %             Y=lsqcurvefit(@Sparams,[real(etguess) imag(etguess)...
70 %                 real(ezguess) imag(ezguess)],...
71 %                 wval,Smeas,[0 lb 0 lb],[ub 0 ub 0],options);
72             Y=lsqcurvefit(@Sparams,[real(etguess) imag(etguess)...
73                 real(ezguess) imag(ezguess)],...
74                 wval,Smeas,[lb lb lb lb],[ub ub ub ub],options);
```

268

```matlab
75            end
76      etsol=Y(1)+1j*Y(2);
77      ezsol=Y(3)+1j*Y(4);
78      mutsol=1;
79      muzsol=1;
80
81      case 5 % uniaxial, non-dielectric, mag -> ez=et=eps0 and muz,mut
82          if strcmp(alg,'LM')==1
83              Y=lsqcurvefit(@Sparams,[real(mutguess) imag(mutguess)...
84                  real(muzguess) imag(muzguess)],...
85                  wval,Smeas,[],[],options);
86          elseif strcmp(alg,'TRR')==1
87              Y=lsqcurvefit(@Sparams,[real(mutguess) imag(mutguess)...
88                  real(muzguess) imag(muzguess)],...
89                  wval,Smeas,[0 lb 0 lb],[ub 0 ub 0],options);
90          end
91      etsol=1;
92      ezsol=1;
93      mutsol=Y(1)+1j*Y(2);
94      muzsol=Y(3)+1j*Y(4);
95
96      case 6 % uniaxial, dielectric, mag -> ez,et and muz,mut
97          if strcmp(alg,'LM')==1
98              Y=lsqcurvefit(@Sparams,[real(etguess) imag(etguess)...
99                  real(ezguess) imag(ezguess) real(mutguess) imag(mutguess)...
100                 real(muzguess) imag(muzguess)],...
101                 wval,Smeas,[],[],options);
102         elseif strcmp(alg,'TRR')==1
103             Y=lsqcurvefit(@Sparams,[real(etguess) imag(etguess)...
104                 real(ezguess) imag(ezguess) real(mutguess) imag(mutguess)...
105                 real(muzguess) imag(muzguess)],...
106                 wval,Smeas,[0 lb 0 lb 0 lb 0 lb],[ub 0 ub 0 ub 0 ub 0],options);
```

269

```
107            end
108      etsol=Y(1)+1j*Y(2);
109      ezsol=Y(3)+1j*Y(4);
110      mutsol=Y(5)+1j*Y(6);
111      muzsol=Y(7)+1j*Y(8);
112
113      case 7 % uniaxial, dielectric, mag with known et and mut
114          if strcmp(alg,'LM')==1
115              Y=lsqcurvefit(@Sparams,[real(ezguess) imag(ezguess) ...
116                  real(muzguess) imag(muzguess)],...
117                  wval,Smeas,[],[],options);
118          elseif strcmp(alg,'TRR')==1
119              Y=lsqcurvefit(@Sparams,[real(ezguess) imag(ezguess) ...
120                  real(muzguess) imag(muzguess)],...
121                  wval,Smeas,[0 lb 0 lb],[ub 0 ub 0],options);
122          end
123      etsol=ket;
124      ezsol=Y(1)+1j*Y(2);
125      mutsol=kmut;
126      muzsol=Y(3)+1j*Y(4);
127
128  end
```

F.3   Sparams.m

This function calculates the theoretical scattering parameters, based on the `solveCase`
variable.

```
1 function Sthy=Sparams(X,wval)
2 % export the theoretical scattering coefficients with the real part on top
3 % and the imaginary part below
```

270

```matlab
% INPUTS:
% 1) the vector X contains the input arguments in the order:
% - real(et), imag(et), real(ez), imag(ez)
% - real(mut), imag(mut), real(muz), imag(muz)
% 2) wval is the angular frequency (single value)
% % Calculation of A coefficients and scattering parameters

global v wi a b dmat eps0 mu0 numModes includeModes solveCase porttouse...
    ket kmut num_int;

k0=sqrt(wval.^2.*eps0.*mu0); % gonna need this later

Sthy=[];
A11=zeros(numModes,numModes);
A12=A11;
Bmat=zeros(2*numModes,1);

% cases:
%  1 - isotropic, dielectric, non-magnetic (et=ez=er) & (mut=muz=mu0)
%  2 - isotropic, non-dielectric, magnetic (et=ez=eps0) & (mut=muz=mur)
%  3 - isotropic, dielectric, magnetic (et=ez=er) & (mut=muz=mur)
%  4 - uniaxial, dielectric, non-magnetic (et,ez) & (mut=muz=mu0)
%  5 - uniaxial, non-dielectric, magnetic (et=ez=eps0) & (mut,muz)
%  6 - uniaxial, dielectric, magnetic (et,ez) & (mut,muz)
switch solveCase
    case 1
        ret=X(1);
        iet=X(2);
        rez=ret;
        iez=iet;
        rmut=1;
        imut=0;
```

271

```matlab
36          rmuz=rmut;
37          imuz=imut;
38
39      case  2
40          ret=1;
41          iet=0;
42          rez=ret;
43          iez=iet;
44          rmut=X(1);
45          imut=X(2);
46          rmuz=rmut;
47          imuz=imut;
48
49      case 3
50          ret=X(1);
51          iet=X(2);
52          rez=ret;
53          iez=iet;
54          rmut=X(3);
55          imut=X(4);
56          rmuz=rmut;
57          imuz=imut;
58
59      case 4
60          ret=X(1);
61          iet=X(2);
62          rez=X(3);
63          iez=X(4);
64          rmut=1;
65          imut=0;
66          rmuz=rmut;
67          imuz=imut;
```

272

```matlab
68
69    case 5
70        ret=1;
71        iet=0;
72        rez=ret;
73        iez=iet;
74        rmut=X(1);
75        imut=X(2);
76        rmuz=X(3);
77        imuz=X(4);
78    case 6
79        ret=X(1);
80        iet=X(2);
81        rez=X(3);
82        iez=X(4);
83        rmut=X(5);
84        imut=X(6);
85        rmuz=X(7);
86        imuz=X(8);
87    case 7
88        ret=real(ket);
89        iet=imag(ket);
90        rez=X(1);
91        iez=X(2);
92        rmut=real(kmut);
93        imut=imag(kmut);
94        rmuz=X(3);
95        imuz=X(4);
96 end
97
98 % put the real and imaginary parts together
99 et=ret+1j*iet;
```

```matlab
100  ez=rez+1j*iez;

101  mut=rmut+1j*imut;

102  muz=rmuz+1j*imuz;

103

104  % % display some useful info

105  % display(['Current Values are:'])

106  % display(['widx = ' num2str(widx)])

107  % display(['et = ' num2str(et)])

108  % display(['ez = ' num2str(ez)])

109  % display(['mut = ' num2str(mut)])

110  % display(['muz = ' num2str(muz)])

111

112  for didx=1:length(dmat) % if we have two thicknesses

113      d=dmat(didx);

114      midx=0;

115      for m=includeModes % source modes

116          midx=midx+1;

117          nidx=0;

118          vm=v(m);

119          wm=wi(m);

120          if wm==0

121              delta0wm = 1;

122          else

123              delta0wm = sqrt(2);

124          end

125

126      % waveguide parameters for m

127          kxm=vm.*pi/a;

128          kym=wm.*pi/b;

129          kcm=sqrt(kxm.^2+kym.^2);

130          kzm=sqrt(k0.^2-kcm.^2);

131
```

```matlab
       % m index normalization coefficients
    if any(m==[4 7 9 12 15 19]) % tmz
        Zm=kzm./(wval.*eps0);   % TMZ m index
        Mhxm=(sqrt(2).*kym.*delta0wm)./(Zm.*kcm*sqrt(a*b));   % TMZ
        Mhym=-(sqrt(2).*kxm.*delta0wm)./(Zm.*kcm*sqrt(a*b));   % TMZ
    else % it's tez
        Zm=wval.*mu0./kzm;   % TEZ m index
        Mhxm=(sqrt(2).*kxm.*delta0wm)./(Zm.*kcm*sqrt(a*b));   % TEZ
        Mhym=(sqrt(2).*kym.*delta0wm)./(Zm.*kcm*sqrt(a*b));   % TEZ
    end

    for n=includeModes  % observation modes
        nidx=nidx+1;
     % the source terms for the MFIE's
        if m==1 && n==1 % only the dominant source is excited
            Bmat(1)=(2./(Zm.^2));
        end
        vn=v(n);
        wn=wi(n);
        if wn==0
            delta0wn = 1;
        else
            delta0wn = sqrt(2);
        end

        deltamn=1.*(m==n);

        % waveguide parameters for n
        kxn=vn.*pi/a;
        kyn=wn.*pi/b;
        kcn=sqrt(kxn.^2+kyn.^2);
        kzn=sqrt(k0.^2-kcn.^2);
```

```matlab
164
165             % n index normalization coefficients
166             if any(n==[4 7 9 12 15 19])
167                 Zn=kzn./(wval.*eps0);   % TMZ n index
168                 Mhxn=(sqrt(2).*kyn.*delta0wn)./(Zn.*kcn*sqrt(a*b));   % TMZ
169                 Mhyn=-(sqrt(2).*kxn.*delta0wn)./(Zn.*kcn*sqrt(a*b));   % TMZ
170             else
171                 Zn=wval.*mu0./kzn;   %  TEZ n index
172                 Mhxn=(sqrt(2).*kxn.*delta0wn)./(Zn.*kcn*sqrt(a*b));   % TEZ
173                 Mhyn=(sqrt(2).*kyn.*delta0wn)./(Zn.*kcn*sqrt(a*b));   % TEZ
174             end
175
176             % % which set of lamy solutions we use depends on wm and wn
177             if num_int==1
178                 intval11=2*quad2d(@(lamx, lamy) SelfIntegral2d(wval,et,ez,...
179                     mut,muz,vm,vn,wm,wn,a,b,d,Mhxm,Mhxn,Mhym,Mhyn,lamx,lamy),...
180                     0,50e3,0,50e3,'abstol',1e-10,'reltol',1e-10);
181                 intval12=2*quad2d(@(lamx, lamy) CouplingIntegral2d(wval,et,ez,...
182                     mut,muz,vm,vn,wm,wn,a,b,d,Mhxm,Mhxn,Mhym,Mhyn,lamx,lamy),...
183                     0,50e3,0,50e3,'abstol',1e-10,'reltol',1e-10);
184             else
185                 if wm == 0 && wn == 0   % Case 1
186                     % quadgk numerically solves the lamx integrals
187 %                     disp(['v_m = ' num2str(vm)  ' and v_n = ' num2str(vn)])
188 %                     disp(['w_m = ' num2str(wm)  ' and w_n = ' num2str(wn)])
189 %                     disp('Using Case 1')
190                     intval11=quadgk(@(lamx) SelfIntegral_1(wval,et,ez...
191                         ,mut,muz,vm,vn,a,b,d,Mhxm,Mhxn,lamx),...
192                         0,50e3,'abstol',1e-10,'reltol',1e-10);
193                     intval12=quadgk(@(lamx) CouplingIntegral_1(wval,et,ez,...
194                         mut,muz,vm,vn,a,b,d,Mhxm,Mhxn,lamx),...
195                         0,50e3,'abstol',1e-10,'reltol',1e-10);
```

276

```matlab
196             elseif wm ~=0 && wn==0 % Case 2
197    %              disp(['v_m = ' num2str(vm)  ' and v_n = ' num2str(vn)])
198    %              disp(['w_m = ' num2str(wm)  ' and w_n = ' num2str(wn)])
199    %              disp('Using Case 2')
200             intval11=quadgk(@(lamx) SelfIntegral_2(wval,et,ez...
201                 ,mut,muz,wm,vm,vn,a,b,d,Mhxm,Mhxn,Mhym,lamx)...
202                 ,0,50e3,'abstol',1e-10,'reltol',1e-10);
203             intval12=quadgk(@(lamx) CouplingIntegral_2(wval,et,ez,...
204                 mut,muz,wm,vm,vn,a,b,d,Mhxm,Mhxn,Mhym,lamx),...
205                 0,50e3,'abstol',1e-10,'reltol',1e-10);
206         elseif wm==0 && wn~=0  % Case 3
207    %              disp(['v_m = ' num2str(vm)  ' and v_n = ' num2str(vn)])
208    %              disp(['w_m = ' num2str(wm)  ' and w_n = ' num2str(wn)])
209    %              disp('Using Case 3')
210             intval11=quadgk(@(lamx) SelfIntegral_3(wval,et,ez,...
211                 mut,muz,wn,vm,vn,a,b,d,Mhxm,Mhxn,Mhyn,lamx),...
212                 0,50e3,'abstol',1e-10,'reltol',1e-10);
213             intval12=quadgk(@(lamx) CouplingIntegral_3(wval,et,ez,...
214                 mut,muz,wn,vm,vn,a,b,d,Mhxm,Mhxn,Mhyn,lamx),...
215                 0,50e3,'abstol',1e-10,'reltol',1e-10);
216         elseif wm~=0 && wn~=0 && wm==wn % Case 4
217    %               disp(['v_m = ' num2str(vm)  ' and v_n = ' num2str(vn)])
218    %               disp(['w_m = ' num2str(wm)  ' and w_n = ' num2str(wn)])
219    %               disp('Using Case 4')
220            intval11=quadgk(@(lamx) SelfIntegral_4(wval,et,ez,...
221                 mut,muz,wm,vm,vn,a,b,d,Mhxm,Mhxn,Mhym,Mhyn,lamx),...
222                 0,50e3,'abstol',1e-10,'reltol',1e-10);
223            intval12=quadgk(@(lamx) CouplingIntegral_4(wval,et,ez,...
224                 mut,muz,wm,vm,vn,a,b,d,Mhxm,Mhxn,Mhym,Mhyn,lamx),...
225                 0,50e3,'abstol',1e-10,'reltol',1e-10);
226         elseif wm~=0 && wn~=0 && wm~=wn % Case 5
227    %               disp(['v_m = ' num2str(vm)  ' and v_n = ' num2str(vn)])
```

277

```matlab
228  %                    disp(['w_m = ' num2str(wm)   ' and w_n = ' num2str(wn)])
229  %                    disp('Using Case 5')
230                       intval11=quadgk(@(lamx) SelfIntegral_5(wval,et,ez,...
231                           mut,muz,wm,wn,vm,vn,a,b,d,Mhxm,Mhxn,Mhym,Mhyn,lamx),...
232                           0,50e3,'abstol',1e-10,'reltol',1e-10);
233                       intval12=quadgk(@(lamx) CouplingIntegral_5(wval,et,ez,...
234                           mut,muz,wm,wn,vm,vn,a,b,d,Mhxm,Mhxn,Mhym,Mhyn,lamx),...
235                           0,50e3,'abstol',1e-10,'reltol',1e-10);
236               end  % end case logic
237           end % end num_int logic
238         % the A & B coefficients
239           A11(midx,nidx)=deltamn./(Zm.*Zn) - ( ( (Zn)./(4) ).* 2.*intval11 );
240           A12(midx,nidx) =  ((Zn)./(4)).* 2.*intval12;
241           A21=A12;
242           A22=A11;
243       end % end of n loop
244    end % end of m loop
245
246  % solve for the C matrix
247    Amat=[A11 A12; A21 A22];
248    Cmat=Amat\Bmat;
249
250  % scattering parameters
251    S11thy=Cmat(1)-1;
252    S21thy=Cmat(numModes+1);
253    S22thy=S11thy;
254    S12thy=S21thy;
255    if porttouse==1
256        Sthy=cat(1,Sthy,real(S11thy),imag(S11thy),real(S21thy),imag(S21thy));
257    elseif porttouse==2
258        Sthy=cat(1,Sthy,real(S12thy),imag(S12thy),real(S22thy),imag(S22thy));
259    else % use all 4
```

278

```
260        Sthy=cat(1,Sthy,real(S11thy),imag(S11thy),real(S21thy),imag(S21thy),...
261            real(S12thy),imag(S12thy),real(S22thy),imag(S22thy));
262 end % end of dmat loop
263
264
265 end % end of function
```

F.4 SelfIntegral_1.m

This is provided as an example of how the code calculates the A-coefficients, specifically, $A^{(11)}$ for Case I.

```
1  function y = SelfIntegral_1(w,et,ez,mut,muz,vm,vn,a,b,d,Mhxm,Mhxn,lamx)
2
3  global eps0 mu0;
4  Clamx= ((1-(-1).^vm.*exp(1j.*lamx.*a)).*(1-(-1).^vn.*exp(-1j.*lamx.*a)))./...
5      ((lamx.^2-(vm.*pi./a).^2).*(lamx.^2-(vn.*pi./a).^2));
6
7  % % tez term
8  % the sum term
9  lmax=100;
10 kt=sqrt(w^2*eps0*et*mu0*mut);
11 ktz=sqrt(w^2*eps0*et*mu0*muz);
12 kzt=sqrt(w^2*eps0*ez*mu0*mut);
13 [l,lamxl] = ndgrid(0:lmax,lamx);
14 lamylth=sqrt(ktz^2)*sqrt(1-((pi^2*l.^2)/(d^2*kt^2))-((lamxl.^2)/(ktz^2)));
15 sumterm1= -((4*pi*mu0*muz.*lamx.^2.*Clamx)./(w*mu0^2*mut^2*d)).*...
16     sum( ( ( (pi*l/d).^2 ).*(1-exp(-1j*lamylth*b) ) )./...
17     ( lamylth.^3.*(lamylth.^2 + lamxl.^2) ),1);
18
19 % the other term
```

```matlab
20   lamztha=kt*sqrt( 1 - ( lamx/ktz ).^2 );

21   term2stable=((1j*2*pi*b.*lamztha.*Clamx)./(w*mut*mu0));

22   term2unstable=((cos(lamztha*d))./(sin(lamztha*d)));

23   term2unstable(isnan(term2unstable))=1j;

24

25   % the whole tez term

26   omega11tez=(term2stable.*term2unstable + sumterm1);

27

28   % % tmz term

29   lamylpsi=sqrt(kzt^2)*sqrt(1-((pi^2*l.^2)/(d^2*kt^2))-((lamxl.^2)/(kzt^2)));

30   omega11tmz=-((4.*pi.*w.*ez.*eps0.*Clamx)./(d)).*...

31       sum( (1-exp(-1j.*lamylpsi.*b))./...

32       (lamylpsi.*(lamylpsi.^2 + lamxl.^2).*(1+1.*(l==0))),1);

33

34   y=( (Mhxm.*Mhxn.*vm.*vn)./ (a^2) ).*(omega11tez+omega11tmz);

35

36   end
```

Bibliography

[1] Agilent Technologies. *Technical Specifications - Agilent Technologies PNA Series Network Analyzers E8362B/C, E8363B/C, and E8364B/C*, October 2008. URL http://cp.literature.agilent.com/litweb/pdf/E8364-90031.pdf.

[2] Alenkowicz, H and B Levitas. "Time domain measurement of complex-permittivity and complex permeability of materials". *Microwaves, Radar and Wireless Communications, 2002. MIKON-2002. 14th International Conference on*, volume 1, 302–305. IEEE, 2002.

[3] Ali, S.M., T.M. Habashy, and J. Au Kong. "Spectral-domain Green's function in layered chiral media". *JOSA A*, 9(3):413–423, 1992.

[4] Arfken, George B, Hans J Weber, and Lawrence Ruby. *Mathematical methods for physicists*, volume 3. Academic press San Diego, 1985.

[5] Bagby, JS and DP Nyquist. "Dyadic Green's functions for integrated electronic and optical circuits". *Microwave Theory and Techniques, IEEE Transactions on*, 35(2):207–210, 1987.

[6] Baker-Jarvis, James, Richard G Geyer, and Paul D Domich. "A nonlinear least-squares solution with causality constraints applied to transmission line permittivity and permeability determination". *Instrumentation and Measurement, IEEE Transactions on*, 41(5):646–652, 1992.

[7] Baker-Jarvis, James, Michael D Janezic, Paul D Domich, and Richard G Geyer. "Analysis of an open-ended coaxial probe with lift-off for nondestructive testing". *Instrumentation and Measurement, IEEE Transactions on*, 43(5):711–718, 1994.

[8] Bakhtiari, Sasan, Stoyan I Ganchev, and Reza Zoughi. "Open-ended rectangular waveguide for nondestructive thickness measurement and variation detection of lossy dielectric slabs backed by a conducting plate". *Instrumentation and Measurement, IEEE Transactions on*, 42(1):19–24, 1993.

[9] Balanis, C.A. *Advanced engineering electromagnetics*, volume 205. Wiley New York, 1989.

[10] Balanis, C.A. *Antenna Theory: Analysis and Design*. NJ: Wiley, 2005.

[11] Ball, JAR and PJ Khan. "Source region electric field derivation by a dyadic green's function approach". *Microwaves, Optics and Antennas, IEE Proceedings H*, 127(5):301–304, 1980.

[12] Belhadj-Tahar, N.-E. and A. Fourrier-Lamer. "Broad-band simultaneous measurement of the complex permittivity tensor for uniaxial materials using a coaxial dis-

continuity". *Microwave Theory and Techniques, IEEE Transactions on*, 39(10):1718 –1724, oct 1991. ISSN 0018-9480.

[13] Belov, P. A. "Backward waves and negative refraction in uniaxial dielectrics with negative dielectric permittivity along the anisotropy axis". *Microwave and Optical Technology Letters*, 37(4):259–263, 2003. ISSN 1098-2760. URL http://dx.doi.org/10.1002/mop.10887.

[14] Belov, Pavel A and Constantin R Simovski. "Homogenization of electromagnetic crystals formed by uniaxial resonant scatterers". *Physical Review E*, 72(2):026615, 2005.

[15] Bois, K.J., A.D. Benally, and R. Zoughi. "Multimode solution for the reflection properties of an open-ended rectangular waveguide radiating into a dielectric half-space: the forward and inverse problems". *Instrumentation and Measurement, IEEE Transactions on*, 48(6):1131 –1140, dec 1999. ISSN 0018-9456.

[16] Caloz, Christophe and Tatsuo Itoh. *Electromagnetic metamaterials: transmission line theory and microwave applications*. Wiley-IEEE Press, 2005.

[17] Chang, CW, KM Chen, and Jian Qian. "Nondestructive measurements of complex tensor permittivity of anisotropic materials using a waveguide probe system". *Microwave Theory and Techniques, IEEE Transactions on*, 44(7):1081–1090, 1996.

[18] Chang, CW, KM Chen, and Jian Qian. "Nondestructive determination of electromagnetic parameters of dielectric materials at X-band frequencies using a waveguide probe system". *Instrumentation and Measurement, IEEE Transactions on*, 46(5):1084–1092, 1997.

[19] Chen, Chun-Ping, Zhewang Ma, Tetsuo Anada, and Jui-Pang Hsu. "Further study on two-thickness-method for simultaneous measurement of complex EM parameters based on open-ended coaxial probe". *Microwave Conference, 2005 European*, volume 1, 4–pp. IEEE, 2005.

[20] Chen, Hollis C. *Theory of electromagnetic waves: a coordinate-free approach*. McGraw-Hill Book Company, 1983.

[21] Chen, K.M. "A simple physical picture of tensor Green's function in source region". *Proceedings of the IEEE*, 65(8):1202–1204, 1977.

[22] Chen, L. *Microwave electronics: measurement and materials characterization*. John Wiley, 2004. ISBN 9780470844922. URL http://books.google.com/books?id=pAhTAAAAMAAJ.

[23] Chew, W.C. "Some observations on the spatial and eigenfunction representations of dyadic Green's functions". *Antennas and Propagation, IEEE Transactions on*, 37(10):1322–1327, 1989.

[24] Chew, W.C. *Waves and fields in inhomogeneous media*. Van Nostrand Reinhold, 1990. ISBN 9780442238162. URL http://books.google.com/books?id=5tLvAAAAMAAJ.

[25] Chew, Weng Cho, E Michielssen, JM Song, and JM Jin. *Fast and efficient algorithms in computational electromagnetics*. Artech House, Inc., 2001.

[26] Collin, RE. "A simple artificial anisotropic dielectric medium". *Microwave Theory and Techniques, IRE Transactions on*, 6(2):206–209, 1958.

[27] Collin, R.E., IEEE Antennas, and Propagation Society. *Field theory of guided waves*. The IEEE/OUP Series on Electromagnetic Wave Theory (Formerly IEEE Only), Series Editor Series. IEEE Press, 1991. ISBN 9780879422370. URL http://books.google.com/books?id=vvRDAQAAIAAJ.

[28] Compton Jr, RT. "The admittance of aperture antennas radiating into lossy media". 1964.

[29] Crowgey, Benjamin R., Ozgur Tuncer, Junyan Tang, Edward J. Rothwell, B. Shanker, Leo C. Kempel, and Michael J. Havrilla. "Characterization of Biaxial Anisotropic Material Using a Reduced Aperture Waveguide". 2013.

[30] Cui, Tie Jun, David Smith, and Ruopeng Liu. *Metamaterials: theory, design, and applications*. Springer, 2009.

[31] Decreton, M. and F.E. Gardiol. "Reflection from a metallic or dielectric sheet into an open ended waveguide". *Antennas and Propagation Society International Symposium, 1976*, volume 14, 362–365. Oct.

[32] Decreton, Marc C and MS Ramachandraiah. "Nondestructive Measurement of Complex Permittivity for Dielectric Slabs (Short Papers)". *Microwave Theory and Techniques, IEEE Transactions on*, 23(12):1077–1080, 1975.

[33] Dester, G. D., E. J. Rothwell, M. J. Havrilla, and M. W. Hyde. "Error analysis of a two-layer method for the electromagnetic characterization of conductor-backed absorbing material using an open-ended waveguide probe". *Progress In Electromagnetics Research*, 26:1–21, 2010.

[34] Dester, Gary D, Edward J Rothwell, and Michael J Havrilla. "An extrapolation method for improving waveguide probe material characterization accuracy". *Microwave and Wireless Components Letters, IEEE*, 20(5):298–300, 2010.

[35] Dester, Gary D, Edward J Rothwell, and Michael J Havrilla. "Two-Iris Method for the Electromagnetic Characterization of Conductor-Backed Absorbing Materials Using an Open-Ended Waveguide Probe". *Instrumentation and Measurement, IEEE Transactions on*, 61(4):1037–1044, 2012.

[36] Dong, X.T., X.S. Rao, Y.B. Gan, B. Guo, and W.Y. Yin. "Perfectly matched layer-absorbing boundary condition for left-handed materials". *Microwave and Wireless Components Letters, IEEE*, 14(6):301 – 303, june 2004. ISSN 1531-1309.

[37] Eleftheriades, George V and Keith G Balmain. *Negative-refraction metamaterials: fundamental principles and applications*. Wiley-IEEE Press, 2005.

[38] Engen, Glenn F and Cletus A Hoer. "Thru-reflect-line: An improved technique for calibrating the dual six-port automatic network analyzer". *Microwave Theory and Techniques, IEEE Transactions on*, 27(12):987–993, 1979.

[39] Engheta, Nader and Richard W Ziolkowski. *Metamaterials: Physics and engineering explorations*. Wiley-IEEE Press, 2006.

[40] Fikioris, J.G. "Electromagnetic Field inside a Current-Carrying Region". *Journal of Mathematical Physics*, 6:1617, 1965.

[41] FOLGERØ, K and T TJOMSLAND. "Permittivity measurement of thin liquid layers using open-ended coaxial probes". *Measurement science & technology*, 7(8):1164–1173, 1996.

[42] Ganchev, S.I., S. Bakhtiari, and R. Zoughi. "A novel numerical technique for dielectric measurement of generally lossy dielectrics". *Instrumentation and Measurement, IEEE Transactions on*, 41(3):361 –365, jun 1992. ISSN 0018-9456.

[43] Ghodgaonkar, DK, VV Varadan, and VK Varadan. "Free-space measurement of complex permittivity and complex permeability of magnetic materials at microwave frequencies". *Instrumentation and Measurement, IEEE Transactions on*, 39(2):387–394, 1990.

[44] Harrington, R.F. *Time-harmonic electromagnetic fields*. McGraw-Hill electrical and electronic engineering series. McGraw-Hill, 1961. URL http://books.google.com/books?id=FtpPAAAAMAAJ.

[45] Harrington, Roger F. *Field computation by moment methods*. Wiley-IEEE Press, 1993.

[46] Havrilla, M. "Electric and magnetic field dyadic Green's functions and depolarizing dyad for a magnetic current immersed in a uniaxial dielectric-filled parallel plate waveguide". *General Assembly and Scientific Symposium, 2011 XXXth URSI*, 1–4. 2011.

[47] Havrilla, M.J. "Scalar Potential Depolarizing Dyad Artifact for a Uniaxial Medium". *Progress In Electromagnetics Research*, 134:151–168, 2013.

[48] Hecht, E. *Optics*. Addison-Wesley, 2002. ISBN 9780805385663. URL http://books.google.com/books?id=7aG6QgAACAAJ.

[49] Hildebrand, Francis B. "Advanced Calculus for Applications, 1976". *Prentice-Hall, Englewood Cliffs, NJ*, 511:256.

284

[50] Hrabar, S., J. Bartolic, and Z. Sipus. "Waveguide miniaturization using uniaxial negative permeability metamaterial". *Antennas and Propagation, IEEE Transactions on*, 53(1):110 – 119, jan. 2005. ISSN 0018-926X.

[51] Hyde, M. W. and M. J. Havrilla. "A non-destructive technique for determining complex permittivity and permeability of magnetic sheet materials using two flanged rectangular waveguides". *Progress In Electromagnetics Research, PIER*, 79:367–386, 2008. URL http://www.jpier.org/PIER/pier79/24.07102405.pdf.

[52] Hyde, Milo W, Michael J Havrilla, Andrew E Bogle, Edward J Rothwell, and Gary D Dester. "An Improved Two-Layer Method for Nondestructively Characterizing Magnetic Sheet Materials Using a Single Rectangular Waveguide Probe". *Electromagnetics*, 32(7):411–425, 2012.

[53] Hyde, MW and MJ Havrilla. "Measurement of complex permittivity and permeability using two flanged rectangular waveguides". *Microwave Symposium, 2007. IEEE/MTT-S International*, 531–534. IEEE, 2007.

[54] Hyde, MW and MJ Havrilla. "Reducing the measurement footprint in the characterization of low-loss materials using the flanged-waveguide measurement geometry". *Electromagnetics in Advanced Applications (ICEAA), 2010 International Conference on*, 43–46. IEEE, 2010.

[55] Hyde, MW, MJ Havrilla, and AE Bogle. "A novel and simple technique for measuring low-loss materials using the two flanged waveguides measurement geometry". *Measurement Science and Technology*, 22(8):085704, 2011.

[56] Hyde IV, M.W., J.W. Stewart, M.J. Havrilla, W.P. Baker, E.J. Rothwell, and D.P. Nyquist. "Nondestructive electromagnetic material characterization using a dual waveguide probe: A full wave solution". *Radio Science*, 44(3):RS3013, 2009.

[57] Jakoby, B. and F. Olyslager. "Singularity in Green dyadics for uniaxial bianisotropic media". *Electronics Letters*, 31(10):779–781, 1995.

[58] Jeffrey, A. *Complex analysis and applications*. Advanced engineering mathematics. CRC Press, 1992. ISBN 9780849386237. URL http://books.google.com/books?id=AoXwAAAAMAAJ.

[59] Krupka, J., K. Derzakowski, A. Abramowicz, M.E. Tobar, and R.G. Geyer. "Use of whispering-gallery modes for complex permittivity determinations of ultra-low-loss dielectric materials". *Microwave Theory and Techniques, IEEE Transactions on*, 47(6):752 –759, jun 1999. ISSN 0018-9480.

[60] Lakhtakia, Akhlesh. "On the genesis of Post constraint in modern electromagnetism". *Optik-International Journal for Light and Electron Optics*, 115(4):151–158, 2004.

[61] Lee, SW. "Ray Theory of Diffraction by Open-Ended Waveguides. I. Field in Waveguides". *Journal of Mathematical Physics*, 11:2830, 1970.

[62] Li, Ching-Lei and Kun-Mu Chen. "Determination of electromagnetic properties of materials using flanged open-ended coaxial probe-full-wave analysis". *Instrumentation and Measurement, IEEE Transactions on*, 44(1):19–27, 1995.

[63] Madsen, K., H. B. Nielsen, and O. Tingleff. "Methods for Non-Linear Least Squares Problems (2nd ed.)", 2004.

[64] Mandel?shtam, LI. "Group velocity in a crystal lattice". *Zh. Eksp. Teor. Fiz*, 15(9):475–478, 1945.

[65] Maode, Niu, Su Yong, Yan Jinkui, Fu Chenpeng, and Xu Deming. "An improved open-ended waveguide measurement technique on parameters ε_γ and μ_γ of high-loss materials". *Instrumentation and Measurement, IEEE Transactions on*, 47(2):476–481, 1998. ID: 1.

[66] McNamara, DA, CWI Pistorius, and JAG Malherbe. *The Uniform Geometrical theory of diffraction*. 1990.

[67] Morita, N. *Integral Equation Methods for Electromagnetics*. The Artech House Antenna Library. Books on Demand, 1990. ISBN 9780608013473. URL http://books.google.com/books?id=EAblAAAACAAJ.

[68] Mostafavi, M. and W.-C. Lan. "Polynomial characterization of inhomogeneous media and their reconstruction using an open-ended waveguide". *Antennas and Propagation, IEEE Transactions on*, 41(6):822 –824, jun 1993. ISSN 0018-926X.

[69] P. Frandsen, H. Nielsen O. Tingleff, K. Jonasson. "Unconstrained Optimization (3rd ed.)", 2004.

[70] Pendry, John B, AJ Holden, DJ Robbins, and WJ Stewart. "Magnetism from conductors and enhanced nonlinear phenomena". *Microwave Theory and Techniques, IEEE Transactions on*, 47(11):2075–2084, 1999.

[71] Pendry, John B, AJ Holden, WJ Stewart, and I Youngs. "Extremely low frequency plasmons in metallic mesostructures". *Physical review letters*, 76(25):4773–4776, 1996.

[72] Pendry, John B, David Schurig, and David R Smith. "Controlling electromagnetic fields". *Science*, 312(5781):1780–1782, 2006.

[73] Pendry, John B and David R Smith. "Reversing light with negative refraction". *Physics Today*, 57:37–43, 2004.

[74] Pendry, John Brian. "Negative refraction makes a perfect lens". *Physical review letters*, 85(18):3966–3969, 2000.

[75] Post, Evert Jan. *Formal structure of electromagnetics: general covariance and electromagnetics*. Courier Dover Publications, 1962.

[76] Pournaropoulos, Christos L and Devendra Misra. "A study on the coaxial aperture electromagnetic sensor and its application in material characterization". *Instrumentation and Measurement, IEEE Transactions on*, 43(2):111–115, 1994.

[77] Przezdziecki, S. S. "On the representation of electromagnetic fiels in gyrotropic media in terms of scalar Hertz potentials". *Journal of mathematical physics*, 23(9):1708, 1982.

[78] Przeziecki, S. and R. A. Hurd. "A note on scalar Hertz potentials for gyrotropic media". *Applied Physics*, 20(4):313 – 317, 1979.

[79] Robin L. Cravey, Kerri Bussell, Pacita I. Tiemsin and Kenneth L. Dudley. *NASA-95-TM110147 Dielectric Property Measurements in Electromagnetic Properties Measurement Laboratory*. Technical report, Electromagnetic Properties Measurement Laboratory, 1995.

[80] Sanadiki, B.A. and M. Mostafavi. "Inversion of inhomogeneous continuously varying dielectric profiles using open-ended waveguides". *Antennas and Propagation, IEEE Transactions on*, 39(2):158 –163, feb 1991. ISSN 0018-926X.

[81] Schultz, J.W. *Focused Beam Methods: Measuring Microwave Materials in Free Space*. Createspace Independent Pub, 2012. ISBN 9781480092853. URL http://books.google.com/books?id=gYVlPZq5CssC.

[82] Scott Jr, Waymond R. "A new technique for measuring the constitutive parameters of planar materials". *Instrumentation and Measurement, IEEE Transactions on*, 41(5):639–645, 1992.

[83] Seal, M. D., M. W. Hyde, and M. J. Havrilla. "Nondestructive complex permittivity and permeability extraction using a two-layer dual-waveguide probe measurement geometry". *Progress In Electromagnetics Research*, 123:123–142, 2012.

[84] Shamonina, E and L Solymar. "Metamaterials: How the subject started". *Metamaterials*, 1(1):12–18, 2007.

[85] Shelby, RA, DR Smith, and S Schultz. "Experimental verification of a negative index of refraction". *Science*, 292(5514):77–79, 2001.

[86] Stewart, James W. *Simultaneous extraction of the permittivity and permeability of conductor-backed lossy materials using open-ended waveguide probes*. Ph.D. thesis, 2006.

[87] Stewart, JW and MJ Havrilla. "Electromagnetic characterization of a magnetic material using an open-ended waveguide probe and a rigorous full-wave multimode model". *Journal of electromagnetic waves and applications*, 20(14):2037–2052, 2006.

[88] Stuchly, Maria A and Stanislaw S Stuchly. "Coaxial line reflection methods for measuring dielectric properties of biological substances at radio and microwave

frequencies-A review". *Instrumentation and Measurement, IEEE Transactions on*, 29(3):176–183, 1980.

[89] Tantot, Olivier, Michel Chatard-Moulin, and Pierre Guillon. "Measurement of complex permittivity and permeability and thickness of multilayered medium by an open-ended waveguide method". *Instrumentation and Measurement, IEEE Transactions on*, 46(2):519–522, 1997.

[90] Teodoridis, V, T Sphicopoulos, and FE Gardiol. "The reflection from an open-ended rectangular waveguide terminated by a layered dielectric medium". *Microwave Theory and Techniques, IEEE Transactions on*, 33(5):359–366, 1985.

[91] Van Bladel, J. "Some remarks on Green's dyadic for infinite space". *Antennas and Propagation, IRE Transactions on*, 9(6):563–566, 1961.

[92] Veselago, Viktor G et al. "The electrodynamics of substances with simultaneously negative values of ε and μ". *Physics-Uspekhi*, 10(4):509–514, 1968.

[93] Viola, M.S. and DP Nyquist. "An observation on the Sommerfeld-integral representation of the electric dyadic Green's function for layered media". *Microwave Theory and Techniques, IEEE Transactions on*, 36(8):1289–1292, 1988.

[94] Weiglhofer, W.S. "Reduction of dyadic Green's functions to scalar Hertz potentials for gyrotropic media". *Radio Science*, 22(2):209 – 215, 1987. Id: 1; issn: print 0048-6604.

[95] Weiglhofer, W.S. "Scalarisation of maxwell's equations in general inhomogeneous bianisotropic media". *Microwaves, Antennas and Propagation, IEE Proceedings H*, 134(4):357 –360, august 1987. ISSN 0950-107X.

[96] Weiglhofer, W.S. "Isotropic chiral media and scalar Hertz potentials". *Journal of physics.A, Mathematical and general*, 21(9):2249–2251, -05 1988.

[97] Weiglhofer, W.S. "Electromagnetic Field Representation in (Inhomogeneous) Isotropic Chiral Media". *Electromagnetics*, 10(3):271–278, 1990. URL http://www.tandfonline.com/doi/abs/10.1080/02726349008908243.

[98] Weiglhofer, W.S. "Green's functions and magnetized ferrites". *International journal of electronics*, 73(4):763–771, 1992.

[99] Weiglhofer, W.S. "Analytic methods and free-space dyadic Green's functions". *Radio Science*, 28(5):847–857, 1993. ISSN 1944-799X. URL http://dx.doi.org/10.1029/93RS00903.

[100] Weiglhofer, W.S. "Frequency-dependent dyadic Green functions for bianisotropic media". *Advanced Electromagnetism: Foundations, Theory, Applications*, 376–389, 1995.

[101] Weiglhofer, W.S. "Electromagnetic field in the source region: A review". *Electromagnetics*, 19(6):563–577, 1999.

[102] Weiglhofer, W.S. *Hertz Potentials in Complex Medium Electromagnetics*. Technical report, DTIC Document, 2000.

[103] Weiglhofer, W.S. *Scalar Hertz potentials for linear bianisotropic mediums*. John Wiley, 2000.

[104] Weiglhofer, W.S. "Scalar Hertz potentials for nonhomogeneous uniaxial dielectric-magnetic mediums". *International Journal of Applied Electromagnetics and Mechanics*, 11(3):131–140, 2000.

[105] Weiglhofer, W.S. and A. Lakhtakia. "The correct constitutive relations of chiroplasmas and chiroferrites". *Microwave and Optical Technology Letters*, 17(6):405–408, 1998.

[106] Weiglhofer, W.S. and A. Lakhtakia. *Introduction to complex mediums for optics and electromagnetics*, volume 123. Society of Photo Optical, 2003.

[107] Weiglhofer, W.S. and I.V. Lindell. "Scalar potential formalism for uniaxial bianisotropic media". *Antennas and Propagation Society International Symposium, 1994. AP-S. Digest*, volume 3, 1586 –1589 vol.3. jun 1994.

[108] Weiglhofer, W.S. and Papousek W. "Scalar Hertz potentials for transversally oriented current density distributions in gyrotropic media". *Archiv Elektronik und Uebertragungstechnik*, 41:41–45, feb 1987. URL http://adsabs.harvard.edu/abs/1987ArElU..41...41W.

[109] Wong, K.-L. and H.-T. Chen. "Electromagnetic scattering by a uniaxially anisotropic sphere". *Microwaves, Antennas and Propagation, IEE Proceedings H*, 139(4):314 –318, aug 1992. ISSN 0950-107X.

[110] Wu, Mingzhong, Xi Yao, and Liangying Zhang. "An improved coaxial probe technique for measuring microwave permittivity of thin dielectric materials". *Measurement Science and Technology*, 11(11):1617, 2000. URL http://stacks.iop.org/0957-0233/11/i=11/a=311.

[111] Yaghjian, A.D. "Electric dyadic Green's functions in the source region". *Proceedings of the IEEE*, 68(2):248–263, 1980.

[112] Ziolkowski, Richard W. "Metamaterial-based antennas: Research and developments". *IEICE transactions on electronics*, 89(9):1267–1275, 2006.

[113] Zoughi, Reza. *Microwave Non-Destructive Testing and Evaluation Principles*, volume 4. Springer, 2000.

Vita

Capt Neil Rogers was born in Tulsa, Oklahoma. After graduating with honors from Union High School, he studied Electrical Engineering at the University of Tulsa. He graduated Cum Laude with his Bachelor's Degree in Electrical Engineering in May of 2003. Capt Rogers commissioned into the United States Air Force in August of 2004 through Officer Training School (OTS) at Maxwell AFB, Montgomery, Alabama. Following OTS, he was assigned to the National Air and Space Intelligence Center (NASIC) where he worked in remote sensing. Following his assignment to NASIC, he entered graduate school at the Air Force Institute of Technology (AFIT) in August of 2007 and completed his Master's Degree in Electrical Engineering in February of 2009. He served for one year as the chief for the Active Denial section and for one year as the chief of the Computational Physics section in the High Powered Microwave Division of the Air Force Research Labs (AFRL/RDHE) at Kirtland AFB, New Mexico. He is currently pursuing his Doctorate in Electrical Engineering at AFIT with a focus in electromagnetics. Capt Rogers has been married to the love of his life for almost 9 years, and has three rambunctious little boys. He is actively involved in his church band, loves being outdoors and hopes to one day finish an ironman distance triathlon.

REPORT DOCUMENTATION PAGE

Form Approved
OMB No. 0704–0188

1. REPORT DATE *(DD–MM–YYYY)*	2. REPORT TYPE	3. DATES COVERED *(From — To)*
18–09–2014	Doctoral Dissertation	Oct 2011–Sep 2014

4. TITLE AND SUBTITLE

Nondestructive Electromagnetic Characterization of Uniaxial Materials

5a. CONTRACT NUMBER

5b. GRANT NUMBER

5c. PROGRAM ELEMENT NUMBER

6. AUTHOR(S)

Rogers, Neil G., Captain, USAF

5d. PROJECT NUMBER

5e. TASK NUMBER

5f. WORK UNIT NUMBER

7. PERFORMING ORGANIZATION NAME(S) AND ADDRESS(ES)

Air Force Institute of Technology
Graduate School of Engineering and Management (AFIT/EN)
2950 Hobson Way
WPAFB, OH 45433-7765

8. PERFORMING ORGANIZATION REPORT NUMBER

AFIT-ENG-DS-14-S-05

9. SPONSORING / MONITORING AGENCY NAME(S) AND ADDRESS(ES)

Intentionally Left Blank

10. SPONSOR/MONITOR'S ACRONYM(S)

11. SPONSOR/MONITOR'S REPORT NUMBER(S)

12. DISTRIBUTION / AVAILABILITY STATEMENT

DISTRIBUTION STATEMENT A:
APPROVED FOR PUBLIC RELEASE; DISTRIBUTION UNLIMITED

13. SUPPLEMENTARY NOTES

This work is declared a work of the U.S. Government and is not subject to copyright protection in the United States.

14. ABSTRACT

In this dissertation, a method for the simultaneous non-destructive extraction of the permittivity and permeability of a dielectric magnetic uniaxial anisotropic media is developed and several key contributions are demonstrated. The method utilizes a single fixture in which the MUT is clamped between two rectangular waveguides with $6" \times 6"$ PEC flanges. The transmission and reflection coefficients are measured, then compared with theoretically calculated coefficients to find a least squares solution to the minimization problem. One of the key contributions of this work is the development of the total parallel plate spectral-domain Green's function by two independent methods. The Green's function is thereby shown to be correct in form and in physical meaning. A second significant contribution of this work to the scientific community is the evaluation of one of the inverse Fourier transform integrals in the complex plane. This significantly enhances the efficiency of the extraction code. A third significant contribution is the measurement of a number of uniaxial anisotropic materials, many of which were envisioned, designed and constructed in-house using 3D printing technology. The results are shown to be good in the transverse dimension, but mildly unstable in the longitudinal dimension. A secondary contribution of this work that warrants mention is the inclusion of a flexible, complete, working code for the extraction process. Although such codes have been written before, they have not been published in the literature for broader use.

15. SUBJECT TERMS

Electromagnetics, Uniaxial, Characterization, Nondestructive, Green's Functions

16. SECURITY CLASSIFICATION OF:			17. LIMITATION OF ABSTRACT	18. NUMBER OF PAGES	19a. NAME OF RESPONSIBLE PERSON
a. REPORT	b. ABSTRACT	c. THIS PAGE			Dr. Michael J. Havrilla (ENG)
U	U	U	UU	313	19b. TELEPHONE NUMBER *(include area code)* (937) 255-3636 x4582 michael.havrilla@afit.edu

Standard Form 298 (Rev. 8–98)
Prescribed by ANSI Std. Z39.18